GLOBAL RADII OF CURVATURE, AND THE BIARC APPROXIMATION OF SPACE CURVES: IN PURSUIT OF IDEAL KNOT SHAPES

THÈSE N^{O} 2981 (2004)

PRÉSENTÉE À LA FACULTÉ SCIENCES DE BASE

Institut de mathématiques B

SECTION DE MATHÉMATIQUES

ÉCOLE POLYTECHNIQUE FÉDÉRALE DE LAUSANNE

POUR L'OBTENTION DU GRADE DE DOCTEUR ÈS SCIENCES

PAR

Jana SMUTNY

mathématicienne diplômée de l'Université de Zürich
de nationalités suisse tchèque et originaire de Windisch (AG)

acceptée sur proposition du jury:

Prof. J.H. Maddocks, directeur de thèse
Prof. P. Buser, rapporteur
Prof. S. Hildebrandt, rapporteur
Prof. A. Quarteroni, rapporteur
Prof. G. Wanner, rapporteur

Lausanne, EPFL
2004

Abstract

The distance from self-intersection of a (smooth and either closed or infinite) curve $\mathbf{q}$ in three dimensions can be characterised via the *global radius of curvature* at $\mathbf{q}(s)$, which is defined as the smallest possible radius amongst all circles passing through the given point and any two other points on the curve. The minimum value of the global radius of curvature along the curve gives a convenient measure of curve *thickness* or normal injectivity radius.

Given the utility of the construction inherent to global curvature, it is natural to consider variants defined in related ways. The first part of the thesis considers all possible circular and spherical distance functions and the associated, single argument, global radius of curvature functions that are constructed by minimisation over all but one argument. It is shown that among all possible global radius of curvature functions there are only five independent ones. And amongst these five there are two particularly useful ones for characterising thickness of a curve. We investigate the geometry of how these two functions, ρ_{pt} and ρ_{tp}, can be achieved. Properties and interrelations of the divers global radius of curvature functions are illustrated with the simple examples of ellipses and helices.

It is known that any Lipschitz continuous curve with positive thickness actually has $C^{1,1}$-regularity. Accordingly, $C^{1,1}$ is the natural space in which to carry out computations involving self-avoiding curves. The second part of the thesis develops the mathematical theory of *biarcs*, which are a geometrically elegant way of discretizing $C^{1,1}$ space curves. A biarc is a pair of circular arcs joined in a C^1 fashion according to certain matching rules. We establish a self-contained theory of the geometry of biarc interpolation of point-tangent data sampled from an underlying base curve, and demonstrate that such biarc curves have attractive convergence properties in both a pointwise and function-space sense, e.g. the two arcs of the biarc interpolating a coalescent point-tangent data pair on a C^2-curve approach the osculating circle of the curve at the limit of the data points, and for a $C^{1,1}$-base curve and a sequence of (possibly non-uniform) meshes, the interpolating biarc curves approach the base curve in the C^1-norm. For smoother base curves, stronger convergence can be obtained, e.g. interpolating biarc curves approach a C^2 base curve in the $C^{1,1}$-norm.

The third part of the thesis concerns the practical utility of biarcs in computation. It is shown that both the global radius of curvature function ρ_{pt} and thickness can be evaluated efficiently (and to an arbitrarily small, prescribed precision) on biarc curves. Moreover, both the notion of a contact set, i.e. the set of points realising thickness, and an approximate contact set can be defined rigorously. The theory is then illustrated

with an application to the computation of *ideal shapes* of knots. Informally ideal knot shapes can be described as the configuration allowing a given knot to be tied with the shortest possible piece of rope of prescribed thickness. The biarc discretization is combined with a simulated annealing code to obtain approximate ideal shapes. These shapes provide rigorous upper bounds for rope length of ideal knots. The approximate contact set and the function ρ_{pt} evaluated on the computed shapes allow us to assess closeness of the computations to ideality. The high accuracy of the computations reveal various, previously unrecognized, features of ideal knot shapes.

Résumé

La distance "d'auto-intersection" d'une courbe tridimensionnelle $\mathbf{q}$ (lisse, fermée ou infinie) peut se caractériser par le *rayon de courbure global* au point $\mathbf{q}(s)$, à savoir le plus petit de tous les rayons des cercles passant par le point $\mathbf{q}(s)$ et deux autres points quelconques de la courbe. Le rayon de courbure global minimal de la courbe est ainsi une mesure de *l'épaisseur* ou du *rayon injectif normal* de la courbe.

L'utilité d'une telle notion pour la caractérisation des courbes "non-intersectantes" pousse à étendre la définition précédente du rayon de courbure global. La première partie de la thèse envisage ainsi toutes les fonctions de distance circulaires et sphériques et les fonctions de rayon de courbure global associées obtenues par minimisation de ces fonctions de distance. Il est ainsi démontré que parmi toutes les fonctions de rayon de courbure global seules cinq sont indépendantes, dont deux particulièrement utiles pour caractériser l'épaisseur d'une courbe. Nous décrivons les géométries particulières "réalisant" ces deux fonctions ρ_{pt} et ρ_{tp}. Les propriétés des fonctions de rayon global de courbure et leurs rélations sont illustrées dans les cas simples des ellipses et des helices.

Il est connu qu'une courbe continue, lipschitzienne et d'épaisseur positive est automatiquement de régularité $C^{1,1}$. $C^{1,1}$ est par conséquent l'espace naturel pour les calculs mettant en jeu des courbes non-intersectantes. La deuxième partie de la thèse présente ainsi la théorie mathématique des *bi-arcs*, objets géométriques qui permettent de discrétiser de façon élégante les courbes spatiales de régularité $C^{1,1}$: Un bi-arc est une paire d'arcs de cercles joints de manière C^1 et suivant certaines règles particulières. Nous proposons une théorie autonome de l'interpolation par bi-arcs d'ensembles de couples point-tangente extraits d'une courbe de base. Nous démontrons en particulier que les courbes de bi-arcs possèdent des propriétés de convergence ponctuelles et uniformes intéressantes. Par exemple, dans la limite où deux point-tangentes d'une courbe C^2 se rejoignent, nous montrons que les deux arcs du bi-arc qui interpole cette paire point-tangente approchent le cercle osculatoire au point limite consideré. Nous montrons aussi que pour une courbe $C^{1,1}$ et une séquence de discrétisation (éventuellement non-uniforme) les courbes bi-arc d'interpolation convergent vers la courbe de base avec la norme C^1 et que pour des courbes de bases plus lisses des convergences plus fortes peuvent être obtenues : les courbes bi-arcs interpolant une courbe de base C^2 convergent vers la courbe de base avec la norme $C^{1,1}$.

La troisième partie de la thèse concerne l'utilité pratique des bi-arcs dans les calculs. Il est démontré que la fonction de rayon de courbure global ρ_{pt} et l'épaisseur des courbes bi-arcs peuvent être évaluées de manière efficace et ce à la précision voulue. Nous définissons de plus de façon rigoureuse la notion d'ensemble de contact, c'est-à-dire

l'ensemble des paires de point qui "réalisent" l'épaisseur, ainsi que la notion d'ensemble de contact "approximatif". La théorie est illustrée par l'étude des *nœuds idéaux* : les configurations des nœuds idéaux correspondent, pour nœud donné et une épaisseur donnée, aux configurations de longueur de corde minimale. Une méthode numérique de minimisation basée sur le principe du recuit-simulé et utilisant la discrétisation en bi-arc permet alors d'obtenir des approximations des configurations de nœuds idéaux. Ces configurations approchées fournissent ainsi des "limites supérieures" rigoureuses de la longueur de corde des nœuds idéaux. L'ensemble de contact approximatif et la fonction ρ_{pt} évalués à partir de ces configurations permettent alors d'estimer l' "écart à l'idéalité" de nos résultats. La grande précision des calculs permet par ailleurs de mettre en lumière diverses propriétés non observées jusqu'à présent.

Acknowledgements

It is a great pleasure to thank my supervisor Prof. John H. Maddocks for sharing his mathematical intuition, his ideas and for his guidance over more than three years. The idea of considering pairs of arcs of circles, which ultimately lead to the biarc discretization, first arose in conversations with Prof. Rémi Langevin; I wish to thank him for interesting discussions in the spirit of conformal geometry. I greatly enjoyed the collaboration with Ben Laurie, who adapted his simulated annealing code to allow computations with biarcs - a big thanks to him. I am very grateful to Prof. Heiko von der Mosel for many fruitful discussions, and all his helpful comments on the analysis. For careful mathematical discussions and reflexions, and a pleasant collaboration I wish to thank Prof. Oscar Gonzalez. I thank Mathias Carlen who ran 4.1-knot annealing computations within the framework of a semester project.

I am grateful to Prof. Eva Bayer-Flückiger for presiding the thesis committee, and Prof. Peter Buser, Prof. Stefan Hildebrandt, Prof. Alfio Quarteroni, and Prof. Gerhard Wanner, for accepting to be part of the committee and for reading the manuscript.

A big thank you to all former and current members of the 'chaire d'analyse appliquée' for their encouragement and interesting discussions, special thanks go to Carine Tschanz and Philippe Caussignac.

I wish to thank my parents, who raised and taught me, and my sister for their encouragement and love. I thank all my friends for being my companions. 'Un grand merci' to my Lausanne friends for wonderful ski and climbing tours, mountain hikes, and enjoyable moments at the lakeside.

Contents

Notation

$\mathbf{x} \cdot \mathbf{y}$	euclidean inner product of $\mathbf{x}$ and $\mathbf{y}$ in $\mathbb{R}^n$
$\lvert\mathbf{x}\rvert$	euclidean norm of $\mathbf{x}$ in $\mathbb{R}^n$
$\angle\mathbf{a}$	swept out angle of a circular arc $\mathbf{a}$
$\mathbf{x} \times \mathbf{y}$	cross product of $\mathbf{x}$ and $\mathbf{y}$ in $\mathbb{R}^3$
$\mathbf{x} \otimes \mathbf{y}$	outer product of $\mathbf{x}$ and $\mathbf{y}$ in $\mathbb{R}^n$
$\mathbf{d}$, $\mathbf{e}$	given two points $\mathbf{q}_0,\ \mathbf{q}_1 \in \mathbb{R}^3$ with $\mathbf{q}_0 \neq \mathbf{q}_1$, we denote the chord by $\mathbf{d} := \mathbf{q}_1 - \mathbf{q}_0$, and unit vector along the chord by $\mathbf{e} := \frac{\mathbf{q}_1 - \mathbf{q}_0}{\lvert\mathbf{q}_1 - \mathbf{q}_0\rvert}$, we use the same notation for two distinct points $\mathbf{q}_0 = \mathbf{q}(\sigma),\ \mathbf{q}_1 = \mathbf{q}(s)$ on a curve $\mathbf{q}$
$\mathbf{I}$	identity matrix in $\mathbb{R}^n$
$\angle(\mathbf{x}, \mathbf{y})$	the angle in $[0, \pi]$ between two non-zero vectors $\mathbf{x}$ and $\mathbf{y}$ in $\mathbb{R}^n$
S^n	unit sphere in $\mathbb{R}^{n+1}$, i.e. $S^n = \{\mathbf{x} \in \mathbb{R}^{n+1}; \lvert\mathbf{x}\rvert = 1\}$
c	a constant (following common practice, the symbol c will always denote a constant, but not necessarily always the same constant during a proof)
$C^k(I, \mathbb{R}^n)$	space of k times continuously differentiable functions from I to $\mathbb{R}^n$
$C^\infty(I, \mathbb{R}^n)$	space of functions from I to $\mathbb{R}^n$ continuously differentiable to any order
$C^{k,1}(I, \mathbb{R}^n)$	space of k times differentiable functions from I to $\mathbb{R}^n$, with the k-th derivative Lipschitz continuous
$K_{\mathbf{q}}$	Lipschitz constant of the curve $\mathbf{q}$
$\lVert\mathbf{q}\rVert_{C(I,\mathbb{R}^n)}$	maximum norm, i.e. $\lVert\mathbf{q}\rVert_{C(I,\mathbb{R}^n)} := \max_{s\in I} \lvert\mathbf{q}(s)\rvert$
$\lVert\mathbf{q}\rVert_{C^k(I,\mathbb{R}^n)}$	maximum norm in $C^k(I, \mathbb{R}^n)$ i.e. $\lVert\mathbf{q}\rVert_{C^k(I,\mathbb{R}^n)} := \sum_{i=0}^k \lVert\mathbf{q}^{(i)}\rVert_{C(I,\mathbb{R}^n)}$, where $\mathbf{q}^{(i)}$ is the i-th derivative of $\mathbf{q}$
$\lambda(\mathbf{q})$	length of the curve $\mathbf{q}$
$\rho, \mathbf{c}_{\text{oc}}$	radius and centre of the osculating circle
$\rho_{\text{os}}, \mathbf{c}_{\text{os}}$	radius and centre of the osculating sphere
$\mathcal{A}$	polar axis, cf. Definition 2.6

We will consider various functions f defined on points $\mathbf{q}(s)$ on a curve Γ. If the curve parameterisation is injective, for example for a simple curve parameterised by arc length, we may identify points $\mathbf{q}(s) \in \Gamma$ on the curve and the arguments $s \in I$. For convenience we may therefore unambiguously use $f(s)$ to stand for $f(\mathbf{q}(s))$, that is, we identify the two functions f and $f \circ \mathbf{q}$. We use the same identification for multi-argument functions.

pp, ppp, tp, pt, pppp, ppt, ptp, tpp, tt, cp, pc	various multi-point radius functions for line segment, circles and spheres, where the number of letter indicates, how many arguments the function has, and p stands for point (contact order zero), t for tangent (contact order one), and c for circle (contact of order two), cf. section 3.1
ρ_{pp}, ρ_{ppp}, ρ_{tp}, ρ_{pt}, ρ_{pppp}, ρ_{ppt}, ρ_{ptp}, ρ_{tpp}, ρ_{tt}, ρ_{cp}, ρ_{pc}	global radius of curvature functions of one argument, obtained from the multi-point radius functions by minimising over all but the first argument, cf. section 3.2

Chapter 1

Introduction

This thesis concerns the analysis, numerical analysis, and computation of self-avoiding curves in $\mathbb{R}^3$. In particular we propose and justify an efficient space discretization that can be exploited in computations involving self-avoiding space curves. Self-avoiding curves arise in several different contexts; for example, what is the longest rope of prescribed, uniform thickness that can be placed in a given container, or, in a more biological context, how is DNA packaged in phage heads? Such optimal packing problems share an underlying and fundamental, mathematical question: for each point on a given space curve Γ, what is the distance from self-intersection? We resolve this question analytically using extensions of the idea of *global radius of curvature* to characterise *thickness* of a given curve. We then consider the numerical analysis and convergence properties of the *biarc* discretization of space curves, and demonstrate that global curvature and thickness can be evaluated straightforwardly on biarc curves to a prescribed tolerance. Finally we use the biarc discretization in the computation of approximate solutions to the specific optimal packing problem of the *ideal shapes* of certain knots.

An overview of the classic, local, differential geometry of space curves is given in chapter 2.1. The classic way to quantify a self-avoidance distance of curves is the idea of *normal injectivity radius*. As is explained in section 2.2 the idea of normal injectivity radius is completely rigorous, but is not so straightforward to exploit in either analysis or computation. Recently an alternative characterisation of normal injectivity radius has been introduced in terms of *global radius of curvature* [18]. The global radius of curvature of a curve Γ involves the radii of circles passing through various sets of three points on the curve. The approach has already proven to be analytically useful; for example it has been exploited to demonstrate that, in a precise sense, any self-avoiding curve has at least $C^{1,1}$ regularity [20].

The primary motivation for this thesis was to develop ideas surrounding the notion of global radius of curvature in the analytical and computational study of ideal knot shapes. Informally, the ideal shape of a curve of prescribed length and knot type can be described as the configuration that is as far as possible from self-intersection. In addition to their intrinsic mathematical interest, ideal knot shapes have been extensively studied in physics and biology [57, 5]. For example there is an experimentally observed, but as yet unexplained, linear relation between the migration speed of knotted DNA molecules in gel-electrophoresis, and the writhe of computed ideal shapes of the corre-

sponding knot type [55, 62]. The ideal shape problem is defined precisely in section 2.3, and known results and prior computations are described. In the direction of analysis, the idea of global radius of curvature has already been exploited to show that ideal knot shapes exist in the space of $C^{1,1}$-curves [20, 6, 17]. Global radius of curvature has also been used in computations of ideal knot shapes [18] and other optimal packing problems for self-avoiding curves [31] that were based on piece-wise linear space discretizations. The primary contribution of this thesis is to demonstrate that the piece-wise linear discretization adopted in such computations can be replaced in a rigorous, but nevertheless efficient, way by the higher-order *biarc* space discretization whose $C^{1,1}$ regularity matches the minimal possible regularity of the underlying self-avoiding curve.

The original part of the presentation starts in chapter 3, where, in a generalisation of the particular global radius of curvature function introduced in [18], we study all thirteen possible multi-point circular and spherical distances defined on curves in terms of the radii of a circle or sphere that intersects the curve, respectively, three or four times, with appropriate account being taken of coalescent points and higher order contacts. We also characterise all distinct radius of curvature functions, which are defined through minimisation of a circular or spherical distance function over all but one of its arguments. Our conclusion is that it suffices to study only two global radius curvature functions $\rho_{\mathsf{pt}}(s) \equiv \min_\sigma \mathsf{pt}(s,\sigma)$ and $\rho_{\mathsf{tp}}(s) \equiv \min_\sigma \mathsf{pt}(\sigma,s)$ where the single, two-argument function $\mathsf{pt}(s,\sigma)$ is in turn defined as the radius of the unique circle passing through two points $\mathbf{q}(s)$ and $\mathbf{q}(\sigma)$ on the curve Γ and which shares the common tangent $\mathbf{q}'(\sigma)$. The properties of $\rho_{\mathsf{pt}}(s)$ and $\rho_{\mathsf{tp}}(s)$, and in particular the special properties of pairs of points $\mathbf{q}(s)$ and $\mathbf{q}(\sigma)$ at which either $\rho_{\mathsf{pt}}(s)$ or $\rho_{\mathsf{tp}}(s)$ are achieved, are described in 3.3. In 3.4 it is shown that the thickness, or normal injectivity radius, of the curve Γ can be characterised as the minimum of either of the global radius of curvature functions ρ_{pt} and ρ_{tp}. Our results are illustrated by application to simple, explicitly parametrised curves, specifically ellipses and helices which suffice to exhibit the range of possible phenomena.

It is of course of more interest to apply the theory of global radius of curvature functions to more complicated curves, and in particular to curves that are only known via numerical computation. Accordingly, chapters 4-6 are devoted to a comprehensive development of the theory of biarcs. Biarcs are special rational quadratic splines that can be used for Hermite interpolation. Their use has been developed in the Computer-Aided Design (CAD) literature [2, 54, 39, 35] with such pragmatic motivations as programming cutting [2, 38, 32] and milling [23, 40] machines, or approximating B-splines [37] and general NURBS [40], but we are unaware of a prior, comprehensive mathematical treatment. As will be explained in chapter 4, a pair of point-tangent data (in arbitrary dimension) can be interpolated by (a one parameter family of) two circular arcs assembled in a C^1 fashion. A biarc curve is made up of such pairs of circular arcs. Biarcs are both a natural, higher-order extension of piece-wise linear Lagrange interpolation, and a geometrically elementary, interpolant for Hermite point-tangent data. In particular biarcs have attractive properties such as simple closed form expressions for arc length and curvature.

We present a self-contained description of the geometrical construction of biarcs in

chapter 4. This material unites and extends results from the CAD literature. Additionally the geometry of biarcs on the tangent indicatrix sphere is introduced. Chapter 5 describes associated local convergence results and approximations of arc length, curvature, and torsion. And it is observed that biarcs have natural analogues of all the classical osculating objects for a space curve, namely the tangent line, the osculating circle and the osculating sphere.

Global convergence results are described in chapter 6, where the point-tangent data pairs are assumed to be sampled from a mesh on curves of various prescribed regularities. Convergence results at divers rates are derived in different norms dependent upon the differing assumed regularities of the underlying curve that is being approximated. Neither the local nor global convergence results depend upon the biarcs being of equal length, so that non uniform meshes are simply handled.

Chapter 7 demonstrates that biarc curves are a particularly attractive choice of space discretization for computations involving evaluation of curve thickness and global radius of curvature functions. For a piece-wise linear curve the thickness always vanishes because of the presence of corners at which the radius of curvature can be regarded as zero. To bypass this problem, the case of thickness being achieved by local curvature is usually ignored. This assumption is appropriate if thickness is known to be achieved globally, but in many problems this is not evident, and indeed the computations of chapter 8 suggest that local curvature is often active or extremely close to being active. Chapter 7 is devoted to the development of concise and efficient methods for the evaluation of thickness and the global radius of curvature function ρ_{pt} on *arc curves*, i.e. on $C^{1,1}$ curves assembled from circular arcs. (Biarc curves are therefore particular arc curves where there is a certain pairing between adjacent arcs that is induced by the underlying interpolation properties.) In particular we present an algorithm to compute an upper and lower bound of thickness of an arc curve up to an arbitrary prescribed precision.

In chapter 8 we turn to the specific problem of computation of ideal knot shapes. First, in 8.1 necessary conditions for smooth ideal shapes are described, and rigorous definitions of contact and μ-contact sets are given. Informally, the contact set is the set of pairs of points that realise the thickness of the curve. For a general curve, and in particular for a curve that is close to, but not precisely ideal, the contact set is likely to be a single pair of points. However the necessary conditions for ideal knot shapes imply that the contact set should be much larger, for example one or more curves of pairs of points. The μ-contact set is a way to quantify closeness to ideality via a construction of a set of pairs of points that are close to contact. The evaluation of ρ_{pt} allows another estimate of closeness to ideality. The ideas developed in 8.1 are then applied to biarc curve approximations of ideal shapes of 3.1 (trefoil) and 4.1 (figure eight) knots that were obtained as output from a simulated annealing code that was developed in collaboration with B. Laurie. The code implemented the biarc space discretization described in chapter 4 and the thickness evaluation algorithm described in chapter 7.1 as modifications to an existing code [26] that was previously based on a piecewise linear space discretization. Because the biarc curves are, by inspection, of the appropriate knot type, and lie in the $C^{1,1}$ regularity class in which an ideal shape is

known to exist, the computed shapes provide rigorous lower bounds for thickness of the ideal shape, independent of how they were found, with the only error being in the numerical evaluation of thickness and arc length. The values we find for thickness are the best published, but are not greatly different from previous computations based on piece-wise linear computations (improvements in the 4th digit). However, as already remarked and in contrast to the piece-wise linear approximation, our computations are true lower bounds independent of any discretization error. Moreover the improved accuracy provided by our biarc computations appears to have resolved the contact set of the trefoil, which has long been expected to have an extremely sensitive dependence on the computed knot shape, and previously unobserved features of the ideal shapes have been revealed.

The results of the thesis, possible generalisations, and suggestions for further work are discussed in chapter 9.

Chapter 2

Local and global properties of a space curve - classic results & overview

In this chapter we describe local properties of space curves that are well-known in the literature of differential geometry, and provide an overview of the ideas of ideal knot shapes and global radius of curvature. Using order of contact we define osculating plane, osculating circle and osculating sphere and study their interrelations. Section 2.2 is devoted to the notion of normal injectivity radius and its various characterisations, all of which are equivalent in the case of smooth curves. One motivation of this thesis is the study of ideal shapes of knots and links, together with the difficulties in computing them. Ideal knot shapes are explained in section 2.3.

2.1 Local circles and spheres - classic osculating objects

By a *curve* Γ we mean the image of a continuous three-dimensional vector function $\mathbf{q} \in C(I, \mathbb{R}^3)$, where $I \subset \mathbb{R}$ is a closed interval, i.e. $\Gamma = \mathbf{q}(I)$. We also use the notion of a *curve* to refer to the vector function $\mathbf{q}$ itself. We call a curve Γ a C^k-curve, when $\mathbf{q} \in C^k(I, \mathbb{R}^3)$. A C^1- curve Γ is parametrised by arc length when $|\mathbf{q}'(s)| = 1$ for all $s \in I$. In the C^1- case we distinguish *finite curves*, when $I = [0, L]$ is a closed finite interval, *semi-infinite curves*, when $I = [0, \infty)$, and *infinite curves*, when I is the the real axis $I = \mathbb{R}$. A curve Γ is *smooth* if the function $\mathbf{q}$ is continuously differentiable to any order and if the tangent vector $\mathbf{q}'(s)$ is nonzero for all $s \in I$. In the smooth case, after reparametrisation if necessary, we interpret s as the arc length parameter. A finite curve Γ is *closed* if $\mathbf{q}(L) = \mathbf{q}(0)$. Moreover, if Γ is smoothly closed, the derivatives of all orders of $\mathbf{q}(s)$ agree at $s = 0$ and $s = L$. Finally, a curve Γ is *simple* if it has no self-intersection, that is $\mathbf{q}(s_1) = \mathbf{q}(s_2)$ only when $s_1 = s_2$.

Definition 2.1 *For an arc-length parametrised curve $\mathbf{q} \in C^3(I, \mathbb{R}^3)$, and for $s \in I$ with $|\mathbf{q}''(s)| \neq 0$, the orthonormal Frenet frame of tangent, principal normal and binormal*

$\{\mathbf{t}(s), \mathbf{n}(s), \mathbf{b}(s)\}$ *at* s *is given by*

$$\begin{aligned} \mathbf{t}(s) &:= \mathbf{q}'(s), \\ \mathbf{n}(s) &:= \frac{\mathbf{q}''(s)}{|\mathbf{q}''(s)|}, \\ \mathbf{b}(s) &:= \mathbf{t}(s) \times \mathbf{n}(s). \end{aligned}$$

We denote the standard local curvature and torsion of $\mathbf{q}$ *at* s *by* $\kappa(s)$ *and* $\tau(s)$*; they are given by the relations*

$$\begin{aligned} \kappa(s) &:= |\mathbf{q}''(s)|, \\ \mathbf{b}'(s) &= -\tau(s)\mathbf{n}(s). \end{aligned}$$

The Frenet frame satisfies the *Serret-Frenet formulæ*:

$$\begin{aligned} \mathbf{t}'(s) &= \kappa(s)\mathbf{n}(s), \\ \mathbf{n}'(s) &= -\kappa(s)\mathbf{t}(s) + \tau(s)\mathbf{b}(s), \\ \mathbf{b}'(s) &= -\tau(s)\mathbf{n}(s). \end{aligned}$$

The local behaviour of a curve Γ at a point $\mathbf{q}(s)$ can be described in terms of various osculating or tangent objects [21, pp. 26, 28, 32, 72], [59, pp. 10, 14, 25]: the tangent line $\mathcal{L}(s)$, osculating plane $\mathcal{P}(s)$, circle $\mathcal{C}(s)$, and sphere $\mathcal{S}(s)$, and the circumsphere $\mathcal{S}^c(s)$. All but the last are standard objects in the differential geometry of curves. We first define the notion of *order of contact*, cf. [59, p. 23][9, p. 171], in terms of which we will define the osculating objects.

Definition 2.2 *For a curve* Γ *given by* $\mathbf{q} \in C^k(I, \mathbb{R}^3)$*, with* $k \in \mathbb{N}$*:*

1. *Let* $\mathbf{f}(\mathbf{x}) = 0$ *be the equation of a surface* Σ*, with* $\mathbf{f} \in C^k(\mathbb{R}^3, \mathbb{R})$*. Then the curve* Γ *is said to have* contact of order k *with the surface* Σ *at* $\mathbf{q}(s)$ *if*

$$\frac{d^i}{ds^i}(\mathbf{f} \circ \mathbf{q})(s) = 0, \quad \text{for } i = 0, \ldots, k. \tag{2.1}$$

2. *Let* $\mathbf{f}_1(\mathbf{x}) = 0$ *and* $\mathbf{f}_2(\mathbf{x}) = 0$ *be the equations defining a curve* Υ*. The curve* Γ *is said to have* contact of order k *with the curve* Υ *at* $\mathbf{q}(s)$ *if*

$$\frac{d^i}{ds^i}(\mathbf{f}_j \circ \mathbf{q})(s) = 0, \quad \text{for } i = 0, \ldots, k, \quad \text{and for } j = 1, 2. \tag{2.2}$$

The Taylor expansion for $\mathbf{f} \circ \mathbf{q}$ reveals that condition (2.1) is equivalent to $\mathbf{f}(\mathbf{q}(s+h)) = o(h^k)$. Equivalently, a surface $\mathbf{f}(\mathbf{x}) = 0$ passing through $k+1$ coalescent points on the curve Γ has contact of order k (Rolle's Theorem cf. [59, p. 10]).

Remark and Definition 2.3 *For an arc-length parametrised curve* $\mathbf{q} \in C^3(I, \mathbb{R}^3)$ *and* $s \in I$*:*

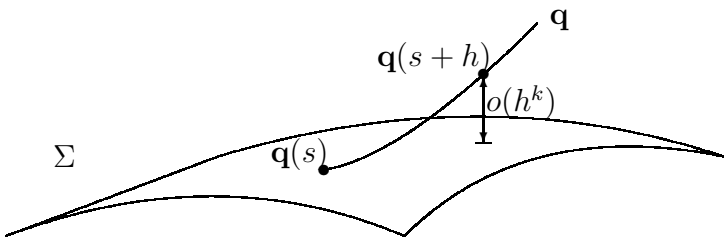

Figure 2.1: Illustration of order of contact k of a curve $\mathbf{q}$ with a surface Σ.

1. *There exists a unique straight line $\mathcal{L}(s)$ that has contact of order one with Γ at $\mathbf{q}(s)$. This line $\mathcal{L}(s)$ is called the* tangent line *at $\mathbf{q}(s)$; it is the line through $\mathbf{q}(s)$ spanned by $\mathbf{t}(s)$.*

2. *When $\kappa(s) \neq 0$, there exists a unique plane $\mathcal{P}(s)$ that has contact of order two with the curve Γ at $\mathbf{q}(s)$. This plane is called the* osculating plane *$\mathcal{P}(s)$ at $\mathbf{q}(s)$; it is the plane through $\mathbf{q}(s)$ spanned by the tangent and principal normal $\{\mathbf{t}(s), \mathbf{n}(s)\}$.*

3. *When $\kappa(s) \neq 0$, there exists a unique circle $\mathcal{C}(s)$ that has contact of order two with the curve Γ at $\mathbf{q}(s)$. This circle is called the* osculating circle *$\mathcal{C}(s)$ at $\mathbf{q}(s)$; it is the circle contained in the osculating plane $\mathcal{P}(s)$ with centre*

$$\mathbf{c}_{\text{oc}}(s) = \mathbf{q}(s) + \rho(s)\mathbf{n}(s), \tag{2.3}$$

and radius

$$\rho(s) = \frac{1}{\kappa(s)}, \tag{2.4}$$

i.e. $\rho(s)$ is the standard local radius of curvature.

4. *When both $\kappa(s) \neq 0$ and $\tau(s) \neq 0$, there exists a unique sphere that has contact of order three with the curve Γ at $\mathbf{q}(s)$. This sphere is called the* osculating sphere *$\mathcal{S}(s)$ at $\mathbf{q}(s)$; it is the sphere through four coalescent points [59, p. 25] and is centred at*

$$\mathbf{c}_{\text{os}}(s) = \mathbf{q}(s) + \rho(s)\mathbf{n}(s) + \frac{\rho'(s)}{\tau(s)}\mathbf{b}(s), \tag{2.5}$$

with radius

$$\rho_{\text{os}}(s) = \sqrt{\rho^2(s) + \left(\frac{\rho'(s)}{\tau(s)}\right)^2}. \tag{2.6}$$

Proof

1. To find the line $\mathcal{L}(s)$ write the two equations $\mathbf{f}_1(\mathbf{x}) := \mathbf{x} \cdot \mathbf{p}_1 - a_1 = 0$ and $\mathbf{f}_2(\mathbf{x}) := \mathbf{x} \cdot \mathbf{p}_2 - a_2 = 0$ with $\mathbf{p}_1 \neq \mathbf{p}_2$ and $\mathbf{p}_1,\ \mathbf{p}_2 \in \mathbb{R}^3$ and $a_1,\ a_2 \in \mathbb{R}$. Solving the equations in (2.2) for $i = 0, 1$ and $j = 1, 2$ yields the result.

2. The general equation of a plane is $\mathbf{f}(\mathbf{x}) := \mathbf{x} \cdot \mathbf{p} - a = 0$ for some $\mathbf{p} \in \mathbb{R}^3$ and $a \in \mathbb{R}$. Solving equations (2.1) for $i = 0, 1, 2$ yields the equation $\mathbf{f}(\mathbf{x}) = \mathbf{x} \cdot \mathbf{b}(s) - \mathbf{q}(s) \cdot \mathbf{b}(s) = 0$, that is, there is only one osculating plane and it is the plane passing through $\mathbf{q}(s)$ perpendicular to $\mathbf{b}(s)$.

3. The general equation of a circle is $\mathbf{f}_1(\mathbf{x}) := \mathbf{x} \cdot \mathbf{p} - a = 0$ and $\mathbf{f}_2(\mathbf{x}) := (\mathbf{x} - \mathbf{c}) \cdot (\mathbf{x} - \mathbf{c}) - r = 0$ for some $\mathbf{p}, \mathbf{c} \in \mathbb{R}^3$ and $a, r \in \mathbb{R}$. Solving equations (2.2) for $i = 0, 1, 2$ and $j = 1$ yields that the circle lies in the osculating plane. Solving equations (2.2) for $i = 0, 1, 2$ and $j = 2$ yields the equations $(\mathbf{q}(s) - \mathbf{c}) \cdot (\mathbf{q}(s) - \mathbf{c}) - r = 0$, $\mathbf{t}(s) \cdot (\mathbf{q}(s) - \mathbf{c}) = 0$ and $1 + \kappa(s)\mathbf{n}(s) \cdot (\mathbf{q}(s) - \mathbf{c}) = 0$, and we find (2.3) and (2.4).

4. The osculating sphere must satisfy (2.1) for $i = 0, 1, 2, 3$ with $\mathbf{f}(\mathbf{x}) := (\mathbf{x} - \mathbf{c}) \cdot (\mathbf{x} - \mathbf{c}) - r = 0$ for some $\mathbf{c} \in \mathbb{R}^3$ and $r \in \mathbb{R}$. As in the previous cases, these four equations have a unique solution given by (2.5) and (2.6).

■

We will also make use of another locally-defined sphere, which we call the *osculating circumsphere*, denoted by $\mathcal{S}^c(s)$, that, for $\kappa(s) \neq 0$, is defined to be the unique sphere of radius $\rho(s)$ that contains the osculating circle $\mathcal{C}(s)$ as a great circle. The osculating circle is always contained in the intersection of the osculating sphere and osculating circumsphere, and, in general, it is all of the intersection because (2.6) reveals that typically $\rho_{os}(s) > \rho(s)$. More precisely, at each point $\mathbf{q}(s)$ on a curve Γ the osculating plane $\mathcal{P}(s)$, circle $\mathcal{C}(s)$, sphere $\mathcal{S}(s)$ and circumsphere $\mathcal{S}^c(s)$ enjoy the following relationships:

$$\begin{aligned}
&\mathcal{C}(s) = \mathcal{P}(s) \cap \mathcal{S}(s), && \kappa(s) \neq 0,\ \tau(s) \neq 0,\\
&\mathcal{C}(s) = \mathcal{P}(s) \cap \mathcal{S}^c(s), && \kappa(s) \neq 0,\\
&\mathcal{C}(s) = \mathcal{S}(s) \cap \mathcal{S}^c(s), && \kappa(s) \neq 0,\ \kappa'(s) \neq 0,\ \tau(s) \neq 0.
\end{aligned}$$

The degenerate cases excluded above can be handled as follows.

Remark 2.4 *For an arc-length parametrised curve $\mathbf{q} \in C^3(I, \mathbb{R}^3)$ and $s \in I$:*

1. *When $\kappa(s) = 0$, the tangent line $\mathcal{L}(s)$ has order of contact two with the curve, we may set $\rho(s) = \infty$, and identify the osculating circle with the tangent line,*

$$\mathcal{C}(s) = \mathcal{L}(s), \qquad \text{for } \kappa(s) = 0.$$

The osculating plane, sphere and circumsphere may or may not be uniquely defined dependent upon the limiting behaviour of κ and τ near s. In all cases it is consistent to set $\rho_{\text{os}}(s) = \infty$, since any limit of (2.6) must be infinite, hence

$$\rho(s) \leq \rho_{\text{os}}(s), \qquad \text{for any } \kappa(s) \text{ and } \tau(s).$$

2. *When $\kappa(s) \neq 0$, $\tau(s) = 0$ and $\kappa'(s) \neq 0$, the only osculating sphere is the osculating plane, which then has contact of order three.*

When $\kappa(s) \neq 0$, $\tau(s) = 0$ and $\kappa'(s) = 0$, then every sphere passing through the osculating circle is an osculating sphere, i.e. has order of contact three. The radii

vary from $\rho(s)$ to ∞, the osculating plane is then a special osculating sphere and has contact of order three. One of these osculating spheres is the sphere with the highest order of contact (in [21, p. 72] this is defined to be the osculating sphere).

Thus, when $\kappa(s) \neq 0$, but $\tau(s) = 0$, the osculating sphere may or may not be uniquely defined depending on the limiting behaviour of κ' near s. Following the contact-order arguments in [21, p. 72] we set

$$\mathcal{S}(s) = \begin{cases} \mathcal{P}(s), & \text{if } \lim_{\sigma\to s} \rho'(\sigma)/\tau(\sigma) \text{ is infinite} \\ \lim_{\sigma\to s} \mathcal{S}(\sigma), & \text{if } \lim_{\sigma\to s} \rho'(\sigma)/\tau(\sigma) \text{ is finite} \\ \mathcal{S}^c(s), & \text{if } \lim_{\sigma\to s} \rho'(\sigma)/\tau(\sigma) \text{ is undefined.} \end{cases}$$

The problematic last case occurs, for example, when Γ is itself a circle. It could be handled differently; for example the osculating sphere of a circle is explicitly left undefined in [21, p. 74].

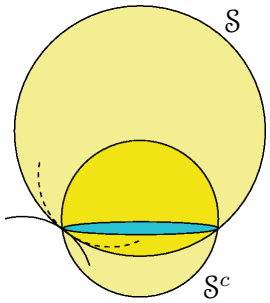

Figure 2.2: Geometric interpretation of the Taylor expansions (2.7) and (2.8). The spheres $\mathcal{S}$ and $\mathcal{S}^c$ intersect on the osculating circle $\mathcal{C}$, and thereby define four spherical quadrants, corresponding to the intersections of the interiors and exteriors of the two spheres. Locally and generically, a curve lies either outside (solid curve) or inside (dashed curve) the (larger) osculating sphere $\mathcal{S}$, whereas it crosses the (smaller) osculating circumsphere $\mathcal{S}^c$, i.e. the curve passes between the four spherical quadrants in a highly constrained way.

While Γ is tangent to both the osculating sphere $\mathcal{S}$ and circumsphere $\mathcal{S}^c$, whenever $\kappa \neq 0 \neq \tau$ we find that, generically and locally, Γ pierces or crosses $\mathcal{S}^c$, but lies on one or other side of the sphere $\mathcal{S}$, as illustrated in Figure 2.2. More precisely:

Remark 2.5 *For an arc-length parametrised curve $\mathbf{q} \in C^\infty(I, \mathbb{R}^3)$ and $s \in I$ with $\kappa(s) \neq 0$:*

1. *When $\kappa'(s) \neq 0$, then the curve Γ locally pierces or crosses $\mathcal{S}^c(s)$. When $\kappa'(s) = 0$ and $\tau^2(s) < \frac{\kappa''(s)}{\kappa(s)}$ both sides are locally inside, and when $\kappa'(s) = 0$ and $\tau^2(s) > \frac{\kappa''(s)}{\kappa(s)}$ both sides are locally outside the circumsphere $\mathcal{S}^c(s)$.*

2. *When $\tau(s) \neq 0$, both sides of the curve Γ are locally inside or outside the osculating sphere $\mathcal{S}$ as $\frac{\tau^2(s)}{2} - \frac{\kappa''(s)}{2\kappa(s)} + \frac{\kappa'^2(s)}{\kappa^2(s)} + \frac{\kappa'(s)\tau'(s)}{2\tau(s)\kappa(s)}$ is negative or positive.*

Proof For $\mathcal{S}^c(s)$ this conclusion follows from the h^3 coefficient in the Taylor expansion

$$|\mathbf{q}(s+h) - \mathbf{c}_{\rm oc}(s)|^2 = \frac{1}{\kappa^2} - \Big(\frac{\kappa'}{3\kappa}\Big)h^3 + \Big(\frac{\tau^2}{12} - \frac{\kappa''}{12\kappa}\Big)h^4 + O(h^5), \tag{2.7}$$

while the result for $\mathcal{S}(s)$ follows from the h^4 coefficient in the Taylor expansion

$$\begin{aligned}|\mathbf{q}(s+h) - \mathbf{c}_{\rm os}(s)|^2 = \frac{1}{\kappa^2} + \frac{\kappa'^2}{\tau^2\kappa^4} \\ + \Big(\frac{\tau^2}{12} - \frac{\kappa''}{12\kappa} + \frac{\kappa'^2}{6\kappa^2} + \frac{\kappa'\tau'}{12\tau\kappa}\Big)h^4 + O(h^5).\end{aligned} \tag{2.8}$$

■

Definition 2.6 *For an arc-length parametrised curve $\mathbf{q} \in C^3(I, \mathbb{R}^3)$ and for $s \in I$ with $\kappa(s) \neq 0$, the* polar axis $\mathcal{A}(s)$ *at s [59, p. 25] is the line passing through the centre of curvature $\mathbf{c}_{\rm oc}(s)$ parallel to the binormal $\mathbf{b}(s)$:*

$$\mathcal{A}(s) = \{\mathbf{q}(s) + \rho(s)\mathbf{n}(s) + \lambda\mathbf{b}(s);\ \lambda \in \mathbb{R}\}.$$

The polar axis is called the polar line in [21, p. 71].

The osculating circumsphere $\mathcal{S}^c(s)$ is not special in the sense that the curve Γ locally pierces or crosses $\mathcal{S}^c(s)$. In fact, generically, it is precisely all spheres, except for the osculating sphere $\mathcal{S}(s)$, with centres on the *polar axis* at s that have this crossing property.

Remark 2.7 *For an arc-length parametrised curve $\mathbf{q} \in C^3(I, \mathbb{R}^3)$ and for $s \in I$ consider all spheres passing through $\mathbf{q}(s)$, tangent to $\mathbf{q}'(s)$ at $\mathbf{q}(s)$, that are locally crossed by the curve Γ at $\mathbf{q}(s)$.*

1. *When $\kappa(s) \neq 0$ and $\tau(s) \neq 0$, the locus of centres of all such spheres is the polar axis $\mathcal{A}(s)$ punctured at $\mathbf{c}_{\rm os}(s)$, the centre of the osculating sphere.*
2. *When $\kappa(s) \neq 0$, $\tau(s) = 0$ and $\kappa'(s) \neq 0$, the locus of centres of all such spheres is the polar axis $\mathcal{A}(s)$.*

Proof The centre $\mathbf{c}$ of a sphere $\mathcal{S}$ passing through $\mathbf{q}(s)$ and tangent to $\mathbf{q}'(s)$ at $\mathbf{q}(s)$ lies in the normal plane,

$$\mathbf{c} = \mathbf{q}(s) + \mu\mathbf{n}(s) + \lambda\mathbf{b}(s),$$

for some μ, $\lambda \in \mathbb{R}$. The Taylor expansion

$$|\mathbf{q}(s+h) - \mathbf{c}|^2 = \mu^2 + \lambda^2 + \big(1 - \kappa(s)\mu\big)h^2 - \frac{1}{3}\big(\kappa(s)\tau(s)\lambda + \kappa'(s)\mu\big)h^3 + o(h^3),$$

shows that the curve Γ locally crosses the sphere $\mathcal{S}$ at $\mathbf{q}(s)$ only when the h^2 coefficient is zero and actually will cross if further the h^3 coefficient is non-zero, i.e. if $\kappa(s) \neq 0$ and $\tau(s) \neq 0$ whenever $\mu = \rho(s)$ and $\lambda \neq \frac{-\kappa'(s)}{\kappa^2(s)\tau(s)}$, and if $\kappa(s) \neq 0$, $\tau(s) = 0$ and $\kappa'(s) \neq 0$ whenever $\mu = \rho(s)$ and $\lambda \in \mathbb{R}$. ■

2.2 Thickness of closed or infinite curves

A measure of the distance from self-intersection of a space curve Γ is given by the *normal injectivity radius*, as treated for example in [10, p. 271] for complete Riemannian manifolds. In the specific case of C^1 curves, normal injectivity radius can be defined as follows [29].

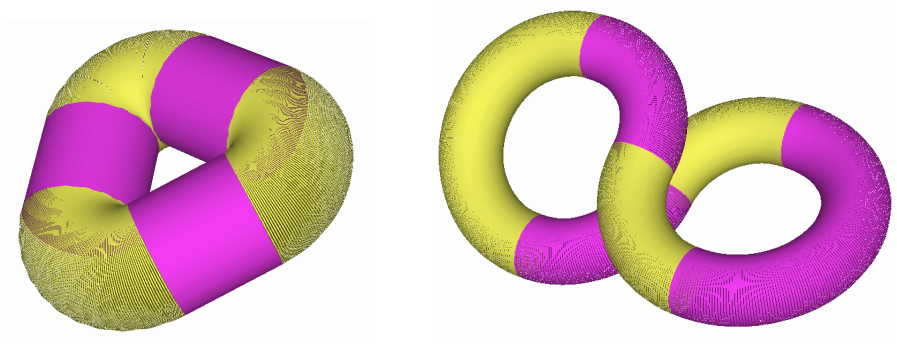

(a) (b)

Figure 2.3: Two curves surrounded by tubular surfaces with radius equal to the actual thicknesses, cf. Proposition 7.2 and equality (2.12). Thickness can be achieved by either (a) the smallest local radius of curvature, as in this planar $C^{1,1}$ curve made up of three circular arcs and three straight lines, or (b) half of the double critical distance as in this $C^{1,1}$ curve made up of six circular arcs.

Let $\mathbf{q}$ be a simple, closed or infinite, C^1-curve parametrised by arc length. Define the normal bundle E of the curve $\mathbf{q}$ by

$$E := \{(\mathbf{q}(s), \mathbf{v}) \in \mathbf{q}(I) \times \mathbb{R}^3; \mathbf{q}'(s) \cdot \mathbf{v} = 0\}, \tag{2.9}$$

and the exponential map

$$exp : E \to \mathbb{R}^3, \qquad exp(\mathbf{x}, \mathbf{v}) := \mathbf{x} + \mathbf{v}.$$

Denote for $r \geq 0$

$$E_r := \{(\mathbf{x}, \mathbf{v}) \in E;\ |\mathbf{v}| \leq r\}.$$

Then the normal injectivity radius $\Delta[\mathbf{q}]$ is defined by

$$\Delta[\mathbf{q}] := \sup\{r \geq 0;\ exp \text{ is injective on } E_r\}. \tag{2.10}$$

By this construction, for any two distinct points $\mathbf{q}(s)$ and $\mathbf{q}(\sigma)$, and for any $0 < r < \Delta[\mathbf{q}]$, the two disks of radius r centred at $\mathbf{q}(s)$ and $\mathbf{q}(\sigma)$ lying in the respective normal planes do not intersect. Intuitively the normal injectivity radius Δ is the radius of the largest tube that can be put around the curve such that the surface of the tube is smooth and such that it does not intersect itself, cf. figure 2.3. Due to this geometrical construction the normal injectivity radius of a curve will here be called its *thickness*.

In [29] it was shown that for $\mathbf{q} \in C^2$ the thickness of a curve is governed by two numbers: the minimal radius of curvature and half of the minimal distance between *double critical points* or *points of stationary approach*, i.e. pairs of distinct points $\mathbf{q}(s)$ and $\mathbf{q}(\sigma)$ and associated curve tangents $\mathbf{q}'(s)$ and $\mathbf{q}'(\sigma)$ satisfying

$$\mathbf{q}'(s) \cdot (\mathbf{q}(s) - \mathbf{q}(\sigma)) = \mathbf{q}'(\sigma) \cdot (\mathbf{q}(s) - \mathbf{q}(\sigma)) = 0. \tag{2.11}$$

More precisely, if we denote by dc the set of arguments $(s, \sigma) \in I \times I$ with $s \neq \sigma$ that satisfy (2.11), then [29]

$$\Delta[\mathbf{q}] = \min \left\{ \min_{s \in I} \rho(s), \tfrac{1}{2} \min_{(s,t) \in dc} |\mathbf{q}(s) - \mathbf{q}(t)| \right\}. \tag{2.12}$$

Furthermore, instead of considering only double critical points, the *single critical points*, i.e. pairs of distinct points $\mathbf{q}(s)$ and $\mathbf{q}(\sigma)$ and associated curve tangents $\mathbf{q}'(s)$ and $\mathbf{q}'(\sigma)$ satisfying

$$\mathbf{q}'(s) \cdot (\mathbf{q}(s) - \mathbf{q}(\sigma)) = 0, \tag{2.13}$$

may be considered. Thickness may also be characterised using these single critical points [29]

$$\Delta[\mathbf{q}] = \min \left\{ \min_{s \in I} \rho(s), \tfrac{1}{2} \min_{(s,t) \in sc} |\mathbf{q}(s) - \mathbf{q}(t)| \right\}, \tag{2.14}$$

where sc denotes the set of arguments $(s, \sigma) \in I \times I$ with $s \neq \sigma$ that satisfy (2.13).

Another approach to characterise thickness was presented in [18] in terms of *global radius of curvature*. The global radius of curvature of a continuous curve $\mathbf{q}$ at $s \in I$ is defined by

$$\rho_g(s) := \inf_{\substack{\sigma, t \in I \\ s \neq \sigma \neq t \neq s}} \mathsf{ppp}(s, \sigma, t), \qquad s \in I, \tag{2.15}$$

where $\mathsf{ppp}(s, \sigma, t)$ denotes the radius of the circle passing through the three points $\mathbf{q}(s)$, $\mathbf{q}(\sigma)$, and $\mathbf{q}(t)$. When the curve $\mathbf{q}$ is simple and smooth, the function ρ_g is continuous and $0 \leq \rho_g(s) \leq \rho(s)$ for all $s \in I$. If a curve Γ has a point with $\rho_g(s) = \infty$, then it is a straight line, in which case the global radius of curvature function is infinite at all points. Moreover, the global radius of curvature function $\rho_g(s)$ at s is achieved either by the local radius of curvature $\rho(s)$, or by a circle passing through $\mathbf{q}(s)$ and some distinct point $\mathbf{q}(\sigma)$ at which the circle is tangent, so that to evaluate $\rho_g(s)$ it suffices to consider the minimisation (2.15) with the restriction $\sigma = t$ [18].

For a continuous curve $\mathbf{q}$ the functional Δ_g was defined [18] by

$$\Delta_g[\mathbf{q}] := \inf_{s \in I} \rho_g(s) = \inf_{\substack{s, \sigma, t \in I \\ s \neq \sigma \neq t \neq s}} \mathsf{ppp}(s, \sigma, t), \tag{2.16}$$

and it was shown that for a simple, smooth curve $\mathbf{q}$

$$\Delta_g[\mathbf{q}] = \Delta[\mathbf{q}]. \tag{2.17}$$

In the smooth case, the infima in (2.15) and (2.16) can be replaced by minima, and the thickness is simply the smallest radius of a circle passing through three points on Γ, where distinct points may be replaced by a higher order of contact at one point.

The description of $\Delta[\mathbf{q}]$ using the global radius of curvature function is analytically attractive because it is explicit and because it simultaneously captures both possibilities manifested in (2.12) and (2.14): that the thickness is achieved by a local radius of curvature or that it is achieved by half of a critical self-distance. This characterisation also offers a way to extend the definition of thickness to continuous, simple curves.

In [20] the functional $\Delta_g[\mathbf{q}]$ was considered for arc-length parametrised, closed $C^{0,1}$-curves. It was shown that for such curves having an additional lower bound on thickness $\Delta_g[\mathbf{q}] \geq \theta > 0$, the curve is differentiable and the tangent curve is Lipschitz continuous with Lipschitz constant $K_{\mathbf{q}'} \leq \theta^{-1}$. In other words, closed, arc-length parametrised, Lipschitz continuous curves with positive thickness, are actually $C^{1,1}$-curves, and therefore the curvature exists almost everywhere.

2.3 Ideal knot shapes

Ideal shapes of knots are certain configurations that maximise thickness in a sense to be made precise below. First we need certain basic notions of knot theory. Further details can be found in classic books such as [49, 4].

Definition 2.8 *1. A* knot *or* knot shape $\mathcal{K} \subset \mathbb{R}^3$ *is the image of a closed, non-self-intersecting, continuous curve* $\mathbf{q}$ *in* $\mathbb{R}^3$.

2. A link $\mathcal{L} \subset \mathbb{R}^3$ *is the union of a finite number of pairwise disjoint knots,* $\mathcal{L} = \mathcal{K}_1 \cup \cdots \cup \mathcal{K}_m$. *A knot is a special case of a link.*

3. An ambient isotopy *is a continuous map* $h : \mathbb{R}^3 \times [0,1] \to \mathbb{R}^3$ *with* $h(\cdot, 0) = id_{\mathbb{R}^3}$ *and* $h(\cdot, t)$ *a homeomorphism for all* $t \in [0,1]$.

4. Two knots $\mathcal{K}_1$ *and* $\mathcal{K}_2$ *are* ambient isotopic *(notation:* $\mathcal{K}_1 \simeq \mathcal{K}_2$*) if an ambient isotopy* $h : \mathbb{R}^3 \times [0,1] \to \mathbb{R}^3$ *exists with* $h(\mathcal{K}_1, 1) = \mathcal{K}_2$.

Two knots are ambient isotopic if one knot can be continuously transformed onto the other. Being ambient isotopic is an equivalence relation which splits the set of all knots into *isotopy classes*. We denote the isotopy class of a knot $\mathcal{K}$ by $[\mathcal{K}]$, i.e. $\mathcal{K} \in [\mathcal{K}^*]$, if $\mathcal{K} \simeq \mathcal{K}^*$.

Definition 2.9 *An* ideal shape $\mathcal{K}$ *[3, 25, 57] of the isotopy class* $[\mathcal{K}^*]$ *is a knot shape* $\mathcal{K}$ *that minimises the functional length/thickness within the isotopy class* $[\mathcal{K}^*]$, *i.e. an ideal shape is a solution of*

$$\frac{\lambda(\mathcal{K})}{\Delta[\mathcal{K}]} \to \min!$$

subject to $\mathcal{K} \in C(S^1, \mathbb{R}^3), \mathcal{K} \simeq \mathcal{K}^*$. *The positive number* $\frac{\lambda(\mathcal{K})}{\Delta[\mathcal{K}]}$ *is called the* rope length $(\lambda/\Delta)[\mathcal{K}]$ *of the knot* $\mathcal{K}$.

The notion of isotopy class and ideal shape can be extended to links in a straightforward way. Note that rope length is a scale invariant number.

It has been proven [20, 6, 17] that ideal shapes exist in the space of $C^{1,1}$-curves, and that the global radius of curvature function ρ_g on an ideal shape is constant on smooth curved segments [18, p. 4771]. For a point $\mathbf{q}(s)$ on an ideal shape, at which the local curvature is not active, i.e. where $\rho_g(s)$ is only achieved by a circle that is tangent at a distinct point $\mathbf{q}(\sigma)$, the principal normal is in the cone of the contact chords [52]. The investigation of the analytic properties of ideal shapes continues to be an active area [51, 11, 12].

Although the problem is easy to state, the only known ideal knot shape is the circle for the trivial knot. For links, several ideal shapes are analytically known with generalisations to families of chain-like links [6] showing that, in general, ideal shapes are not unique and have no better regularity than $C^{1,1}$.

Several groups performed computations using either a sequence of points to approximate a curve or a piece-wise linear curve discretization, divers definitions of thickness and various minimisation methods both for closed knots and links [25, 56, 41, 26, 45, 48, 18, 31] and open knots [43, 8]. In [25] a Monte Carlo method was carried out on a sequence of points, while [41] used a curve shortening on a sequence of points. The step from a point to a continuous discretization was accomplished by [26] who performed simulated annealing computations with a piece-wise linear curve discretization. All these computations produce very satisfactory approximations of rope length to three or four significant digits. However, with the notable exception of [45], no error estimate between the discrete and the underlying continuous problem is given. This is mainly for two reasons: First, the point or piece-wise linear discretization does not match the known minimal $C^{1,1}$ regularity of the solution. The other significant issue is that closed piece-wise linear curves always have thickness zero because they have corners. Therefore some number of neighbouring points or line segments must be ignored. But the number of neighbours to be excluded is not clear. For instance, when computing the thickness of the ideal unknot, i.e. the circle, the number of excluded neighbours dominates the computation of thickness until all but the diametrically opposite point or line segment is excluded. Rigorous error estimates of the rope length of a piece-wise linear curve were given by Rawdon [45, 46, 47], who bypasses both problems by inscribing arcs of circles to the corners of a piece-wise linear curve. Another approach to circumvent the problem of the local case of thickness was introduced in [18] with the global radius of curvature for smooth curves. It was also shown that there is a version of global radius of curvature appropriate for a point discretization, which was later adopted in [31]. The earlier point discretization ideal shape computations in [25, 55, 56] did not satisfy the necessary condition of constancy of the discrete global radius of curvature function ρ_g to a reasonable accuracy, essentially because of the difficulties with ruling out nearest neighbours, and in [18] a local discretized curve shortening algorithm was applied to obtain improved shapes which did satisfy the necessary condition of a constant global radius of curvature function ρ_g. However, as we shall see in chapter 8, this approach in turn missed features related to local curvature that appear to be robust in our computations using the biarc discretization. The first consideration of a contact set for the ideal trefoil was

introduced in [18] by visualising the diameters of all circles realising $\Delta_g[\mathbf{q}]$ to a rather small tolerance. This computation indicated that the results are very sensitive to error in shape. Subsequently, the series of three articles [41, 42, 44] concluded that the contact set of the ideal trefoil is still unresolved. Our approach combines the idea of global radius of curvature with a $C^{1,1}$ space discretization, the *biarcs*. We therefore handle the local case of thickness in a simple way and compute in the right class, but in contrast to [45, 46, 47] where the data format is piece-wise linear, the biarc-discretization provides higher convergence rates from the discretized to the underlying continuous problem.

Chapter 3

Local and global properties of a space curve

In the study of ideal knot shapes, as explained in sections 2.2 and 2.3, it has recently proven useful to consider a global radius of curvature of the curve at $\mathbf{q}(s)$ defined as the smallest possible radius amongst all circles passing through this point and any two other points on the curve, coalescent or not. In particular, the minimum value of the global radius of curvature gives a convenient measure of curve thickness. Given the utility of the construction inherent to global curvature, it is also natural to consider variants of global radii of curvature defined in related ways involving circles and spheres intersecting the given curve. Then single argument, global radius of curvature functions can be constructed by minimising over all but one argument. In sections 3.1 and 3.2 we describe the interrelations between all possible global radius of curvature functions of this type, and show that there are two of particular interest. Properties of the divers global radius of curvature functions are illustrated with the simple examples of ellipses and helices, including certain critical helices that arise in the optimal shapes of compact filaments, in α-helical proteins, and in B-form DNA.

3.1 Global circles and spheres

Just as the local behaviour of a curve can be described in terms of local osculating lines, circles and spheres, aspects of the global behaviour of a curve can be described by analogous multi-point objects: two-point line segments $\mathcal{L}(s,t)$, three-point circles $\mathcal{C}(s,t,\sigma)$ and four-point spheres $\mathcal{S}(s,t,\sigma,\tau)$. Here we study these objects and use them to introduce various generalised global radius of curvature functions for curves.

Hypothesis 3.1 *Throughout this chapter and unless explicit mention to the contrary is made, all curves will be assumed to be parametrised by arc length, and to be simple, smooth, and either (a) finite and closed, or (b) infinite with the property that* $|\mathbf{q}(s)| \to \infty$ *as* $|s| \to \infty$. *For the sake of simplicity, in this chapter we shall give full consideration only to generic sets of points (and coalescent limits thereof) on smooth curves, so that sets of three points are assumed non-collinear sets of four points non-coplanar, and*

so on. We shall implicitly assume throughout that the infima of various functionals considered in this chapter are attained at finite points $\mathbf{q}(s)$ *on the curve.*

3.1.1 Definitions

Let Γ be a simple curve. Then for any two distinct points $\mathbf{q}(s)$ and $\mathbf{q}(t)$ we define $\mathcal{L}(s,t)$ to be the unique line segment between them with half-length

$$\mathsf{pp}(s,t) = \frac{1}{2}|\mathbf{q}(s) - \mathbf{q}(t)|. \tag{3.1}$$

For any three non-collinear points $\mathbf{q}(s)$, $\mathbf{q}(t)$ and $\mathbf{q}(\sigma)$ we define $\mathcal{C}(s,t,\sigma)$ to be the unique circle (the circumcircle) that contains them, with radius (the circumradius) given by any of the classic formulæ [7, p. 13]:

$$\mathsf{ppp}(s,t,\sigma) = \frac{2\mathsf{pp}(s,t)\mathsf{pp}(s,\sigma)\mathsf{pp}(t,\sigma)}{\mathcal{A}(s,t,\sigma)} \tag{3.2}$$

where $\mathcal{A}(s,t,\sigma)$ is the area of the triangle with vertices $\mathbf{q}(s)$, $\mathbf{q}(t)$ and $\mathbf{q}(\sigma)$, or

$$\mathsf{ppp}(s,t,\sigma) = \frac{\mathsf{pp}(s,\sigma)}{|\sin\theta_{st\sigma}|} = \frac{\mathsf{pp}(t,s)}{|\sin\theta_{t\sigma s}|} = \frac{\mathsf{pp}(\sigma,t)}{|\sin\theta_{\sigma st}|} \tag{3.3}$$

where $\theta_{st\sigma}$ is the angle between the edge vectors $\mathbf{q}(s)-\mathbf{q}(t)$ and $\mathbf{q}(\sigma)-\mathbf{q}(t)$, and so on. The three forms in (3.3) all coincide by the Sine Rule of elementary geometry. (Note that typically these formulæ are written in terms of edge lengths, but for us the factor of one half in the definition (3.1) of pp is convenient, so we work with half of the edge lengths.) The circle radius can also be written as a ratio involving a Cayley-Menger determinant [1, p. 241], namely

$$\mathsf{ppp}^2(s,t,\sigma) = -2\frac{\Delta_{(3)}}{\Gamma_{(3)}}, \tag{3.4}$$

where

$$\Delta_{(3)} = \begin{vmatrix} 0 & \mathsf{pp}^2(s,t) & \mathsf{pp}^2(s,\sigma) \\ \mathsf{pp}^2(s,t) & 0 & \mathsf{pp}^2(t,\sigma) \\ \mathsf{pp}^2(s,\sigma) & \mathsf{pp}^2(t,\sigma) & 0 \end{vmatrix}, \tag{3.5}$$

and

$$\Gamma_{(3)} = \begin{vmatrix} 0 & \mathsf{pp}^2(s,t) & \mathsf{pp}^2(s,\sigma) & 1 \\ \mathsf{pp}^2(s,t) & 0 & \mathsf{pp}^2(t,\sigma) & 1 \\ \mathsf{pp}^2(s,\sigma) & \mathsf{pp}^2(t,\sigma) & 0 & 1 \\ 1 & 1 & 1 & 0 \end{vmatrix}. \tag{3.6}$$

It is the Cayley-Menger form of the circle radius formula that generalises to spheres [1, p. 241]. For any four non-coplanar points $\mathbf{q}(s)$, $\mathbf{q}(t)$, $\mathbf{q}(\sigma)$ and $\mathbf{q}(\tau)$ we define

$\mathcal{S}(s,t,\sigma,\tau)$ to be the unique sphere that contains them. The radius of this sphere, denoted $\mathsf{pppp}(s,t,\sigma,\tau)$, satisfies

$$\mathsf{pppp}^2(s,t,\sigma,\tau) = -2\frac{\Delta_{(4)}}{\Gamma_{(4)}}, \tag{3.7}$$

where the 4×4 determinant $\Delta_{(4)}$ and 5×5 determinant $\Gamma_{(4)}$ are the natural generalisations of (3.5) and (3.6) written in terms of the six edge half-lengths.

Remark 3.2 *1. At any distinct pair, non-collinear triple, or non-coplanar quadruple of points, the functions* pp, ppp *and* pppp *are, respectively, continuous and symmetric in their arguments.*

2. When (s,t,σ) *are distinct but collinear, we set* $\mathsf{ppp}(s,t,\sigma)=\infty$. *Similarly, when* (s,t,σ,τ) *are distinct but coplanar, we set* $\mathsf{pppp}(s,t,\sigma,\tau)=\infty$, *unless these points are co-circular in which case we set* $\mathsf{pppp}(s,t,\sigma,\tau)=\mathsf{ppp}(s,t,\sigma)$.

3. The sphere $\mathcal{S}(s,t,\sigma,\tau)$ *enjoys several equivalent geometric characterisations at any quadruple of non-coplanar points. For example, it is the unique sphere defined by the point* $\mathbf{q}(s)$ *and the circle* $\mathcal{C}(t,\sigma,\tau)$, *but is also the unique sphere defined by the point* $\mathbf{q}(t)$ *and the circle* $\mathcal{C}(s,\sigma,\tau)$ *and so on. These equivalent characterisations will be exploited below.*

3.1.2 Coalescent functions

Various radius functions can be derived from ppp and pppp by considering (generic) coalescent limits along the curve Γ. To that end we adopt a mnemonic notation where p stands for point (contact order zero), t for tangent (contact order one), and c for circle (contact of order two). For example, from the three-point function we obtain

$$\mathsf{ppp}(s,t,\sigma) \overset{\sigma\to t}{\to} \mathsf{pt}(s,t) \overset{t\to s}{\to} \rho(s), \quad (s,t,\sigma \quad \text{non-collinear}).$$

Here $\mathsf{pt}(s,t)$ is the radius of the unique circle that passes through $\mathbf{q}(s)$ and is tangent to Γ at $\mathbf{q}(t)$. We denote this circle by $\mathcal{C}(s,t,t)$ and note that it is actually the limit of $\mathcal{C}(s,t,\sigma)$ as $\mathbf{q}(\sigma)\to\mathbf{q}(t)$ along Γ. As before, $\rho(s)$ is the radius of the standard osculating circle $\mathcal{C}(s)$ at $\mathbf{q}(s)$. Thus we recover the classic result that the osculating circle may be interpreted as $\mathcal{C}(s,s,s)$, namely the limit of $\mathcal{C}(s,t,\sigma)$ as $\mathbf{q}(\sigma),\mathbf{q}(t)\to\mathbf{q}(s)$ along Γ.

By changing the order of the first limit we obtain a slightly different result, namely

$$\mathsf{ppp}(s,t,\sigma) \overset{t\to s}{\to} \mathsf{tp}(s,\sigma) \overset{\sigma\to s}{\to} \rho(s), \quad (s,t,\sigma \quad \text{non-collinear}).$$

Here $\mathsf{tp}(s,t)$ is the radius of the unique circle $\mathcal{C}(s,s,t)$ that passes through $\mathbf{q}(t)$ and is tangent to Γ at $\mathbf{q}(s)$. In particular, we have $\mathsf{tp}(s,t)=\mathsf{pt}(t,s)$, but $\mathsf{tp}(s,t)\neq\mathsf{tp}(t,s)=\mathsf{pt}(s,t)$, because, in general, both of the two-point circular radius functions are non-symmetric in their arguments.

Analogous limits may also be considered for the four-point function pppp. For example,

$$\mathsf{pppp}(s,t,\sigma,\tau) \overset{\tau\to\sigma}{\to} \mathsf{ppt}(s,t,\sigma) \overset{\sigma\to t}{\to} \mathsf{pc}(s,t) \overset{t\to s}{\to} \rho_{\text{os}}(s), \quad (s,t,\sigma,\tau \quad \text{non-coplanar}).$$

Here $\mathsf{ppt}(s,t,\sigma)$ is the radius of the unique sphere defined by the point $\mathbf{q}(s)$ and the circle $\mathcal{C}(t,\sigma,\sigma)$. Similarly, $\mathsf{pc}(s,t)$ is the radius of the unique sphere defined by the point $\mathbf{q}(s)$ and the osculating circle $\mathcal{C}(t,t,t)$. As before, $\rho_{\text{os}}(s)$ is the radius of the osculating sphere at $\mathbf{q}(s)$.

By changing the order of the limits we obtain various different three-point functions analogous to ppt, and various different two-point functions analogous to pc. The different functions may be represented in the following way:

$$\mathsf{pppp} \overset{\text{4pt}\to\text{3pt}}{\to} \left\{ \begin{array}{c} \mathsf{ppt} \\ \mathsf{ptp} \\ \mathsf{tpp} \end{array} \right\} \overset{\text{3pt}\to\text{2pt}}{\to} \left\{ \begin{array}{c} \mathsf{pc} \\ \mathsf{cp} \\ \mathsf{tt} \end{array} \right\} \overset{\text{2pt}\to\text{1pt}}{\to} \rho_{\text{os}}.$$

For example, $\mathsf{ptp}(s,t,\sigma)$ is the radius of the unique sphere defined by the point $\mathbf{q}(s)$ and the circle $\mathcal{C}(t,t,\sigma)$, or, equivalently, defined by the point $\mathbf{q}(\sigma)$ and the circle $\mathcal{C}(s,t,t)$. The two-point function $\mathsf{tt}(s,t)$ is the radius of the unique sphere defined by the two circles $\mathcal{C}(s,s,t)$ and $\mathcal{C}(s,t,t)$. In particular, $\mathsf{tt}(s,t)$ is the radius of the sphere that is tangent to Γ at both $\mathbf{q}(s)$ and $\mathbf{q}(t)$.

3.1.3 Explicit formulæ

Explicit formulæ for the coalescent limit functions are available whenever the remaining arguments are in generic position. For the two-point circular functions pt and tp we have

$$\mathsf{pt}(s,\sigma) = \mathsf{tp}(\sigma,s) = \frac{\mathsf{pp}(s,\sigma)}{|\sin\theta_{s\sigma'}|}, \quad (s \neq \sigma) \tag{3.8}$$

where $\theta_{s\sigma'}$ is the angle between $\mathbf{q}(s) - \mathbf{q}(\sigma)$ and the tangent vector to $\mathcal{C}$ at $\mathbf{q}(\sigma)$. When $\sin\theta_{s\sigma'} = 0$ we set $\mathsf{pt}(s,\sigma) = \infty$. Note that (3.8) is the limit of (3.3) as the triangle closes.

For the two-point spherical function tt we find

$$\mathsf{tt}^2(s,\sigma) = \mathsf{pp}^2(s,\sigma)\,\frac{1 - \big(\mathbf{t}(\sigma)\cdot\mathbf{R}(\mathbf{e})\mathbf{t}(s)\big)^2}{|\mathbf{t}(s)\times\mathbf{t}(\sigma)\cdot\mathbf{e}|^2}, \quad (s \neq \sigma) \tag{3.9}$$

where $\mathbf{t}(s)\times\mathbf{t}(\sigma)\cdot\mathbf{e}$ is the standard scalar triple product,

$$\mathbf{e} = \frac{\mathbf{q}(s) - \mathbf{q}(\sigma)}{|\mathbf{q}(s) - \mathbf{q}(\sigma)|} \tag{3.10}$$

is the unit vector along the chord, and

$$\mathbf{R}(\mathbf{e}) = 2\mathbf{e}\otimes\mathbf{e} - \mathbf{I} \tag{3.11}$$

with $\mathbf{e}\otimes\mathbf{e}$ being the usual vector outer product so that $\mathbf{R}(\mathbf{e})$ is the (symmetric) proper rotation matrix that maps the curve tangent $\mathbf{t}(\sigma)$ into the (compatibly oriented) tangent

$\mathbf{t}^\star(s,\sigma)$ at $\mathbf{q}(s)$ of the circle $\mathcal{C}(\sigma,\sigma,s)$ (which was defined as the circle with tangent $\mathbf{t}(\sigma)$ at $\mathbf{q}(\sigma)$ passing through the point $\mathbf{q}(s)$). Formula (3.9) is valid whenever the two tangents and the chord associated with (s,σ) are linearly independent. In the case when they are linearly dependent we set $\mathsf{tt}(s,\sigma)=\infty$, unless they are co-circular in the sense that $\mathcal{C}(s,\sigma,\sigma)=\mathcal{C}(s,s,\sigma)$, in which case we set $\mathsf{tt}(s,\sigma)=\mathsf{pt}(s,\sigma)=\mathsf{tp}(s,\sigma)$. By considering a curve $\mathbf{q}$ lying on a sphere $\mathcal{S}$ of radius R, that has a part forming a non-great circle of radius $r<R$ we find that the two argument function tt is not continuous, because $\mathsf{tt}(s,\sigma)=R$, except for pairs of points where $\mathbf{q}(s)-\mathbf{q}(\sigma),\mathbf{q}'(s)$, and $\mathbf{q}'(\sigma)$ are co-planar, in which case $\mathsf{tt}(s,\sigma)=r$.

As $\mathbf{t}(s)$ and $\mathbf{t}(\sigma)$ are unit vectors and $\mathbf{R}(\mathbf{e})$ is a rotation matrix, $\mathbf{t}(\sigma)\cdot\mathbf{R}(\mathbf{e})\mathbf{t}(s)$ is the cosine of the angle $\alpha(s,\sigma)$ between the unit vectors $\mathbf{t}(s)$ and $\mathbf{t}^\star(s,\sigma)$ and we may rewrite (3.9) as

$$\mathsf{tt}(s,\sigma)=\mathsf{pp}(s,\sigma)\,\frac{|\sin\alpha(s,\sigma)|}{|\mathbf{t}(s)\times\mathbf{t}(\sigma)\cdot\mathbf{e}|},\quad(s\neq\sigma).\tag{3.12}$$

The angle α has previously been considered in various knot energies [24, p. 318], [36, p. 294].

Formulæ for the two-point spherical functions cp and pc are also available. In particular, let (α,β,γ) be the coordinates of $\mathbf{q}(\sigma)$ with respect to the Frenet frame at $\mathbf{q}(s)$ in the sense that

$$\mathbf{q}(\sigma)=\mathbf{q}(s)+\alpha\mathbf{t}(s)+\beta\mathbf{n}(s)+\gamma\mathbf{b}(s).\tag{3.13}$$

Then we find

$$\mathsf{cp}(s,\sigma)=\mathsf{pc}(\sigma,s)=\sqrt{\rho^2(s)+\frac{[\alpha^2+\beta^2+\gamma^2-2\beta\rho(s)]^2}{4\gamma^2}},\quad(s\neq\sigma).\tag{3.14}$$

This formula is valid whenever $\gamma\neq0$, that is, $\mathbf{q}(\sigma)\notin\mathcal{P}(s)$. When $\mathbf{q}(\sigma)\in\mathcal{P}(s)$ we set $\mathsf{cp}(s,\sigma)=\infty$, unless $\mathbf{q}(\sigma)\in\mathcal{C}(s)$ in which case we set $\mathsf{cp}(s,\sigma)=\rho(s)$.

For points s at which $\tau(s)\neq0$, formula (3.14) suggests the definition

$$\mathsf{cp}(s,s)=\lim_{\sigma\to s}\mathsf{cp}(s,\sigma)=\rho_{os}(s).\tag{3.15}$$

However, just as in Remarks 2.4, the most appropriate definition for $\mathsf{cp}(s,s)$ at points with $\tau(s)=0$ is unclear.

3.1.4 Multi-point radius inequalities

The functions pp, ppp and pppp satisfy the basic inequalities:

$$0\leq\mathsf{pp}(s,t)\leq\mathsf{ppp}(s,t,\sigma)\leq\mathsf{pppp}(s,t,\sigma,\tau),\quad(s,t,\sigma,\tau\quad\text{distinct}),\tag{3.16}$$

which follow from the facts that the half-length of any chord on a circle is bounded by the circle radius, and the radius of any circle on a sphere is bounded by the sphere radius.

By considering various coalescent limits in (3.16) we arrive at inequalities involving the associated limit functions. For example, for the limit functions with three-point arguments we find

$$\mathsf{ppp}(s,t,\sigma) \leq \begin{cases} \mathsf{ppt}(s,t,\sigma) \\ \mathsf{ptp}(s,t,\sigma) \\ \mathsf{tpp}(s,t,\sigma) \end{cases} \qquad (s,t,\sigma \quad \text{distinct}), \tag{3.17}$$

and for the limit functions with two-point arguments we find

$$\mathsf{pp}(s,t) \leq \begin{cases} \mathsf{pt}(s,t) & \leq \begin{cases} \mathsf{pc}(s,t) \\ \mathsf{tt}(s,t) \end{cases} \\ \mathsf{tp}(s,t) & \leq \begin{cases} \mathsf{tt}(s,t) \\ \mathsf{cp}(s,t) \end{cases} \end{cases} \qquad (s,t \quad \text{distinct}), \tag{3.18}$$

where in (3.17) and (3.18) it is to be understood that the braces indicate alternatives.

Table 3.1 summarises all thirteen, distinct, multi-point distance functions which arise as radii of line segments, circles and spheres that are defined by various orders of contact to a given curve at one, two, three or four distinct points. The row in the table indicates whether it is the radius of a line segment, circle, or sphere (which may be interpreted as zero-, one- or two-dimensional spheres), while the column indicates the number of distinct arguments in the corresponding function. In particular, we find that while there is generally no ordering among the functions contained in any one block of the table, within one column a function appearing in a higher row is bounded above by any function appearing in a lower row. The only exceptions to this rule are the two functions cp and pc that are marked with asterisks; there are only partial orderings between these functions and those appearing above them.

	1	2	3	4
line	0	pp		
circle	ρ	pt tp	ppp	
sphere	ρ_{os}	$\mathsf{cp}^\star$ $\mathsf{pc}^\star$ tt	tpp ptp ppt	pppp

Table 3.1: All possible multi-point radius functions that are defined in terms of line segments, circles and spheres. Rows correspond to the type of object, while columns correspond to the number of arguments associated with each radius function. With the exception of the two asterisked functions, the following inequalities hold: within a given column, and when evaluated at the same arguments, any function appearing in a higher of the three rows is smaller than any function appearing in a lower row.

There exist curves Γ with pairs of points (s,t) such that all of the inequalities (3.18) are sharp. Contrariwise, pairs of points of stationary approach, i.e. pairs of distinct points $\mathbf{q}(s)$ and $\mathbf{q}(t)$ and associated curve tangents $\mathbf{t}(s)$ and $\mathbf{t}(t)$ satisfying (2.11) are

very special because at such pairs we always have equality between four of the two-point radius functions

$$\mathsf{pp}(s,t) = \mathsf{pt}(s,t) = \mathsf{tp}(s,t) = \mathsf{tt}(s,t). \tag{3.19}$$

As seen in section 2.2 thickness can be characterised using such pairs of points of stationary approach.

3.2 Global radius of curvature functions

To any simple curve Γ and any of the multi-point radius functions displayed in Table 3.1 we may associate a global radius of curvature function defined by minimising over all but the first argument, namely

$$\begin{array}{lcll}
\rho_{\mathsf{pppp}}(s) & := & \inf_{t,\sigma,\tau} \mathsf{pppp}(s,t,\sigma,\tau) & (s,t,\sigma,\tau \quad \text{distinct}) \\
\rho_{\mathsf{ppp}}(s) & := & \inf_{t,\sigma} \mathsf{ppp}(s,t,\sigma) & (s,t,\sigma \quad \text{distinct}) \\
\rho_{\mathsf{pt}}(s) & := & \inf_{t} \mathsf{pt}(s,t) & (s,t \quad \text{distinct}) \\
 & \vdots & & \\
\rho_{\mathsf{pp}}(s) & := & \inf_{t} \mathsf{pp}(s,t) = 0 & (s,t \quad \text{distinct}).
\end{array}$$

These functions may be viewed as generalisations of the standard local radius of curvature functions $\rho(s)$ and $\rho_{\mathrm{os}}(s)$. Here we study various properties of these global radius of curvature functions, and discuss the non-local information that they contain about Γ.

3.2.1 Radius of curvature inequalities

The radius of curvature functions are nested at each point $\mathbf{q}(s)$. In particular, for the circular radius of curvature functions we have

$$\rho \geq \left\{ \begin{array}{l} \rho_{\mathsf{tp}} \\ \rho_{\mathsf{pt}} \end{array} \right\} \geq \rho_{\mathsf{ppp}}. \tag{3.20}$$

These inequalities follow from the observation that any circle which achieves any radius function on the left is a competitor (or limit of competitors) for any function on the right. Similarly, the spherical radius functions satisfy

$$\rho_{\mathrm{os}} \geq \left\{ \begin{array}{lcl} \left.\begin{array}{l} \rho_{\mathsf{pc}} \\ \rho_{\mathsf{tt}} \\ \rho_{\mathsf{cp}} \end{array}\right\} & \geq & \rho_{\mathsf{ppt}} = \rho_{\mathsf{ptp}} \\ \left.\begin{array}{l} \rho_{\mathsf{tt}} \\ \rho_{\mathsf{cp}} \end{array}\right\} & \geq & \rho_{\mathsf{tpp}} \end{array} \right\} \geq \rho_{\mathsf{pppp}}. \tag{3.21}$$

Because the minimisation of the two-point radius function pp yields the zero function $\rho_{\mathsf{pp}}(s) \equiv 0$, there remain twelve nontrivial global radius of curvature functions as shown in Table 3.2. In addition to the column inequalities carried over from Table 3.1, there are now also row inequalities. Specifically, (and for simplicity again ignoring the two asterisked functions) it can be shown that along each row, any function dominates any other function appearing in a column to its right.

	0	1	2	3
line	0	$\rho_{\mathsf{pp}} = 0$		
circle	ρ	ρ_{pt} ρ_{tp}	ρ_{ppp}	
sphere	ρ_{os}	$\rho_{\mathsf{cp}}{}^{\star}$ $\rho_{\mathsf{pc}}{}^{\star}$ ρ_{tt}	ρ_{tpp} ρ_{ptp} ρ_{ppt}	ρ_{pppp}

Table 3.2: Global radius of curvature functions. Each function of a single variable is defined by minimisation of the multi-point functions of Table 3.1 over all but their first argument. Rows correspond to the type of object, while columns correspond to the number of minimisations associated with the function. It can be shown that only five of the twelve functions are distinct on smooth curves that are closed or infinite.

3.2.2 Distinct radius of curvature functions

When Γ is a simple, closed or infinite, curve we find that there are various identities between the circular and spherical radius of curvature functions.

Proposition 3.3 *Under hypothesis 3.1 the following equalities hold:*

$$\rho_{\mathsf{pt}} = \rho_{\mathsf{ppp}} = \rho_{\mathsf{ptp}} = \rho_{\mathsf{ppt}} = \rho_{\mathsf{pppp}}, \tag{3.22}$$

and

$$\rho_{\mathsf{tt}} = \rho_{\mathsf{tpp}} = \rho_{\mathsf{tp}}. \tag{3.23}$$

The first equality in (3.22) was derived in [18, p. 4770], and the further relations in (3.22) and (3.23) are implied by similar arguments. The central idea in most of the demonstrations is that a sphere realising the minimum in the definition of a global radius of curvature function at the point s, cannot have only zero-order intersections at distinct points, for otherwise the sphere could be shrunk, while retaining the same number of intersections with the curve Γ, and the same order of contact at s, contradicting optimality.

Proof

1. $\rho_{\mathsf{ppt}} = \rho_{\mathsf{ptp}}$:
   By symmetry in the last two arguments, i.e. $\mathsf{ppt}(s,t,\sigma) = \mathsf{ptp}(s,\sigma,t)$, the minimisation is over the same set.

2. $\rho_{\mathsf{ppp}} = \rho_{\mathsf{pt}}$:
   By (3.20) we have $\rho_{\mathsf{ppp}} \leq \rho_{\mathsf{pt}}$. Now assume that there exist s, t, and σ such that $\mathsf{ppp}(s,t,\sigma) = \rho_{\mathsf{ppp}}(s) < \rho_{\mathsf{pt}}(s)$. If $t \neq s \neq \sigma$, then there must be a tangency at either t or σ, because if not the curve crosses at t and σ and the circumsphere of $\mathcal{C}(s,t,\sigma)$ could be shrunk to obtain $\mathsf{ppp}(s,\tilde{t},\tilde{\sigma}) < \rho_{\mathsf{ppp}}(s)$, a contradiction of the definition of $\rho_{\mathsf{ppp}}(s)$. And if there is a tangency at say t, then $\mathsf{pt}(s,t) =$

$\mathsf{ppp}(s,t,t) < \rho_{\mathsf{pt}}(s)$, another contradiction. The case $t = s \neq \sigma$ is excluded by the same two contradictions. And if $t = s = \sigma$, then $\mathsf{pt}(s,s) = \mathsf{ppp}(s,s,s) < \rho_{\mathsf{pt}}(s)$, a contradiction.

3. $\rho_{\mathsf{pt}} = \rho_{\mathsf{ppt}}$:
We know $\rho_{\mathsf{pt}} \leq \rho_{\mathsf{ppt}}$. Now assume $\rho_{\mathsf{pt}}(s) < \rho_{\mathsf{ppt}}(s)$ for some $s \in I$. Then, by continuity of pt, there exists a $\sigma \neq s$ such that $\mathsf{pt}(s,\sigma) < \rho_{\mathsf{ppt}}(s)$.

   If the curve is tangent to the circumsphere of $\mathcal{C}(s,\sigma,\sigma)$ at s we get $\rho_{\mathsf{tt}}(s) \leq \mathsf{pt}(s,\sigma) < \rho_{\mathsf{ppt}}(s)$, contradicting (3.21). If the curve crosses the circumsphere of $\mathcal{C}(s,\sigma,\sigma)$ at s it must re-cross it at a distinct point $t \neq s$. Then, for $t \neq \sigma$ we have $\mathsf{ppt}(s,t,\sigma) = \mathsf{pt}(s,\sigma) < \rho_{\mathsf{ppt}}(s)$, a contradiction. For $t = \sigma$ we have contact of order two at σ (at least one, but the curve crosses, thus two). Therefore $\rho_{\mathsf{ppt}}(s) \leq \mathsf{pc}(s,t) = \mathsf{pt}(s,t) < \rho_{\mathsf{ppt}}(s)$, a contradiction.

4. $\rho_{\mathsf{pppp}} = \rho_{\mathsf{ppt}}$:
By (3.21) we have $\rho_{\mathsf{pppp}} \leq \rho_{\mathsf{ppt}}$. Now assume $\rho_{\mathsf{pppp}}(s) < \rho_{\mathsf{ppt}}(s)$ for some $s \in I$. Then there exist t,σ,τ such that $\mathsf{pppp}(s,t,\sigma,\tau) < \rho_{\mathsf{ppt}}(s)$. In the case that three or four points coincide with s, say $s = t = \sigma$, then a contradiction arises from $\mathsf{pppp}(s,s,s,\tau) = \mathsf{ptp}(s,s,\tau) < \rho_{\mathsf{ppt}}(s)$. If no or one point coincides with s then there must be a tangency at one of the distinct arguments, else the sphere $\mathcal{S}(s,t,\sigma,\tau)$ can be shrunk maintaining intersections until we get a tangency say at $\tilde{\tau}$ to $\mathcal{S}(s,t,\tilde{\tau},\tilde{\tau})$, contradicting $\mathsf{ppt}(s,t,\tilde{\tau}) < \mathsf{pppp}(s,t,\sigma,\tau) < \rho_{\mathsf{ppt}}(s)$. And if there is a tangency at $\tau \neq s$ say then a contradiction follows from $\mathsf{ppt}(s,t,\tau) = \mathsf{pppp}(s,t,\sigma,\tau) < \rho_{\mathsf{ppt}}(s)$.

5. $\rho_{\mathsf{tp}} = \rho_{\mathsf{tt}}$:
As a consequence of (3.18) we have $\rho_{\mathsf{tp}} \leq \rho_{\mathsf{tt}}$. Assume $\rho_{\mathsf{tp}}(s) < \rho_{\mathsf{tt}}(s)$ for some $s \in I$. Then there exists a σ such that $\mathsf{tp}(s,\sigma) = \rho_{\mathsf{tp}}(s)$. If $\sigma \neq s$ we obtain, analogously to before, a contradiction of $\mathsf{tp}(s,\sigma) = \rho_{\mathsf{tp}}(s)$ unless the curve is tangent at σ to the circumsphere of $\mathcal{C}(s,s,\sigma)$. If $\sigma = s$, then the curve either has third order contact at s so that $\mathsf{tt}(s,s) = \mathsf{tp}(s,s) = \rho_{\mathsf{tp}}(s) < \rho_{\mathsf{tt}}(s)$, a contradiction, or the curve crosses the circumsphere of curvature at s. And if the curve crosses the sphere at s, it must recross at a distinct point t. Then either the curve is tangent at t to the circumsphere of $\mathcal{C}(s,s,t)$, contradicting $\mathsf{tt}(s,t) = \mathsf{tp}(s,t) = \mathsf{tp}(s,s) = \rho_{\mathsf{tp}}(s) < \rho_{\mathsf{tt}}(s)$, or we get another contradiction by a shrinking argument.

6. $\rho_{\mathsf{tpp}} = \rho_{\mathsf{tt}}$:
By (3.21) we have $\rho_{\mathsf{tpp}} \leq \rho_{\mathsf{tt}}$. On the other hand $\mathsf{tp}(s,t) \leq \mathsf{tpp}(s,t,\sigma)$ for all (s,t,σ), thus $\rho_{\mathsf{tp}}(s) \leq \rho_{\mathsf{tpp}}(s)$ for all $s \in I$. Using part 5. we find $\rho_{\mathsf{tt}} = \rho_{\mathsf{tp}} \leq \rho_{\mathsf{tpp}} \leq \rho_{\mathsf{tt}}$.

■

Lemma 3.4 *Under hypothesis 3.1 and at each point* $\mathbf{q}(s)$ *at which either* $\kappa'(s) \neq 0$ *or* $\tau(s) \neq 0$ *we have*

$$\rho = \rho^{\star}_{\mathsf{cp}}. \tag{3.24}$$

The equality (3.24) is of a different character than (3.22) and (3.23) as it relates the entirely local object ρ with a global radius of curvature. Moreover here the asterisk indicates that the equality only holds at points at which either $\kappa'(s) \neq 0$ or $\tau(s) \neq 0$. At points where $\kappa'(s) = \tau(s) = 0$ the very definition of $\rho_{\mathsf{cp}}(s)$ is unclear.

Proof For the demonstration of the generic case, note first that $\mathsf{cp}(s, \sigma) \geq \rho(s)$ because any sphere with second-order contact at s contains the osculating circle at s. Thus $\rho_{\mathsf{cp}}(s) \geq \rho(s)$. If $\kappa'(s) \neq 0$ the opposite inequality (and therefore equality) follows from the Taylor expansion (2.7). In particular, the curve locally crosses the osculating circumsphere $\mathcal{S}^c$ near $\mathbf{q}(s)$. Since the curve Γ is simple and has no end-points (it is closed or infinite) it must re-cross the sphere $\mathcal{S}^c$ at some distinct point $\mathbf{q}(\sigma)$, which leads to the conclusion that $\mathsf{cp}(s, \sigma) = \rho(s)$, so that $\rho_{\mathsf{cp}}(s) \leq \rho(s)$. When $\kappa'(s) = 0$ but $\tau(s) \neq 0$, we have by (3.15) and (2.6) that $\lim_{\sigma \to s} \mathsf{cp}(s, \sigma) = \rho_{\mathrm{os}}(s) = \rho(s)$, so $\rho_{\mathsf{cp}}(s) \leq \rho(s)$. ■

Thus for simple, closed or infinite, curves we have the seven equalities (3.22)–(3.24) which imply that of the possible twelve radius of curvature functions there are only five distinct ones. The functions $\{\rho_{\mathsf{pt}}, \rho_{\mathsf{tp}}, \rho_{\mathsf{pc}}, \rho, \rho_{\mathrm{os}}\}$ can be taken as an independent set. Combining inequalities (3.20) and (3.21) with equalities (3.22)–(3.24), implies that these five functions are nested in the sense

$$\rho_{\mathrm{os}} \geq \left\{ \begin{array}{c} \rho \geq \rho_{\mathsf{tp}} \\ \rho_{\mathsf{pc}} \end{array} \right\} \geq \rho_{\mathsf{pt}} \geq 0. \tag{3.25}$$

We can then address the question of identifying special points along the curve at which equalities can occur between some or all of the five independent curvature functions. For example, equalities between the two global radius of curvature functions ρ_{pt} and ρ_{tp} can arise at points of stationary approach (cf. (2.11)) as described in Section 3.1.4. Equality between the local and a global radius of curvature functions can occur only at certain special points along Γ.

Lemma 3.5 *Under the hypothesis 3.1, equality between ρ_{pt} and ρ or between ρ_{tp} and ρ can occur only at extremal points of the local curvature κ in the sense that*

$$\rho_{\mathsf{pt}} = \rho \quad \Rightarrow \quad \kappa' = 0 \quad \textit{and} \quad \kappa'' \leq \kappa\tau^2, \tag{3.26}$$

$$\rho_{\mathsf{tp}} = \rho \quad \Rightarrow \quad \kappa' = 0 \quad \textit{and} \quad \kappa'' \leq \kappa\tau^2. \tag{3.27}$$

Notice that these extremal points must be maxima (to second order) of the local curvature whenever the torsion is zero, as is the case for planar curves.

Proof First note, that $\rho_{\mathsf{pt}}(s) = \infty$ for some $s \in I$ if and only if the curve is a straight, infinite line in which case the right hand side of both (3.26) and (3.27) are fulfilled.

Now consider the case when Γ is not a straight, infinite line, that is assume $\rho_{\mathsf{pt}}(s) = \rho(s) \neq \infty$: The results follow then from the Taylor expansion (2.7). The proofs are by contradiction: When $\kappa(s) \neq 0$ and $\kappa'(s) \neq 0$ then Γ locally pierces the osculating circumsphere $\mathcal{S}^c(s)$ of radius $\rho(s)$. Since Γ is simple and has no end-points (it is closed or infinite) it must re-cross $\mathcal{S}^c(s)$ at a distinct point $\mathbf{q}(\sigma)$. Then we can shrink $\mathcal{S}^c(s)$ to

find a sphere of smaller radius than $\rho(s)$ that is tangent at $\mathbf{q}(s)$ and which intersects Γ near $\mathbf{q}(\sigma)$. In the case $\rho_{\mathsf{tp}}(s) = \rho(s)$ this is an immediate contradiction and therefore $\kappa'(s) = 0$. In the case $\rho_{\mathsf{pt}}(s) = \rho(s) \neq \infty$ consideration of circles on the shrunken sphere implies that $\rho_{\mathsf{tp}}(s) < \rho(s) = \rho_{\mathsf{pt}}(s)$, a contradiction of (3.25). Thus $\kappa'(s) = 0$ is a necessary condition (in both cases). If the second condition $\kappa'' \leq \kappa\tau^2$ were violated the expansion (2.7) reveals that the curve would locally lie inside the osculating circumsphere $\mathcal{S}^c(s)$, and a similar shrinking argument would lead to a contradiction as before. ■

Notice that if $\rho_{\mathsf{pt}} = \rho$, then all the circular radius of curvature functions (both local and global) must be equal by virtue of (3.20) and (3.22). If moreover $\tau \neq 0$, then all the radius of curvature functions introduced thus far (both circular and spherical, local and global) must be equal by virtue of (2.6), (3.21), (3.22) and (3.23).

3.3 The global radius of curvature functions ρ_{pt} and ρ_{tp}

In this section we complement the results of Lemma 3.5 characterising the circumstances in which ρ_{pt} and ρ_{tp} can be achieved locally, by a study of how the global radius of curvature functions ρ_{pt} and ρ_{tp} can be achieved non-locally. We first consider the function ρ_{pt} and ask: what is the geometry of the curve at distinct points s and σ that realise the global radius of curvature $\mathsf{pt}(s, \sigma) = \rho_{\mathsf{pt}}(s)$?

To this end assume $\mathsf{pt}(s, \sigma) = \rho_{\mathsf{pt}}(s) < \rho(s)$, i.e. $\rho_{\mathsf{pt}}(s)$ is not achieved locally. Denote the circumsphere of the circle $\mathcal{C}(s, \sigma, \sigma)$ by $\mathcal{S}$. Then, generically, three cases can occur: either the curve $\mathbf{q}$ at σ lies locally inside $\mathcal{S}$, locally outside $\mathcal{S}$ or it locally crosses the sphere $\mathcal{S}$. First assume that the curve $\mathbf{q}$ at σ lies locally inside $\mathcal{S}$. Shrinking the sphere (keeping the contact at $\mathbf{q}(s)$) leads to a slightly smaller sphere that intersects the curve at two distinct points $\mathbf{q}(t) \neq \mathbf{q}(t')$. Thus, $\mathsf{ppp}(s, t, t') < \rho_{\mathsf{pt}}(s)$, which contradicts (3.22), and the first case cannot arise.

Now assume the curve $\mathbf{q}$ at σ lies locally outside $\mathcal{S}$. If $\mathbf{q}'(\sigma) \cdot (\mathbf{q}(\sigma) - \mathbf{q}(s)) \neq 0$, rotating the sphere around the axis $\mathbf{q}(\sigma) - \mathbf{q}(s)$ (keeping the contact at $\mathbf{q}(s)$) leads to a sphere that intersects the curve at two distinct points $\mathbf{q}(t) \neq \mathbf{q}(t')$. Shrinking this sphere then produces a sphere that still intersects at two distinct points $\mathbf{q}(u) \neq \mathbf{q}(u')$ and $\mathsf{ppp}(s, u, u') < \rho_{\mathsf{pt}}(s)$, which contradicts (3.22). This yields that the second case can only occur if $\mathbf{q}'(\sigma) \cdot (\mathbf{q}(\sigma) - \mathbf{q}(s)) = 0$.

Finally assume that the curve $\mathbf{q}$ at σ locally crosses $\mathcal{S}$. Remark 2.7 implies that the centre of the circle $\mathcal{C}(s, \sigma, \sigma)$ must lie on the polar axis $\mathcal{A}(\sigma)$ at σ.

We summarise the possible cases and provide more rigorous analytic proofs in:

Lemma 3.6 *For a given curve $\mathbf{q} \in C^3(I, \mathbb{R}^3)$, and for $s \in I$, only the following five cases can occur:*

1. *Γ is a straight infinite line so that $\rho_{\mathsf{pt}} \equiv \rho \equiv \infty$,*
2. *$\mathbf{q}(s)$ is a self-intersection point, i.e. $\mathbf{q}(s) = \mathbf{q}(\sigma)$ for some $\sigma \neq s$ in which case $\rho_{\mathsf{pt}}(s) = 0$,*

3. $0 < \rho_{\mathsf{pt}}(s) = \rho(s) < \infty$, *i.e.* $\rho_{\mathsf{pt}}(s)$ *is achieved locally, in which case* $\rho'(s) = 0$,

4. $0 < \rho_{\mathsf{pt}}(s) = \mathsf{pt}(s,\sigma) < \infty$ *with* $s \neq \sigma$ *and* $\mathbf{q}'(\sigma) \cdot (\mathbf{q}(\sigma) - \mathbf{q}(s)) = 0$ *, i.e.* $\rho_{\mathsf{pt}}(s)$ *is achieved by half of the distance between a pair of single critical points (cf. (2.13)),*

5. $0 < \rho_{\mathsf{pt}}(s) = \mathsf{pt}(s,\sigma) < \infty$ *with* $s \neq \sigma$*, and* $\kappa(\sigma) \neq 0$ *and the centre* $\mathbf{c}$ *of the circle* $\mathcal{C}(s,\sigma,\sigma)$ *lies on the polar axis* $\mathcal{A}(\sigma)$ *at* σ*.*

Proof Both cases 1 and 2 can arise. By Lemma 3.5 we know that $\rho_{\mathsf{pt}}(s) = \rho(s)$ implies $\rho'(s) = 0$. Now assume $\rho_{\mathsf{pt}}(s) < \rho(s)$, i.e. $\rho_{\mathsf{pt}}(s)$ is achieved non-locally. Then $\rho_{\mathsf{pt}}(s) = \mathsf{pt}(s,\sigma)$ with $s \neq \sigma$. Recall the formula (3.8)

$$\mathsf{pt}(s,\sigma) = \frac{\mathsf{pp}(s,\sigma)}{|\sin\theta_{s\sigma'}|} = \frac{|\mathbf{q}(s) - \mathbf{q}(\sigma)|^2}{2|(\mathbf{q}(s) - \mathbf{q}(\sigma)) \times \mathbf{q}'(\sigma)|}, \quad (s \neq \sigma).$$

We study the non-local critical points of ρ_{pt} or roots of $\partial_\sigma \mathsf{pt}(s,\sigma) = 0$:

$$\begin{aligned}\partial_\sigma \left(\mathsf{pt}(s,\sigma)^2\right) =& \frac{|\mathbf{q}(s) - \mathbf{q}(\sigma)|^2\, \mathbf{q}'(\sigma) \cdot (\mathbf{q}(s) - \mathbf{q}(\sigma))}{2|(\mathbf{q}(s) - \mathbf{q}(\sigma)) \times \mathbf{q}'(\sigma)|^4} \Big[|\mathbf{q}(s) - \mathbf{q}(\sigma)|^2 \mathbf{q}''(\sigma) \cdot (\mathbf{q}(s) - \mathbf{q}(\sigma)) \\ & - 2|(\mathbf{q}(s) - \mathbf{q}(\sigma)) \times \mathbf{q}'(\sigma)|^2 \Big]\end{aligned}$$

We find that $\partial_\sigma \mathsf{pt}(s,\sigma) = 0$ when

$$\mathbf{q}'(\sigma) \cdot (\mathbf{q}(s) - \mathbf{q}(\sigma)) = 0,$$

which is case 4, or when

$$|\mathbf{q}(s) - \mathbf{q}(\sigma)|^2 \mathbf{q}''(\sigma) \cdot (\mathbf{q}(s) - \mathbf{q}(\sigma)) - 2|(\mathbf{q}(s) - \mathbf{q}(\sigma)) \times \mathbf{q}'(\sigma)|^2 = 0,$$

which, whenever $\kappa(\sigma) \neq 0$, may be rewritten using the notation

$$\mathbf{d} = \mathbf{q}(s) - \mathbf{q}(\sigma) \tag{3.28}$$

for the chord between $\mathbf{q}(\sigma)$ and $\mathbf{q}(s)$, and the notation (3.10) as

$$\kappa(\sigma)\mathbf{n}(\sigma) \cdot \mathbf{d} - 2|\mathbf{e} \times \mathbf{q}'(\sigma)|^2 = 0, \tag{3.29}$$

and which reduces in the case $\kappa(\sigma) = 0$ to

$$|\mathbf{e} \times \mathbf{q}'(\sigma)| = 0. \tag{3.30}$$

In the case $\kappa(\sigma) = 0$ condition (3.30) yields that $\mathbf{e}$ and $\mathbf{q}'(\sigma)$ are colinear and therefore $\rho_{\mathsf{pt}}(s) = \mathsf{pt}(s,\sigma) = \infty$, in which case the curve is a straight line. This case is already covered by case 1.

It remains to show that in the case $\kappa(\sigma) \neq 0$ condition (3.29) is equivalent to case 5. First consider the projection $\hat{\mathbf{q}}(s)$ of $\mathbf{q}(s)$ onto the $\mathbf{n}(\sigma)$-$\mathbf{b}(\sigma)$-plane, cf. Figure 3.1

$$\hat{\mathbf{q}}(s) = \mathbf{q}(\sigma) + \mathbf{d} - \mathbf{d} \cdot \mathbf{q}'(\sigma)\mathbf{q}'(\sigma).$$

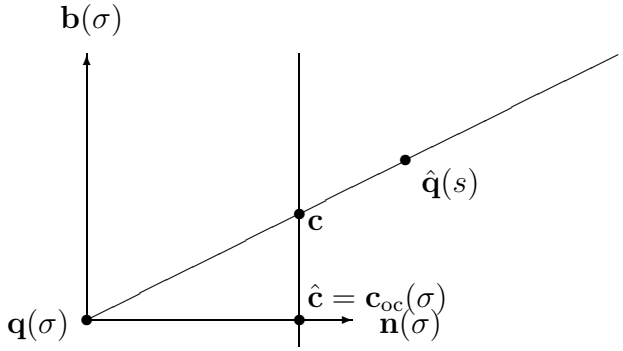

Figure 3.1: The $\mathbf{n}(\sigma)$-$\mathbf{b}(\sigma)$-plane containing the centre $\mathbf{c}$ of the circle $\mathcal{C}(s,\sigma,\sigma)$ and the projection $\hat{\mathbf{q}}(s)$ of $\mathbf{q}(s)$.

The centre $\mathbf{c}$ of the circle $\mathcal{C}(s,\sigma,\sigma)$ lies in the intersection of the $\mathbf{n}(\sigma)$-$\mathbf{b}(\sigma)$-plane with the $\mathbf{t}(\sigma)$-$\mathbf{d}$-plane, that is on the straight line passing through $\mathbf{q}(\sigma)$ and $\hat{\mathbf{q}}(s)$ and is given by

$$\mathbf{c} = \mathbf{q}(\sigma) + \mathsf{pt}(s,\sigma)\frac{\hat{\mathbf{q}}(s)-\mathbf{q}(\sigma)}{|\hat{\mathbf{q}}(s)-\mathbf{q}(\sigma)|} = \mathbf{q}(\sigma) + \frac{\mathbf{d}-\mathbf{d}\cdot\mathbf{q}'(\sigma)\mathbf{q}'(\sigma)}{2|\mathbf{e}\times\mathbf{q}'(\sigma)|^2}.$$

The projection of the centre $\mathbf{c}$ onto the line through $\mathbf{q}(\sigma)$ parallel to $\mathbf{n}(\sigma)$ is given by

$$\hat{\mathbf{c}} = \mathbf{q}(\sigma) + (\mathbf{c}-\mathbf{q}(\sigma))\cdot\mathbf{n}(\sigma)\mathbf{n}(\sigma) = \mathbf{q}(\sigma) + \frac{\mathbf{d}\cdot\mathbf{n}(\sigma)}{2|\mathbf{e}\times\mathbf{q}'(\sigma)|^2}\mathbf{n}(\sigma).$$

Thus

$$|\hat{\mathbf{c}}-\mathbf{q}(\sigma)| = \frac{\mathbf{d}\cdot\mathbf{n}(\sigma)}{2|\mathbf{e}\times\mathbf{q}'(\sigma)|^2},$$

and the centre $\mathbf{c}$ of the circle $\mathcal{C}(s,\sigma,\sigma)$ lies on the polar axis $\mathcal{A}(\sigma)$ at σ, i.e. $|\hat{\mathbf{c}}-\mathbf{q}(\sigma)| = \frac{1}{\kappa(\sigma)}$, if and only if equation (3.29) is true. ■

Lemma 3.7 *For a given curve $\mathbf{q} \in C^3(I,\mathbb{R}^3)$, and for $s \in I$, only the four following cases can occur:*

1. *Γ is a straight infinite line so that $\rho_{\mathsf{pt}} \equiv \rho \equiv \infty$,*
2. *$\mathbf{q}(s)$ is a self-intersection point, i.e. $\mathbf{q}(s) = \mathbf{q}(\sigma)$ for some $\sigma \neq s$ in which case $\rho_{\mathsf{pt}}(s) = 0$,*
3. *$0 < \rho_{\mathsf{tp}}(s) = \rho(s) < \infty$, i.e. $\rho_{\mathsf{tp}}(s)$ is achieved locally, in which case $\rho'(s) = 0$,*
4. *$0 < \rho_{\mathsf{tp}}(s) = \mathsf{tp}(s,\sigma) < \infty$ with $s \neq \sigma$, and the tangent $\mathbf{q}'(\sigma)$ lies in the tangent plane of the circumsphere $\mathcal{S}$ of the circle $\mathcal{C}(s,s,\sigma)$ at $\mathbf{q}(\sigma)$.*

Proof Both cases 1 and 2 can arise. By Lemma 3.5 we know that $\rho_{\mathsf{tp}}(s) = \rho(s)$ implies $\rho'(s) = 0$. Now assume $\rho_{\mathsf{tp}}(s) < \rho(s)$, i.e. $\rho_{\mathsf{tp}}(s)$ is not achieved locally. Then

$\rho_{\mathsf{tp}}(s) = \mathsf{tp}(s,\sigma)$ with $s \neq \sigma$. We differentiate the formula (3.8) (where the roles of s and σ are interchanged)

$$\begin{aligned}\partial_\sigma \left(\mathsf{tp}(s,\sigma)^2\right) =& \frac{|\mathbf{q}(\sigma)-\mathbf{q}(s)|^2}{2|(\mathbf{q}(\sigma)-\mathbf{q}(s))\times\mathbf{q}'(s)|^4}\Big[2\mathbf{q}'(\sigma)\cdot(\mathbf{q}(\sigma)-\mathbf{q}(s))\,|(\mathbf{q}(\sigma)-\mathbf{q}(s))\times\mathbf{q}'(s)|^2 \\ & - |\mathbf{q}(\sigma)-\mathbf{q}(s)|^2\,(\mathbf{q}'(\sigma)\cdot(\mathbf{q}(\sigma)-\mathbf{q}(s)) - \mathbf{q}'(s)\cdot(\mathbf{q}(\sigma)-\mathbf{q}(s))\mathbf{q}'(s)\cdot\mathbf{q}'(\sigma))\Big].\end{aligned}$$

We use the notation (3.10) and (3.28), then the non-local critical points $\partial_\sigma \mathsf{tp}(s,\sigma) = 0$ are achieved when

$$-2\mathbf{q}'(\sigma)\cdot\mathbf{d}\,|\mathbf{d}\times\mathbf{q}'(s)|^2 - |\mathbf{d}|^2\,(\mathbf{q}'(s)\cdot\mathbf{d}\,\mathbf{q}'(s)\cdot\mathbf{q}'(\sigma) - \mathbf{q}'(\sigma)\cdot\mathbf{d}) = 0,$$

that is, when

$$\mathbf{q}'(\sigma)\cdot\left[-2\mathbf{d}\,|\mathbf{d}\times\mathbf{q}'(s)|^2 - |\mathbf{d}|^2\,(\mathbf{q}'(s)\cdot\mathbf{d}\,\mathbf{q}'(s) - \mathbf{d})\right] = 0. \tag{3.31}$$

Consider the circumsphere $\mathcal{S}$ of the circle $\mathcal{C}(s,s,\sigma)$. The tangent plane at $\mathbf{q}(\sigma)$ is spanned by the vectors

$$\mathbf{R}(\mathbf{e})\mathbf{q}'(s), \quad \text{and} \quad \mathbf{e}\times\mathbf{q}'(s),$$

where $\mathbf{R}(\mathbf{e})$ is the proper rotation matrix given by (3.11). Therefore the tangent $\mathbf{q}'(\sigma)$ lies in the tangent plane of the circumsphere $\mathcal{S}$ of the circle $\mathcal{C}(s,s,\sigma)$ at $\mathbf{q}(\sigma)$ when

$$\mathbf{q}'(\sigma)\cdot[\mathbf{R}(\mathbf{e})\mathbf{q}'(s)\times(\mathbf{e}\times\mathbf{q}'(s))] = 0. \tag{3.32}$$

It remains to show that this condition is equivalent to equation (3.31). Dividing equation (3.31) by $|\mathbf{d}|^3$ yields

$$0 = \mathbf{q}'(\sigma)\cdot\left[-2\mathbf{e}\,|\mathbf{e}\times\mathbf{q}'(s)|^2 - (\mathbf{q}'(s)\cdot\mathbf{e}\,\mathbf{q}'(s) - \mathbf{e})\right].$$

We continue with algebra to find

$$\begin{aligned}0 &= \mathbf{q}'(\sigma)\cdot\left[-2\mathbf{e}\,(1-(\mathbf{e}\cdot\mathbf{q}'(s))^2) - (\mathbf{q}'(s)\cdot\mathbf{e}\,\mathbf{q}'(s) - \mathbf{e})\right] \\ &= \mathbf{q}'(\sigma)\cdot[2\mathbf{e}\otimes\mathbf{e} - \mathbf{I}]\;(\mathbf{q}'(s)\cdot\mathbf{e}\,\mathbf{q}'(s) - \mathbf{e}) \\ &= \mathbf{q}'(\sigma)\cdot\mathbf{R}(\mathbf{e})\,(\mathbf{q}'(s)\cdot\mathbf{e}\,\mathbf{q}'(s) - \mathbf{e}) \\ &= \mathbf{R}(\mathbf{e})\,\mathbf{q}'(\sigma)\cdot(\mathbf{q}'(s)\cdot\mathbf{e}\,\mathbf{q}'(s) - \mathbf{e}) \\ &= \mathbf{R}(\mathbf{e})\,\mathbf{q}'(\sigma)\cdot((\mathbf{e}\times\mathbf{q}'(s))\times\mathbf{q}'(s)) \\ &= \mathbf{R}(\mathbf{e})\,\mathbf{q}'(\sigma)\cdot(\mathbf{R}(\mathbf{e})(-(\mathbf{e}\times\mathbf{q}'(s)))\times\mathbf{q}'(s)) \\ &= \mathbf{q}'(\sigma)\cdot((-(\mathbf{e}\times\mathbf{q}'(s)))\times\mathbf{R}(\mathbf{e})\mathbf{q}'(s)) \\ &= \mathbf{q}'(\sigma)\cdot(\mathbf{R}(\mathbf{e})\mathbf{q}'(s)\times(\mathbf{e}\times\mathbf{q}'(s))),\end{aligned}$$

so that equation (3.31) is indeed equivalent to (3.32). ■

As a consequence of Lemma 3.7 we find, that if $\rho_{\mathsf{tp}}(s)$ is achieved non-locally, then $\rho_{\mathsf{tp}}(s) = \rho_{\mathsf{tt}}(s)$. Moreover, if $\rho_{\mathsf{tp}}(s)$ is achieved locally, then, in the generic case $\tau(s) \neq 0$, Lemma 3.5 yields $\rho(s) = \rho_{\mathrm{os}}(s)$, so that $\rho_{\mathsf{tp}}(s) = \rho_{\mathsf{tt}}(s)$. This confirms that the two global radius of curvature functions ρ_{tp} and ρ_{tt} are identical (cf. (3.23)).

3.4 Thickness of closed or infinite curves

Let Γ be a simple, closed or infinite, curve. Then to each of the five distinct radius of curvature functions $\{\rho_{\mathsf{pt}}, \rho_{\mathsf{tp}}, \rho_{\mathsf{pc}}, \rho, \rho_{\mathrm{os}}\}$ we may associate a functional (or number) corresponding to its infimum:

$$\Delta_{\mathsf{pt}}[\Gamma] = \inf_s \rho_{\mathsf{pt}}(s), \quad \Delta_{\mathsf{tp}}[\Gamma] = \inf_s \rho_{\mathsf{tp}}(s),$$

and so on.

Lemma 3.8 *Under the hypothesis 3.1 we have the ordering*

$$\Delta_{\rho_{\mathrm{os}}}[\Gamma] \geq \Delta^{\star}_{\mathsf{pc}}[\Gamma] = \Delta_{\rho}[\Gamma] \geq \Delta_{\mathsf{tp}}[\Gamma] = \Delta_{\mathsf{pt}}[\Gamma], \tag{3.33}$$

with the exception indicated by the asterisk, that the relations involving $\Delta_{\mathsf{pc}}[\Gamma]$ are only valid for curves with non-vanishing torsion, i.e. if $\tau(s) \neq 0$ for all $s \in I$.

In the case of zero torsion $\tau(s) = 0$, $\mathsf{pc}(s, s)$ is left undefined, which forces us to exclude this case.

Proof By (3.25) we have immediately

$$\Delta_{\rho_{\mathrm{os}}} \geq \left\{ \begin{array}{c} \Delta_{\rho} \geq \Delta_{\mathsf{tp}} \\ \Delta^{\star}_{\mathsf{pc}} \end{array} \right\} \geq \Delta_{\mathsf{pt}} \geq 0,$$

and it remains to show: $\Delta_{\mathsf{tp}}[\Gamma] = \Delta_{\mathsf{pt}}[\Gamma]$ and $\Delta^{\star}_{\mathsf{pc}}[\Gamma] = \Delta_{\rho}[\Gamma]$. We have,

$$\Delta_{\mathsf{pt}}[\Gamma] = \inf_s \rho_{\mathsf{pt}}(s) = \inf_{(s,\sigma)} \mathsf{pt}(s, \sigma) = \inf_{(s,\sigma)} \mathsf{tp}(\sigma, s) = \inf_{\sigma} \rho_{\mathsf{tp}}(\sigma) = \Delta_{\mathsf{tp}}[\Gamma],$$

which gives the first equality. To prove the second equality, first note that trivially $\Delta^{\star}_{\mathsf{pc}}[\Gamma] \geq \Delta_{\rho}[\Gamma]$. Assume $\Delta^{\star}_{\mathsf{pc}}[\Gamma] > \Delta_{\rho}[\Gamma] = \rho(s)$, for some $s \in I$. Then, κ achieves a maximum at s, thus $\kappa'(s) = 0$ and $\kappa''(s) \leq 0$. If $\tau(s) \neq 0$, then $\rho(s) = \rho_{\mathrm{os}}(s) = \mathsf{pc}(s, s)$ and we find a contradiction. ■

Thus for simple, closed or infinite, curves we have only three distinct functionals of this type, namely Δ_{pt}, Δ_{ρ} and $\Delta_{\rho_{\mathrm{os}}}$. The number Δ_{ρ} is just the minimal value of the local osculating circle radius of curvature ρ along the curve, while $\Delta_{\rho_{\mathrm{os}}}$ is the minimal value of the local osculating sphere radius of curvature ρ_{os}. For smooth curves with non-vanishing torsion, formula (2.6) reveals that $\rho_{\mathrm{os}}(s) = \rho(s)$ whenever $\rho'(s) = 0$. Consequently $\Delta_{\rho_{\mathrm{os}}}[\Gamma] = \Delta_{\rho}[\Gamma]$ for closed curves with $\tau(s) \neq 0$ at the minimum of ρ. However in general the two numbers are different, as can be seen, for example, by consideration of smooth, non-circular closed curves lying on a given sphere.

The number Δ_{pt} is more interesting. As mentioned in section 2.2, it was first introduced in [18] within the context of the study of ideal or tight knots, where it was shown that $\Delta_{\mathsf{pt}} = \Delta_{\mathsf{ppp}}$ gives an explicit characterisation of the normal injectivity radius or thickness of the curve Γ. With the last equality in (3.33), we see that the thickness could also be computed via a numerical evaluation of $\Delta_{\mathsf{tp}}[\Gamma]$. Consideration of smooth, simple

curves that are close to a figure eight, demonstrates that strict inequality between Δ_ρ and Δ_{pt} is possible.

In the whole present chapter we excluded curves with end-points, whose presence may cause several identities to fail. For example, the last equality of (3.33) relies on the fact that a simple, closed or infinite, curve has no end-point. In particular, this equality is violated for the curve with end-points that is sketched in Figure 3.2. Here $\rho_{\mathsf{tp}}(s) = R = 2r > r = \rho_{\mathsf{pt}}(s)$. And, by taking r as small as necessary, we see that $\Delta_{\mathsf{tp}}[\Gamma] = \rho_{\mathsf{tp}}(s)$ while $\Delta_{\mathsf{pt}}[\Gamma] = \rho_{\mathsf{pt}}(s)$, so that the last equality in (3.33) fails. Moreover $\rho_{\mathsf{tp}}(\sigma) = r < \rho_{\mathsf{tt}}(\sigma)$, which shows that the identity (3.23) can also fail in the presence of end-points.

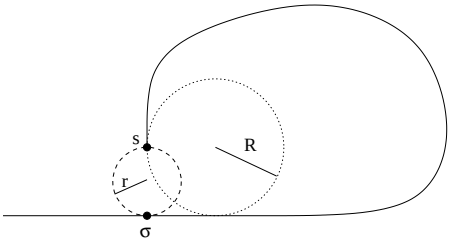

Figure 3.2: A curve Γ that illustrates possible effects of end-points on global radius of curvature functions and curve thickness. The curve is drawn such that $\Delta_{\mathsf{tp}}[\Gamma] = \rho_{\mathsf{tp}}(s) = R = 2r > r = \rho_{\mathsf{pt}}(s) = \Delta_{\mathsf{pt}}[\Gamma]$.

3.5 Examples

3.5.1 Ellipses

Here we illustrate various properties of the standard local radius of curvature function ρ, and the global radius of curvature functions ρ_{pt} and ρ_{tp} for the case when Γ is an ellipse. See section 7.2.1 for the corresponding plots on an ellipse discretized with biarcs.

Figure 3.3 displays the two dimensional plot of pt for an ellipse with principal axes of length 1.0 and 0.6. The minimum of a horizontal cut $\mathsf{pt}(s, \cdot)$ is $\rho_{\mathsf{pt}}(s)$ whereas the minimum of a vertical cut $\mathsf{pt}(\cdot, \sigma)$ is $\rho_{\mathsf{tp}}(\sigma)$.

Figure 3.4 shows plots of ρ, ρ_{pt} and ρ_{tp} along the same ellipse. Nestedness between all three functions is in agreement with (3.25). Moreover, equality between all three functions occurs only at local minima of ρ (equivalently, local maxima of κ), which is in accordance with (3.26) and (3.27) in the case of zero torsion. The two global radius of curvature functions also coincide at the ends of the minor axes, which are a pair of points of stationary approach as defined in (2.11). While ρ_{tp} is smooth, ρ_{pt} has corners near each of its local maxima. As discussed below, these corners are associated with a discontinuity in the family of minimising circles for ρ_{pt} corresponding to a switch between case 4 and case 5 in Lemma 3.6 that describes how ρ_{pt} is achieved.

Figure 3.5 illustrates various properties of the osculating and minimising circles associated with the functions ρ, ρ_{pt} and ρ_{tp} on an ellipse. Panel (a) shows the locus of centres of all osculating circles, and the loci of the centres of all minimising circles

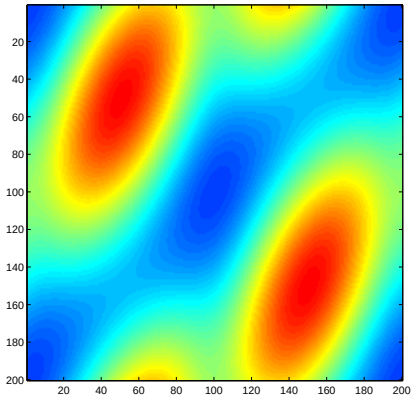

Figure 3.3: Plot of $\mathsf{pt}(s, \sigma)$ for an ellipse with principal axes of length 1.0 and 0.6. The vertical axis is for the point argument s, and the horizontal axis is for the tangent argument σ. Colour indicates the height of the function pt: from blue for low to red for high.

associated with ρ_{tp} and ρ_{pt}. The osculating and ρ_{pt} loci actually coincide on the two arrow-head portions, which fact is explained later. Panel (b) illustrates the classic result that for planar curves the osculating circles are nested between extremal points, or vertices, of the local radius of curvature ρ (see, e.g. [22, Theorem 3-12, p. 48], [61, p. 403]). In panel (c) we plot the minimising circles associated with ρ_{tp} for various points along the ellipse. These circles are actually osculating circles at the two local minima of ρ, i.e. at the left and right end-points of the line segment, but minimising circles with centres at interior points are instead doubly tangent at distinct points of the ellipse. Panels (d)–(f) illustrate the minimising circles for ρ_{pt}. Panel (d) depicts the continuous, nested, family of minimising circles with centres on the arrow-head portion of the locus of centres. The minimising circles are non-unique at the point illustrated in panel (e), and then the (non-nested) family of minimising circles smoothly evolves, as shown in panel (f). It is this transition between two smooth families of minimising circles that explains the corner in the graph of $\rho_{\mathsf{pt}}(s)$ that can be seen in Figure 3.4 (b).

It remains to discuss the nestedness of the circles appearing in Figure 3.5 (d). The numerics indicate that the minimising circle at s has zeroth-order contact with the ellipse at s. The minimising circle for ρ_{pt} must, by definition, have a first-order intersection or tangency to the ellipse at some point σ. For all but one of the circles in part (d) the point σ is distinct from s, and, moreover, there is no other intersection between each minimising circle and the ellipse. By a crossing argument this means that the order of contact between the ellipse and circle (i.e. two closed planar curves) at σ must be at least of second-order. Thus the circle realising the minimum in $\rho_{\mathsf{pt}}(s)$ is in fact the osculating circle to the ellipse at σ, so that $\rho_{\mathsf{pt}}(s) = \rho(\sigma)$. Therefore the loci of centres of minimising circles for ρ_{pt} and the osculating circles coincide locally, and local nestedness follows from the known nestedness of osculating circles. Thus, the circles appearing in Figure 3.5 (d) correspond to the case 5 of Lemma 3.6. Contrariwise, the circles appearing in Figure 3.5 (f) correspond to the case 4 of Lemma 3.6 as will become evident for the discretized ellipse with biarcs in Figure 7.11.

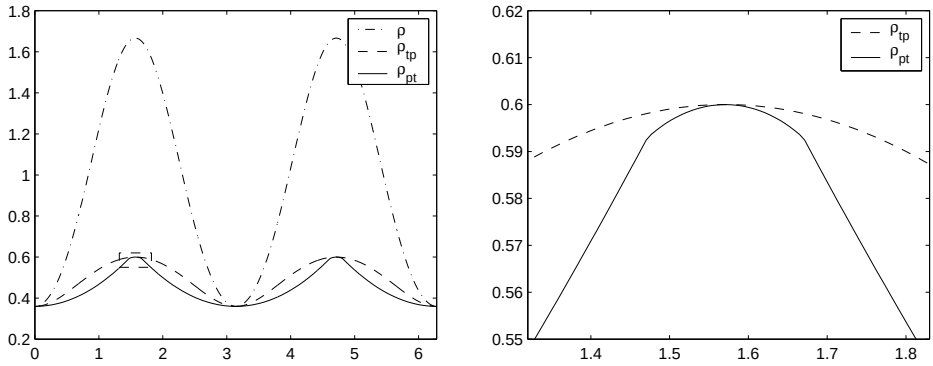

(a) (b)

Figure 3.4: Plots of local and global radius of curvature functions for an ellipse with principal axes of length 1.0 and 0.6: (a) ρ, ρ_{pt} and ρ_{tp} versus the polar angular coordinate around the ellipse (with $\theta = 0$ corresponding to a vertex of minimal radius of curvature), (b) magnified view of ρ_{pt} and ρ_{tp} near their common maxima at $\theta = \pi/2$ (corresponding to the inset of part a).

3.5.2 Helices

Helices are perhaps the simplest non-planar curves. Because helices are uniform, any radius of curvature function must be constant. However for helices it is interesting to consider how the various radius of curvature functions are realised as minima of the linear pp, circular $\{\mathsf{pt}, \mathsf{tp}\}$ and spherical $\{\mathsf{cp}, \mathsf{pc}, \mathsf{tt}\}$ two-point radius functions. Precisely because helices are uniform, it suffices to fix an arbitrary point s on the helix and to examine how the two-point radius functions vary with the second argument σ. It can be shown that helices possess a discrete symmetry which implies $\mathsf{pt}(s, \sigma) = \mathsf{tp}(s, \sigma)$ and $\mathsf{pc}(s, \sigma) = \mathsf{cp}(s, \sigma)$. Accordingly, we consider only one independent circular function pt and two independent spherical functions $\{\mathsf{cp}, \mathsf{tt}\}$.

Figures 3.6 (a,b) show plots of pp, pt, cp and tt as functions of the difference in arc length $\eta = \sigma - s$ for a helix of pitch 1.2. (In all our examples the helices are scaled to have radius one.) Nestedness between the linear, circular and spherical functions is in agreement with (3.18), as is the non-nestedness of the spherical functions cp and tt. (For helices the function tt tends to infinity near distinct points (s, σ) where the associated tangents are parallel.) Notice that the circular function pt and the spherical function tt enjoy the same global minimal value, as asserted by the last equality in (3.33), that the global minimum of cp is strictly larger (i.e. the second inequality in (3.33) is actually strict for this curve), and that, trivially, the global minimum of pp is zero.

Figure 3.6 (c) illustrates how the minima of various two-point functions depend on the helix pitch. For the helices with pitches 4 and 2.8, $\mathsf{pt}(s, \sigma)$ achieves its global minimum at $\eta = \sigma - s = 0$. For pitch 4 the global minimum is the only local minimum, whereas for pitch 2.8 there are two other local minima. The fact that the global minimum is achieved at $\eta = 0$ implies the thickness equality $\Delta_\rho[\Gamma] = \Delta_{\mathsf{pt}}[\Gamma]$ since the limit function $\mathsf{pt}(s, s)$ is just the standard local radius of curvature $\rho(s)$. For the helix with pitch 1.5, pt achieves its global minimum for $\eta \neq 0$; moreover, this minimum value is strictly less than

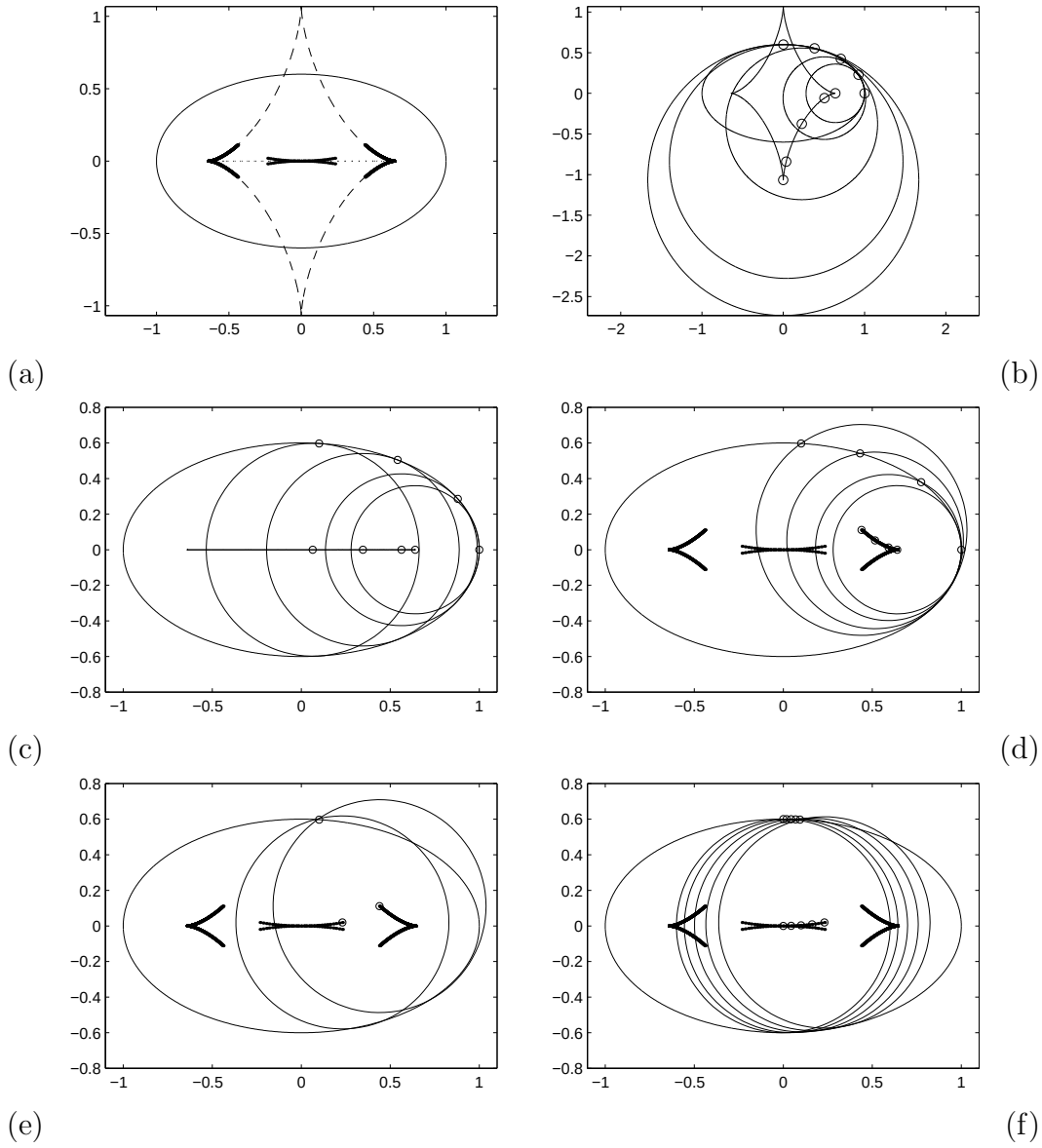

Figure 3.5: Osculating circles associated with ρ and minimising circles associated with ρ_{tp} and ρ_{pt} for an ellipse: (a) three loci of the centres of i) the osculating circles (diamond-shaped curve drawn in dashes), ii) the minimising circles realising ρ_{tp} (horizontal line segment drawn in small dots), and iii) the minimising circles realising ρ_{pt} (thick curve with discontinuities), (b) various osculating circles with centres and tangency points marked in open dots, (c) various minimising circles for ρ_{tp}, (d)-(f) minimising circles for ρ_{pt} with (d) centres on the arrow-head portion of the locus of centres, (e) two minimising circles with the same radius, but different centres lying on either side of the discontinuity in the locus, and (f) non-nested minimising circles with centres on the central portion of the locus.

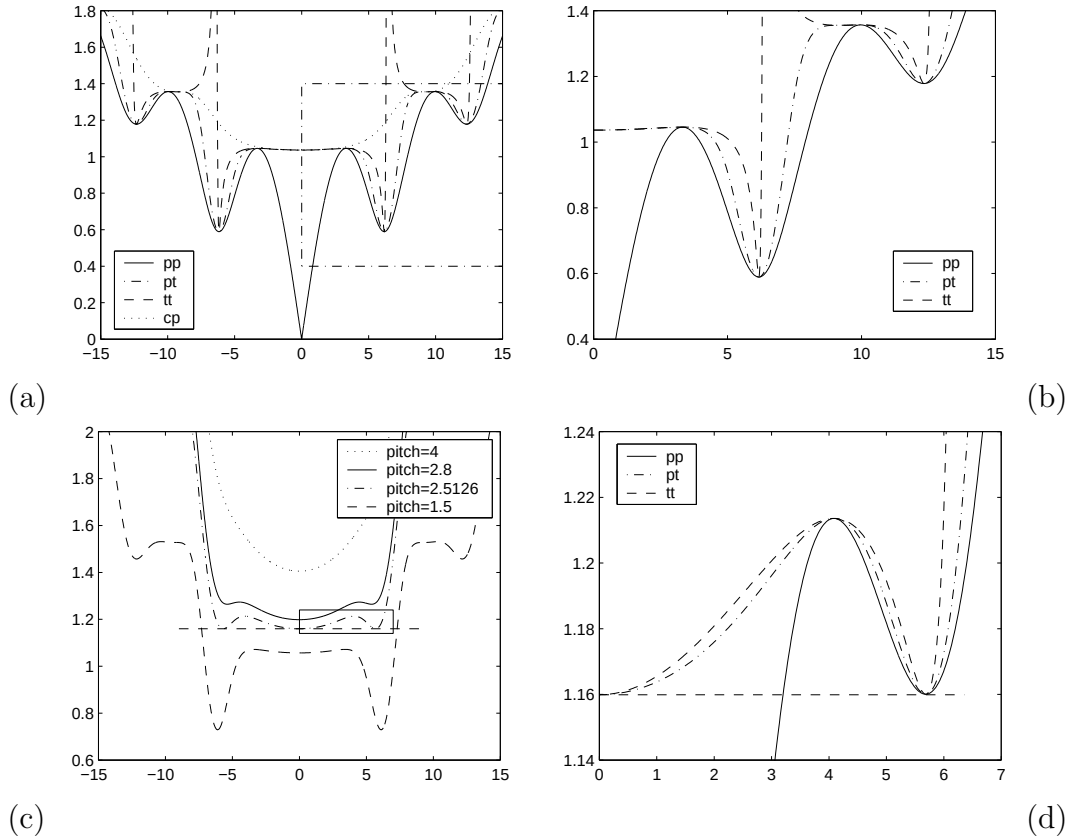

Figure 3.6: Plots of linear, circular, and spherical, two-point radius functions for helices: (a) pp, pt, cp, and tt versus $\eta = \sigma - s$ for a helix of pitch 1.2, (b) magnification of the inset shown in part (a), (c) plots of the single function pt for four helices with different pitches 1.5, 2.5126, 2.8 and 4. The horizontal line segment emphasises the equality of the three local minima for the critical pitch 2.5126 of Maritan *et al* [31], (d) plots of the three functions pp, pt and tt on the single critical-pitch helix within the inset indicated in part (c).

its value at the local minimum $\eta = 0$. Thus for pitch 1.5 we have the strict inequality $\Delta_\rho[\Gamma] > \Delta_{\mathsf{pt}}[\Gamma]$, and the thickness is achieved by a circle (or sphere) that intersects the helix at two distinct points. For the helix with pitch 2.5126..., pt achieves its global minimum both at $\eta = 0$ and at $\eta \neq 0$. Thus the thickness of a helix with this critical pitch is determined simultaneous by local and global properties of the curve. Maritan *et al* [31] originally identified this critical pitch in their work on the optimal packing of filaments. They also observed that many crystal structures of helical proteins have the same critical pitch. The critical helix is further illustrated in Figure 3.7.

In all of our discussions we are by no means restricted to consider only connected curves. Curves made up of multiple helices with a common axis, diameter and pitch, remain uniform (cf. Figure 3.8), and therefore have constant radius of curvature functions. Accordingly, just as for single helices, we can plot linear, circular and spherical two-point radius functions for various double helices. In Figure 3.9, panels (a) and (c) show the symmetric case of diametrically opposed strands (an offset angle of π), and in (b) and (d) an asymmetric case in which the strands are offset by an angle of $\frac{2}{3}\pi$.

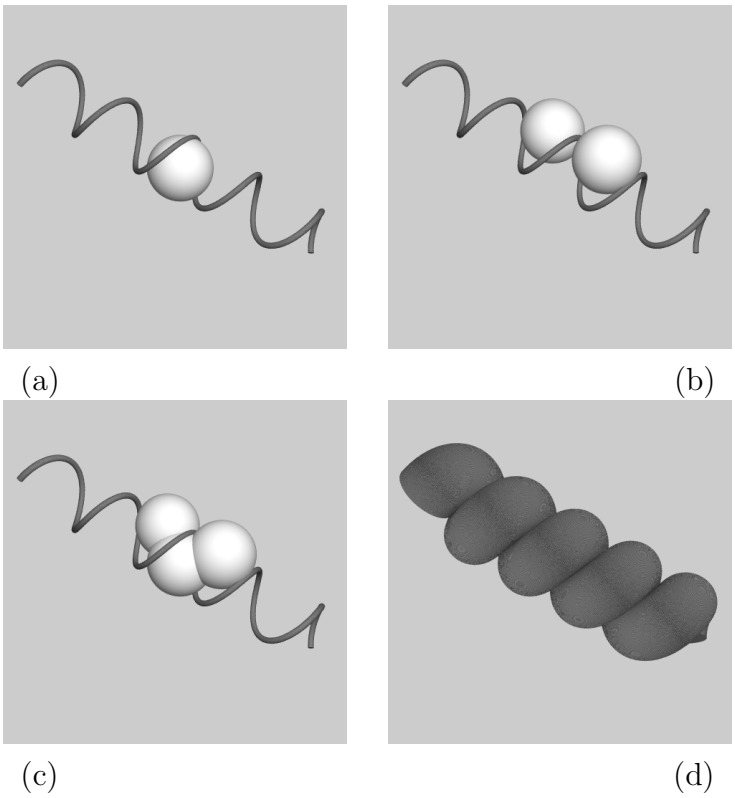

Figure 3.7: Visualisation of the pitch 2.5126 critical single helix: (a) the local osculating circumsphere (which is also the osculating sphere) associated with ρ, (b) two doubly-tangent spheres of radius ρ that achieve ρ_{pt}, (c) superposition of the local and global spheres, (d) the tube formed as the envelope of all spheres with radius equal to the thickness $\Delta_{\mathsf{pt}}[\Gamma]$ that are centred on the helix.

Panels (a) and (b) each plot the functions pp, pt and tt for one double-helical structure (pitch = 2.5126), while panels (c) and (d) plot the single function pt for a range of pitches. It can be shown that in all cases, $\Delta_{\mathsf{pt}}[\Gamma] = \Delta_{\mathsf{tt}}[\Gamma]$ is achieved by a circle that intersects both strands, or, equivalently, by a sphere that sits between the two strands with tangencies at either side. Panel (c) shows that as the pitch is decreased, there is a critical value at which a global minimum of pt, achieved across the diameter of the helical structure, splits into two global minima, achieved by asymmetric leading and trailing spheres (and a symmetric local maximum). Unlike the single helix, this transition, or bifurcation, for the double helix is local and for this reason it is easy to calculate analytically that the critical pitch is exactly 2π. In [58] it was observed that this critical pitch value corresponds to the standard parameters for the B-form DNA double helix. For asymmetrically offset double helices, as shown in panel (d), there is a critical pitch below which there are multiple local minima of the function pt. However for all pitch values there is always a unique global minimum that varies smoothly.

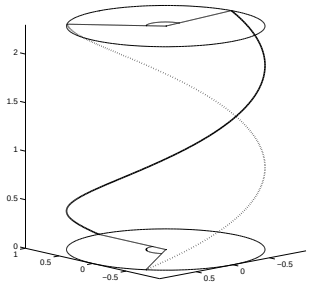

Figure 3.8: Structure formed by two helices with common axis, diameter and pitch, and constant offset angle (here 0.7π).

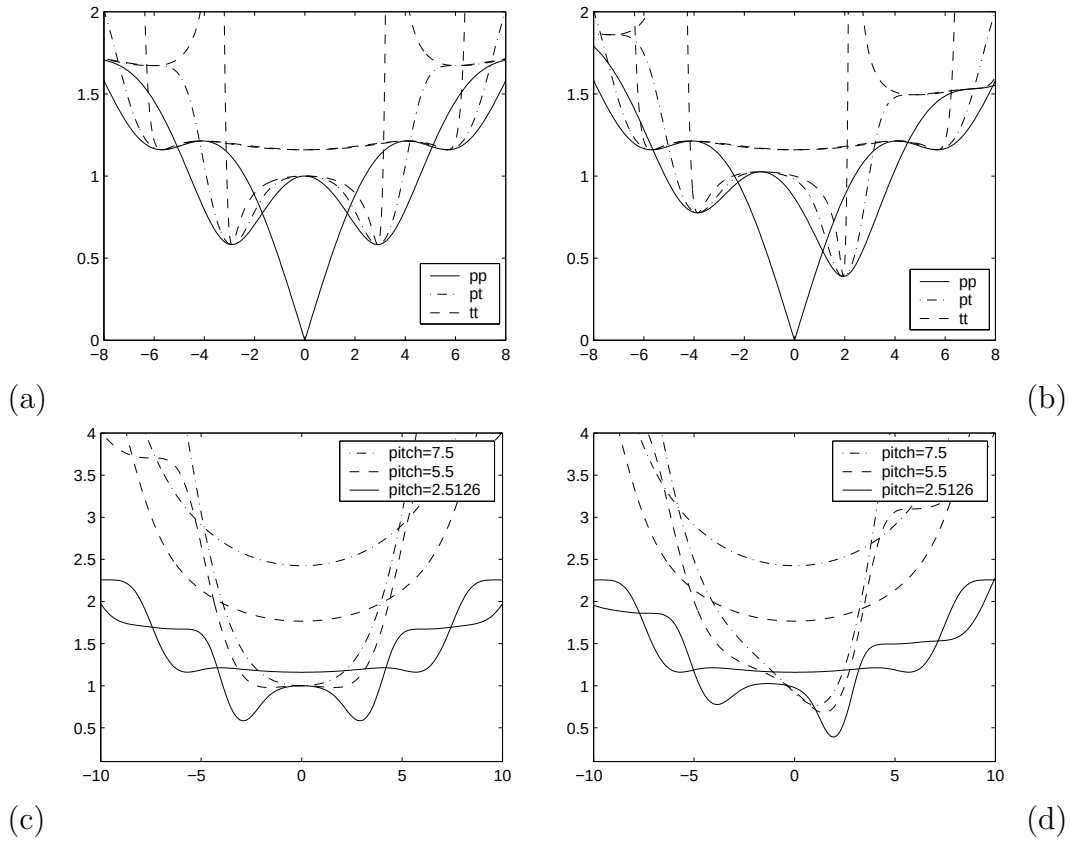

Figure 3.9: Plots of linear, circular, and spherical, two-point radius functions on double helices. The arc-length parameter $\eta = \sigma - s$ now assumes all real values twice, once corresponding to pairs of points on the same strand, and once with the pair on opposite strands (with phasing chosen such that $\eta = 0$ corresponds to points on opposite strands that lie in the same orthogonal cross-section of the double helical structure). Accordingly, the plot of each function generates two curves (one for each strand): (a) pp, pt, and tt for pitch 2.5126, and offset angle π (i.e. the diametrically opposed double helix), (b) same as (a) but with offset angle $\frac{2}{3}\pi$, (c) pt for three different pitches, all with offset angle π, (d) same as (c), but with offset angle $\frac{2}{3}\pi$.

Chapter 4

Biarcs

The examples of chapter 3 involve evaluation of global radius of curvature functions and thickness on analytically known curves. However we are also interested in computations involving curves with thickness. To that end we need to consider a discretization of space curves that allows an efficient thickness evaluation to a given accuracy, and that has simple closed form expressions for arc length, curvature and torsion. Moreover we want the discretization to live in the space of $C^{1,1}$ curves, where minimisers are known to exist. This allows us for example to give rigorous upper bounds for rope length in the examples of ideal knot shapes described in chapter 2.3 and 8. The above mentioned properties are all provided by curves assembled from biarcs in a C^1 fashion.

In this chapter we give a self-contained description of the construction of biarcs in three dimensional space. Local convergence results, and approximations of arc length, curvature and torsion are described in chapter 5. In chapter 6, point-tangent data pairs sampled from a (non-uniform) mesh on curves are interpolated with biarc curves and convergence results in different norms are obtained.

4.1 Construction and description

The basic building block in our convergence results is a single *biarc*, that is a pair of circular arcs used for Hermite interpolation. We first review, refine, and set notation for the theory of single biarcs, cf. [2], [54], [64].

Definition 4.1 Point-tangent data *is of the form* $(\mathbf{q}, \mathbf{t}) \in \mathcal{J} := \mathbb{R}^3 \times S^2$*, where* $S^2 \subset \mathbb{R}^3$ *denotes the unit 2-sphere. A* point-tangent data pair *is of the form* $((\mathbf{q}_0, \mathbf{t}_0), (\mathbf{q}_1, \mathbf{t}_1)) \in \mathcal{J} \times \mathcal{J}$ *with* $\mathbf{q}_0 \neq \mathbf{q}_1$.

Definition 4.2 *A* biarc $(\mathbf{a}, \bar{\mathbf{a}})$ *is a pair of circular arcs in* $\mathbb{R}^3$*, joined continuously and with continuous tangents, that interpolate a point-tangent data pair. The common end point* $\mathbf{m}$ *of the two arcs* $\mathbf{a}$ *and* $\bar{\mathbf{a}}$ *is the* matching point *of the biarc.*

The notions from Definitions 4.1 and 4.2 are illustrated in Figure 4.1. Hereafter the word arc will always mean a circular arc, and, for any arc $\mathbf{a}$, $\angle\mathbf{a}$ will denote the angle swept out by the arc. It is convenient to include straight line segments as being arcs,

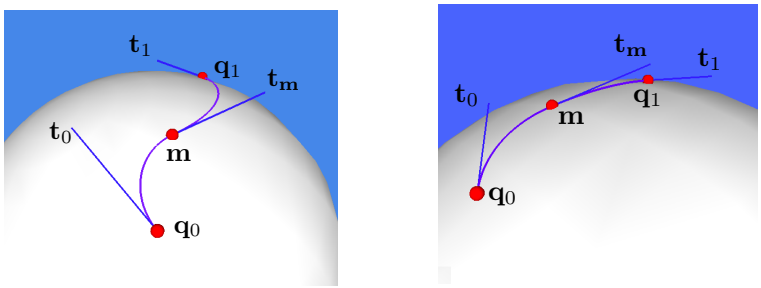

Figure 4.1: A *biarc* is a pair of circular arcs, assembled with a common tangent $\mathbf{t_m}$ at a matching point $\mathbf{m}$, that interpolates a given pair of point-tangent data $((\mathbf{q}_0, \mathbf{t}_0), (\mathbf{q}_1, \mathbf{t}_1))$. The biarc lies entirely on the (generically unique) sphere $\mathcal{S}$ defined by the data.

and planes as being spheres. Note that interpolation is taken to mean with orientation, so that $\mathbf{t}_0$ points to the interior of the first arc, while $-\mathbf{t}_1$ points to the interior of the second arc. The case $\mathbf{q}_0 = \mathbf{q}_1$ can be excluded in Definition 4.1 because there can be no interpolating biarc except in the trivial case in which $\mathbf{t}_0 = \mathbf{t}_1$.

We now discuss existence and multiplicity of interpolating biarcs, but first we need further notation. Given two points $\mathbf{q}_0,\ \mathbf{q}_1 \in \mathbb{R}^3$ with $\mathbf{q}_0 \neq \mathbf{q}_1$, we denote the chord, and unit vector along the chord, by

$$\mathbf{d} := \mathbf{q}_1 - \mathbf{q}_0, \quad \text{and} \quad \mathbf{e} := \frac{\mathbf{q}_1 - \mathbf{q}_0}{|\mathbf{q}_1 - \mathbf{q}_0|}, \tag{4.1}$$

and recall the definition (3.11) of the symmetric, proper rotation matrix

$$\mathbf{R}(\mathbf{e}) := 2\mathbf{e} \otimes \mathbf{e} - \mathbf{I}. \tag{4.2}$$

The matrix $\mathbf{R}(\mathbf{e})$ maps a vector $\mathbf{t} \in S^2$ into the (compatibly oriented) tangent $\mathbf{t}^\star$ at $\mathbf{q}_0$ of the circle with tangent $\mathbf{t}$ at $\mathbf{q}_1$ passing through the point $\mathbf{q}_0$, cf. Figure 4.2. Note that $\mathbf{R}(\mathbf{e})$ represents a reflexion in the unit vector $\mathbf{e}$, and $\mathbf{R}^{-1}(\mathbf{e}) = \mathbf{R}^T(\mathbf{e}) = \mathbf{R}(\mathbf{e}) = \mathbf{R}(-\mathbf{e})$. Given a point-tangent data pair $((\mathbf{q}_0, \mathbf{t}_0), (\mathbf{q}_1, \mathbf{t}_1)) \in \mathcal{J} \times \mathcal{J}$ we denote

$$\mathbf{t}_0^\star := \mathbf{R}(\mathbf{e})\mathbf{t}_0, \quad \mathbf{t}_1^\star := \mathbf{R}(\mathbf{e})\mathbf{t}_1. \tag{4.3}$$

Definition 4.3 *For a pair of point-tangent data $((\mathbf{q}_0, \mathbf{t}_0), (\mathbf{q}_1, \mathbf{t}_1)) \in \mathcal{J} \times \mathcal{J}$, the circle with tangent $\mathbf{t}_0$ at $\mathbf{q}_0$ passing through $\mathbf{q}_1$ is denoted by $\mathcal{C}_0$, and the circle with tangent $\mathbf{t}_1$ at $\mathbf{q}_1$ passing through $\mathbf{q}_0$ by $\mathcal{C}_1$. If $\mathbf{t}_0 + \mathbf{t}_1^\star \neq 0$, the circle with tangent $\mathbf{t}_0 + \mathbf{t}_1^\star$ at $\mathbf{q}_0$ passing through $\mathbf{q}_1$ is denoted by $\mathcal{C}_+$, while if $\mathbf{t}_0 - \mathbf{t}_1^\star \neq 0$, the circle with tangent $\mathbf{t}_0 - \mathbf{t}_1^\star$ at $\mathbf{q}_0$ passing through $\mathbf{q}_1$ is denoted $\mathcal{C}_-$.*

For any circle $\mathcal{C}$ passing through $\mathbf{q}_0$ and $\mathbf{q}_1$ we denote by $\mathcal{C}'$ the circle $\mathcal{C}$ punctured at $\mathbf{q}_0$ and $\mathbf{q}_1$.

Definition 4.4 *A pair of point-tangent data $((\mathbf{q}_0, \mathbf{t}_0), (\mathbf{q}_1, \mathbf{t}_1)) \in \mathcal{J} \times \mathcal{J}$ will be described as* cocircular *if $\mathcal{C}_0 = \mathcal{C}_1$. A cocircular pair of point-tangent data can be classified as either* compatible *or* incompatible *dependent upon the orientations they induce for their common circle.*

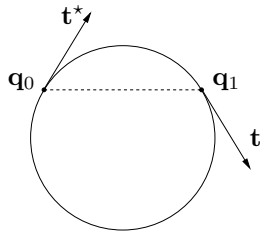

Figure 4.2: Given two distinct points $\mathbf{q}_0$ and $\mathbf{q}_1$ and a vector $\mathbf{t}$, there is a unique circle passing through $\mathbf{q}_0$ and $\mathbf{q}_1$ with tangent $\mathbf{t}$ at $\mathbf{q}_1$. The rotation matrix $\mathbf{R}(\mathbf{e})$ defined in equation (4.2) maps the vector $\mathbf{t}$ into the compatibly oriented tangent $\mathbf{t}^\star$ at $\mathbf{q}_0$.

We remark that the case of compatible cocircular data is equivalent to $\mathbf{t}_0 - \mathbf{t}_1^\star = 0$, so that in Definition 4.3 $\mathcal{C}_-$ is not defined, while the incompatible cocircular case has $\mathbf{t}_0 + \mathbf{t}_1^\star = 0$, so that $\mathcal{C}_+$ is not defined.

Elementary geometry demonstrates that any pair of point-tangent data that are non-cocircular define a unique sphere $\mathcal{S}$ containing both points and with each tangent contained in the corresponding tangent plane to the sphere (cf. Figure 4.1). We shall call $\mathcal{S}$ the double tangent sphere generated by $((\mathbf{q}_0, \mathbf{t}_0), (\mathbf{q}_1, \mathbf{t}_1))$. In the case $|\mathbf{t}_0 \times \mathbf{t}_1 \cdot \mathbf{e}| = 0$ with $((\mathbf{q}_0, \mathbf{t}_0), (\mathbf{q}_1, \mathbf{t}_1))$ coplanar, but non-cocircular, the double tangent sphere is the plane. When $|\mathbf{t}_0 \times \mathbf{t}_1 \cdot \mathbf{e}| \neq 0$, the radius of $\mathcal{S}$ is given by

$$R = \frac{|\mathbf{d}|}{2} \frac{|\sin\alpha|}{|\mathbf{t}_0 \times \mathbf{t}_1 \cdot \mathbf{e}|} = \frac{|\mathbf{d}|}{2} \frac{\sqrt{1 - (\mathbf{t}_1^\star \cdot \mathbf{t}_0)^2}}{|\mathbf{t}_0 \times \mathbf{t}_1 \cdot \mathbf{e}|},$$

where α is the angle between the unit vectors $\mathbf{t}_0$ and $\mathbf{t}_1^\star$, and the centre $\mathbf{c}$ is given by

$$\mathbf{c} = \mathbf{q}_0 + \frac{|\mathbf{d}|}{2} \frac{\mathbf{t}_1^\star \times \mathbf{t}_0}{\mathbf{t}_0 \times \mathbf{t}_1 \cdot \mathbf{e}}.$$

In the non-cocircular case all four circles introduced in Definition 4.3 exist, pass through $\mathbf{q}_0$ and $\mathbf{q}_1$, and lie on the sphere $\mathcal{S}$. The circles $\mathcal{C}_+$ and $\mathcal{C}_-$ are mutually perpendicular and bisect the angles between $\mathcal{C}_0$ and $\mathcal{C}_1$, see Figure 4.3.

For a compatible, cocircular pair of point-tangent data their common arc can be considered as a family of biarcs. Incompatible pairs of point-tangent data are degenerate in another way, but we first discuss the more typical case of non-cocircular pairs of point-tangent data. Suppose therefore that $((\mathbf{q}_0, \mathbf{t}_0), (\mathbf{q}_1, \mathbf{t}_1)) \in \mathcal{J} \times \mathcal{J}$ is a non-cocircular point-tangent data pair. Do there exist one or more biarcs interpolating this data? That is, can one draw a circle $\mathbf{a}$ passing through $\mathbf{q}_0$, tangent to $\mathbf{t}_0$ at $\mathbf{q}_0$, and a circle $\bar{\mathbf{a}}$ passing through $\mathbf{q}_1$, tangent to $\mathbf{t}_1$ at $\mathbf{q}_1$, such that the two circles $\mathbf{a}$ and $\bar{\mathbf{a}}$ intersect at some point $\mathbf{m}$ with a common tangent? This question was answered (for the three dimensional case) in [53, pp. 52, 68, 70] and [54, pp. 396-401]. Their results can be summarised in our notation as:

Proposition 4.5 *(Sharrock) For a point-tangent data pair $((\mathbf{q}_0, \mathbf{t}_0), (\mathbf{q}_1, \mathbf{t}_1)) \in \mathcal{J} \times \mathcal{J}$ that is non-cocircular, there is a nonempty set of possible matching points $\mathbf{m}$ corresponding to compatibly oriented arcs. For each matching point $\mathbf{m}$ the biarc is unique. Moreover*

1. *The set $\Sigma_+ \subset \mathbb{R}^3$ of all possible matching points is a circle (punctured at $\mathbf{q}_0$ and $\mathbf{q}_1$).*

2. *All biarcs lie on the double tangent sphere generated by $((\mathbf{q}_0, \mathbf{t}_0), (\mathbf{q}_1, \mathbf{t}_1))$.*

3. *There is a unique biarc through every point on the double tangent sphere punctured at $\mathbf{q}_0$ and $\mathbf{q}_1$ (i.e. the set of all possible biarcs is a simple covering of the double tangent sphere $\mathcal{S}$).*

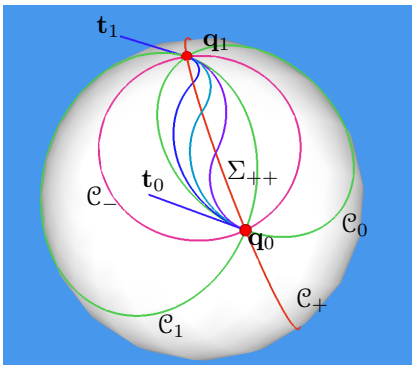

Figure 4.3: A proper (cf. Definition 4.10) point-tangent data pair with the circles $\mathcal{C}_0$, $\mathcal{C}_1$, $\mathcal{C}_+$, $\mathcal{C}_-$ introduced in Definition 4.3, and three proper biarcs with matching points on Σ_{++} (cf. Definition 4.8). Every biarc and every circle lie on the double tangent sphere $\mathcal{S}$.

We remark that a point-tangent data pair $((\mathbf{q}_0, \mathbf{t}_0), (\mathbf{q}_1, \mathbf{t}_1)) \in \mathcal{J}_n \times \mathcal{J}_n$, where $\mathcal{J}_n = \mathbb{R}^n \times S^{n-1}$ with $n \geq 3$, naturally and generically defines a three dimensional affine subspace $\mathcal{V}$, with $\mathbf{q}_0$, $\mathbf{q}_0 + \mathbf{t}_0$, $\mathbf{q}_1$, and $\mathbf{q}_1 + \mathbf{t}_1 \in \mathcal{V}$. Therefore the same biarc construction is also possible for point-tangent data associated with $\mathbb{R}^n$, $n > 3$. A treatment of this case, along with a discussion of biarcs on the $(n-1)$ dimensional sphere S^{n-1}, can be found in [64]. See also the discussion in section 9 below.

Two proofs of Proposition 4.5 can be found in [53, p. 194]. One approach uses the fact that the biarc construction is invariant under inversions in spheres [7, p. 77] to reduce to an equivalent planar problem. We re-use this approach in the proof of the sharpened results described in Proposition 4.7, for which we need

Definition 4.6 *(cf. [7, p. 85]) A* tangent pencil $\mathcal{P}(\mathbf{q}, \mathcal{C})$ of oriented coaxal circles *is the two parameter family of oriented circles that touch the oriented circle $\mathcal{C}$ at the point $\mathbf{q}$ with common oriented tangent.*

Proposition 4.7 *For a given point-tangent data pair $((\mathbf{q}_0, \mathbf{t}_0), (\mathbf{q}_1, \mathbf{t}_1)) \in \mathcal{J} \times \mathcal{J}$, consider the circles $\mathcal{C}_0$, $\mathcal{C}_1$, $\mathcal{C}_+$, and $\mathcal{C}_-$ defined in Definition 4.3, denote by $\Sigma_+ \subset \mathbb{R}^3$ the set of matching points of all biarcs interpolating $((\mathbf{q}_0, \mathbf{t}_0), (\mathbf{q}_1, \mathbf{t}_1))$, and by $\Sigma_- \subset \mathbb{R}^3$ the set of matching points of all biarcs interpolating $((\mathbf{q}_0, \mathbf{t}_0), (\mathbf{q}_1, -\mathbf{t}_1))$. Then:*

1. *If $((\mathbf{q}_0, \mathbf{t}_0), (\mathbf{q}_1, \mathbf{t}_1))$ is non-cocircular, then Σ_+ is the punctured circle $\mathcal{C}'_+$, and Σ_- is the punctured circle $\mathcal{C}'_-$.*

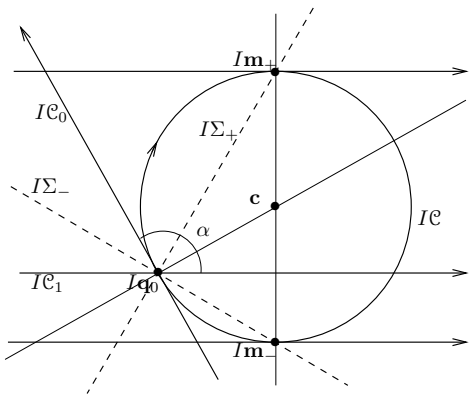

Figure 4.4: Geometry on the double tangent plane $I\mathcal{S}$.

2. *If* $((\mathbf{q}_0, \mathbf{t}_0), (\mathbf{q}_1, \mathbf{t}_1))$ *is cocircular, then*

   (a) *if the data is compatible,* Σ_+ *is the common punctured circle* $\mathcal{C}'_+ = \mathcal{C}'_0 = \mathcal{C}'_1$*, and* Σ_- *is the punctured sphere passing through* $\mathbf{q}_0$ *and* $\mathbf{q}_1$ *perpendicular to the circle* $\mathcal{C}_+$*, while*

   (b) *if the data is incompatible,* Σ_- *is the common punctured circle* $\mathcal{C}'_- = \mathcal{C}'_0 = \mathcal{C}'_1$*, and* Σ_+ *is the punctured sphere passing through* $\mathbf{q}_0$ *and* $\mathbf{q}_1$ *perpendicular to the circle* $\mathcal{C}_-$*.*

3. *The locus* Σ_+ *is a punctured straight line if and only if* $\mathbf{t}_0 = \mathbf{t}_1$ *with* $\mathbf{t}_0 \cdot \mathbf{e} \neq 0$*.*

4. *The locus* Σ_+ *is a punctured plane if and only if* $\mathbf{t}_0 = \mathbf{t}_1$ *with* $\mathbf{t}_0 \cdot \mathbf{e} = 0$*.*

Thus the matching locus $\Sigma_\pm$ is (respectively) the circle $\mathcal{C}_\pm$ whenever it exists, and is otherwise an associated sphere. The matching locus Σ_+ has infinite radius if and only if $\mathbf{t}_0 = \mathbf{t}_1$.

Proof

1. The inversion I in a sphere centred at the data point $\mathbf{q}_1$ and passing through $\mathbf{q}_0$, sends $\mathbf{q}_1$ to infinity and therefore transforms the double tangent sphere $\mathcal{S}$ into a plane $I\mathcal{S}$. Similarly, the tangent pencil $\mathcal{P}(\mathbf{q}_1, \mathcal{C}_1)$ is transformed into a pencil $\mathcal{P}(I\mathbf{q}_1, I\mathcal{C}_1)$ of oriented straight lines, all parallel to the straight line $I\mathcal{C}_1$ passing through $I\mathbf{q}_0$. Because the data is non-cocircular, $I\mathcal{C}_0$ is another, non-parallel, line also passing through $\mathbf{q}_0$, and so $I\mathcal{C}_0$ and $I\mathcal{C}_1$ span the plane $I\mathcal{S}$.

   To obtain the locus of possible matching points of a biarc $(\mathbf{a}, \bar{\mathbf{a}})$, we note that the inversion $I\bar{\mathbf{a}}$ of the arc $\bar{\mathbf{a}}$ passing through $\mathbf{q}_1$ must be an oriented half-line drawn from the pencil $\mathcal{P}(I\mathbf{q}_1, I\mathcal{C}_1)$, while the inversion $I\mathbf{a}$ of the arc $\mathbf{a}$ passing through $\mathbf{q}_0$ must be drawn from a member $I\mathcal{C}$ of the pencil $\mathcal{P}(I\mathbf{q}_0, I\mathcal{C}_0)$. To satisfy the matching condition between sub-arcs, $I\mathcal{C}$ must be tangent to an element of $\mathcal{P}(I\mathbf{q}_1, I\mathcal{C}_1)$. But because $I\mathcal{C}_0$ and $I\mathcal{C}_1$ span the plane $I\mathcal{S}$, this is only possible if $I\mathcal{C} \subset I\mathcal{S}$. We therefore see that all biarcs $(\mathbf{a}, \bar{\mathbf{a}})$ lie on the double tangent sphere $\mathcal{S}$ and it suffices to study the geometry within the double tangent plane $I\mathcal{S}$, see Figure 4.4.

Each circle $I\mathcal{C} \in \mathcal{P}(I\mathbf{q}_0, I\mathcal{C}_0)$ contained in $I\mathcal{S}$ touches elements of the pencil $\mathcal{P}(I\mathbf{q}_1, I\mathcal{C}_1)$ at two diametrically opposed points $I\mathbf{m}_+$ and $I\mathbf{m}_-$, with the sign induced by compatible or incompatible orientations. By construction the diameter through $I\mathbf{m}_+$ and $I\mathbf{m}_-$ is perpendicular to elements of $\mathcal{P}(I\mathbf{q}_1, I\mathcal{C}_1)$, and the radius of $I\mathcal{C}$ through $I\mathbf{q}_0$ is perpendicular to $I\mathcal{C}_0$. We denote the angle between $I\mathcal{C}_0$ and $I\mathcal{C}_1$ by α. It follows by elementary geometry that the angle $\angle(I\mathbf{q}_0, \mathbf{c}, I\mathbf{m}_+)$ equals α. Then the angle $\angle(I\mathbf{q}_0, I\mathbf{m}_+, \mathbf{c}) = \frac{1}{2}(\pi - \alpha)$. But the angle between the line $I\mathcal{C}_1$ and the line between $I\mathbf{m}_+$ and $I\mathbf{q}_0$ is the complement $\frac{1}{2}\pi - \frac{1}{2}(\pi - \alpha) = \frac{1}{2}\alpha$. Thus an arbitrary matching point $I\mathbf{m}_+$ respecting orientation lies on a line bisecting the angle between $I\mathcal{C}_0$ and $I\mathcal{C}_1$.

Moreover the line through $I\mathbf{m}_+$ and $I\mathbf{q}_0$ is perpendicular to the line through $I\mathbf{m}_-$ and $I\mathbf{q}_0$ because they subtend a diameter of $I\mathcal{C}$. Therefore $I\mathbf{m}_-$ lies on the other bisector of the angle between $I\mathcal{C}_0$ and $I\mathcal{C}_1$.

Consequently Σ_+ is contained in one of the two perpendicular circles lying on $\mathcal{S}$, passing through $\mathbf{q}_0$ and $\mathbf{q}_1$, that bisect the angle between $\mathcal{C}_0$ and $\mathcal{C}_1$. But the construction is reversible so that Σ_+ equals one of these two (punctured) circles. Examining all possible cases yields that $\mathbf{t}_0 + \mathbf{t}_1^\star$ is the tangent to Σ_+, so that $\Sigma_+ = \mathcal{C}'_+$, and $\mathbf{t}_0 - \mathbf{t}_1^\star$ is tangent to Σ_-, so that $\Sigma_- = \mathcal{C}'_-$.

2. If the data is cocircular, we apply the same inversion I as above. This time $I\mathcal{C}_0$ is parallel or anti-parallel to the elements of the pencil $\mathcal{P}(I\mathbf{q}_1, I\mathcal{C}_1)$. A member $I\mathcal{C}$ of $\mathcal{P}(I\mathbf{q}_0, I\mathcal{C}_0)$ can touch one of the straight parallel lines in $\mathcal{P}(I\mathbf{q}_1, I\mathcal{C}_1)$ only in the plane perpendicular to $I\mathcal{C}_0$ at $I\mathbf{q}_0$, or on $I\mathcal{C}_0$ when $I\mathcal{C} = I\mathcal{C}_0$. Depending on whether the data is incompatible or compatible, the plane corresponds to the matching points on Σ_+, and any point on the line $I\mathcal{C}_0$ corresponds to the matching points on Σ_-, or vice versa.

3. By parts 1. and 2. when the locus Σ_+ is a punctured straight line, then the straight line is $\mathcal{C}_+$, and the data therefore can not be incompatible cocircular, i.e. $\mathbf{t}_0 + \mathbf{t}_1^\star \neq 0$. In particular the case $\mathbf{t}_0 = \mathbf{t}_1$ with $\mathbf{t}_0 \cdot \mathbf{e} = \mathbf{t}_1 \cdot \mathbf{e} = 0$ can not arise. Because $\mathcal{C}_+$ is straight, its tangent $\mathbf{t}_0 + \mathbf{t}_1^\star$ is parallel to $\mathbf{e}$. Using (4.2) and (4.3) we deduce that $\mathbf{t}_0 - \mathbf{t}_1$ is parallel to $\mathbf{e}$, i.e. $\mathbf{t}_0 - \mathbf{t}_1 = \lambda\mathbf{e}$, for some $\lambda \in \mathbb{R}$. Because $\mathbf{t}_0$ and $\mathbf{t}_1$ are both unit vectors the case $\lambda \neq 0$ can only occur when the data is incompatible cocircular, a contradiction. Hence $\lambda = 0$, and $\mathbf{t}_0 = \mathbf{t}_1$.

   Contrariwise, if $\mathbf{t}_0 = \mathbf{t}_1$ and $\mathbf{t}_0 \cdot \mathbf{e} \neq 0$, the data is not incompatible cocircular, so that $\mathcal{C}_+$ is defined, and $\Sigma_+ = \mathcal{C}'_+$. But by (4.3)

$$\mathbf{t}_0 + \mathbf{t}_1^\star = \mathbf{t}_0 + 2\mathbf{t}_1 \cdot \mathbf{e}\, \mathbf{e} - \mathbf{t}_1 = \mathbf{t}_0 + 2\mathbf{t}_0 \cdot \mathbf{e}\, \mathbf{e} - \mathbf{t}_0 = 2\mathbf{t}_0 \cdot \mathbf{e}\, \mathbf{e},$$

   so that $\mathcal{C}_+$ is in fact the straight line through $\mathbf{q}_0$ and $\mathbf{q}_1$.

4. By parts 1. and 2. when the locus Σ_+ is a punctured plane, then the data is incompatible cocircular, i.e. $0 = \mathbf{t}_0 + \mathbf{t}_1^\star = \mathbf{t}_0 + 2(\mathbf{t}_1 \cdot \mathbf{e})\mathbf{e} - \mathbf{t}_1$. It only remains to show that $\mathbf{t}_1 \cdot \mathbf{e} = 0$, but, again by part 2., the punctured plane Σ_+ passing through $\mathbf{q}_0$ and $\mathbf{q}_1$ is perpendicular to the circle $\mathcal{C}_1$, thus $\mathbf{t}_1 \cdot \mathbf{e} = 0$.

On the other hand, if $\mathbf{t}_0 = \mathbf{t}_1$ and $\mathbf{t}_0 \cdot \mathbf{e} = 0$, then $\mathbf{t}_0 + \mathbf{t}_1^\star = \mathbf{t}_0 + 2(\mathbf{t}_1 \cdot \mathbf{e})\mathbf{e} - \mathbf{t}_1 = 0$, so the data is incompatible cocircular. By part 2.(b), Σ_+ is the punctured sphere passing through $\mathbf{q}_0$ and $\mathbf{q}_1$ perpendicular to the circle $\mathcal{C}_0$. But $\mathcal{C}_0$ has tangent $\mathbf{t}_0$ at $\mathbf{q}_0$, and as $\mathbf{t}_0 \cdot \mathbf{e} = 0$, Σ_+ is a (punctured) plane.

■

We emphasise that the matching set Σ_+ is truly punctured at $\mathbf{q}_0$ and $\mathbf{q}_1$ in the following sense. Given any matching point $\mathbf{m}$ on Σ_+ the mutual tangent at the matching point is given by the formulæ

$$\mathbf{t}_\mathbf{m} = \mathbf{R}(\mathbf{e}_\mathbf{m})\mathbf{t}_0 = \mathbf{R}(\bar{\mathbf{e}}_\mathbf{m})\mathbf{t}_1, \tag{4.4}$$

where $\mathbf{R}(\mathbf{e}_\mathbf{m})$ is the matrix defined in (4.2) applied to the unit chords

$$\mathbf{e}_\mathbf{m} := \frac{\mathbf{m} - \mathbf{q}_0}{|\mathbf{m} - \mathbf{q}_0|}, \qquad \text{and} \qquad \bar{\mathbf{e}}_\mathbf{m} := \frac{\mathbf{q}_1 - \mathbf{m}}{|\mathbf{q}_1 - \mathbf{m}|}. \tag{4.5}$$

Then given a point-tangent data pair $((\mathbf{q}_0, \mathbf{t}_0), (\mathbf{q}_1, \mathbf{t}_1)) \in \mathcal{J} \times \mathcal{J}$ that is not compatible cocircular, in the limit as $\mathbf{m} \in \Sigma_+$ approaches the point $\mathbf{q}_0$, $\mathbf{t}_\mathbf{m} = \mathbf{t}_1^\star \neq \mathbf{t}_0$, and the limiting arc does not interpolate the data. In the same limit the radius of the arc $\mathbf{a}$ tends to zero, while $\angle\mathbf{a}$ approaches the angle α between $\mathbf{t}_0$ and $\mathbf{t}_1^\star$, and the radius of the arc $\bar{\mathbf{a}}$ tends to the radius of $\mathcal{C}_1$. Similarly, as $\mathbf{m}$ approaches the point $\mathbf{q}_1$, the radius of the arc $\mathbf{a}$ tends to the radius of $\mathcal{C}_0$, the radius of the arc $\bar{\mathbf{a}}$ tends to zero, and $\angle\bar{\mathbf{a}}$ approaches the angle α between $\mathbf{t}_0^\star$ and $\mathbf{t}_1$. Due to this puncturing it is useful to further divide Σ_+ according to:

Definition 4.8 *Given a point-tangent data pair $((\mathbf{q}_0, \mathbf{t}_0), (\mathbf{q}_1, \mathbf{t}_1)) \in \mathcal{J} \times \mathcal{J}$ that is not incompatible cocircular, i.e. $\mathbf{t}_0 + \mathbf{t}_1^\star \neq 0$, we denote by Σ_{++} the sub-arc of Σ_+ from $\mathbf{q}_0$ to $\mathbf{q}_1$ with the orientation induced by the tangent $\mathbf{t}_0 + \mathbf{t}_1^\star$.*

4.2 Tangent indicatrix

Given a C^1 curve $\mathbf{q}$ parametrised by arc length s we may study the *tangent indicatrix*, i.e. the curve $\mathbf{q}'$ of tangents on the unit sphere S^2. Given a point-tangent data pair $((\mathbf{q}_0, \mathbf{t}_0), (\mathbf{q}_1, \mathbf{t}_1)) \in \mathcal{J} \times \mathcal{J}$, how does the construction described in Proposition 4.7 translate to the sphere? The tangent indicatrix of a circle is a great circle, so that the tangent indicatrix of a biarc is two arcs of great circles that intersect, but which in general form a corner.

Proposition 4.9 *For a point-tangent data pair $((\mathbf{q}_0, \mathbf{t}_0), (\mathbf{q}_1, \mathbf{t}_1)) \in \mathcal{J} \times \mathcal{J}$, consider $\mathbf{t}_0, \mathbf{t}_1, \mathbf{e}$, and $\mathbf{t}_0^\star$ and $\mathbf{t}_1^\star$ defined in (4.3) as points on S^2, cf. figure 4.5. Denote by $\Theta \subset S^2$ the set of matching tangents $\mathbf{t}_\mathbf{m}$ of all biarcs interpolating $((\mathbf{q}_0, \mathbf{t}_0), (\mathbf{q}_1, \mathbf{t}_1))$, and when the data is not incompatible cocircular denote by $\Theta_{++} \subset \Theta$ the set of matching tangents $\mathbf{t}_\mathbf{m}$ at matching points $\mathbf{m} \in \Sigma_{++}$. Then:*

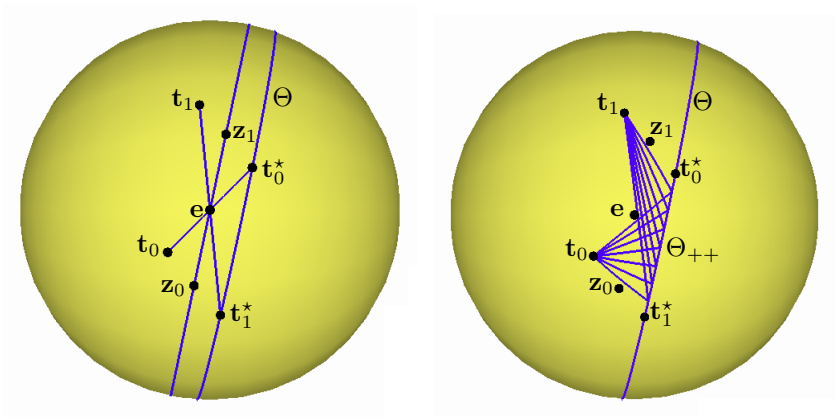

(a) (b)

Figure 4.5: The tangent indicatrix for a generic, non-cocircular case with $\mathbf{t}_0 \neq \mathbf{t}_1$. The unit chord $\mathbf{e}$, tangents $\mathbf{t}_0$ and $\mathbf{t}_1$, rotated tangents $\mathbf{t}_0^\star$ and $\mathbf{t}_1^\star$, and points $\mathbf{z}_0 = \frac{\mathbf{t}_0+\mathbf{t}_1^\star}{|\mathbf{t}_0+\mathbf{t}_1^\star|}$ and $\mathbf{z}_1 = \frac{\mathbf{t}_1+\mathbf{t}_0^\star}{|\mathbf{t}_1+\mathbf{t}_0^\star|}$ appear in both parts (a) and (b). Then part (a) depicts the punctured circle Θ of matching tangents $\mathbf{t_m}$ that is parallel to the tangent indicatrix of Σ_+, while (b) illustrates the tangent indicatrices of seven biarcs with matching tangents $\mathbf{t_m}$ on Θ_{++}, corresponding to matching points $\mathbf{m} \in \Sigma_{++}$.

1. *If* $((\mathbf{q}_0, \mathbf{t}_0), (\mathbf{q}_1, \mathbf{t}_1))$ *is non-cocircular with* $\mathbf{t}_0 \neq \mathbf{t}_1$*, then* Θ *is the circle punctured at* $\mathbf{t}_0^\star$ *and* $\mathbf{t}_1^\star$ *that passes through* $\mathbf{t}_0^\star$*,* $\mathbf{t}_1^\star$*,* $-\mathbf{t}_0$*, and* $-\mathbf{t}_1$*, and so is a great circle if and only if* $\mathbf{e} \cdot \mathbf{t}_0 \times \mathbf{t}_1 = 0$*. The circle is always parallel to the tangent indicatrix of the physical matching circle* $\mathcal{C}_+$*, i.e. to the great circle through* $\mathbf{e}$*,* $\mathbf{z}_0 := \frac{\mathbf{t}_0+\mathbf{t}_1^\star}{|\mathbf{t}_0+\mathbf{t}_1^\star|}$*, and* $\mathbf{z}_1 := \frac{\mathbf{t}_1+\mathbf{t}_0^\star}{|\mathbf{t}_1+\mathbf{t}_0^\star|}$.

2. *If* $((\mathbf{q}_0, \mathbf{t}_0), (\mathbf{q}_1, \mathbf{t}_1))$ *is cocircular with* $\mathbf{t}_0 \neq \mathbf{t}_1$*, then*

   (a) *if the data is compatible, the conclusions are as in case 1., except that* Θ *is necessarily a (punctured) great circle, while*

   (b) *if the data is incompatible,* Θ *is the whole sphere* S^2 *punctured at* $\mathbf{t}_1^\star = -\mathbf{t}_0$ *and* $\mathbf{t}_0^\star = -\mathbf{t}_1$.

3. *If* $\mathbf{t}_0 = \mathbf{t}_1$*, then* $\Theta = \{\mathbf{t}_0^\star\} = \{\mathbf{t}_1^\star\}$*, i.e. the only possible matching tangent is* $\mathbf{t_m} = \mathbf{t}_0^\star = \mathbf{t}_1^\star$.

4. *If* $\mathbf{t}_0 \neq \mathbf{t}_1$*, and the data is not incompatible cocircular, then* Θ_{++} *is the open arc of* Θ *between* $\mathbf{t}_1^\star$ *and* $\mathbf{t}_0^\star$ *with orientation induced by the parallel great circle passing through, and oriented by,* $\mathbf{z}_0$*,* $\mathbf{e}$ *and* $\mathbf{z}_1$.

Proof

1. For a given $\mathbf{m} \in \Sigma_+$ we use the notation (4.5) for the unit chord $\mathbf{e_m}$, and by (4.4), the matching tangent satisfies

$$\mathbf{t_m} = \mathbf{R}(\mathbf{e_m})\mathbf{t}_0 = 2(\mathbf{e_m} \cdot \mathbf{t}_0)\mathbf{e_m} - \mathbf{t}_0.$$

Denote the binormal to the physical matching circle $\mathcal{C}_+$ by $\mathbf{b} = \mathbf{e_m} \times \bar{\mathbf{e}}_\mathbf{m}$, which is well defined because $\mathbf{t}_0 \neq \mathbf{t}_1$. Then

$$\mathbf{t_m} \cdot \mathbf{b} = 2(\mathbf{e_m} \cdot \mathbf{t}_0)(\mathbf{e_m} \cdot \mathbf{b}) - \mathbf{t}_0 \cdot \mathbf{b} = -\mathbf{t}_0 \cdot \mathbf{b},$$

a constant independent of $\mathbf{m} \in \Sigma_+$. This shows that all matching tangents $\mathbf{t_m}$ lie on the circle through $-\mathbf{t}_0$, with binormal $\mathbf{b}$. Analogously we find $\mathbf{t_m} \cdot \mathbf{b} = -\mathbf{t}_1 \cdot \mathbf{b}$ for each matching tangent $\mathbf{t_m}$. From $(\mathbf{t}_0^\star + \mathbf{t}_1) \cdot \mathbf{b} = 0$ and $(\mathbf{t}_1^\star + \mathbf{t}_0) \cdot \mathbf{b} = 0$, we obtain $\mathbf{t}_0^\star \cdot \mathbf{b} = -\mathbf{t}_1 \cdot \mathbf{b}$ and $\mathbf{t}_1^\star \cdot \mathbf{b} = -\mathbf{t}_0 \cdot \mathbf{b}$. This shows that all four points $\mathbf{t}_0^\star$, $\mathbf{t}_1^\star$, $-\mathbf{t}_0$, and $-\mathbf{t}_1$ lie on the *circle of matching tangents* $\mathbf{t_m}$. By construction the circle is great if and only if $\mathbf{e} \cdot \mathbf{t}_0 \times \mathbf{t}_1 = 0$.

On the other hand, given a point $\mathbf{t}$ on the circle of matching tangents, $\mathbf{t}_1^\star \neq \mathbf{t} \neq \mathbf{t}_0^\star$, and because $\mathbf{t}_1 \neq \mathbf{t}_0$, at least one of the great circles through $\mathbf{t}$ and $\mathbf{t}_0$, or through $\mathbf{t}$ and $\mathbf{t}_1$, is uniquely defined. Therefore at least one of the chords $\mathbf{e_m}$ and $\bar{\mathbf{e}}_\mathbf{m}$ is well-defined as the intersection between the tangent indicatrix of $\mathcal{C}_+$ and one of the great circles. Assuming $\mathbf{e_m}$ is so fixed, the corresponding matching point $\mathbf{m}$ is the intersection of $\mathcal{C}_+$ and the straight line $\mathbf{q}_0 + \mu \mathbf{e_m},\ \mu \in \mathbb{R}$.

2. (a) In this case Σ_+ is still the punctured circle $\mathcal{C}'_+$, and the proof is identical with that of part 1., except that necessarily $\mathbf{e} \cdot \mathbf{t}_0 \times \mathbf{t}_1 = 0$ for cocircular data.

   (b) If the data $((\mathbf{q}_0, \mathbf{t}_0), (\mathbf{q}_1, \mathbf{t}_1))$ is incompatible cocircular then Σ_+ is a sphere punctured at $\mathbf{q}_0$ and $\mathbf{q}_1$ with either $\mathbf{t}_0$ and $\mathbf{t}_1$ or $-\mathbf{t}_0$ and $-\mathbf{t}_1$ pointing to the centre. Arcs tangent at $\mathbf{q}_0$ to $\mathbf{t}_0$ intersect this sphere anywhere on its surface, but always orthogonally. That is any direction except $-\mathbf{t}_0$ (at $\mathbf{q}_0$) and $-\mathbf{t}_1$ (at $\mathbf{q}_1$) is a possible matching tangent.

3. If $\mathbf{t}_0 = \mathbf{t}_1$, then by Proposition 4.7 the locus Σ_+ is either a straight (punctured) line, or the (punctured) plane perpendicular to $\mathbf{t}_0$ passing through $\mathbf{q}_0$, so that each arc $\bar{\mathbf{a}}$ sweeps out an angle of π. In either case the result follows from the elementary reflector formula (4.2).

4. Suppose $\mathbf{t}_0 + \mathbf{t}_1^\star \neq 0$ and $\mathbf{t}_0 \neq \mathbf{t}_1$. Then as $\mathbf{m} \in \Sigma_{++}$ moves from $\mathbf{q}_0$ to $\mathbf{q}_1$, the chord $\mathbf{e_m}$ moves from $\mathbf{z}_0 = \frac{\mathbf{t}_0 + \mathbf{t}_1^\star}{|\mathbf{t}_0 + \mathbf{t}_1^\star|}$ to $\mathbf{e}$, and the chord $\bar{\mathbf{e}}_\mathbf{m}$ moves from $\mathbf{e}$ to $\mathbf{z}_1 = \frac{\mathbf{t}_0^\star + \mathbf{t}_1}{|\mathbf{t}_0^\star + \mathbf{t}_1|}$, cf. Figure 4.5(b). By (4.4) the matching tangent $\mathbf{t_m}$ is the reflection of $\mathbf{t}_0$ on the chord $\mathbf{e_m}$, and therefore moves from $\mathbf{t}_1^\star$ to $\mathbf{t}_0^\star$, following the orientation of the indicatrix of the physical matching circle.

■

Definition 4.10 *The point-tangent data pair* $((\mathbf{q}_0, \mathbf{t}_0), (\mathbf{q}_1, \mathbf{t}_1)) \in \mathcal{J} \times \mathcal{J}$ *will be called* proper *if*

$$\begin{aligned} &(\mathbf{q}_1 - \mathbf{q}_0) \cdot \mathbf{t}_0 > 0, \\ \textit{and} \qquad & \\ &(\mathbf{q}_1 - \mathbf{q}_0) \cdot \mathbf{t}_1 > 0. \end{aligned} \tag{4.6}$$

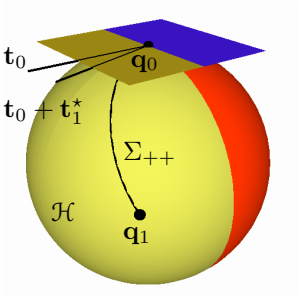

Figure 4.6: For proper point-tangent data pairs, the arc Σ_{++} lies entirely in the hemisphere $\mathcal{H}$ (4.7) of the double tangent sphere $\mathcal{S}$.

Recall that for any arc $\mathbf{a}$, $\angle\mathbf{a}$ denotes the swept out angle.

Proposition 4.11 *For a proper point-tangent data pair* $((\mathbf{q}_0, \mathbf{t}_0), (\mathbf{q}_1, \mathbf{t}_1)) \in \mathcal{J} \times \mathcal{J}$,

1. $\angle\Sigma_{++} < \pi$, *and*
2. *for any biarc* $(\mathbf{a}, \bar{\mathbf{a}})$ *with matching point* $\mathbf{m} \in \Sigma_{++}$, $\angle\mathbf{a} < \pi$ *and* $\angle\bar{\mathbf{a}} < \pi$.

Proof

1. The data $((\mathbf{q}_0, \mathbf{t}_0), (\mathbf{q}_1, \mathbf{t}_1)) \in \mathcal{J} \times \mathcal{J}$ is proper, therefore
$$(\mathbf{t}_0 + \mathbf{t}_1^\star) \cdot \mathbf{d} = \mathbf{t}_0 \cdot \mathbf{d} + \mathbf{t}_1^\star \cdot \mathbf{d} = \mathbf{t}_0 \cdot \mathbf{d} + \mathbf{t}_1 \cdot \mathbf{d} > 0.$$
Thus, as $\mathbf{t}_0 + \mathbf{t}_1^\star$ is the tangent to Σ_{++} at $\mathbf{q}_0$, and $\mathbf{d}$ is the chord subtending the arc Σ_{++}, $\angle\Sigma_{++} < \pi$.

2. Denote by $\mathcal{H}$ the hemisphere of the double tangent sphere $\mathcal{S}$ satisfying
$$\mathcal{H} = \{\mathbf{p} \in \mathcal{S} : (\mathbf{p} - \mathbf{q}_0) \cdot \mathbf{t}_0 > 0\}, \tag{4.7}$$
and remark that $\mathcal{H}$ is the set of all points on $\mathcal{S}$ that are endpoints of an arc through $\mathbf{q}_0$ with (oriented) tangent $\mathbf{t}_0$ at $\mathbf{q}_0$, and with swept out angle less than π. Then:
   (a) $\mathbf{q}_1 \in \mathcal{H}$, because $\mathbf{d} \cdot \mathbf{t}_0 > 0$.
   (b) $(\mathbf{t}_0 + \mathbf{t}_1^\star) \cdot \mathbf{t}_0 > 0$, because $(\mathbf{t}_0 + \mathbf{t}_1^\star) \cdot \mathbf{t}_0 = 1 + \mathbf{t}_1^\star \cdot \mathbf{t}_0 > 0$ unless $\mathbf{t}_1^\star = -\mathbf{t}_0$. And if $\mathbf{t}_1^\star = -\mathbf{t}_0$, $\mathbf{t}_1 \cdot \mathbf{d} = \mathbf{t}_1^\star \cdot \mathbf{d} = -\mathbf{t}_0 \cdot \mathbf{d}$, which contradicts the data being proper.
   (c) $\Sigma_{++} \subset \mathcal{H}$ is a consequence of (a) and (b), see Figure 4.6.
   (d) By (c) any $\mathbf{m} \in \Sigma_{++}$ lies in $\mathcal{H}$, thus $\angle\mathbf{a} < \pi$.

   By a symmetry argument we deduce $\angle\bar{\mathbf{a}} < \pi$.

■

Definition 4.12 *We call a biarc* proper *if it interpolates a proper point-tangent data pair* $((\mathbf{q}_0, \mathbf{t}_0), (\mathbf{q}_1, \mathbf{t}_1)) \in \mathcal{J} \times \mathcal{J}$ *with a matching point* $\mathbf{m} \in \Sigma_{++}$.

Our goal is to approximate a given curve by interpolation of sampled point-tangent data. For sufficiently smooth curves, and a sufficiently fine sampling, the prescribed data will be proper, and Proposition 4.11 shows that it suffices to consider only proper biarcs.

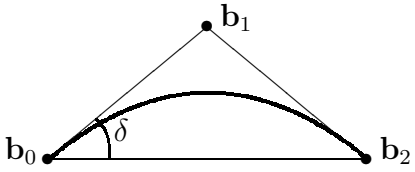

Figure 4.7: The isosceles Bézier control triangle of an arc.

4.3 Bézier points of Proper Biarcs

Dependent upon the situation, we regard a biarc either as a geometric subset of $\mathbb{R}^3$, or as a curve in $\mathbb{R}^3$, which may, for example, be parametrised by arc length or by using Bézier control points. Any conic section can be described by rational quadratic Bézier splines. In particular a circular arc $\mathbf{a}$ with $\angle\mathbf{a} < \pi$ can be parametrised using a Bézier control polygon that is a single isosceles triangle [15, p. 228],

$$\mathbf{a}(\tau) = \frac{(1-\tau)^2\mathbf{b}_0 + 2\omega\tau(1-\tau)\mathbf{b}_1 + \tau^2\mathbf{b}_2}{(1-\tau)^2 + 2\omega\tau(1-\tau) + \tau^2}, \qquad \tau \in [0,1], \tag{4.8}$$

where ω is the cosine of the base angle δ of the isosceles control triangle, that is,

$$\omega = \frac{(\mathbf{b}_1 - \mathbf{b}_0)\cdot(\mathbf{b}_2 - \mathbf{b}_0)}{|\mathbf{b}_1 - \mathbf{b}_0|\,|\mathbf{b}_2 - \mathbf{b}_0|} > 0,$$

where $\mathbf{b}_0, \mathbf{b}_1, \mathbf{b}_2$ are the control points, i.e. the vertices of the control triangle, cf. figure 4.7. By base length we refer to the distance $|\mathbf{b}_2 - \mathbf{b}_0|$, and by side length we understand the distance $|\mathbf{b}_1 - \mathbf{b}_0|$. Note that τ is not a uniform parameter in the sense that it is not a constant scaling of arc length, unless the arc is a straight line segment, that is unless $\mathbf{b}_1 = \frac{1}{2}(\mathbf{b}_0 + \mathbf{b}_2)$.

Lemma 4.13 *Given a proper point-tangent data pair* $((\mathbf{q}_0, \mathbf{t}_0), (\mathbf{q}_1, \mathbf{t}_1)) \in \mathcal{J} \times \mathcal{J}$ *and a proper biarc* $(\mathbf{a}, \bar{\mathbf{a}})$*, then:*

1. *The Bézier control points of the arc* Σ_{++} *are given by*

$$\mathbf{b}_0 = \mathbf{q}_0, \quad \mathbf{b}_1 = \frac{(\mathbf{t}_0\cdot\mathbf{d})\mathbf{q}_0 + (\mathbf{t}_1\cdot\mathbf{d})\mathbf{q}_1}{\mathbf{t}_0\cdot\mathbf{d} + \mathbf{t}_1\cdot\mathbf{d}} + \frac{|\mathbf{d}|^2(\mathbf{t}_0 - \mathbf{t}_1)}{2(\mathbf{t}_0\cdot\mathbf{d} + \mathbf{t}_1\cdot\mathbf{d})}, \quad \mathbf{b}_2 = \mathbf{q}_1.$$

2. *The Bézier control points of the arc* $\mathbf{a}$ *are*

$$\mathbf{b}_0 = \mathbf{q}_0, \quad \mathbf{b}_1 = \mathbf{q}_0 + \Lambda\frac{|\mathbf{d}|^2}{2\mathbf{t}_0\cdot\mathbf{d}}\mathbf{t}_0, \quad \mathbf{b}_2 = \mathbf{m}, \tag{4.9}$$

and the Bézier control points of the arc $\bar{\mathbf{a}}$ *are*

$$\mathbf{b}_0 = \mathbf{m}, \quad \mathbf{b}_1 = \mathbf{q}_1 - \bar{\Lambda}\frac{|\mathbf{d}|^2}{2\mathbf{t}_1\cdot\mathbf{d}}\mathbf{t}_1, \quad \mathbf{b}_2 = \mathbf{q}_1, \tag{4.10}$$

where $\mathbf{m} \in \Sigma_{++}$ *is the matching point given by the formula*

$$\mathbf{m} = \frac{\bar{\Lambda}(\mathbf{t}_0\cdot\mathbf{d})\mathbf{q}_0 + \Lambda(\mathbf{t}_1\cdot\mathbf{d})\mathbf{q}_1}{\Lambda\mathbf{t}_1\cdot\mathbf{d} + \bar{\Lambda}\mathbf{t}_0\cdot\mathbf{d}} + \frac{\Lambda\bar{\Lambda}|\mathbf{d}|^2(\mathbf{t}_0 - \mathbf{t}_1)}{2(\Lambda\mathbf{t}_1\cdot\mathbf{d} + \bar{\Lambda}\mathbf{t}_0\cdot\mathbf{d})}, \tag{4.11}$$

and Λ *and* $\bar{\Lambda} \in (0,1)$ *are two parameters that are roots of the equation*

$$0 = \Lambda\bar{\Lambda}(1 - \mathbf{t}_0 \cdot \mathbf{t}_1) + (\Lambda + \bar{\Lambda} - 1)\, 2\mathbf{t}_0 \cdot \mathbf{e}\, \mathbf{t}_1 \cdot \mathbf{e}. \tag{4.12}$$

If Λ *is regarded as the independent variable,* $\bar{\Lambda}$ *is given by*

$$\begin{aligned} \bar{\Lambda} &= \frac{2(1-\Lambda)\ (\mathbf{t}_0 \cdot \mathbf{e})\ (\mathbf{t}_1 \cdot \mathbf{e})}{\Lambda(1 - \mathbf{t}_0 \cdot \mathbf{t}_1) + 2(\mathbf{t}_0 \cdot \mathbf{e})\ (\mathbf{t}_1 \cdot \mathbf{e})} \\ &= \frac{2(1-\Lambda)\ (\mathbf{t}_0 \cdot \mathbf{d})\ (\mathbf{t}_1 \cdot \mathbf{d})}{\Lambda(1 - \mathbf{t}_0 \cdot \mathbf{t}_1)|\mathbf{d}|^2 + 2(\mathbf{t}_0 \cdot \mathbf{d})\ (\mathbf{t}_1 \cdot \mathbf{d})}. \end{aligned} \tag{4.13}$$

Alternatively if a matching point $\mathbf{m}$ *on* Σ_{++} *is given, the biarc parameters* Λ *and* $\bar{\Lambda}$ *are*

$$\Lambda = \frac{\mathbf{t}_0 \cdot \mathbf{d}\ |\mathbf{m} - \mathbf{q}_0|^2}{\mathbf{t}_0 \cdot (\mathbf{m} - \mathbf{q}_0)\ |\mathbf{d}|^2} \qquad \textit{and} \qquad \bar{\Lambda} = \frac{\mathbf{t}_1 \cdot \mathbf{d}\ |\mathbf{q}_1 - \mathbf{m}|^2}{\mathbf{t}_1 \cdot (\mathbf{q}_1 - \mathbf{m})\ |\mathbf{d}|^2}. \tag{4.14}$$

Proof

1. Consider the Bézier control triangle of Σ_{++}. The control point $\mathbf{b}_1$ is given by $\mathbf{b}_1 = \mathbf{q}_0 + l\frac{\mathbf{t}_0 + \mathbf{t}_1^\star}{|\mathbf{t}_0 + \mathbf{t}_1^\star|}$, where l is the side length of the Bézier control triangle. We know that the base angle δ of the isosceles Bézier control triangle satisfies

$$\frac{(\mathbf{t}_0 + \mathbf{t}_1^\star) \cdot (\mathbf{q}_1 - \mathbf{q}_0)}{|\mathbf{t}_0 + \mathbf{t}_1^\star|\ |\mathbf{q}_1 - \mathbf{q}_0|} = \cos\delta = \frac{\frac{1}{2}|\mathbf{q}_1 - \mathbf{q}_0|}{l}.$$

But from (4.1) and (4.3) we have $\mathbf{t}_1^\star \cdot \mathbf{d} = \mathbf{t}_1 \cdot \mathbf{d}$. Therefore

$$l = \frac{|\mathbf{d}|^2 |\mathbf{t}_0 + \mathbf{t}_1^\star|}{2(\mathbf{d} \cdot \mathbf{t}_0 + \mathbf{d} \cdot \mathbf{t}_1)},$$

and

$$\begin{aligned} \mathbf{b}_1 &= \mathbf{q}_0 + \frac{|\mathbf{d}|^2}{2(\mathbf{d} \cdot \mathbf{t}_0 + \mathbf{d} \cdot \mathbf{t}_1)}(\mathbf{t}_0 + \mathbf{t}_1^\star) \\ &= \frac{\mathbf{t}_0 \cdot \mathbf{d}\ \mathbf{q}_0 + \mathbf{t}_1 \cdot \mathbf{d}\ \mathbf{q}_1}{\mathbf{t}_0 \cdot \mathbf{d} + \mathbf{t}_1 \cdot \mathbf{d}} + \frac{|\mathbf{d}|^2(\mathbf{t}_0 - \mathbf{t}_1)}{2(\mathbf{t}_0 \cdot \mathbf{d} + \mathbf{t}_1 \cdot \mathbf{d})}. \end{aligned}$$

2. The side length of the Bézier triangle of the sub-arc of $\mathcal{C}_0$ from $\mathbf{q}_0$ to $\mathbf{q}_1$ following the orientation induced by the tangent $\mathbf{t}_0$ is

$$\frac{|\mathbf{d}|^2}{2\mathbf{t}_0 \cdot \mathbf{d}},$$

and the side length of the Bézier triangle of the sub-arc of $\mathcal{C}_1$ from $\mathbf{q}_1$ to $\mathbf{q}_0$ following the orientation induced by the tangent $-\mathbf{t}_1$ is

$$\frac{|\mathbf{d}|^2}{2\mathbf{t}_1 \cdot \mathbf{d}}.$$

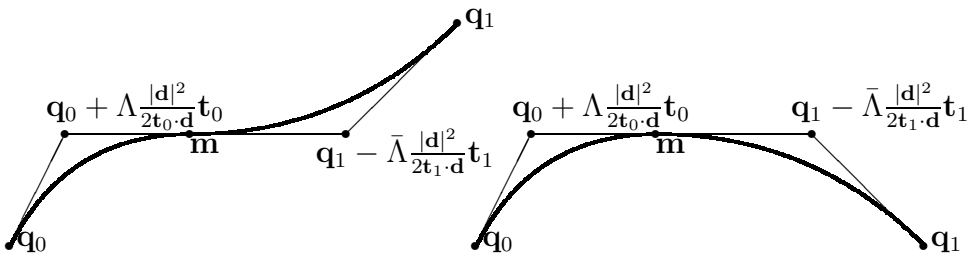

Figure 4.8: Two planar biarcs—with and without an inflection point—with the corresponding Bézier triangles. The *biarc parameters* Λ and $\bar{\Lambda}$ are the fraction of the maximal possible side length of the Bézier triangle of the corresponding arcs $\mathbf{a}$ and $\bar{\mathbf{a}}$.

Therefore for a proper biarc $(\mathbf{a}, \bar{\mathbf{a}})$, the Bézier control points of the arc $\mathbf{a}$ are

$$\mathbf{b}_0 = \mathbf{q}_0, \quad \mathbf{b}_1 = \mathbf{q}_0 + \Lambda\frac{|\mathbf{d}|^2}{2\mathbf{t}_0\cdot\mathbf{d}}\mathbf{t}_0, \quad \mathbf{b}_2 = \mathbf{m},$$

for some $\Lambda \in (0,1)$, and the Bézier control points of the arc $\bar{\mathbf{a}}$ are

$$\mathbf{b}_0 = \mathbf{m}, \quad \mathbf{b}_1 = \mathbf{q}_1 - \bar{\Lambda}\frac{|\mathbf{d}|^2}{2\mathbf{t}_1\cdot\mathbf{d}}\mathbf{t}_1, \quad \mathbf{b}_2 = \mathbf{q}_1,$$

for some $\bar{\Lambda} \in (0,1)$. The *biarc parameters* Λ and $\bar{\Lambda}$ are the fraction of the maximal possible side length of the associated Bézier triangle. The biarc parameters and matching point $\mathbf{m}$ are dependent. By the triangle inequality the distance between the Bézier control point $\mathbf{b}_1$ of $\mathbf{a}$, and the Bézier control point $\mathbf{b}_1$ of $\bar{\mathbf{a}}$ is smaller or equal to the sum of the side lengths of the Bézier triangles of $\mathbf{a}$ and of $\bar{\mathbf{a}}$. The condition that the unit tangents of the arcs $\mathbf{a}$ and $\bar{\mathbf{a}}$ at $\mathbf{m}$ are equal, implies the equality (cf. Figure 4.8 for the planar case)

$$\left(\Lambda\frac{|\mathbf{d}|^2}{2\mathbf{t}_0\cdot\mathbf{d}} + \bar{\Lambda}\frac{|\mathbf{d}|^2}{2\mathbf{t}_1\cdot\mathbf{d}}\right)^2 = \left|\left(\mathbf{q}_1 - \bar{\Lambda}\frac{|\mathbf{d}|^2}{2\mathbf{t}_1\cdot\mathbf{d}}\mathbf{t}_1\right) - \left(\mathbf{q}_0 + \Lambda\frac{|\mathbf{d}|^2}{2\mathbf{t}_0\cdot\mathbf{d}}\mathbf{t}_0\right)\right|^2,$$

which is equivalent to (4.12), and (4.13) follows from algebra.

The matching point $\mathbf{m}$ is the weighted average of the control points $\mathbf{b}_1$ of the corresponding triangles, that is

$$\mathbf{m} \;=\; \frac{\Lambda\frac{|\mathbf{d}|^2}{2\mathbf{t}_0\cdot\mathbf{d}}\;\left(\mathbf{q}_0 + \Lambda\frac{|\mathbf{d}|^2}{2\mathbf{t}_0\cdot\mathbf{d}}\mathbf{t}_0\right) + \bar{\Lambda}\frac{|\mathbf{d}|^2}{2\mathbf{t}_1\cdot\mathbf{d}}\;\left(\mathbf{q}_1 - \bar{\Lambda}\frac{|\mathbf{d}|^2}{2\mathbf{t}_1\cdot\mathbf{d}}\mathbf{t}_1\right)}{\Lambda\frac{|\mathbf{d}|^2}{2\mathbf{t}_0\cdot\mathbf{d}} + \bar{\Lambda}\frac{|\mathbf{d}|^2}{2\mathbf{t}_1\cdot\mathbf{d}}}$$

and (4.11) follows. The side length l of the Bézier triangle of $\mathbf{a}$ given in (4.9) is

$$l = \Lambda\frac{|\mathbf{d}|^2}{2\mathbf{t}_0\cdot\mathbf{d}}. \tag{4.15}$$

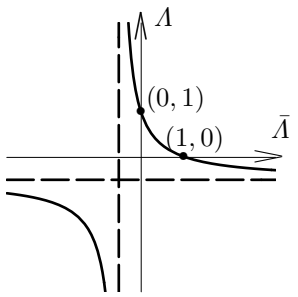

Figure 4.9: The biarc parameters Λ and $\bar{\Lambda}$ are coupled through equation (4.12) of a hyperbola.

But, using trigonometry, the side length l can be written as

$$l = \frac{\frac{1}{2}|\mathbf{m} - \mathbf{q}_0|}{\cos\delta} = \frac{\frac{1}{2}|\mathbf{m} - \mathbf{q}_0|}{\frac{(\mathbf{m}-\mathbf{q}_0)}{|\mathbf{m}-\mathbf{q}_0)|} \cdot \mathbf{t}_0}, \tag{4.16}$$

where δ is the base angle. Solving equations (4.15) and (4.16) for Λ yields the first part of (4.14). The proof of the formula for $\bar{\Lambda}$ is analogous.

■

We remark that equation (4.12) relating Λ and $\bar{\Lambda}$ involves only angles so that the condition is scale invariant. When $\mathbf{t}_0 = \mathbf{t}_1$ it reduces to $\bar{\Lambda} = 1 - \Lambda$. For $\mathbf{t}_0 \neq \mathbf{t}_1$, equation (4.12) is the equation of a hyperbola with orthogonal asymptotes parallel to the coordinate axes, and centred at $(-p, -p)$, where

$$p = \frac{2\mathbf{t}_0 \cdot \mathbf{e}\ \mathbf{t}_1 \cdot \mathbf{e}}{1 - \mathbf{t}_0 \cdot \mathbf{t}_1},$$

cf. Figure 4.9. In other words, with the coordinate transformation $X = \Lambda + p,\ \bar{X} = \bar{\Lambda} + p$, equation (4.12) becomes

$$X\bar{X} = p^2 + p.$$

Chapter 5

Local convergence results for biarcs

In this chapter we consider biarcs $(\mathbf{a}, \bar{\mathbf{a}})_h$ that interpolate point-tangent data pairs sampled from a space curve $\mathbf{q}$, i.e. point-tangent data pairs of the form $((\mathbf{q}(s), \mathbf{q}'(s)), (\mathbf{q}(s+h), \mathbf{q}'(s+h)))$. We study the local behaviour of biarcs, i.e. the properties of the interpolating biarc $(\mathbf{a}, \bar{\mathbf{a}})_h$ in the limit $h \to 0$.

As a curve with non-vanishing curvature is defined up to a rigid body displacement by the curvature $\kappa(s) > 0$ and torsion $\tau(s)$ given as functions of the arc-length argument s, we seek pointwise approximations of these quantities in terms of either the interpolating biarcs $(\mathbf{a}, \bar{\mathbf{a}})_h$ or directly in terms of the point-tangent data pairs $((\mathbf{q}(s), \mathbf{q}'(s)), (\mathbf{q}(s+h), \mathbf{q}'(s+h)))$. A related question is to find natural osculating objects associated with the biarc $(\mathbf{a}, \bar{\mathbf{a}})_h$ and to study whether they converge in the limit $h \to 0$ to the osculating objects of the curve $\mathbf{q}$ at $\mathbf{q}(s)$.

5.1 Biarcs and Taylor expansions

We will work with curves that have at least $C^{1,1}$-regularity, i.e. differentiable curves whose tangent field is Lipschitz continuous. Therefore we start by reviewing some properties of such curves.

Definition 5.1 *Let $I \subset \mathbb{R}$ be a closed interval of the form $I = [l_0, l_1]$ or $I = [l_0, \infty)$. The curve $\mathbf{q}$ belongs to the space $C^{0,1}(I, \mathbb{R}^3)$ if there exists a constant $K_{\mathbf{q}} < \infty$ such that*

$$|\mathbf{q}(s) - \mathbf{q}(\sigma)| \leq K_{\mathbf{q}} |s - \sigma|, \qquad \forall s, \sigma \in I.$$

The constant $K_{\mathbf{q}}$ is called the Lipschitz constant *of $\mathbf{q}$. The curve $\mathbf{q}$ belongs to the space $C^{1,1}(I, \mathbb{R}^3)$ if $\mathbf{q}$ is differentiable and the curve $\mathbf{q}'$ belongs to $C^{0,1}(I, \mathbb{R}^3)$. The space $C^{1,1}(I, \mathbb{R}^3)$ is equipped with the norm*

$$\|\mathbf{q}\|_{C^{1,1}(I,\mathbb{R}^3)} = \|\mathbf{q}\|_{C^1(I,\mathbb{R}^3)} + \sup_{s,\sigma \in I} \frac{|\mathbf{q}'(s) - \mathbf{q}'(\sigma)|}{|s - \sigma|}. \tag{5.1}$$

Hypothesis 5.2 *$I \subset \mathbb{R}$ is a finite closed interval $I = [l_0, l_1]$ or a semi-infinite closed interval $I = [l_0, \infty)$.*

Hypothesis 5.3 *The curve* $\mathbf{q} \in C^{1,1}(I, \mathbb{R}^3)$ *is parametrised by arc length, with Lipschitz constant* $K_{\mathbf{q}'}$ *for the tangent curve* $\mathbf{q}'$.

Let Hypotheses 5.2-5.3 hold. By Rademacher's theorem [14, p. 81] a Lipschitz continuous function has a derivative a.e. equal to the weak derivative a.e., and we have the isomorphism $C^{1,1}(I, \mathbb{R}^3) \equiv W^{2,\infty}(I, \mathbb{R}^3)$ [14, pp. 81, 131, 235]. Accordingly we may unambiguously use $\mathbf{q}'' \in L_\infty$ to stand for the weak second derivative of $\mathbf{q}$, and

$$K_{\mathbf{q}'} \leq \|\mathbf{q}''\|_{L_\infty}. \tag{5.2}$$

We may write

$$\mathbf{q}'(s) = \mathbf{q}'(\sigma) + \int_\sigma^s \mathbf{q}''(\tau) d\tau. \tag{5.3}$$

Integration of this equation yields

$$\mathbf{q}(s) = \mathbf{q}(\sigma) + \mathbf{q}'(\sigma)(s-\sigma) + \int_\sigma^s \int_\sigma^\phi \mathbf{q}''(\tau) d\tau d\phi. \tag{5.4}$$

We introduce the notation

$$\mathbf{w}(s,\sigma) := \frac{\mathbf{q}'(s) - \mathbf{q}'(\sigma)}{s-\sigma} = \frac{1}{s-\sigma} \int_\sigma^s \mathbf{q}''(\tau) d\tau, \tag{5.5}$$

$$\widetilde{\mathbf{w}}(s,\sigma) := \frac{\mathbf{q}(s) - \mathbf{q}(\sigma) - \mathbf{q}'(\sigma)(s-\sigma)}{(s-\sigma)^2} = \frac{1}{(s-\sigma)^2} \int_\sigma^s \int_\sigma^\phi \mathbf{q}''(\tau) d\tau d\phi. \tag{5.6}$$

Simple estimation of the integrals on the right hand sides of (5.5) and (5.6) implies the bounds

$$|\mathbf{w}(s,\sigma)| \leq \|\mathbf{q}''\|_{L_\infty}, \tag{5.7}$$

$$|\widetilde{\mathbf{w}}(s,\sigma)| \leq \frac{(s-\sigma)(\phi-\sigma)}{(s-\sigma)^2} \|\mathbf{q}''\|_{L_\infty} \leq \|\mathbf{q}''\|_{L_\infty}. \tag{5.8}$$

With (5.3)-(5.4) and (5.5)-(5.6) we may write

$$\mathbf{q}(s) = \mathbf{q}(\sigma) + \mathbf{q}'(\sigma)(s-\sigma) + \widetilde{\mathbf{w}}(s,\sigma)(s-\sigma)^2, \tag{5.9}$$

$$\mathbf{q}'(s) = \mathbf{q}'(\sigma) + \mathbf{w}(s,\sigma)(s-\sigma). \tag{5.10}$$

If the curve $\mathbf{q}$ is parametrised by arc length so that $|\mathbf{q}'(s)| = 1$, we can exploit equation (5.10) to obtain

$$2\mathbf{q}'(\sigma) \cdot \mathbf{w}(s,\sigma) + |\mathbf{w}(s,\sigma)|^2 |s-\sigma| = 0,$$

which implies

$$\mathbf{q}'(\sigma) \cdot \mathbf{w}(s,\sigma) = O(|s-\sigma|). \tag{5.11}$$

Using in turn the definition of $\widetilde{\mathbf{w}}$, the definition of $\mathbf{w}$, and equality (5.11) we find

$$\begin{aligned}
|\mathbf{q}'(\sigma)\cdot\widetilde{\mathbf{w}}(s,\sigma)| &= \left|\mathbf{q}'(\sigma)\cdot\left(\frac{1}{(s-\sigma)^2}\int_\sigma^s\int_\sigma^\phi \mathbf{q}''(\tau)d\tau d\phi\right)\right| \\
&= \left|\int_\sigma^s \frac{(\phi-\sigma)}{(s-\sigma)^2}\mathbf{q}'(\sigma)\cdot\left(\frac{1}{(\phi-\sigma)}\int_\sigma^\phi \mathbf{q}''(\tau)d\tau\right)d\phi\right| \\
&= \left|\int_\sigma^s \frac{(\phi-\sigma)}{(s-\sigma)^2}\mathbf{q}'(\sigma)\cdot\mathbf{w}(\phi,\sigma)d\phi\right| \\
&\le \int_\sigma^s \frac{(\phi-\sigma)^2}{(s-\sigma)^2}\left|\frac{\mathbf{q}'(\sigma)\cdot\mathbf{w}(\phi,\sigma)}{(\phi-\sigma)}\right|d\phi \;\le \int_\sigma^s \mathsf{c}\;d\phi,
\end{aligned}$$

where c denotes some constant, and

$$\mathbf{q}'(\sigma)\cdot\widetilde{\mathbf{w}}(s,\sigma) = O(|s-\sigma|). \tag{5.12}$$

In other words, the sequences $\mathbf{w}(s,\sigma)$ and $\widetilde{\mathbf{w}}(s,\sigma)$ approach the normal plane at $\mathbf{q}(\sigma)$, as $s\to\sigma$. Note that for a C^2-curve we have $\lim_{s\to\sigma}\mathbf{w}(s,\sigma)=\mathbf{q}''(\sigma)$, and $\lim_{s\to\sigma}\widetilde{\mathbf{w}}(s,\sigma)=\frac{1}{2}\mathbf{q}''(\sigma)$.

Now we derive a number of Taylor expansions that will be used in the proofs of the convergence results to be presented in Lemmas 5.8, 5.9, and 6.7. For convenience we introduce

Notation 5.4 *For a curve $\mathbf{q}\in C^{1,1}(I,\mathbb{R}^3)$ parametrised by arc length and for $s\in I$ and $h\neq 0$ with $s+h\in I$ we denote*

$$\mathbf{q}_0=\mathbf{q}(s),\ \mathbf{t}_0=\mathbf{q}'(s),\ \mathbf{q}_h=\mathbf{q}(s+h),\ \mathbf{t}_h=\mathbf{q}'(s+h). \tag{5.13}$$

Hypothesis 5.5 *For $s\in I$ and $h\neq 0$ with $s+h\in I$ the point-tangent data $((\mathbf{q}_0,\mathbf{t}_0),(\mathbf{q}_h,\mathbf{t}_h))$ is interpolated by a biarc $(\mathbf{a},\bar{\mathbf{a}})_h$ with matching point $\mathbf{m}_h\in\Sigma_{++}$ that for h sufficiently small corresponds to a biarc parameter $\Lambda_h\in(0,1)$ (cf. Lemma 4.13).*

Lemma 5.6 (Taylor expansions) *Let Hypotheses 5.2-5.3, and 5.5 hold, then*

$$\Lambda_h+\bar{\Lambda}_h = 1+O(h^2), \tag{5.14}$$

$$\frac{|\mathbf{m}_h-\mathbf{q}_0|}{h}-\Lambda_h = O(h^2), \tag{5.15}$$

$$\frac{|\mathbf{m}_h-\mathbf{q}_h|}{h}-\bar{\Lambda}_h = O(h^2), \tag{5.16}$$

$$1-\frac{\mathbf{m}_h-\mathbf{q}_0}{|\mathbf{m}_h-\mathbf{q}_0|}\cdot\mathbf{t}_0 = O(h^2), \tag{5.17}$$

and

$$1-\frac{\mathbf{q}_h-\mathbf{m}_h}{|\mathbf{q}_h-\mathbf{m}_h|}\cdot\mathbf{t}_h = O(h^2), \tag{5.18}$$

where the constants depend only on $K_{\mathbf{q}'}$, in particular they do not depend on s.

Proof In the more compact notation (5.13), the expansions (5.9) and (5.10) translate to

$$\left\{ \begin{array}{rcl} \mathbf{q}_h &=& \mathbf{q}_0 + \mathbf{t}_0 h + \widetilde{\mathbf{w}}_h h^2, \\ \mathbf{t}_h &=& \mathbf{t}_0 + \mathbf{w}_h h, \end{array} \right. \tag{5.19}$$

where $\widetilde{\mathbf{w}}_h := \widetilde{\mathbf{w}}(s+h, s)$ and $\mathbf{w}_h := \mathbf{w}(s+h, s)$. By (5.7) and (5.8) the vector functions $\widetilde{\mathbf{w}}_h$ and $\mathbf{w}_h$ are bounded by the same number $\|\mathbf{q}''\|_{L_\infty}$. Denote by

$$\left. \begin{array}{rcll} \eta_h &=& \mathbf{t}_0 \cdot \mathbf{w}_h, & |\eta_h| \le K_{\mathbf{q}'}, \\ \nu_h &=& |\mathbf{w}_h|^2, & |\nu_h| \le K_{\mathbf{q}'}^2, \\ \mu_h &=& \mathbf{t}_0 \cdot \widetilde{\mathbf{w}}_h, & |\mu_h| \le K_{\mathbf{q}'}, \\ \lambda_h &=& |\widetilde{\mathbf{w}}_h|^2, & |\lambda_h| \le K_{\mathbf{q}'}^2, \\ \tau_h &=& \widetilde{\mathbf{w}}_h \cdot \mathbf{w}_h, & |\tau_h| \le K_{\mathbf{q}'}^2, \\ \mathbf{d}_h &=& \mathbf{q}_h - \mathbf{q}_0. & \end{array} \right\} \tag{5.20}$$

All of $\eta_h, \nu_h, \mu_h, \lambda_h$, and τ_h depend on h, but are bounded by a constant that depends only on the constant $K_{\mathbf{q}'}$. With the approximations (5.19), notation (5.20) and the fact that $|\mathbf{q}'(s)| = 1$ we have

$$\left. \begin{array}{rcl} \mathbf{d}_h &=& \mathbf{t}_0 h + \widetilde{\mathbf{w}}_h h^2, \\ |\mathbf{d}_h|^2 &=& h^2 + 2\mu_h h^3 + \lambda_h h^4, \\ \mathbf{d}_h \cdot \mathbf{t}_0 &=& h + \mu_h h^2, \\ \mathbf{d}_h \cdot \mathbf{t}_h &=& h + \mu_h h^2 + \eta_h h^2 + \tau_h h^3, \\ \mathbf{t}_0 \cdot \mathbf{t}_h &=& 1 + \eta_h h. \end{array} \right\} \tag{5.21}$$

In this notation, (5.11) and (5.12) become

$$\eta_h = O(h), \tag{5.22}$$

$$\mu_h = O(h). \tag{5.23}$$

We use elementary algebra to rearrange equation (4.11) for the matching point $\mathbf{m}_h$,

$$\mathbf{m}_h = \mathbf{q}_0 + \frac{\Lambda_h \mathbf{t}_h \cdot \mathbf{d}_h}{\Lambda_h \mathbf{t}_h \cdot \mathbf{d}_h + \bar{\Lambda}_h \mathbf{t}_0 \cdot \mathbf{d}_h} \left[\mathbf{d}_h + \frac{\bar{\Lambda}_h |\mathbf{d}_h|^2}{2\mathbf{t}_h \cdot \mathbf{d}_h} (\mathbf{t}_0 - \mathbf{t}_h) \right] \tag{5.24}$$

$$= \mathbf{q}_h + \frac{\bar{\Lambda}_h \mathbf{t}_0 \cdot \mathbf{d}_h}{\Lambda_h \mathbf{t}_h \cdot \mathbf{d}_h + \bar{\Lambda}_h \mathbf{t}_0 \cdot \mathbf{d}_h} \left[\frac{\Lambda_h |\mathbf{d}_h|^2}{2\mathbf{t}_0 \cdot \mathbf{d}_h} (\mathbf{t}_0 - \mathbf{t}_h) - \mathbf{d}_h \right]. \tag{5.25}$$

For convenience we drop the subscript h where it does not induce confusion. We now indicate the computations yielding equations (5.14)-(5.18).

- Equation (5.14): Insert the expansions (5.21) into

$$\bar{\Lambda} = \frac{(1-\Lambda)\, 2\mathbf{t}_0 \cdot \mathbf{d}\ \mathbf{t}_h \cdot \mathbf{d}}{\Lambda(1 - \mathbf{t}_0 \cdot \mathbf{t}_h)|\mathbf{d}|^2 + 2\mathbf{t}_0 \cdot \mathbf{d}\ \mathbf{t}_h \cdot \mathbf{d}} = 1 - \Lambda + O(h^2),$$

  where equation (5.22) implies the simplification.

- Equation (5.15): From equation (5.24), and the fact that the data is proper,

$$|\mathbf{m}_h - \mathbf{q}_0| = \frac{\Lambda \mathbf{t}_h \cdot \mathbf{d}}{\Lambda \mathbf{t}_h \cdot \mathbf{d} + \bar{\Lambda} \mathbf{t}_0 \cdot \mathbf{d}} \left| \mathbf{d} + \frac{\bar{\Lambda}|\mathbf{d}|^2}{2\mathbf{t}_h \cdot \mathbf{d}} (\mathbf{t}_0 - \mathbf{t}_h) \right|. \tag{5.26}$$

We insert the expansions (5.14) and (5.21) and equations (5.22) and (5.23) into the first factor on the right hand side to find

$$\frac{\Lambda \mathbf{t}_h \cdot \mathbf{d}}{\Lambda \mathbf{t}_h \cdot \mathbf{d} + \bar{\Lambda} \mathbf{t}_0 \cdot \mathbf{d}} = \Lambda + O(h^2), \tag{5.27}$$

and, using expansions (5.19) and (5.21) and equations (5.22) and (5.23), compute that

$$\begin{aligned} \left| \mathbf{d} + \frac{\bar{\Lambda}|\mathbf{d}|^2}{2\mathbf{t}_h \cdot \mathbf{d}} (\mathbf{t}_0 - \mathbf{t}_h) \right|^2 &= \left| \mathbf{d} - \frac{\bar{\Lambda}|\mathbf{d}|^2}{2\mathbf{t}_h \cdot \mathbf{d}} \mathbf{w} h \right|^2 \\ &= |\mathbf{d}|^2 - \frac{\bar{\Lambda}|\mathbf{d}|^2}{\mathbf{t}_h \cdot \mathbf{d}} \mathbf{d} \cdot \mathbf{w} h + \frac{\bar{\Lambda}^2 |\mathbf{d}|^4}{4(\mathbf{t}_h \cdot \mathbf{d})^2} |\mathbf{w}|^2 h^2 \\ &= h^2[1 + h(2\mu - \eta\bar{\Lambda}) + h^2(\lambda - \tau\bar{\Lambda} + \tfrac{1}{4}\nu\bar{\Lambda}^2) + O(h^3)] \\ &= h^2[1 + O(h^2)]. \end{aligned} \tag{5.28}$$

Combining (5.27) and (5.28) yields

$$|\mathbf{m}_h - \mathbf{q}_0|^2 = (\Lambda^2 + O(h^2))h^2[1 + O(h^2)] = \Lambda^2 h^2[1 + O(h^2)]$$

as required.

- Equation (5.16): From equation (5.25)

$$|\mathbf{m}_h - \mathbf{q}_h| = \frac{\bar{\Lambda} \mathbf{t}_0 \cdot \mathbf{d}}{\Lambda \mathbf{t}_h \cdot \mathbf{d} + \bar{\Lambda} \mathbf{t}_0 \cdot \mathbf{d}} \left| \frac{\Lambda|\mathbf{d}|^2}{2\mathbf{t}_0 \cdot \mathbf{d}} (\mathbf{t}_0 - \mathbf{t}_h) - \mathbf{d} \right|.$$

We insert the expansions (5.14) and (5.21) and equations (5.22) and (5.23) into the first factor of the right hand side to get

$$\frac{\bar{\Lambda} \mathbf{t}_0 \cdot \mathbf{d}}{\Lambda \mathbf{t}_h \cdot \mathbf{d} + \bar{\Lambda} \mathbf{t}_0 \cdot \mathbf{d}} = \bar{\Lambda} + O(h^2), \tag{5.29}$$

and, with the expansions (5.19) and (5.21) and equations (5.22) and (5.23), we find

$$\begin{aligned} \left| \frac{\Lambda|\mathbf{d}|^2}{2\mathbf{t}_0 \cdot \mathbf{d}} (\mathbf{t}_0 - \mathbf{t}_h) - \mathbf{d} \right|^2 &= \left| \frac{\Lambda|\mathbf{d}|^2}{2\mathbf{t}_0 \cdot \mathbf{d}} \mathbf{w} h + \mathbf{d} \right|^2 \\ &= |\mathbf{d}|^2 + \frac{\Lambda|\mathbf{d}|^2}{\mathbf{t}_0 \cdot \mathbf{d}} \mathbf{d} \cdot \mathbf{w} h + \frac{\Lambda^2 |\mathbf{d}|^4}{4(\mathbf{t}_0 \cdot \mathbf{d})^2} |\mathbf{w}|^2 h^2 \\ &= h^2[1 + h(2\mu + \Lambda\eta) + h^2(\lambda + \Lambda\tau + \Lambda^2\nu) + O(h^3)] \\ &= h^2[1 + O(h^2)]. \end{aligned} \tag{5.30}$$

Combining (5.29) and (5.30) yields

$$|\mathbf{m}_h - \mathbf{q}_h|^2 = (\bar{\Lambda}^2 + O(h^2))h^2[1 + O(h^2)] = \bar{\Lambda}^2 h^2(1 + O(h^2))$$

as required.

- Equation (5.17): Equation (5.24) and $|\mathbf{t}_0| = 1$ yield

$$\frac{\mathbf{m}_h - \mathbf{q}_0}{|\mathbf{m}_h - \mathbf{q}_0|} \cdot \mathbf{t}_0 = \frac{\mathbf{t}_0 \cdot \mathbf{d} + \frac{\bar{\Lambda}|\mathbf{d}|^2}{2\mathbf{t}_h \cdot \mathbf{d}}(1 - \mathbf{t}_0 \cdot \mathbf{t}_h)}{\left|\mathbf{d} + \frac{\bar{\Lambda}|\mathbf{d}|^2}{2\mathbf{t}_h \cdot \mathbf{d}}(\mathbf{t}_0 - \mathbf{t}_h)\right|}. \tag{5.31}$$

Expansion of the numerator in the right hand side of (5.31), use of the expansions (5.21) and equations (5.22) and (5.23), imply

$$\begin{aligned} \mathbf{t}_0 \cdot \mathbf{d} + \frac{\bar{\Lambda}|\mathbf{d}|^2}{2\mathbf{t}_h \cdot \mathbf{d}}(1 - \mathbf{t}_0 \cdot \mathbf{t}_h) &= h + \mu h^2 + \tfrac{1}{2}\bar{\Lambda} h(1 + (\mu - \eta)h + O(h^2))(-\eta h) \\ &= h[1 + O(h^2)]. \end{aligned} \tag{5.32}$$

From (5.28) we deduce the expansion of the denominator in the right hand side of (5.31), namely

$$\frac{\mathbf{m}_h - \mathbf{q}_0}{|\mathbf{m}_h - \mathbf{q}_0|} \cdot \mathbf{t}_0 = \frac{\mathbf{t}_0 \cdot \mathbf{d} + \frac{\bar{\Lambda}|\mathbf{d}|^2}{2\mathbf{t}_h \cdot \mathbf{d}}(1 - \mathbf{t}_0 \cdot \mathbf{t}_h)}{\left|\mathbf{d} + \frac{\bar{\Lambda}|\mathbf{d}|^2}{2\mathbf{t}_h \cdot \mathbf{d}}(\mathbf{t}_0 - \mathbf{t}_h)\right|} = \frac{h[1 + O(h^2)]}{h[1 + O(h^2)]} = 1 + O(h^2).$$

- Equation (5.18): Equation (5.25) and $|\mathbf{t}_h| = 1$ yields

$$\frac{\mathbf{m}_h - \mathbf{q}_h}{|\mathbf{m}_h - \mathbf{q}_h|} \cdot \mathbf{t}_h = \frac{\frac{\Lambda|\mathbf{d}|^2}{2\mathbf{t}_0 \cdot \mathbf{d}}(\mathbf{t}_0 \cdot \mathbf{t}_h - 1) - \mathbf{d} \cdot \mathbf{t}_h}{\left|\frac{\Lambda|\mathbf{d}|^2}{2\mathbf{t}_0 \cdot \mathbf{d}}(\mathbf{t}_0 - \mathbf{t}_h) - \mathbf{d}\right|}. \tag{5.33}$$

The expansion of the numerator in the right hand side of (5.33), use of the expansions (5.21) and equations (5.22) and (5.23), imply

$$\begin{aligned} \frac{\Lambda|\mathbf{d}|^2}{2\mathbf{t}_0 \cdot \mathbf{d}}(\mathbf{t}_0 \cdot \mathbf{t}_h - 1) - \mathbf{d} \cdot \mathbf{t}_h &= \tfrac{1}{2}\Lambda h(1 + O(h^2))(\eta h) - [h + \mu h^2 + \eta h^2 + \tau h^3] \\ &= h[-1 + O(h^2)]. \end{aligned}$$

The expansion of the denominator in the right hand side of (5.33) is given by (5.30), thus

$$\frac{\mathbf{m}_h - \mathbf{q}_h}{|\mathbf{m}_h - \mathbf{q}_h|} \cdot \mathbf{t}_h = \frac{\frac{\Lambda|\mathbf{d}|^2}{2\mathbf{t}_0 \cdot \mathbf{d}}(\mathbf{t}_0 \cdot \mathbf{t}_h - 1) - \mathbf{d} \cdot \mathbf{t}_h}{\left|\frac{\Lambda|\mathbf{d}|^2}{2\mathbf{t}_0 \cdot \mathbf{d}}(\mathbf{t}_0 - \mathbf{t}_h) - \mathbf{d}\right|} = \frac{h[-1 + O(h^2)]}{h[1 + O(h^2)]} = -1 + O(h^2).$$

■

5.2 Arc length

Notation 5.7 *We denote the arc length of a curve* $\mathbf{q}$ *by* $\lambda(\mathbf{q})$*. In particular, given a biarc* $(\mathbf{a}, \bar{\mathbf{a}})$*, we denote the arc length of the biarc by* $\lambda((\mathbf{a}, \bar{\mathbf{a}}))$*.*

The length $\lambda(\mathbf{a})$ of an arc $\mathbf{a}$ with end points $\mathbf{q}_0$ and $\mathbf{q}_1$ which is tangent to $\mathbf{t}_0$ at $\mathbf{q}_0$ is given by $\lambda(\mathbf{a}) = \angle\mathbf{a}\, r(\mathbf{q}_0, \mathbf{t}_0, \mathbf{q}_1)$, where $\angle\mathbf{a}$ is the angle swept out by the arc $\mathbf{a}$,

$$\angle\mathbf{a} = 2\arccos\left(\frac{\mathbf{q}_1 - \mathbf{q}_0}{|\mathbf{q}_1 - \mathbf{q}_0|} \cdot \mathbf{t}_0\right), \tag{5.34}$$

and $r(\mathbf{q}_0, \mathbf{t}_0, \mathbf{q}_1)$ is the radius of the circle passing through $\mathbf{q}_0$ and $\mathbf{q}_1$, tangent at $\mathbf{q}_0$ to $\mathbf{t}_0$ given by

$$r(\mathbf{q}_0, \mathbf{t}_0, \mathbf{q}_1) \;=\; \frac{|\mathbf{q}_1 - \mathbf{q}_0|}{2\left|\frac{\mathbf{q}_1 - \mathbf{q}_0}{|\mathbf{q}_1 - \mathbf{q}_0|} \times \mathbf{t}_0\right|} = \frac{|\mathbf{q}_1 - \mathbf{q}_0|}{2\sqrt{1 - \left(\frac{\mathbf{q}_1 - \mathbf{q}_0}{|\mathbf{q}_1 - \mathbf{q}_0|} \cdot \mathbf{t}_0\right)^2}}. \tag{5.35}$$

From (5.35) and (5.34) we obtain the length of the arc $\mathbf{a}$

$$\lambda(\mathbf{a}) = \angle\mathbf{a}\, r(\mathbf{q}_0, \mathbf{t}_0, \mathbf{q}_1) = \frac{|\mathbf{q}_1 - \mathbf{q}_0| \arccos\left(\frac{\mathbf{q}_1 - \mathbf{q}_0}{|\mathbf{q}_1 - \mathbf{q}_0|} \cdot \mathbf{t}_0\right)}{\sqrt{1 - \left(\frac{\mathbf{q}_1 - \mathbf{q}_0}{|\mathbf{q}_1 - \mathbf{q}_0|} \cdot \mathbf{t}_0\right)^2}}. \tag{5.36}$$

Lemma 5.8 (Arc length of a biarc) *Let Hypotheses 5.2-5.3 and 5.5 hold, then*

$$\lambda((\mathbf{a}, \bar{\mathbf{a}})_h) - h = O(h^3),$$

where the constant depends only on $K_{\mathbf{q}'}$, in particular it is independent on s.

Proof We use the expansion

$$\frac{\arccos(y)}{\sqrt{(1 - y^2)}} = 1 + O((1 - y)), \tag{5.37}$$

and apply the expansions (5.14)-(5.18) of Lemma 5.6 to the formula (5.36), to find

$$\begin{aligned}
\lambda((\mathbf{a}, \bar{\mathbf{a}})_h) \;&=\; \frac{|\mathbf{m}_h - \mathbf{q}_0| \arccos(\frac{\mathbf{m}_h - \mathbf{q}_0}{|\mathbf{m}_h - \mathbf{q}_0|} \cdot \mathbf{t}_0)}{\sqrt{1 - (\frac{\mathbf{m}_h - \mathbf{q}_0}{|\mathbf{m}_h - \mathbf{q}_0|} \cdot \mathbf{t}_0)^2}} + \frac{|\mathbf{m}_h - \mathbf{q}_h| \arccos(\frac{\mathbf{m}_h - \mathbf{q}_h}{|\mathbf{m}_h - \mathbf{q}_h|} \cdot \mathbf{t}_h)}{\sqrt{1 - (\frac{\mathbf{m}_h - \mathbf{q}_h}{|\mathbf{m}_h - \mathbf{q}_h|} \cdot \mathbf{t}_h)^2}} \\
&=\; |\mathbf{m}_h - \mathbf{q}_0| \left[1 + O\left(1 - \frac{\mathbf{m}_h - \mathbf{q}_0}{|\mathbf{m}_h - \mathbf{q}_0|} \cdot \mathbf{t}_0\right)\right] \\
&\quad + |\mathbf{m}_h - \mathbf{q}_h| \left[1 + O\left(1 - \frac{\mathbf{m}_h - \mathbf{q}_h}{|\mathbf{m}_h - \mathbf{q}_h|} \cdot \mathbf{t}_h\right)\right] \\
&=\; |\mathbf{m}_h - \mathbf{q}_0| \left[1 + O(h^2)\right] + |\mathbf{m}_h - \mathbf{q}_h| \left[1 + O(h^2)\right] \\
&=\; [\Lambda h + O(h^3)] \left[1 + O(h^2)\right] + [\bar{\Lambda} h + O(h^3)] \left[1 + O(h^2)\right] \\
&=\; [\Lambda h + O(h^3)] + [\bar{\Lambda} h + O(h^3)] = (\Lambda + \bar{\Lambda}) h + O(h^3) \\
&=\; (1 + O(h^2)) h + O(h^3) = h + O(h^3),
\end{aligned}$$

as was to be shown. ■

5.3 Curvature

By construction, the biarc $(\mathbf{a}, \bar{\mathbf{a}})_h$ interpolating the point-tangent data $((\mathbf{q}_0, \mathbf{t}_0), (\mathbf{q}_h, \mathbf{t}_h))$ for some $\Lambda_h \in (0, 1)$ has contact of order one with the curve $\mathbf{q}$ at $\mathbf{q}(s) = \mathbf{q}_0$. We next show that for a C^2-curve, and in the limit $h \to 0$, the arc $\mathbf{a}$ of the biarc $(\mathbf{a}, \bar{\mathbf{a}})_h$ approaches contact of order two at $\mathbf{q}_0$. For this we need the Taylor expansion for a curve $\mathbf{q} \in C^2(I, \mathbb{R}^3)$:

$$\begin{aligned} \mathbf{q}(s+h) &= \mathbf{q}(s) + h\mathbf{q}'(s) + \tfrac{1}{2}h^2\mathbf{q}''(s) + o(h^2), && (5.38)\\ \mathbf{q}'(s+h) &= \mathbf{q}'(s) + h\mathbf{q}''(s) + o(h), && (5.39)\\ \mathbf{q}''(s+h) &= \mathbf{q}''(s) + o(1). && (5.40) \end{aligned}$$

Note that the estimates are uniform in $s \in I$ when $\mathbf{q}''$ is uniformly continuous, in particular when I is a finite interval.

Consider a circular arc $\mathbf{a}$ as a curve $\mathbf{a}(s)$ parametrised by arc length s. Then the second derivative at s is given by

$$\mathbf{a}''(s) = \frac{1}{r(\mathbf{a}(s), \mathbf{a}'(s), \mathbf{a}(\sigma))}\mathbf{n}(s),$$

where $\mathbf{a}(\sigma)$ is some other point on the arc, $r(\mathbf{a}(s), \mathbf{a}'(s), \mathbf{a}(\sigma))$ is the radius of the circle passing through $\mathbf{a}(s)$ and $\mathbf{a}(\sigma)$, tangent at $\mathbf{a}(s)$ to $\mathbf{a}'(s)$ cf. (5.35), and $\mathbf{n}(s)$ is the normal at s. The vector

$$\frac{\mathbf{a}(\sigma) - \mathbf{a}(s)}{|\mathbf{a}(\sigma) - \mathbf{a}(s)|} - \frac{[\mathbf{a}(\sigma) - \mathbf{a}(s)] \cdot \mathbf{t}(s)}{|\mathbf{a}(\sigma) - \mathbf{a}(s)|}\mathbf{t}(s)$$

points in the direction of the normal $\mathbf{n}(s)$, thus, from formula (5.35), we find

$$\mathbf{a}''(s) = \frac{2[\mathbf{a}(\sigma) - \mathbf{a}(s)]}{|\mathbf{a}(\sigma) - \mathbf{a}(s)|^2} - \frac{2[\mathbf{a}(\sigma) - \mathbf{a}(s)] \cdot \mathbf{t}(s)}{|\mathbf{a}(\sigma) - \mathbf{a}(s)|^2}\mathbf{t}(s). \tag{5.41}$$

Note that formula (5.41) remains valid for straight arcs, but reduces to $\mathbf{a}''(s) = (0, 0, 0)$.

Proposition 5.9 *Let Hypotheses 5.2-5.3 and 5.5 hold, and in addition assume that $\mathbf{q} \in C^2(I, \mathbb{R}^3)$ is parametrised by arc length, with Lipschitz constant $K_{\mathbf{q}'} = \|\mathbf{q}''\|_C$. Moreover assume that the biarc parameters Λ_h are bounded from below by a positive constant, that is there exists a constant $\Lambda_{\min}$ such that*

$$0 < \Lambda_{\min} \leq \Lambda_h \tag{5.42}$$

for all $h > 0$. Then the arc $\mathbf{a}$ of the biarc $(\mathbf{a}, \bar{\mathbf{a}})_h$ approaches the osculating circle at the data point $\mathbf{q}_0$, or equivalently,

$$\left|\mathbf{q}''(s) - \mathbf{a}_h''^{+}\right| = o(1). \tag{5.43}$$

The speed of convergence is independent of s if in addition $\mathbf{q}''$ is uniformly continuous.

Proof Similarly to the formulation introduced in Notation 5.4 we denote

$$\begin{array}{lllllllll} \mathbf{q}_0 & = & \mathbf{q}(s), & \mathbf{t}_0 & = & \mathbf{q}'(s), & \kappa_0\mathbf{n}_0 & = & \mathbf{q}''(s), \\ \mathbf{q}_h & = & \mathbf{q}(s+h), & \mathbf{t}_h & = & \mathbf{q}'(s+h), & \kappa_h\mathbf{n}_h & = & \mathbf{q}''(s+h), \end{array} \tag{5.44}$$

where κ_0 and κ_h are the curvatures, and $\mathbf{n}_0$ and $\mathbf{n}_h$ are the normalised second derivatives (or principal normals). Then the expansions (5.38)-(5.40) translate to

$$\mathbf{q}_h = \mathbf{q}_0 + \mathbf{t}_0 h + \tfrac{1}{2}\kappa_0\mathbf{n}_0 h^2 + o(h^2), \tag{5.45}$$

$$\mathbf{t}_h = \mathbf{t}_0 + \kappa_0\mathbf{n}_0 h + o(h), \tag{5.46}$$

$$\kappa_h\mathbf{n}_h = \kappa_0\mathbf{n}_0 + o(1). \tag{5.47}$$

We use formula (5.41), notation (5.44), and equations (5.24), (5.26), and (5.31) to find

$$\begin{aligned} \mathbf{a}_h''^{+} &= \frac{2(\mathbf{m}_h - \mathbf{q}_0)}{|\mathbf{m}_h - \mathbf{q}_0|^2} - \frac{2(\mathbf{m}_h - \mathbf{q}_0)\cdot\mathbf{t}_0}{|\mathbf{m}_h - \mathbf{q}_0|^2}\mathbf{t}_0 \\ &= 2\frac{\left(\mathbf{d} + \frac{\bar\Lambda_h|\mathbf{d}|^2}{2\mathbf{t}_h\cdot\mathbf{d}}(\mathbf{t}_0 - \mathbf{t}_h)\right) - \left(\mathbf{d}\cdot\mathbf{t}_0 + \frac{\bar\Lambda_h|\mathbf{d}|^2}{2\mathbf{t}_h\cdot\mathbf{d}}(1 - \mathbf{t}_h\cdot\mathbf{t}_0)\right)\mathbf{t}_0}{\frac{\Lambda_h\mathbf{t}_h\cdot\mathbf{d}}{\Lambda_h\mathbf{t}_h\cdot\mathbf{d}+\bar\Lambda_h\mathbf{t}_0\cdot\mathbf{d}}\left|\mathbf{d} + \frac{\bar\Lambda_h|\mathbf{d}|^2}{2\mathbf{t}_h\cdot\mathbf{d}}(\mathbf{t}_0 - \mathbf{t}_h)\right|^2}. \end{aligned} \tag{5.48}$$

Equations (5.22) and (5.23) and notation (5.21) imply

$$\frac{\bar\Lambda_h|\mathbf{d}|^2}{2\mathbf{t}_h\cdot\mathbf{d}} = \frac{\bar\Lambda_h(h^2 + 2\mu h^3 + \lambda h^4)}{2(h + \mu h^2 + \eta h^2 + \tau h^3)} = \tfrac{1}{2}\bar\Lambda_h h + O(h^3).$$

Applying this result in formula (5.48), and using equations (5.32), (5.27), and (5.28), we obtain

$$\mathbf{a}_h''^{+} = 2\frac{\mathbf{d} + [\frac{1}{2}\bar\Lambda_h h + O(h^3)](\mathbf{t}_0 - \mathbf{t}_h) - (h + O(h^3))\,\mathbf{t}_0}{[\Lambda_h + O(h^2)]\,[h^2 + O(h^4)]}, \tag{5.49}$$

which we transform with the help of the expansions (5.45)-(5.46) to get

$$\begin{aligned} \mathbf{a}_h''^{+} &= 2\frac{\frac{1}{2}\kappa_0\mathbf{n}_0 h^2 + o(h^2) + [\frac{1}{2}\bar\Lambda_h h + O(h^3)](-\kappa_0\mathbf{n}_0 h + o(h))}{\Lambda_h h^2 + O(h^4)} \\ &= 2\frac{\frac{1}{2}\kappa_0\mathbf{n}_0 + o(1) + [\frac{1}{2}\bar\Lambda_h + O(h^2)](-\kappa_0\mathbf{n}_0 + o(1))}{\Lambda_h + O(h^2)} \\ &= \frac{(1 - \bar\Lambda_h)\kappa_0\mathbf{n}_0 + o(1)}{\Lambda_h + O(h^2)}. \end{aligned}$$

With the expansion (5.14), condition (5.42), and notation (5.44) we find

$$\mathbf{a}_h''^{+} = \kappa_0\mathbf{n}_0 + o(1) = \mathbf{q}''(s) + o(1).$$

■

Note that in the previous proof we used a combination of results for $C^{1,1}$-curves with, where necessary, expansions valid only for C^2-curves.

We next consider another approximation of curvature at the point $\mathbf{q}(s)$ with the same order of accuracy as (5.43) but now expressed in terms of the radii of the two circles $\mathcal{C}_0^h$ and $\mathcal{C}_1^h$ defined in:

Notation 5.10 *(cf. Definition 4.3) For the point-tangent data pair of the form* $((\mathbf{q}(s), \mathbf{q}'(s)), (\mathbf{q}(s+h), \mathbf{q}'(s+h)))$ *the circle with tangent* $\mathbf{q}'(s)$ *at* $\mathbf{q}(s)$ *passing through* $\mathbf{q}(s+h)$ *is denoted by* $\mathcal{C}_0^h$*, and the circle with tangent* $\mathbf{q}'(s+h)$ *at* $\mathbf{q}(s+h)$ *passing through* $\mathbf{q}(s)$ *by* $\mathcal{C}_1^h$*.*

Proposition 5.11 *Let Hypothesis 5.2 hold, and in addition assume that* $\mathbf{q} \in C^2(I, \mathbb{R}^3)$ *is parametrised by arc length. Then for* $s \in I$*, with* $\kappa(s) \neq 0$*,*

$$\rho(s) = r(\mathcal{C}_0^h) + o(1), \quad \textit{and} \quad \rho(s) = r(\mathcal{C}_1^h) + o(1).$$

If in addition $\mathbf{q}''$ *is uniformly continuous the speed of convergence is independent on* s*.*

We note that Proposition 5.11 provides approximations for $\rho(s)$ purely in terms of the data, independent of the biarc interpolation.

Proof We use the notation (5.44) and expansions (5.45)-(5.46) to compute

$$\begin{aligned} \mathbf{d}_h :=& \mathbf{q}_h - \mathbf{q}_0 = h\mathbf{t}_0 + \tfrac{1}{2}h^2\kappa_0\mathbf{n}_0 + o(h^2) \\ |\mathbf{d}_h|^2 =& h^2 + o(h^3), \\ \mathbf{t}_h =& \mathbf{t}_0 + h\kappa_0\mathbf{n}_0 + o(h), \\ \mathbf{d}_h \times \mathbf{t}_0 =& -\tfrac{1}{2}h^2\kappa_0\mathbf{b}_0 + o(h^2), \\ \mathbf{d}_h \times \mathbf{t}_h =& \tfrac{1}{2}h^2\kappa_0\mathbf{b}_0 + o(h^2), \\ |\mathbf{d}_h \times \mathbf{t}_0| = |\mathbf{d}_h \times \mathbf{t}_h| =& \tfrac{1}{2}h^2\kappa_0 + o(h^2). \end{aligned} \tag{5.50}$$

The radii $r(\mathcal{C}_0^h)$ and $r(\mathcal{C}_1^h)$ of the circles $\mathcal{C}_0^h$ and $\mathcal{C}_1^h$ are given by the formula (5.35) in which we insert the expansions (5.50):

$$r(\mathcal{C}_0^h) = \frac{|\mathbf{d}_h|^2}{2|\mathbf{d}_h \times \mathbf{t}_0|} = \frac{h^2 + o(h^3)}{2(\frac{1}{2}h^2\kappa_0 + o(h^2))} = \frac{1}{\kappa_0} + o(1).$$

The expansion for $r(\mathcal{C}_1^h)$ is analogous. ■

We next establish a higher order approximation for curvature at the point $\mathbf{q}(s)$ in terms of the radii of the two circles $\mathcal{C}_0^h$ and $\mathcal{C}_1^h$ assuming a higher regularity of the curve $\mathbf{q}$. For this we need the following expansions for a curve $\mathbf{q} \in C^3(I, \mathbb{R}^3)$:

$$\mathbf{q}(s+h) = \mathbf{q}(s) + h\mathbf{q}'(s) + \tfrac{1}{2}h^2\mathbf{q}''(s) + \tfrac{1}{6}h^3\mathbf{q}'''(s) + o(h^3), \tag{5.51}$$

$$\mathbf{q}'(s+h) = \mathbf{q}'(s) + h\mathbf{q}''(s) + \tfrac{1}{2}h^2\mathbf{q}'''(s) + o(h^2). \tag{5.52}$$

Note that the estimates are uniform in $s \in I$ when $\mathbf{q}'''$ is uniformly continuous, in particular whenever I is a finite interval.

Proposition 5.12 *Let Hypothesis 5.2 hold, and in addition assume that* $\mathbf{q} \in C^3(I, \mathbb{R}^3)$ *is parametrised by arc length. Then for* $s \in I$ *with* $\kappa(s) \neq 0$

$$\begin{aligned} r(\mathcal{C}_0^h) &= \frac{1}{\kappa(s)} - \frac{\kappa'(s)}{3\kappa^2(s)}h + o(h), \\ r(\mathcal{C}_1^h) &= \frac{1}{\kappa(s)} + \frac{2\kappa'(s)}{3\kappa^2(s)}h + o(h). \end{aligned}$$

In particular

$$\rho(s) = \frac{2r(\mathcal{C}_0^h) + r(\mathcal{C}_1^h)}{3} + o(h), \tag{5.53}$$

$$\rho'(s) = \frac{r(\mathcal{C}_0^h) - r(\mathcal{C}_1^h)}{h} + o(1). \tag{5.54}$$

If in addition $\mathbf{q}'''$ *is uniformly continuous the speed of convergence is independent on* s*.*

Proof Similar to the formulation introduced in Notation 5.4 and Proposition 5.9 we denote

$$\begin{array}{rclrclrcl} \mathbf{q}_0 &=& \mathbf{q}(s), & \mathbf{t}_0 &=& \mathbf{q}'(s), & \kappa_0\mathbf{n}_0 &=& \mathbf{q}''(s), \\ \mathbf{q}_h &=& \mathbf{q}(s+h), & \mathbf{t}_h &=& \mathbf{q}'(s+h), & \mathbf{b}_0 &=& \mathbf{t}_0 \times \mathbf{n}_0, \end{array} \tag{5.55}$$

where κ_0 is the curvature, and $\mathbf{n}_0$ and $\mathbf{n}_h$ are the principal normals, $\mathbf{b}_0$ is the binormal, and we denote the torsion at s by τ_0. Then the expansions (5.51)-(5.52) translate to

$$\mathbf{q}_h = \mathbf{q}_0 + h\mathbf{t}_0 + \tfrac{1}{2}h^2\kappa_0\mathbf{n}_0 + \tfrac{1}{6}h^3(\kappa_0'\mathbf{n}_0 - \kappa_0^2\mathbf{t}_0 + \kappa_0\tau_0\mathbf{b}_0) + o(h^3), \tag{5.56}$$

$$\mathbf{t}_h = \mathbf{t}_0 + h\kappa_0\mathbf{n}_0 + \tfrac{1}{2}h^2(\kappa_0'\mathbf{n}_0 - \kappa_0^2\mathbf{t}_0 + \kappa_0\tau_0\mathbf{b}_0) + o(h^2). \tag{5.57}$$

We write the chord $\mathbf{d}_h$ and tangent $\mathbf{t}_h$ in the $(\mathbf{t}_0, \mathbf{n}_0, \mathbf{b}_0)$ frame, and compute the squared norm of $\mathbf{d}_h$:

$$\begin{aligned} \mathbf{d}_h :=& \mathbf{q}_h - \mathbf{q}_0 = h\mathbf{t}_0 + \tfrac{1}{2}h^2\kappa_0\mathbf{n}_0 + \tfrac{1}{6}h^3(\kappa_0'\mathbf{n}_0 - \kappa_0^2\mathbf{t}_0 + \kappa_0\tau_0\mathbf{b}_0) + o(h^3) \\ =& \mathbf{t}_0(h - \tfrac{1}{6}h^3\kappa_0^2) + \mathbf{n}_0(\tfrac{1}{2}h^2\kappa_0 + \tfrac{1}{6}h^3\kappa_0') + \mathbf{b}_0(\tfrac{1}{6}h^3\kappa_0\tau_0) + o(h^3), \\ |\mathbf{d}_h|^2 =& h^2 - \frac{1}{12}\kappa_0^2h^4 + o(h^4), \\ \mathbf{t}_h =& \mathbf{t}_0(1 - \tfrac{1}{2}h^2\kappa_0^2) + \mathbf{n}_0(h\kappa_0 + \tfrac{1}{2}h^2\kappa_0') + \mathbf{b}_0(\tfrac{1}{2}h^2\kappa_0\tau_0) + o(h^2). \end{aligned} \tag{5.58}$$

We set $\mathbf{v}_0^h := \mathbf{t}_0 \times \mathbf{d}_h$ and compute the norm $|\mathbf{v}_0^h|$

$$\begin{aligned} \mathbf{v}_0^h :=& \mathbf{t}_0 \times \mathbf{d}_h = -\tfrac{1}{6}h^3\kappa_0\tau_0\mathbf{n}_0 + (\tfrac{1}{2}h^2\kappa_0 + \tfrac{1}{6}h^3\kappa_0')\mathbf{b}_0 + o(h^3), \\ |\mathbf{v}_0^h|^2 =& \tfrac{1}{4}h^4\kappa_0^2 + \tfrac{1}{6}h^5\kappa_0\kappa_0' + o(h^5), \\ |\mathbf{v}_0^h| =& \tfrac{1}{2}\kappa_0h^2 + \tfrac{1}{6}\kappa_0'h^3 + o(h^3). \end{aligned} \tag{5.59}$$

We set $\mathbf{v}_1^h := \mathbf{d}_h \times \mathbf{t}_h$ and compute the norm $|\mathbf{v}_1^h|$

$$\begin{aligned} \mathbf{v}_1^h :=& \mathbf{d}_h \times \mathbf{t}_h = -\tfrac{1}{3}h^3\kappa_0\tau_0\mathbf{n}_0 + (\tfrac{1}{2}h^2\kappa_0 + \tfrac{1}{3}h^3\kappa_0')\mathbf{b}_0 + o(h^3), \\ |\mathbf{v}_1^h|^2 =& \tfrac{1}{4}h^4\kappa_0^2 - \tfrac{1}{3}h^5\kappa_0\kappa_0' + o(h^5), \\ |\mathbf{v}_1^h| =& \tfrac{1}{2}\kappa_0h^2 - \tfrac{1}{3}\kappa_0'h^3 + o(h^3). \end{aligned} \tag{5.60}$$

The radii $r(\mathcal{C}_0^h)$ and $r(\mathcal{C}_1^h)$ of the circles $\mathcal{C}_0^h$ and $\mathcal{C}_1^h$ are given by the formula (5.35) in which we insert the expansions (5.58) and (5.59) to find

$$r(\mathcal{C}_0^h) = \frac{|\mathbf{d}_h|^2}{2|\mathbf{d}_h \times \mathbf{t}_0|} = \frac{h^2 - \frac{1}{12}\kappa_0^2h^4 + o(h^4)}{2(\frac{1}{2}\kappa_0h^2 + \frac{1}{6}\kappa_0'h^3 + o(h^3))} = \frac{1}{\kappa_0} - \frac{\kappa_0'}{3\kappa_0^2}h + o(h),$$

and insert the expansions (5.58) and (5.60) to get

$$r(\mathcal{C}_1^h) = \frac{|\mathbf{d}_h|^2}{2|\mathbf{d}_h \times \mathbf{t}_h|} = \frac{h^2 - \frac{1}{12}\kappa_0^2h^4 + o(h^4)}{2(\frac{1}{2}\kappa_0h^2 - \frac{1}{3}\kappa_0'h^3 + o(h^3))} = \frac{1}{\kappa(s)} + \frac{2\kappa_0'}{3\kappa_0^2}h + o(h),$$

and with $\rho'(s) = \frac{-\kappa'(s)}{\kappa^2(s)}$ (5.53)-(5.54) follow. ■

5.4 Torsion

By construction the biarc $(\mathbf{a}, \bar{\mathbf{a}})_h$ interpolating the point-tangent data $((\mathbf{q}_0, \mathbf{t}_0), (\mathbf{q}_h, \mathbf{t}_h))$ for some $\Lambda_h \in (0,1)$ has contact of order one with the curve $\mathbf{q}$ at $\mathbf{q}(s) = \mathbf{q}_0$ and $\mathbf{q}(s+h) = \mathbf{q}_h$. If the underlying base curve $\mathbf{q}$ is a C^3-curve, in the limit $h \to 0$ the sphere tangent to the curve at both $\mathbf{q}_0$ and $\mathbf{q}_h$ approaches the osculating sphere at $\mathbf{q}(s) = \mathbf{q}_0$. This is true for any Hermite interpolation, but the biarc interpolation has the special property that the biarcs lie entirely on the double tangent sphere.

We now establish an approximation of torsion at a data point $\mathbf{q}(s)$ in terms of the angle between the planes of the two circles $\mathcal{C}_0^h$ and $\mathcal{C}_1^h$.

Proposition 5.13 *Let Hypotheses 5.2 hold, and assume $\mathbf{q} \in C^3(I, \mathbb{R}^3)$ is parametrised by arc length and $s \in I$ with $\kappa(s) \neq 0$. Denote by $0 \leq \psi_h \leq \pi$ the angle between the planes of the circle $\mathcal{C}_0^h$ and $\mathcal{C}_1^h$, cf. Notation 5.10. Then*

$$|\tau(s)| = \frac{3 \sin \psi_h}{|h|} + o(1).$$

If in addition $\mathbf{q}'''$ is uniformly continuous the speed of convergence is independent on s.

Proof We use the notation (5.55) and additionally denote the torsion at s by τ_0. We then exploit the expansions (5.56)-(5.57). The chord $\mathbf{d}_h$ and the tangent $\mathbf{t}_h$ in the $(\mathbf{t}_0, \mathbf{n}_0, \mathbf{b}_0)$ coordinates are given in (5.58). Expansions related to the normal vectors $\mathbf{v}_0^h$ and $\mathbf{v}_1^h$ to the planes of $\mathcal{C}_0^h$ and $\mathcal{C}_1^h$ are provided in (5.59) and (5.60) respectively. The angle $0 \leq \psi_h \leq \pi$ between the planes of the circles $\mathcal{C}_0^h$ and $\mathcal{C}_1^h$ is now defined by

$$\sin \psi_h := \frac{|\mathbf{v}_0^h \times \mathbf{v}_1^h|}{|\mathbf{v}_0^h|\,|\mathbf{v}_1^h|}. \tag{5.61}$$

Therefore we compute

$$\mathbf{v}_0^h \times \mathbf{v}_1^h = \frac{1}{12} h^5 \kappa_0^2 \tau_0 \mathbf{t}_0 + o(h^5), \quad \text{and} \quad |\mathbf{v}_0^h \times \mathbf{v}_1^h|^2 = \frac{1}{144} h^{10} \kappa_0^4 \tau_0^2 + o(h^{10}). \tag{5.62}$$

We now use expansions (5.59), (5.60) and (5.62) in (5.61) to obtain

$$\begin{aligned}
\sin^2 \psi_h &= \frac{\frac{1}{144} h^{10} \kappa_0^4 \tau_0^2 + o(h^{10})}{(\frac{1}{4} h^4 \kappa_0^2 + \frac{1}{6} h^5 \kappa_0 \kappa_0' + o(h^5))\,(\frac{1}{4} h^4 \kappa_0^2 - \frac{1}{3} h^5 \kappa_0 \kappa_0' + o(h^5))} \\
&= \frac{\frac{1}{144} h^2 \kappa_0^4 \tau_0^2 + o(h^2)}{\frac{1}{16} \kappa_0^4 - \frac{1}{24} h \kappa_0^3 \kappa_0' + o(h)} = \frac{\frac{1}{9} h^2 \kappa_0^4 \tau_0^2 + o(h^2)}{\kappa_0^4 - \frac{2}{3} h \kappa_0^3 \kappa_0' + o(h)} \\
&= \frac{1}{9} h^2 \tau_0^2 + o(h^2),
\end{aligned}$$

or

$$\sin \psi_h = \tfrac{1}{3} |h| |\tau_0| + o(h),$$

as was to be shown. ■

Chapter 6

Biarc curves and global convergence results

6.1 Interpolation with Biarc curves

We now consider interpolation by biarc curves of a set of point-tangent data sampled from a base curve $\mathbf{q}$, and study convergence of the curve assembled from individual biarcs to the underlying base curve $\mathbf{q}$. First we need:

Definition 6.1 *A* biarc curve $\boldsymbol{\beta}$ *is a space curve assembled from biarcs in a* C^1 *fashion, where the biarcs interpolate a sequence* $\{(\mathbf{q}_i, \mathbf{t}_i)\}$ *of point-tangent data (cf. Definition 4.1).*

Notation 6.2 *Given a finite closed interval* $I = [l_0, l_1] \subset \mathbb{R}$*, a* mesh $\mathcal{M}$ of mesh size $h > 0$ on I *will mean a sequence* $\{s_i\}$*,*

$$l_0 = s_0 < s_1 < \cdots < s_m = l_1,$$

for some $m \in \mathbb{N}$*, and* $h = \max_{i=1,\ldots,m} |s_i - s_{i-1}| < \infty$*.*

We will consider a sequence of meshes $\mathcal{M}_j$*,* $j \in \mathbb{N}$ *on* I *with mesh size* $h_j \to 0$ *(and wlog we assume that the mesh size* h_j *is monotone decreasing). We denote by* $\bar{\mathcal{N}}_j := \{0, \ldots, m\}$ *the set of indices of the mesh* $\mathcal{M}_j$*, and its members by* $s_{j,i}$*,* $i \in \bar{\mathcal{N}}_j$*. For* $i \in \mathcal{N}_j := \{0, \ldots, m-1\}$ *we set* $h_{j,i} := s_{j,i+1} - s_{j,i}$*. We assume that for all* $j > k$ *there is a mapping* $\iota_{k\to j} : \bar{\mathcal{N}}_k \to \bar{\mathcal{N}}_j$ *such that*

$$s_{k,i} = s_{j,\iota_{k\to j}(i)}, \qquad i \in \bar{\mathcal{N}}_k, \tag{6.1}$$

i.e. the meshes are nested.

Notation 6.3 *Let* $\mathbf{q} \in C^{1,1}(I, \mathbb{R}^3)$ *be parametrised by arc length. For a given sequence of meshes* $\mathcal{M}_j$ *as described in Notation 6.2,* $\boldsymbol{\beta}_{h_j}$ *is a biarc curve interpolating the data* $(\mathbf{q}(s_{j,i}), \mathbf{q}'(s_{j,i})) \in \mathcal{J}$ *with matching points on* Σ_{++}*.*

We denote by $(\mathbf{a}, \bar{\mathbf{a}})_{j,i}$ *the* i*-th biarc of the biarc curve* $\boldsymbol{\beta}_{h_j}$*, i.e. the biarc interpolating* $((\mathbf{q}(s_{j,i}), \mathbf{q}'(s_{j,i})), (\mathbf{q}(s_{j,i+1}), \mathbf{q}'(s_{j,i+1})))$*. We denote the arc-length parameter interval of*

the biarc curve $\boldsymbol{\beta}_{h_j}$ by I_j. The arc-length parameter corresponding to the matching point of the biarc $(\mathbf{a}, \bar{\mathbf{a}})_{j,i}$ is denoted by $m_{j,i} \in I_j$. The radii of the biarc $(\mathbf{a}, \bar{\mathbf{a}})_{j,i}$ are denoted by $r_{j,i}$ and $\bar{r}_{j,i}$, and the curvatures by $\kappa_{j,i}$ and $\bar{\kappa}_{j,i}$.

Note that for each point-tangent data pair we may choose the matching points independently. If the mesh size h_j is small enough, each point-tangent data pair $((\mathbf{q}(s_{j,i}), \mathbf{q}'(s_{j,i})), (\mathbf{q}(s_{j,i+1}), \mathbf{q}'(s_{j,i+1})))$ and each biarc $(\mathbf{a}, \bar{\mathbf{a}})_{j,i}$ will be proper in the sense of Definitions 4.10 and 4.12, in which case the biarc matching points correspond to biarc parameters $\Lambda_{j,i} \in (0, 1)$ (cf. Lemma 4.13).

The question we address is in what sense do the biarc curves $\boldsymbol{\beta}_{h_j}$ tend to the base curve $\mathbf{q}$ as $j \to \infty$?

Hypothesis 6.4 *$I \subset \mathbb{R}$ is a finite closed interval $I = [l_0, l_1]$.*

Hypothesis 6.5 *A sequence of biarc curves $\boldsymbol{\beta}_{h_j}$ is generated as in Notation 6.2 and 6.3.*

Hypothesis 6.6 *There exist two constants $\Lambda_{\min}, \Lambda_{\max}$ with $0 < \Lambda_{\min} < \Lambda_{\max} < 1$ such that*

$$\Lambda_{\min} \leq \Lambda_{j,i} \leq \Lambda_{\max} \tag{6.2}$$

for the biarc parameter $\Lambda_{j,i}$ of each biarc $(\mathbf{a}, \bar{\mathbf{a}})_{j,i}$ of every biarc curve $\boldsymbol{\beta}_{h_j}$, $j \in \mathbb{N}$.

Hypothesis 6.6 is needed to ensure finite curvature and C^1 continuity of the biarc curve $\boldsymbol{\beta}_{h_j}$, see remark on page 45. Hereafter, and following common practice, the symbol c will always denote a constant, but not necessarily always the same constant.

Lemma 6.7 *Let Hypotheses 6.4, 5.3, 6.5 and 6.6 hold. Then the radii of the arcs of the biarc curves $\boldsymbol{\beta}_{h_j}$ are bounded away from zero, that is, for all $j \in \mathbb{N}, i \in \mathcal{N}_j$ there exists a positive constant $\mathsf{c} = \mathsf{c}(K_{\mathbf{q}'}, \Lambda_{\min}) > 0$ with*

$$r_{j,i} \geq \mathsf{c} \quad \textit{and} \quad \bar{r}_{j,i} \geq \mathsf{c}.$$

Equivalently, the curvatures of the biarc curves $\boldsymbol{\beta}_{h_j}$ are bounded from above,

$$\kappa_{j,i} \leq \frac{1}{\mathsf{c}} < \infty \quad \textit{and} \quad \bar{\kappa}_{j,i} \leq \frac{1}{\mathsf{c}} < \infty.$$

Proof The radius of the circle passing through $\mathbf{q}_0$ and $\mathbf{q}_1$, tangent at $\mathbf{q}_0$ to $\mathbf{t}_0$ is given by (5.35). We use the Notation 5.4, where s is now a mesh point $s_{j,i}$ and where $s+h$ corresponds to $s_{j,i}+h_{j,i} = s_{j,i+1}$. Combining the formula (5.35) with the expansions (5.15) and (5.17) yields

$$\begin{aligned} r(\mathbf{q}_0, \mathbf{t}_0, \mathbf{m}_h)^2 &= \frac{|\mathbf{m}_h - \mathbf{q}_0|^2}{4\left[1 - \left(\frac{\mathbf{m}_h - \mathbf{q}_0}{|\mathbf{m}_h - \mathbf{q}_0|} \cdot \mathbf{t}_0\right)^2\right]} = \frac{h_i^2(\Lambda^2 + O(h_i^2))}{4[1 - (1 + O(h_i^2))]} \\ &= \frac{\Lambda^2 + O(h_i^2)}{O(1)} \geq \frac{\Lambda_{\min}^2 + O(h_i^2)}{\mathsf{c}} \geq \frac{\Lambda_{\min}^2}{2\mathsf{c}}, \end{aligned}$$

for j sufficiently large, because the constants involved in the expansions (5.15) and (5.17) are independent of $s \in I$, and so are independent of $i \in \mathcal{N}_j$. Thus there exists a constant c such that

$$r_{j,i} \geq \mathsf{c}, \qquad \forall j \in \mathbb{N}, \quad i \in \mathcal{N}_j.$$

By a symmetry argument we obtain $\bar{r}_{j,i} \geq \mathsf{c}$, for $j \in \mathbb{N}$, $i \in \mathcal{N}_j$. ■

6.2 Convergence of arc length

Lemma 6.8 (Arc length of a biarc) *Let Hypotheses 6.4,5.3 and 6.5 hold. Then*

$$\lambda((\mathbf{a}, \bar{\mathbf{a}})_{j,i}) - h_{j,i} = O(h_{j,i}^3)$$

where the convergence is uniform in $i \in \mathcal{N}_j$.

Proof This is the statement in Lemma 5.8 combined with the fact that the constant involved depends only on $K_{\mathbf{q}'}$, and in particular does not depend on $i \in \mathcal{N}_j$. ■

Corollary 6.9 (Convergence of arc length) *Let Hypotheses 6.4, 5.3 and 6.5 hold. Then the arc length of the biarc curve $\boldsymbol{\beta}_{h_j}$ converges to the arc length of the curve $\mathbf{q}$ quadratically:*

$$\frac{\lambda(\boldsymbol{\beta}_{h_j})}{\lambda(\mathbf{q})} - 1 = O(h_j^2),$$

and the constant depends only on $K_{\mathbf{q}'}$.

Proof The length of the curves $\mathbf{q}$ and $\boldsymbol{\beta}_{h_j}$ is the sum of the corresponding lengths between the data points, hence

$$\begin{aligned} \lambda(\boldsymbol{\beta}_{h_j}) - \lambda(\mathbf{q}) &= \sum_{i \in \mathcal{N}_j} (\lambda((\mathbf{a}, \bar{\mathbf{a}})_{j,i}) - h_{j,i}) = \sum_{i \in \mathcal{N}_j} h_{j,i}^3 \frac{\lambda((\mathbf{a}, \bar{\mathbf{a}})_{j,i}) - h_{j,i}}{h_{j,i}^3} \\ &\leq \sum_{i \in \mathcal{N}_j} h_{j,i}^3 \, \mathsf{c} \leq h_j^2 \, \mathsf{c} \left(\sum_{i \in \mathcal{N}_j} h_{j,i} \right) = h_j^2 \, \mathsf{c} \, \lambda(\mathbf{q}), \end{aligned}$$

as required. ■

6.3 Parametrisation of the biarc curve

In general the two curves $\mathbf{q} : I \to \mathbb{R}^3$ and $\boldsymbol{\beta}_{h_j} : I_j \to \mathbb{R}^3$ have different arc lengths so that in order to compare them, and in particular to estimate an error bound between them, we have to pick a reparametrisation of the biarc curve $\boldsymbol{\beta}_{h_j}$. We consider reparametrisations

$$\varphi_j : I \to I_j$$

which satisfy the following seven conditions:

(C1) $\varphi_j \in C^{2,1}(I, I_j)$, with $\varphi_j \in C^3$ on the intervals $[s_{j,i}, m_{j,i}]$ and $[m_{j,i}, s_{j,i+1}]$ for all $i \in \mathcal{N}_j,\ j \in \mathbb{N}$,

(C2) φ_j is monotone increasing for j sufficiently large,

(C3) $\mathbf{q}(s_{j,i}) = \boldsymbol{\beta}_{h_j}(\varphi_j(s_{j,i}))$, for $i \in \mathcal{N}_j,\ j \in \mathbb{N}$,

(C4) $\varphi_j'(s_{j,i}) = \frac{\lambda(\boldsymbol{\beta}_{h_j})}{\lambda(\mathbf{q})}$, for $i \in \mathcal{N}_j,\ j \in \mathbb{N}$,

(C5) $\varphi_j''(s_{j,i}) = 0$, for $i \in \mathcal{N}_j,\ j \in \mathbb{N}$,

(C6) $\|\varphi_j' - 1\|_{C(I,\mathbb{R})} \to 0$, $\|\varphi_j''\|_{C(I,\mathbb{R})} \to 0$ as $j \to \infty$,

and

(C7) $\|\varphi_j'''\|_{L^\infty} \leq \mathsf{c}$ for all $j \in \mathbb{N}$.

Condition (C1) imposes regularity, and condition (C2) implies that the function φ_j used in the reparametrisation is a bijection for j sufficiently large. Condition (C3) constrains the biarc curve to pass through the data points at the mesh points. Conditions (C4)-(C7) are convenient for the proofs. For finite intervals, as assumed here, condition (C6) implies $\|\varphi_j - id\|_{C(I,\mathbb{R})} \to 0$, where id denotes the identity mapping. See Figure 6.1 for an illustration of such a reparametrisation function φ_j.

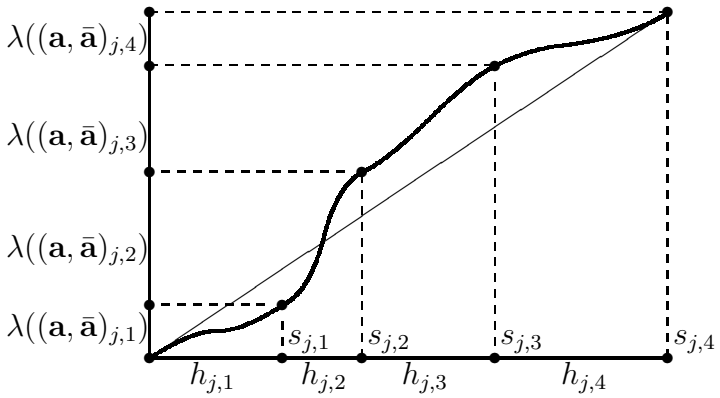

Figure 6.1: A reparametrisation function φ_j, which maps arc-length parameters of the base curve $\mathbf{q}$ to arc-length parameters of the biarc curve $\boldsymbol{\beta}_{h_j}$.

We denote the reparametrised biarc curve by $\mathbf{B}_{h_j}$, or explicitly

$$\mathbf{B}_{h_j} := \boldsymbol{\beta}_{h_j} \circ \varphi_j : I \to I_j \to \mathbb{R}^3. \tag{6.3}$$

The arc-length parametrised, biarc curve $\boldsymbol{\beta}_{h_j}$ is piecewise C^∞, therefore the biarc curve $\mathbf{B}_{h_j}$ is as smooth (piecewise) as the reparametrisation function φ_j, which we here assume to be $C^{2,1}$. The convergence results of section 5 are independent of the particular reparametrisation chosen. However it is important to know that at least one choice satisfying (C1)-(C7) exists. An explicit construction of one simple sequence $\{\varphi_j\}$ is given in Appendix A.

Hypothesis 6.10 *The function φ_j is a reparametrisation function satisfying conditions (C1)-(C7), for all $j \in \mathbb{N}$ and the reparametrised biarc curve $\mathbf{B}_{h_j}$ is given by (6.3).*

6.4 C^1-convergence for $\mathbf{q} \in C^{1,1}(I, \mathbb{R}^3)$

Notation 6.11 *Let Hypotheses 6.4, 5.3, 6.5, and 6.10 hold. For $j \in \mathbb{N}$ we denote the Lipschitz constant of the tangent of the difference curve $\mathbf{q} - \mathbf{B}_{h_j}$ by*

$$K_j := \sup_{s,\sigma \in I, s \neq \sigma} \frac{|(\mathbf{q} - \mathbf{B}_{h_j})'(s) - (\mathbf{q} - \mathbf{B}_{h_j})'(\sigma)|}{|s - \sigma|}.$$

Lemma 6.12 *Let Hypotheses 6.4, 5.3, 6.5, 6.6 and 6.10 hold. Then there exists a constant $\mathsf{c} > 0$, such that $K_j \leq \mathsf{c}$ for all $j \in \mathbb{N}$.*

Proof Consider the following series of inequalities, whose derivation is explained below.

$$\begin{aligned}
K_j &\leq \sup_{s,\sigma} \frac{|\mathbf{q}'(s) - \mathbf{q}'(\sigma)|}{|s - \sigma|} + \sup_{s,\sigma} \frac{|\mathbf{B}'_{h_j}(s) - \mathbf{B}'_{h_j}(\sigma)|}{|s - \sigma|} && (6.4)\\
&= K_{\mathbf{q}'} + \sup_{s,\sigma} \frac{|\boldsymbol{\beta}'_{h_j}(\varphi_j(s))\varphi'_j(s) - \boldsymbol{\beta}'_{h_j}(\varphi_j(\sigma))\varphi'_j(\sigma)|}{|s - \sigma|} && (6.5)\\
&\leq K_{\mathbf{q}'} + \sup_{s,\sigma} \frac{|\boldsymbol{\beta}'_{h_j}(\varphi_j(s)) - \boldsymbol{\beta}'_{h_j}(\varphi_j(\sigma))|}{|s - \sigma|} \mathsf{c}_1 + \mathsf{c}_2 && (6.6)\\
&\leq K_{\mathbf{q}'} + \sup_{\tilde{s},\tilde{\sigma} \in I_j} \frac{|\boldsymbol{\beta}'_{h_j}(\tilde{s}) - \boldsymbol{\beta}'_{h_j}(\tilde{\sigma})|}{|\tilde{s} - \tilde{\sigma}|} \quad \mathsf{c}_3 + \mathsf{c}_2 && (6.7)\\
&\leq K_{\mathbf{q}'} + \max_{i \in \mathcal{N}_j} \{\kappa_{j,i}, \bar{\kappa}_{j,i}\} \; \mathsf{c}_3 + \mathsf{c}_2 \; \leq \mathsf{c}. && (6.8)
\end{aligned}$$

We use the triangle inequality in (6.4). Applying the definition of $K_{\mathbf{q}'}$ and the chain rule we transform the right hand side of (6.4) to (6.5). To obtain (6.6) from (6.5) follow

the steps from (6.9) to (6.12) below:

$$
\begin{aligned}
& \sup_{s,\sigma} \frac{|\boldsymbol{\beta}'_{h_j}(\varphi_j(s))\varphi'_j(s) - \boldsymbol{\beta}'_{h_j}(\varphi_j(\sigma))\varphi'_j(\sigma)|}{|s-\sigma|} \\
\leq \; & \sup_{s,\sigma} \frac{|\boldsymbol{\beta}'_{h_j}(\varphi_j(s))\varphi'_j(s) - \boldsymbol{\beta}'_{h_j}(\varphi_j(\sigma))\varphi'_j(s)|}{|s-\sigma|} \\
& + \sup_{s,\sigma} \frac{|\boldsymbol{\beta}'_{h_j}(\varphi_j(\sigma))\varphi'_j(s) - \boldsymbol{\beta}'_{h_j}(\varphi_j(\sigma))\varphi'_j(\sigma)|}{|s-\sigma|} && (6.9) \\
\leq \; & \sup_{s,\sigma} \frac{|\boldsymbol{\beta}'_{h_j}(\varphi_j(s)) - \boldsymbol{\beta}'_{h_j}(\varphi_j(\sigma))|}{|s-\sigma|} \|\varphi'_j\|_C + \sup_{s,\sigma} \frac{|\varphi'_j(s) - \varphi'_j(\sigma)|}{|s-\sigma|} && (6.10) \\
\leq \; & \sup_{s,\sigma} \frac{|\boldsymbol{\beta}'_{h_j}(\varphi_j(s)) - \boldsymbol{\beta}'_{h_j}(\varphi_j(\sigma))|}{|s-\sigma|} \mathsf{c}_1 + \|\varphi''_j\| && (6.11) \\
\leq \; & \sup_{s,\sigma} \frac{|\boldsymbol{\beta}'_{h_j}(\varphi_j(s)) - \boldsymbol{\beta}'_{h_j}(\varphi_j(\sigma))|}{|s-\sigma|} \mathsf{c}_1 + \mathsf{c}_2. && (6.12)
\end{aligned}
$$

The estimate in (6.9) is a simple triangle inequality, and to get (6.10) we use the facts that $\|\varphi'_j\|_C$ is finite by (C6) and $\|\boldsymbol{\beta}'_{h_j} \circ \varphi_j\|_C = 1$. To go from (6.10) to (6.11) we use $\varphi_j \in C^2$ by (C1). To find (6.12) we reapply (C6).

To derive (6.7) from (6.6) consider (6.13) to (6.17). In the equality in (6.13) we exploit the fact that φ_j is a bijection, which is a consequence of (C1)-(C3). To obtain the right factor in (6.15) from the right factor in (6.14) we again use that φ_j is a bijection. We may rewrite (6.15) as (6.16) because $\|\varphi'_j\|_C$ is finite. Finally with (C6) we obtain (6.17).

$$
\begin{aligned}
\sup_{s,\sigma\in I} \; & \frac{|\boldsymbol{\beta}'_{h_j}(\varphi_j(s)) - \boldsymbol{\beta}'_{h_j}(\varphi_j(\sigma))|}{|s-\sigma|} \\
= \; & \sup_{\tilde{s},\tilde{\sigma}\in I_j} \left(\frac{|\boldsymbol{\beta}'_{h_j}(\tilde{s}) - \boldsymbol{\beta}'_{h_j}(\tilde{\sigma})|}{|\tilde{s}-\tilde{\sigma}|} \frac{|\tilde{s}-\tilde{\sigma}|}{|\varphi_j^{-1}(\tilde{s}) - \varphi_j^{-1}(\tilde{\sigma})|} \right) && (6.13) \\
\leq \; & \sup_{\tilde{s},\tilde{\sigma}\in I_j} \frac{|\boldsymbol{\beta}'_{h_j}(\tilde{s}) - \boldsymbol{\beta}'_{h_j}(\tilde{\sigma})|}{|\tilde{s}-\tilde{\sigma}|} \sup_{\tilde{s},\tilde{\sigma}\in I_j} \frac{|\tilde{s}-\tilde{\sigma}|}{|\varphi_j^{-1}(\tilde{s}) - \varphi_j^{-1}(\tilde{\sigma})|} && (6.14) \\
= \; & \sup_{\tilde{s},\tilde{\sigma}\in I_j} \frac{|\boldsymbol{\beta}'_{h_j}(\tilde{s}) - \boldsymbol{\beta}'_{h_j}(\tilde{\sigma})|}{|\tilde{s}-\tilde{\sigma}|} \sup_{s,\sigma\in I} \frac{|\varphi_j(s) - \varphi_j(\sigma)|}{|s-\sigma|} && (6.15) \\
= \; & \sup_{\tilde{s},\tilde{\sigma}\in I_j} \frac{|\boldsymbol{\beta}'_{h_j}(\tilde{s}) - \boldsymbol{\beta}'_{h_j}(\tilde{\sigma})|}{|\tilde{s}-\tilde{\sigma}|} \quad \|\varphi'_j\|_C && (6.16) \\
\leq \; & \sup_{\tilde{s},\tilde{\sigma}\in I_j} \frac{|\boldsymbol{\beta}'_{h_j}(\tilde{s}) - \boldsymbol{\beta}'_{h_j}(\tilde{\sigma})|}{|\tilde{s}-\tilde{\sigma}|} \quad \mathsf{c}. && (6.17)
\end{aligned}
$$

To bound (6.7) by (6.8) we used the following fact: Let $\boldsymbol{\alpha}$ be a curve consisting of m arcs of circles with a continuous tangent everywhere, parametrised by arc length. Then

$$
\sup_{s\neq\sigma} \frac{|\boldsymbol{\alpha}'(s) - \boldsymbol{\alpha}'(\sigma)|}{|s-\sigma|} \leq \max\{\kappa_1, \cdots, \kappa_m\},
$$

where the κ_i are the curvatures of the different arcs. Because $\boldsymbol{\beta}_{h_j}$ is parametrised by arc length with curvatures $\kappa_{j,i}$, $\bar{\kappa}_{j,i}$ we may use this bound. The last inequality in (6.8) is given by Lemma 6.7. ■

Theorem 6.13 (C^1-convergence) *Let Hypotheses 6.4, 5.3, 6.5, 6.6 and 6.10 hold. Then the biarc curves $\mathbf{B}_{h_j}$ converge to the curve $\mathbf{q}$ in the space $C^1(I,\mathbb{R}^3)$ as $j\to\infty$. More precisely, as $j\to\infty$*

$$\|\mathbf{q}-\mathbf{B}_{h_j}\|_{C^0}=O(h_j^2),\qquad \|\mathbf{q}'-\mathbf{B}'_{h_j}\|_{C^0}=O(h_j).$$

Proof Both the curve $\mathbf{q}$ and the biarc curves $\mathbf{B}_{h_j}$ are $C^{1,1}$-curves, thus we may use the expansions (5.9) and (5.10) for $\mathbf{q}-\mathbf{B}_{h_j}$, simplify with the chain rule and conditions (C3)-(C4) to get

$$\begin{aligned}
(\mathbf{q}-\mathbf{B}_{h_j})(s) &= (\mathbf{q}-\mathbf{B}_{h_j})(s_{j,i})+(\mathbf{q}-\mathbf{B}_{h_j})'(s_{j,i})(s-s_{j,i})\\
&\quad +\widetilde{\boldsymbol{\omega}}_{h_j}(s,s_{j,i})\tfrac{1}{2}(s-s_{j,i})^2\\
&= \mathbf{q}'(s_{j,i})\left(1-\frac{\lambda(\boldsymbol{\beta}_{h_j})}{\lambda(\mathbf{q})}\right)(s-s_{j,i})+\widetilde{\boldsymbol{\omega}}_{h_j}(s,s_{j,i})\tfrac{1}{2}(s-s_{j,i})^2,\\
(\mathbf{q}-\mathbf{B}_{h_j})'(s) &= (\mathbf{q}-\mathbf{B}_{h_j})'(s_{j,i})+\boldsymbol{\omega}_{h_j}(s,s_{j,i})(s-s_{j,i})\\
&= \mathbf{q}'(s_{j,i})\left(1-\frac{\lambda(\boldsymbol{\beta}_{h_j})}{\lambda(\mathbf{q})}\right)+\boldsymbol{\omega}_{h_j}(s,s_{j,i})(s-s_{j,i}).
\end{aligned}$$

The vector functions $\boldsymbol{\omega}_{h_j}$ and $\widetilde{\boldsymbol{\omega}}_{h_j}$ are bounded by the Lipschitz constant K_j of $\mathbf{q}'-\mathbf{B}'_{h_j}$, i.e. $|\widetilde{\boldsymbol{\omega}}_{h_j}|,|\boldsymbol{\omega}_{h_j}|\le K_j$. The Lipschitz constant K_j is uniformly bounded by Lemma 6.12. Then $|\mathbf{q}'(s)|=1$, and Corollary 6.9 yields the rest. ■

6.5 $C^{1,1}$-convergence for $\mathbf{q}\in C^2(I,\mathbb{R}^3)$

As the underlying curve $\mathbf{q}$ is at least $C^{1,1}$ by assumption, and the biarc curves are $C^{1,1}$ by construction, it is natural to seek convergence in the $C^{1,1}$ norm. We next obtain $C^{1,1}$ convergence, but only under an additional regularity assumption on $\mathbf{q}$. Recall that for any Lipschitz curve $\mathbf{q}$ the Lipschitz constant for that curve is denoted $K_{\mathbf{q}}$.

Lemma 6.14 *Let Hypotheses 6.4, 5.3, 6.5, 6.6 and 6.10 hold. Then*

$$\|\mathbf{q}-\mathbf{B}_{h_j}\|_{C^{1,1}}\to 0,\qquad \text{as } j\to\infty,$$

if and only if

$$K_{\{\mathbf{B}'_{h_j}-\mathbf{B}'_{h_k}\}}\to 0,\qquad \text{as } j,k\to\infty.$$

Proof If $\{\mathbf{q}-\mathbf{B}_{h_j}\}\to 0$ in $C^{1,1}$, then $\{\mathbf{q}-\mathbf{B}_{h_j}\}$ is a Cauchy sequence in $C^{1,1}$. This implies that $\{\mathbf{B}_{h_j}\}$ is a Cauchy sequence in $C^{1,1}$, that is $\|\mathbf{B}_{h_j}-\mathbf{B}_{h_k}\|_{C^{1,1}}\to 0$ as

$j,k \to \infty$. In particular $K_{\{\mathbf{B}'_{h_j} - \mathbf{B}'_{h_k}\}} \to 0$, as $j,k \to \infty$, by the definition (5.1) of the $C^{1,1}$ norm.

On the other hand, let $K_{\{\mathbf{B}'_{h_j} - \mathbf{B}'_{h_k}\}} \to 0$, for $j,k \to \infty$. All conditions of Theorem 6.13 are fulfilled, thus $\mathbf{B}_{h_j} \to \mathbf{q}$ in C^1, and therefore $\{\mathbf{B}_{h_j}\}$ is a Cauchy sequence in C^1. With definition (5.1) of the norm, it follows that $\{\mathbf{B}_{h_j}\}$ is a Cauchy sequence in $C^{1,1}$. But $C^{1,1}$ is a Banach space, hence $\{\mathbf{B}_{h_j}\}$ converges in $C^{1,1}$ to some $\mathbf{B} \in C^{1,1}$. In particular $\{\mathbf{B}_{h_j}\} \to \mathbf{B}$ in C^1. By uniqueness of limits, $\mathbf{B} = \mathbf{q}$ which yields the result. ■

Thus to obtain a sharp characterisation of how smooth $\mathbf{q}$ must be for $C^{1,1}$ convergence one could study the Lipschitz constants $K_{\{\mathbf{B}'_{h_j} - \mathbf{B}'_{h_k}\}}$ on sequences of biarc curves. However we instead obtain a $C^{1,1}$ convergence result assuming $\mathbf{q} \in C^2$. For $\mathbf{q} \in C^2(I,\mathbb{R}^3)$ we next review the result that the arcs of the biarc curves $\boldsymbol{\beta}_{h_j}$ approach the osculating circles at the data points. This implies convergence in the space $C^{1,1}(I,\mathbb{R}^3)$, and a faster rate of convergence in the space $C^1(I,\mathbb{R}^3)$ than was shown for $C^{1,1}$-curves, cf. Theorem 6.13.

The Taylor expansions for $\mathbf{q} \in C^2(I,\mathbb{R}^3)$ are given in (5.38)-(5.40). Note that the estimates are uniform in $\sigma \in I$, because I is a finite interval, thus $\mathbf{q}''$ is uniformly continuous. We denote the right- and left-sided second derivatives of the biarc curve $\boldsymbol{\beta}_{h_j}$ by ${\boldsymbol{\beta}''_{h_j}}^{\pm}$.

Proposition 6.15 *Let Hypotheses 6.4, 5.3, 6.5, 6.6 and 6.10 hold, and in addition assume $\mathbf{q} \in C^2(I,\mathbb{R}^3)$ is parametrised by arc length, with Lipschitz constant $K_{\mathbf{q}'} = \|\mathbf{q}''\|_C$. Then the arcs of the biarc curves $\boldsymbol{\beta}_{h_j}$ approach the osculating circles at the data points, or equivalently,*

$$\left|\mathbf{q}''(s_{j,i}) - {\boldsymbol{\beta}''_{h_j}}^{\pm}(\varphi_j(s_{j,i}))\right| = o(1),$$

uniformly in $i \in \mathcal{N}_j$ as $j \to \infty$, i.e. for $\epsilon > 0$ there exists $N \in \mathbb{N}$ s.t.

$$\left|\mathbf{q}''(s_{j,i}) - {\boldsymbol{\beta}''_{h_j}}^{\pm}(\varphi_j(s_{j,i}))\right| < \epsilon,$$

for all $i \in \mathcal{N}_j$ and $j > N$.

Proof This is the fact that the speed of convergence in Proposition 5.9 is independent of $s \in I$, a consequence of the uniform continuity of $\mathbf{q}''$. ■

Lemma 6.16 *Let Hypotheses 6.4, 5.3, 6.5, 6.6 and 6.10 hold, and in addition assume $\mathbf{q} \in C^2(I,\mathbb{R}^3)$ is parametrised by arc length, with Lipschitz constant $K_{\mathbf{q}'} = \|\mathbf{q}''\|_C$. For all $\epsilon > 0$ there exists $\delta > 0$, and $N \in \mathbb{N}$ s.t. for all $i \in \mathcal{N}_j$, $j > N$*

$$|\mathbf{B}''_{h_j}(s) - \mathbf{B}''_{h_j}(\sigma)| \leq \epsilon$$

for all $|s - \sigma| \leq \delta$, with either $s, \sigma \in [s_{j,i}, m_{j,i}]$ or $s, \sigma \in [m_{j,i}, s_{j,i+1}]$.

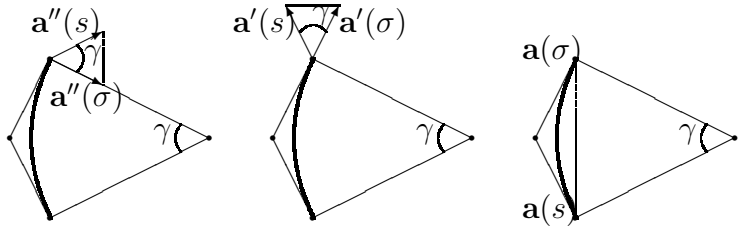

Figure 6.2: Cosine rule for (from left to right) difference of second derivatives, difference of tangents, and distance between points along a circular arc.

In other words, the estimate of uniformness of the second derivative of the biarc curve $\mathbf{B}_{h_j}$ restricted to the subintervals, is uniform in $i \in \mathcal{N}_j,\ j > N$ (where second derivatives at ends of the intervals are always understood to be the one-sided second derivatives).

Proof Using the chain rule on intervals of the form $[s_{j,i}, m_{j,i}]$ or $[m_{j,i}, s_{j,i+1}]$ we find

$$\mathbf{B}''_{h_j}(s) = \boldsymbol{\beta}''_{h_j}(\varphi_j(s)){\varphi'_j}^2(s) + \boldsymbol{\beta}'_{h_j}(\varphi_j(s))\varphi''_j(s). \tag{6.18}$$

With the triangle inequality we get

$$\begin{aligned}
|\mathbf{B}''_{h_j}(s) - \mathbf{B}''_{h_j}(\sigma)| &= |\boldsymbol{\beta}''_{h_j}(\varphi_j(s)){\varphi'_j}^2(s) + \boldsymbol{\beta}'_{h_j}(\varphi_j(s))\varphi''_j(s) \\
&\quad -\boldsymbol{\beta}''_{h_j}(\varphi_j(\sigma)){\varphi'_j}^2(\sigma) - \boldsymbol{\beta}'_{h_j}(\varphi_j(\sigma))\varphi''_j(\sigma)| \\
&\leq |\boldsymbol{\beta}''_{h_j}(\varphi_j(s)) - \boldsymbol{\beta}''_{h_j}(\varphi_j(\sigma))|\ |{\varphi'_j}^2(s)| \\
&\quad +|{\varphi'_j}^2(s) - {\varphi'_j}^2(\sigma)|\ |\boldsymbol{\beta}''_{h_j}(\varphi_j(\sigma))| \\
&\quad +|\boldsymbol{\beta}'_{h_j}(\varphi_j(s)) - \boldsymbol{\beta}'_{h_j}(\varphi_j(\sigma))|\ |\varphi''_j(s)| \\
&\quad +|\varphi''_j(s) - \varphi''_j(\sigma)|\ |\boldsymbol{\beta}'_{h_j}(\varphi_j(\sigma))|.
\end{aligned}$$

With condition (C6), Lemma 6.7 and the arc-length parametrisation of $\boldsymbol{\beta}_{h_j}$ we obtain

$$\begin{aligned}
|\mathbf{B}''_{h_j}(s) - \mathbf{B}''_{h_j}(\sigma)| &\leq |\boldsymbol{\beta}''_{h_j}(\varphi_j(s)) - \boldsymbol{\beta}''_{h_j}(\varphi_j(\sigma))|\ \mathsf{c} + |{\varphi'_j}^2(s) - {\varphi'_j}^2(\sigma)|\ \mathsf{c} \\
&\quad +|\boldsymbol{\beta}'_{h_j}(\varphi_j(s)) - \boldsymbol{\beta}'_{h_j}(\varphi_j(\sigma))|\ \mathsf{c} + |\varphi''_j(s) - \varphi''_j(\sigma)|.
\end{aligned}$$

Using again condition (C6), it remains to show that for a given $\epsilon > 0$ there exists $\delta > 0$ and $N \in \mathbb{N}$ s.t.

$$|\boldsymbol{\beta}''_{h_j}(\varphi_j(s)) - \boldsymbol{\beta}''_{h_j}(\varphi_j(\sigma))| \leq \epsilon, \tag{6.19}$$

$$|\boldsymbol{\beta}'_{h_j}(\varphi_j(s)) - \boldsymbol{\beta}'_{h_j}(\varphi_j(\sigma))| \leq \epsilon, \tag{6.20}$$

for all $|s - \sigma| \leq \delta$, with either $s, \sigma \in [s_{j,i}, m_{j,i}]$ or $s, \sigma \in [m_{j,i}, s_{j,i+1}]$ and for all $i \in \mathcal{N}_j,\ j > N$.

In order to prove the estimates (6.19) and (6.20), consider an arc $\mathbf{a}$ as a curve $\mathbf{a}(s)$ parametrised by arc length s. We exploit the cosine rule three times as shown in Figure 6.2. First we apply it to the difference between the two second derivatives:

$$|\mathbf{a}''(s) - \mathbf{a}''(\sigma)|^2 = \frac{2}{r^2}(1 - \cos\gamma), \tag{6.21}$$

where γ is the angle between the second derivatives at s and σ, and $r = \frac{1}{|\mathbf{a}''|}$ is the radius of the arc $\mathbf{a}$. By simple geometry we find that the angle between the tangents at s and σ equals γ. Thus, with the cosine rule, and the fact that $\mathbf{a}(s)$ is parametrised by arc length we get

$$|\mathbf{a}'(s) - \mathbf{a}'(\sigma)|^2 = 2(1 - \cos\gamma). \tag{6.22}$$

Applying the cosine rule again we find

$$|\mathbf{a}(s) - \mathbf{a}(\sigma)|^2 = 2r^2(1 - \cos\gamma). \tag{6.23}$$

Using the arc-length parametrisation, and combining (6.21) and (6.23), and (6.22) and (6.23), yields

$$|\mathbf{a}''(s) - \mathbf{a}''(\sigma)| \;=\; \frac{1}{r^2}|\mathbf{a}(s) - \mathbf{a}(\sigma)| \le \frac{1}{r^2}|s - \sigma|, \tag{6.24}$$

and

$$|\mathbf{a}'(s) - \mathbf{a}'(\sigma)| \;=\; \frac{1}{r}|\mathbf{a}(s) - \mathbf{a}(\sigma)| \le \frac{1}{r}|s - \sigma|. \tag{6.25}$$

Let $\epsilon > 0$ be given. By Lemma 6.7 there is a constant c, such that $\frac{1}{r_{j,i}}, \frac{1}{r^2_{j,i}}, \frac{1}{\bar{r}_{j,i}}, \frac{1}{\bar{r}^2_{j,i}} \le \mathsf{c}$ for all $i \in \mathcal{N}_j,\ j \in \mathbb{N}$. Applying (6.24) and (6.25) we find

$$\begin{aligned} |\boldsymbol{\beta}''_{h_j}(\varphi_j(s)) - \boldsymbol{\beta}''_{h_j}(\varphi_j(\sigma))| &\le \mathsf{c}|\varphi_j(s) - \varphi_j(\sigma)|, \\ |\boldsymbol{\beta}'_{h_j}(\varphi_j(s)) - \boldsymbol{\beta}'_{h_j}(\varphi_j(\sigma))| &\le \mathsf{c}|\varphi_j(s) - \varphi_j(\sigma)|. \end{aligned}$$

Condition (C6) implies that there exists $N \in \mathbb{N}$ such that $\|\varphi_j - id\|_C \le \frac{\epsilon}{3\mathsf{c}}$, for $j \ge N$, where id denotes the identity mapping. The triangle inequality then yields

$$\begin{aligned} \mathsf{c}|\varphi_j(s) - \varphi_j(\sigma)| &\le \mathsf{c}(|\varphi_j(s) - s| + |s - \sigma| + |\sigma - \varphi_j(\sigma)|) \\ &\le \mathsf{c}(\frac{\epsilon}{3\mathsf{c}} + |s - \sigma| + \frac{\epsilon}{3\mathsf{c}}) \le \epsilon, \end{aligned}$$

for all $|s - \sigma| \le \delta := \frac{\epsilon}{3\mathsf{c}}$, with either $s, \sigma \in [s_{j,i}, m_{j,i}]$ or $s, \sigma \in [m_{j,i}, s_{j,i+1}]$ and for all $i \in \mathcal{N}_j$ for all $j \ge N$. This proves the estimates (6.19) and (6.20). ■

Theorem 6.17 ($C^{1,1}$-convergence) *Let Hypotheses 6.4, 5.3, 6.5, 6.6 and 6.10 hold, and assume $\mathbf{q} \in C^2(I, \mathbb{R}^3)$ is parametrised by arc length, with Lipschitz constant $K_{\mathbf{q}'} = \|\mathbf{q}''\|_C$. Then as $j \to \infty$ the biarc curves $\mathbf{B}_{h_j}$ converge to the curve $\mathbf{q}$ in $C^{1,1}(I, \mathbb{R}^3)$. More precisely, as $j \to \infty$*

$$\|\mathbf{q} - \mathbf{B}_{h_j}\|_{C^0} = o(h_j^2), \qquad \|\mathbf{q}' - \mathbf{B}'_{h_j}\|_{C^0} = o(h_j), \qquad K_j = o(1).$$

Proof The curve $\mathbf{q} - \mathbf{B}_{h_j}$ restricted to the subintervals $[s_{j,i}, m_{j,i}]$ and $[m_{j,i}, s_{j,i+1}]$ is C^2, for all $i \in \mathcal{N}_j,\ j \in \mathbb{N}$. We now consider such an interval $[s_{j,i}, m_{j,i}]$, then with the

expansions (5.38)-(5.40), and conditions (C3) and (C4), we find

$$\begin{aligned}(\mathbf{q}-\mathbf{B}_{h_j})(s) &= (\mathbf{q}-\mathbf{B}_{h_j})(s_{j,i})+(\mathbf{q}-\mathbf{B}_{h_j})'(s_{j,i})(s-s_{j,i})\\ &\quad +\tfrac{1}{2}(\mathbf{q}-\mathbf{B}_{h_j})''^{+}(s_{j,i})(s-s_{j,i})^2+o((s-s_{j,i})^2)\\ &= \mathbf{q}'(s_{j,i})\left(1-\frac{\lambda(\mathbf{B}_{h_j})}{\lambda(\mathbf{q})}\right)(s-s_{j,i})+\tfrac{1}{2}(\mathbf{q}-\mathbf{B}_{h_j})''^{+}(s_{j,i})(s-s_{j,i})^2\\ &\quad +o((s-s_{j,i})^2), \qquad (6.26)\\ (\mathbf{q}-\mathbf{B}_{h_j})'(s) &= (\mathbf{q}-\mathbf{B}_{h_j})'(s_{j,i})+(\mathbf{q}-\mathbf{B}_{h_j})''^{+}(s_{j,i})(s-s_{j,i})+o((s-s_{j,i}))\\ &= \mathbf{q}'(s_{j,i})\left(1-\frac{\lambda(\mathbf{B}_{h_j})}{\lambda(\mathbf{q})}\right)+(\mathbf{q}-\mathbf{B}_{h_j})''^{+}(s_{j,i})(s-s_{j,i})\\ &\quad +o((s-s_{j,i})), \qquad (6.27)\end{aligned}$$

and

$$(\mathbf{q}-\mathbf{B}_{h_j})''(s) = (\mathbf{q}-\mathbf{B}_{h_j})''^{+}(s_{j,i})+o(1), \qquad (6.28)$$

for $s\in[s_{j,i},m_{j,i}]$. Analogous expansions at $s_{j,i+1}$ are valid on the intervals of the form $[m_{j,i},s_{j,i+1}]$, where right-sided second derivatives are replaced by left-sided second derivatives. Note that by Lemma 6.16 all the estimates in equations (6.26)-(6.28) are uniform in $i\in\mathcal{N}_j$. We next use the chain rule (6.18) at $s_{j,i}$ with conditions (C4) and (C5), followed by the triangle inequality, and finally Corollary 6.9, Lemma 6.7 and Proposition 6.15 to find

$$\begin{aligned}\left|\mathbf{q}''(s_{j,i})-\mathbf{B}_{h_j}''^{\pm}(s_{j,i})\right| &= \left|\mathbf{q}''(s_{j,i})-\boldsymbol{\beta}_{h_j}''^{\pm}(\varphi_j(s_{j,i}))\left(\frac{\lambda(\boldsymbol{\beta}_{h_j})}{\lambda(\mathbf{q})}\right)^2\right|\\ &\le \left|\mathbf{q}''(s_{j,i})-\boldsymbol{\beta}_{h_j}''^{\pm}(\varphi_j(s_{j,i}))\right| \qquad (6.29)\\ &\quad +\left|\boldsymbol{\beta}_{h_j}''^{\pm}(\varphi_j(s_{j,i}))\right|\left(1-\left(\frac{\lambda(\boldsymbol{\beta}_{h_j})}{\lambda(\mathbf{q})}\right)^2\right)=o(1),\end{aligned}$$

uniformly in $i\in\mathcal{N}_j$ as $j\to\infty$.

We may apply Corollary 6.9, and the limit (6.29) in equations (6.26) and (6.27) to obtain

$$\|\mathbf{q}-\mathbf{B}_{h_j}\|_{C^0}=o(h_j^2), \qquad \|\mathbf{q}'-\mathbf{B}'_{h_j}\|_{C^0}=o(h_j).$$

With equations (6.28) and (6.29) we find

$$(\mathbf{q}-\mathbf{B}_{h_j})''(s) = o(1),$$

uniformly on I. With the bound (5.2) we get

$$K_j\le\|(\mathbf{q}-\mathbf{B}_{h_j})''\|_{L_\infty}=o(1).$$

■

6.6 $C^{1,1}$-convergence for $\mathbf{q} \in C^{2,1}(I, \mathbb{R}^3)$

If we know that the curve $\mathbf{q}$ that we interpolate is twice differentiable and moreover that the second derivative is Lipschitz continuous, that is $\mathbf{q} \in C^{2,1}(I, \mathbb{R}^3)$, then we can slightly improve the results obtained for C^2 curves, cf. Proposition 6.15 and Theorem 6.17. The proofs are analogous, but take advantage of a higher order Taylor expansion. Lemma 6.19 assumes the role of Lemma 6.16.

In analogy to the expansions (5.9) and (5.10) we may establish

$$\begin{aligned} \mathbf{q}(s) &= \mathbf{q}(\sigma) + \mathbf{q}'(\sigma)(s-\sigma) + \tfrac{1}{2}\mathbf{q}''(\sigma)(s-\sigma)^2 + \widetilde{\mathbf{v}}(s,\sigma)(s-\sigma)^3, && (6.30)\\ \mathbf{q}'(s) &= \mathbf{q}'(\sigma) + \mathbf{q}''(\sigma)(s-\sigma) + \mathbf{v}(s,\sigma)(s-\sigma)^2, && (6.31)\\ \mathbf{q}''(s) &= \mathbf{q}''(\sigma) + \widehat{\mathbf{v}}(s,\sigma)(s-\sigma). && (6.32) \end{aligned}$$

where $\mathbf{v}, \widetilde{\mathbf{v}}$ and $\widehat{\mathbf{v}}$ are vector functions bounded by the Lipschitz constant $K_{\mathbf{q}''}$ of $\mathbf{q}''$, i.e. $|\mathbf{v}(s,\sigma)|,\ |\widetilde{\mathbf{v}}(s,\sigma)|,\ |\widehat{\mathbf{v}}(s,\sigma)| \le K_{\mathbf{q}''}$ for all $s, \sigma \in I$.

Proposition 6.18 *Let Hypotheses 6.4, 5.3, 6.5, 6.6 and 6.10 hold, and in addition assume $\mathbf{q} \in C^{2,1}(I, \mathbb{R}^3)$ is parametrised by arc length, with Lipschitz constant $K_{\mathbf{q}'} = \|\mathbf{q}''\|_C$. Then the arcs of the biarc curves $\boldsymbol{\beta}_{h_j}$ approach the osculating circles at the data points, or equivalently,*

$$\left| \mathbf{q}''(s_{j,i}) - \boldsymbol{\beta}_{h_j}''^{\,\pm}(\varphi_j(s_{j,i})) \right| = O(h_j),$$

uniformly in $i \in \mathcal{N}_j$ as $j \to \infty$.

Proof This proof is analogous to that of Proposition 5.9. We use the notation (5.44), where s is now a mesh point $s_{j,i}$ and where $s+h$ corresponds to $s_{j,i}+h_{j,i} = s_{j,i+1}$. Then the expansions (6.30)-(6.32) translate to

$$\begin{aligned} \mathbf{q}_h &= \mathbf{q}_0 + \mathbf{t}_0 h_{j,i} + \tfrac{1}{2}\kappa_0 \mathbf{n}_0 h_{j,i}^2 + \widetilde{\mathbf{v}}_{h_{j,i}} h_{j,i}^3, && (6.33)\\ \mathbf{t}_h &= \mathbf{t}_0 + \kappa_0 \mathbf{n}_0 h_{j,i} + \mathbf{v}_{h_{j,i}} h_{j,i}^2, && (6.34)\\ \kappa_h \mathbf{n}_h &= \kappa_0 \mathbf{n}_0 + \widehat{\mathbf{v}}_{h_{j,i}} h_{j,i}. && (6.35) \end{aligned}$$

We insert the expansions (6.33) and (6.34) into (5.49):

$$\begin{aligned} \boldsymbol{\beta}_{h_j}''^{\,+}(\varphi_j(s_{j,i})) &= 2\frac{\left(\mathbf{d} + [\frac{1}{2}\bar{\Lambda} h_{j,i} + O(h_{j,i}^3)](\mathbf{t}_0 - \mathbf{t}_h)\right) - \left(h_{j,i} + O(h_{j,i}^3)\right)\mathbf{t}_0}{[\Lambda + O(h_{j,i}^2)]\,[h_{j,i}^2 + O(h_{j,i}^4)]}\\ &= 2\frac{[\frac{1}{2}\kappa_0 \mathbf{n}_0 + \widetilde{\mathbf{v}}_{h_{j,i}} h_{j,i}] + [\frac{1}{2}\bar{\Lambda} + O(h_{j,i}^2)](-\kappa_0 \mathbf{n}_0 - \mathbf{v}_{h_{j,i}} h_{j,i}) - O(h_{j,i})\mathbf{t}_0}{\Lambda + O(h_{j,i}^2)}\\ &= \frac{(1-\bar{\Lambda})\kappa_0 \mathbf{n}_0 + O(h_{j,i})}{\Lambda + O(h_{j,i}^2)}. \end{aligned}$$

We obtain the same expression as for C^2 curves, only the $o(1)$ is replaced by $O(h)$. With the expansion (5.14) and notation (5.44) we find

$$\boldsymbol{\beta}_{h_j}''^{\,+}(\varphi_j(s_{j,i})) = \kappa_0 \mathbf{n}_0 + O(h_{j,i}) = \mathbf{q}''(s_{j,i}) + O(h_{j,i}),$$

and the estimate is uniform in $i \in \mathcal{N}_j$. The result for ${\boldsymbol{\beta}''_{h_j}}^-(\varphi_j(s_{j,i}))$ is derived similarly. ■

Lemma 6.19 *Let Hypotheses 6.4, 5.3, 6.5, 6.6 and 6.10 hold. Then there exists a constant* c *with*

$$\sup_{i\in N(j)} \|\mathbf{B}'''_{h_j}\|_{C((s_{j,i},m_{j,i}),\mathbb{R}^3)} \le \mathsf{c}, \qquad \textit{and} \qquad \sup_{i\in N(j)} \|\mathbf{B}'''_{h_j}\|_{C((m_{j,i},s_{j,i+1}),\mathbb{R}^3)} \le \mathsf{c}$$

for all $j \in \mathbb{N}$.

Proof For $s \in (s_{j,i}, m_{j,i})$ we use the chain rule

$$\mathbf{B}'''_{h_j}(s) = \boldsymbol{\beta}'''_{h_j} \circ \varphi_j(s)\varphi'_j(s)^3 + 3\boldsymbol{\beta}''_{h_j} \circ \varphi_j(s)\varphi'_j(s)\varphi''_j(s) + \boldsymbol{\beta}'_{h_j} \circ \varphi_j(s)\varphi'''_j(s).$$

Note that the norm of the second derivative of an arc-length parametrised arc is $\frac{1}{r}$, while the norm of the third derivative is $\frac{1}{r^2}$, where r is the radius of the arc. With Lemma 6.7 we find

$$\begin{aligned}
\|\boldsymbol{\beta}''_{h_j}\|_{C((s_{j,i},m_{j,i}),\mathbb{R}^3)} &\le \max_{i\in\mathcal{N}_j}\{\kappa_{j,i}, \bar\kappa_{j,i}\} \le \mathsf{c},\\
\|\boldsymbol{\beta}'''_{h_j}\|_{C((s_{j,i},m_{j,i}),\mathbb{R}^3)} &\le \max_{i\in\mathcal{N}_j}\{\kappa^2_{j,i}, \bar\kappa^2_{j,i}\} \le \mathsf{c},
\end{aligned}$$

for all $j \in \mathbb{N}$. Conditions (C6) and (C7), and the fact that $|\boldsymbol{\beta}'_{h_j}(s)| = 1$ imply $\|\mathbf{B}'''_{h_j}\|_{C((s_{j,i},m_{j,i}),\mathbb{R}^3)} \le \mathsf{c}$ for all $j \in \mathbb{N}$. The proof for intervals of the form $(m_{j,i}, s_{j,i+1})$ is analogous. ■

Theorem 6.20 ($C^{1,1}$-convergence) *Let Hypotheses 6.4, 5.3, 6.5, 6.6 and 6.10 hold, and in addition assume* $\mathbf{q} \in C^{2,1}(I,\mathbb{R}^3)$ *is parametrised by arc length, with Lipschitz constant* $K_{\mathbf{q}'} = \|\mathbf{q}''\|_C$. *Then the biarc curves* $\mathbf{B}_{h_j}$ *converge to the curve* $\mathbf{q}$ *in the space* $C^{1,1}(I,\mathbb{R}^3)$ *as* $j \to \infty$, *more precisely, as* $j \to \infty$

$$\|\mathbf{q} - \mathbf{B}_{h_j}\|_{C^0} = O(h_j^3), \qquad \|\mathbf{q}' - \mathbf{B}'_{h_j}\|_{C^0} = O(h_j^2), \qquad K_j = O(h_j).$$

Proof The curve $\mathbf{q} - \mathbf{B}_{h_j}$ restricted to the subintervals $(s_{j,i}, m_{j,i})$ and $(m_{j,i}, s_{j,i+1})$ is $C^{2,1}$, for all $i \in \mathcal{N}_j$, $j \in \mathbb{N}$. For an interval $(s_{j,i}, m_{j,i})$, expansions (6.30)-(6.32) and conditions (C3) and (C4) imply

$$\begin{aligned}
(\mathbf{q} - \mathbf{B}_{h_j})(s) &= (\mathbf{q} - \mathbf{B}_{h_j})(s_{j,i}) + (\mathbf{q} - \mathbf{B}_{h_j})'(s_{j,i})(s - s_{j,i})\\
&\quad + \tfrac{1}{2}(\mathbf{q} - \mathbf{B}_{h_j})''^+(s_{j,i})(s - s_{j,i})^2 + \tfrac{1}{6}\widetilde{\mathbf{v}}_{j,i}(s)(s - s_{j,i})^3\\
&= \mathbf{q}'(s_{j,i})\left(1 - \frac{\lambda(\mathbf{B}_{h_j})}{\lambda(\mathbf{q})}\right)(s - s_{j,i}) + \tfrac{1}{2}(\mathbf{q} - \mathbf{B}_{h_j})''^+(s_{j,i})(s - s_{j,i})^2\\
&\quad + \tfrac{1}{6}\widetilde{\mathbf{v}}_{j,i}(s)(s - s_{j,i})^3, \qquad (6.36)\\
(\mathbf{q} - \mathbf{B}_{h_j})'(s) &= (\mathbf{q} - \mathbf{B}_{h_j})'(s_{j,i}) + (\mathbf{q} - \mathbf{B}_{h_j})''^+(s_{j,i})(s - s_{j,i})\\
&\quad + \tfrac{1}{2}\mathbf{v}_{j,i}(s)(s - s_{j,i})^2\\
&= \mathbf{q}'(s_{j,i})\left(1 - \frac{\lambda(\mathbf{B}_{h_j})}{\lambda(\mathbf{q})}\right) + (\mathbf{q} - \mathbf{B}_{h_j})''^+(s_{j,i})(s - s_{j,i})\\
&\quad + \tfrac{1}{2}\mathbf{v}_{j,i}(s)(s - s_{j,i})^2, \qquad (6.37)
\end{aligned}$$

and

$$(\mathbf{q}-\mathbf{B}_{h_j})''(s) \;=\; (\mathbf{q}-\mathbf{B}_{h_j})''^{+}(s_{j,i}) + \widehat{\mathbf{v}}_{j,i}(s)(s-s_{j,i}), \tag{6.38}$$

for $s \in (s_{j,i}, s_{j,i+1})$, where $\widetilde{\mathbf{v}}_{j,i}, \mathbf{v}_{j,i}, \widehat{\mathbf{v}}_{j,i}$ are vector functions bounded by the Lipschitz constant of the restriction of $(\mathbf{q}-\mathbf{B}_{h_j})''$ on the subinterval $(s_{j,i}, m_{j,i})$. Moreover, with Lemma 6.19 we find

$$\begin{aligned} |\widetilde{\mathbf{v}}_{j,i}|,\ |\mathbf{v}_{j,i}|,\ |\widehat{\mathbf{v}}_{j,i}| \;&\le\; K_{(\mathbf{q}-\mathbf{B}_{h_j})''|_{(s_{j,i},m_{j,i})}} \\ &\le\; K_{\mathbf{q}''} + K_{\mathbf{B}''_{h_j}|_{(s_{j,i},m_{j,i})}} \le K_{\mathbf{q}''} + \|\mathbf{B}'''_{h_j}\|_{C(s_{j,i},m_{j,i})} \le \mathsf{c}, \end{aligned} \tag{6.39}$$

that is, the vector functions $\widetilde{\mathbf{v}}_{j,i}, \mathbf{v}_{j,i}, \widehat{\mathbf{v}}_{j,i}$ are each bounded by a constant independent of $i \in \mathcal{N}_j,\ j \in \mathbb{N}$. Analogously to (6.29), but using Proposition 6.18, we derive the uniform convergence

$$\left|\mathbf{q}''(s_{j,i}) - \mathbf{B}''^{\,\pm}_{h_j}(s_{j,i})\right| = O(h_j). \tag{6.40}$$

Expansions (6.36) and (6.37), equation (6.40), the uniform bound (6.39) and Corollary 6.9 yield

$$\|\mathbf{q}-\mathbf{B}_{h_j}\|_{C^0} = O(h_j^3), \qquad \|\mathbf{q}'-\mathbf{B}'_{h_j}\|_{C^0} = O(h_j^2).$$

Applying (5.2) and using equation (6.38), the uniform convergence in (6.40) and the uniform bound (6.39) we obtain

$$\begin{aligned} K_j \;&\le\; \|(\mathbf{q}-\mathbf{B}_{h_j})''\|_{L_\infty} \le \sup_{i\in\mathcal{N}_j}\Big(|(\mathbf{q}-\mathbf{B}_{h_j})''^{+}(s_{j,i})| + \|\widehat{\mathbf{v}}_{j,i}\|h_j\Big) \\ &\le\; O(h_j) + \mathsf{c}\ h_j = O(h_j). \end{aligned}$$

■

6.7 Infinite curves

In this section we consider semi-infinite curves, that is curves which are defined on an interval of the form $I = [l_0, \infty) \subset \mathbb{R}$. We outline how results similar to those of the previous sections may be obtained. The basic idea is that the results are valid for any finite subinterval of I, and that the constants involved do not depend on the choice of the subintervals. Infinite curve, i.e. curves defined on the interval $I = (-\infty, \infty) = \mathbb{R}$, may be considered as a union of two semi-infinite curves, so that all the results obtained in this section also apply immediately to this case.

For infinite and semi-infinite intervals I the isomorphism $C^{1,1}(I, \mathbb{R}^3) \equiv W^{2,\infty}(I, \mathbb{R}^3)$ that was exploited to obtain (5.2) is not a standard result. We accordingly justify the Taylor expansions in a different way. For a curve $\mathbf{q} \in C^{1,1}(I, \mathbb{R}^3)$ with Lipschitz constant $K_{\mathbf{q}'}$ we introduce the notation

$$\mathbf{w}(s,\sigma) \;:=\; \frac{\mathbf{q}'(s)-\mathbf{q}'(\sigma)}{s-\sigma}, \tag{6.41}$$

$$\widetilde{\mathbf{w}}(s,\sigma) \;:=\; \int_\sigma^s \frac{\mathbf{w}(\tau,\sigma)(\tau-\sigma)}{(s-\sigma)^2}d\tau. \tag{6.42}$$

Simple estimation of the right hand sides of (6.41) and (6.42) implies the bounds

$$|\mathbf{w}(s,\sigma)| \leq K_{\mathbf{q}'}, \tag{6.43}$$
$$|\widetilde{\mathbf{w}}(s,\sigma)| \leq K_{\mathbf{q}'}. \tag{6.44}$$

We rearrange (6.41) to find the expansion

$$\mathbf{q}'(s) = \mathbf{q}'(\sigma) + \mathbf{w}(s,\sigma)(s-\sigma). \tag{6.45}$$

Integration of (6.45) yields

$$\mathbf{q}(s) = \mathbf{q}(\sigma) + \mathbf{q}'(\sigma)(s-\sigma) + \widetilde{\mathbf{w}}(s,\sigma)(s-\sigma)^2. \tag{6.46}$$

Finally the expansions (6.45)-(6.46) are equivalent to the expansions (5.9) and (5.10) for finite curves on which all the proofs are based .

Notation 6.21 *Given a semi-infinite interval $I = [l_0, \infty) \subset \mathbb{R}$, a* mesh $\mathcal{M}$ of mesh size $h > 0$ on I *will mean a sequence $\{s_i\}_{i\in\mathbb{N}}$ with*

$$s_0 = l_0 \quad \textit{and} \quad s_i < s_{i+1} \quad \textit{for} \quad i \in \mathbb{N},$$

and $h = \sup_{i\in\mathbb{N}} |s_{i+1} - s_i| < \infty$.

We will consider a sequence of meshes $\mathcal{M}_j$, $j \in \mathbb{N}$ on I with mesh size $h_j \to 0$ (and wlog we assume that the mesh size h_j is monotone decreasing). For $j \in \mathbb{N}$ we denote the members of the mesh $\mathcal{M}_j$ by $s_{j,i}$, $i \in \mathbb{N}$ and set $h_{j,i} := s_{j,i+1} - s_{j,i}$. We assume that for all $j > k$ there is a mapping $\iota_{k\to j} : \mathbb{N} \to \mathbb{N}$ such that

$$s_{k,i} = s_{j,\iota_{k\to j}(i)}, \qquad i \in \mathbb{N}, \tag{6.47}$$

i.e. the meshes are nested. For compatability we set $\mathcal{N}_j := \mathbb{N}$ for $j \in \mathbb{N}$.

In analogy to Notation 6.3 we note

Notation 6.22 *Let $\mathbf{q} \in C^{1,1}(I, \mathbb{R}^3)$ be parametrised by arc length. For a given sequence of meshes $\mathcal{M}_j$ as described in Notation 6.21, $\boldsymbol{\beta}_{h_j}$ is a biarc curve interpolating the data $(\mathbf{q}(s_{j,i}), \mathbf{q}'(s_{j,i})) \in \mathcal{J}$ with matching points on Σ_{++}.*

We denote by $(\mathbf{a}, \bar{\mathbf{a}})_{j,i}$ the i-th biarc of the biarc curve $\boldsymbol{\beta}_{h_j}$, i.e. the biarc interpolating $((\mathbf{q}(s_{j,i}), \mathbf{q}'(s_{j,i})), (\mathbf{q}(s_{j,i+1}), \mathbf{q}'(s_{j,i+1})))$. We denote the arc-length parameter interval of the biarc curve $\boldsymbol{\beta}_{h_j}$ by I_j. The arc-length parameter corresponding to the matching point of the biarc $(\mathbf{a}, \bar{\mathbf{a}})_{j,i}$ is denoted by $m_{j,i} \in I_j$. The radii of the biarc $(\mathbf{a}, \bar{\mathbf{a}})_{j,i}$ are denoted by $r_{j,i}$ and $\bar{r}_{j,i}$, and the curvatures by $\kappa_{j,i}$ and $\bar{\kappa}_{j,i}$.

Hypothesis 6.23 *$I \subset \mathbb{R}$ is a semi-infinite closed interval $I = [l_0, \infty)$.*

Hypothesis 6.24 *A sequence of biarc curves $\boldsymbol{\beta}_{h_j}$ is generated as in Notation 6.21 and 6.22.*

In the semi-infinite case the arc length $\lambda(\mathbf{q})$ of the curve $\mathbf{q}$ is infinite and therefore Corollary 6.9 has no sense. But it does have sense for any finite subinterval, and moreover the constant involved is independent of the choice of the subinterval.

Corollary 6.25 (Convergence of arc length) *Let Hypotheses 6.23, 5.3 and 6.24 hold. Then, for any subinterval of the form $I_{i,m} = [s_{j,i}, s_{j,i+m}]$, the arc length $\lambda(\boldsymbol{\beta}_{h_j}|_{I_{i,m}})$ of the biarc curve $\boldsymbol{\beta}_{h_j}$ restricted to $I_{i,m}$ converges quadratically to the arc length $\lambda(\mathbf{q}|_{I_{i,m}})$ of the curve $\mathbf{q}$ restricted to $I_{i,m}$:*

$$\frac{\lambda(\boldsymbol{\beta}_{h_j}|_{I_{i,m}})}{\lambda(\mathbf{q}|_{I_{i,m}})} - 1 = O(h_j^2),$$

and the convergence is uniform in i and $m \in \mathbb{N}$. In other words, there exists a constant c such that for all subintervals of the form $I_{i,m} = [s_{j,i}, s_{j,i+m}]$ we have

$$\frac{\lambda(\boldsymbol{\beta}_{h_j}|_{I_{i,m}})}{\lambda(\mathbf{q}|_{I_{i,m}})} - 1 \leq \mathsf{c}h_j^2.$$

Proof By Corollary 6.9 the constant depends only on $K_{\mathbf{q}'}$. ■

Now, condition (C4) (see p. 68) for the reparametrisation function φ_j which implies that the tangent of the reparametrised biarc curve $\mathbf{B}_{h_j}$ has length $\frac{\lambda(\boldsymbol{\beta}_{h_j})}{\lambda(\mathbf{q})}$ has to be replaced by the condition

(C4*) $\varphi_j'(s_{j,i}) = 1$, for $i, j \in \mathbb{N}$,

Hypothesis 6.26 *The function φ_j is a reparametrisation function satisfying conditions (C1)-(C3), (C4*), and (C5)-(C7), for all $j \in \mathbb{N}$ and the reparametrised biarc curve $\mathbf{B}_{h_j}$ is given by (6.3).*

Lemma 6.27 *Let Hypotheses 6.23, 5.3, 6.24 and 6.6 hold. Then the radii of the arcs of the biarc curves $\boldsymbol{\beta}_{h_j}$ are bounded away from zero, that is, for all $i, j \in \mathbb{N}$ there exists a positive constant $\mathsf{c} = \mathsf{c}(K_{\mathbf{q}'}, \Lambda_{\min}) > 0$ with*

$$r_{j,i} \geq \mathsf{c} \quad \textit{and} \quad \bar{r}_{j,i} \geq \mathsf{c}.$$

Proof The proof is analogous to the proof of Lemma 6.7 that is based on the expansions stated in Lemma 5.6 which remain valid in the semi-infinite case. ■

Lemma 6.28 *Let Hypotheses 6.23, 5.3, 6.24, 6.6 and 6.26 hold. Then there exists a constant $\mathsf{c} > 0$, such that $K_j \leq \mathsf{c}$ for all $j \in \mathbb{N}$.*

Proof The proof is similar to the proof of Lemma 6.12, with Lemma 6.27 replacing Lemma 6.7. ■

Theorem 6.29 (C^1-convergence) *Let Hypotheses 6.23, 5.3, 6.24, 6.6 and 6.26 hold. Then the biarc curves $\mathbf{B}_{h_j}$ converge to the curve $\mathbf{q}$ in the space $C^1(I, \mathbb{R}^3)$ as $j \to \infty$. More precisely, as $j \to \infty$*

$$\|\mathbf{q} - \mathbf{B}_{h_j}\|_{C^0} = O(h_j^2), \qquad \|\mathbf{q}' - \mathbf{B}_{h_j}'\|_{C^0} = O(h_j).$$

Proof The proof is analogous to, but even simpler than, the proof of Theorem 6.13, because by Hypothesis 6.26 $(\mathbf{q} - \mathbf{B}_{h_j})'(s_{j,i}) = 0$ for all $i, j \in \mathbb{N}$. ■

Chapter 7

Evaluation of curvature functions and thickness on arc curves

Our goal in this chapter is to present algorithms that allow the efficient and accurate evaluation of thickness and the global radius of curvature function ρ_{pt} on biarc curves. Efficiency and accuracy in the evaluation of thickness is important, because the thickness computation is repeated frequently during simulated annealing computations of the ideal shapes described in chapter 8. Accuracy in the evaluation of ρ_{pt} is important because its variations in s determine the intricate, approximate contact sets that will be described in section 8.1. The algorithms presented in this chapter work for any arc curve, as defined in Definition 7.1 below, that is they are not specific to biarc curves.

7.1 Evaluation of thickness on arc curves

In order to set the material of this chapter in context, we first make some remarks concerning the evaluation of distance between circles. Evaluation of a distance between two circular arcs (forming part of an arc curve) and the evaluation of a distance between two complete circles are of different characters; in many cases the minimal distance between two arcs does not correspond to a minimal distance between the whole circles, but is instead achieved at end points. Nevertheless the two problems are related, and all degeneracies for the complete circle case can also arise in the arc case. Computing the euclidean distance between two circles is a classic problem of computational geometry and computer graphics. The standard approach is to compute the roots of a certain polynomial of degree eight [13, pp. 69–73], [34, 63], and as illustrated in Figure 7.1 the distance function can have eight distinct critical points. In particular it is known that there is no closed-form expression for the distance between two arbitrary circles in three dimensional space [34].

It is also the case that two circles can be arranged to have a constant distance between them. Consider a circle $\mathcal{C}$ with radius r_1 and the surface of the torus with second radius r_2 around $\mathcal{C}$. Trivially any plane parallel to $\mathcal{C}$ cutting the torus does so in two parallel circles that are a constant distance from $\mathcal{C}$. Equally trivially, any plane passing through the centre of $\mathcal{C}$ and cutting $\mathcal{C}$ perpendicularly intersects the torus in

two circles each of which is perpendicular to $\mathcal{C}$ and at a constant distance. What is much less trivial is that through any point on the torus there are four circles lying on the surface of the torus, all of which are at a constant distance from $\mathcal{C}$. Two are the perpendicular and parallel circles already described. The other two *Villarceaux circles* lie in a common plane that is skew to $\mathcal{C}$ [33, pp. 63–72]. This construction reveals that there may be non-trivial cases of arcs that have a constant distance between them, which could pose problems in algorithms for evaluating the minimal distance.

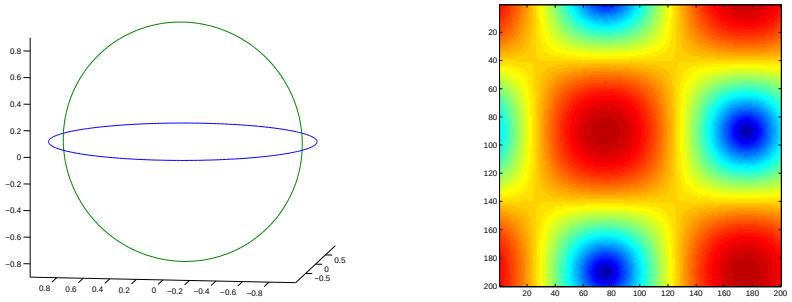

(a) (b)

Figure 7.1: (a) Two co-centric circles of different radii lying in perpendicular planes, (b) plot of pp showing eight critical points, specifically two maxima, two minima and four saddle points.

Definition 7.1 *An* arc curve $\boldsymbol{\alpha}$ *is a space curve assembled in a* C^1 *fashion from circular arcs with swept out angles less than* π *.*

A biarc curve is a special arc curve; on the other hand an arc curve is also a special biarc curve, because every circular arc can be considered as a biarc interpolating the end point data with any point on the arc, except the end points, as matching point. We will use the notion of arc curve to emphasise that throughout this chapter the results do not depend on the fact that the arcs interpolate point-tangent data, and in particular are independent of any matching rule. An arc curve has only $C^{1,1}$ regularity, therefore we can not apply the definition (2.12) of thickness which is valid for C^2 curves. Instead we have to use the definition (2.10), which simplifies for arc curves to:

Proposition 7.2 *For a given non-intersecting arc curve* $\boldsymbol{\alpha} \in C^{1,1}(I, \mathbb{R}^3)$ *composed of* n *arcs* $\mathbf{a}_i$ *with radii* r_i*,* $1 \leq i \leq n$*, the thickness is the minimum of the smallest radius of the arcs and half of the minimal distance between double critical points:*

$$\Delta[\boldsymbol{\alpha}] = \min \left\{ \min_{1 \leq i \leq n} r_i, \tfrac{1}{2} \min_{(s,t) \in dc} |\boldsymbol{\alpha}(s) - \boldsymbol{\alpha}(t)| \right\},$$

where dc *is the set of arguments* $(s, \sigma) \in I \times I$ *with* $s \neq \sigma$ *that satisfy (2.11).*

Proof The thickness $\Delta[\mathbf{q}]$ of a $C^{1,1}$ curve is given in (2.10). First define

$$\delta := \min \left\{ \min_{1 \leq i \leq n} r_i, \tfrac{1}{2} \min_{(s,t) \in dc} |\boldsymbol{\alpha}(s) - \boldsymbol{\alpha}(t)| \right\}.$$

We will show that 1) $\Delta < \delta$ yields a contradiction, while 2) for $r > \delta$, *exp* is not injective on E_r, so $\Delta \leq \delta$.

1) Assume $\Delta < \delta$. For $r > 0$ denote by T_r the set

$$T_r := \{\boldsymbol{\alpha}(s) + \mathbf{v} \in \mathbb{R}^3; (\boldsymbol{\alpha}(s), \mathbf{v}) \in E \text{ and } |\mathbf{v}| = r\},$$

where E is the normal bundle defined in (2.9). Because $\boldsymbol{\alpha}$ is an arc curve, the set T_r is a union of parts of tori with one radius equal to r. For $0 < r < \Delta$ the set T_r is a non-intersecting surface. Moreover, because $\delta \leq \min_{1\leq i\leq n} r_i$, for any $0 < r < \delta$ and for any pair of adjacent arcs $(\mathbf{a}_i, \mathbf{a}_{i+1})$ the part of T_r associated with the two arcs is a C^1 surface having no corner. We consider the continuous family T_r passing from $r = r_1$ to $r = r_2$ with $0 < r_1 < \Delta < r_2 < \delta$. By definition of Δ the exponential map *exp* is not injective on E_r for some $r_1 < r \leq \Delta$. This must happen non-locally by two part of tori associated with non-adjacent arcs $\mathbf{a}_i$ and $\mathbf{a}_j$ at a point $\mathbf{p}$ where the tangent planes are equal. That is, $\mathbf{p} = \boldsymbol{\alpha}(s_i) + \mathbf{v}_i = \boldsymbol{\alpha}(s_j) + \mathbf{v}_j$. The vector $\mathbf{v}_i$ is perpendicular to the common tangent plane at $\mathbf{p}$ and perpendicular to $\boldsymbol{\alpha}'(s_i)$, similarly the vector $\mathbf{v}_j$ is perpendicular to the common tangent plane at $\mathbf{p}$ and perpendicular to $\boldsymbol{\alpha}'(s_j)$. Therefore we have $\boldsymbol{\alpha}'(s_i) \cdot (\boldsymbol{\alpha}(s_i) - \boldsymbol{\alpha}(s_j)) = 0 = \boldsymbol{\alpha}'(s_j) \cdot (\boldsymbol{\alpha}(s_i) - \boldsymbol{\alpha}(s_j))$, thus $(s_i, s_j) \in dc$. By the definition of δ we have $\delta \leq |\boldsymbol{\alpha}(s_i) - \boldsymbol{\alpha}(s_j)|$, which contradicts $|\boldsymbol{\alpha}(s_i) - \boldsymbol{\alpha}(s_j)| = r \leq \Delta < \delta$.

2) If $r > \delta = r_i$ for some i, then two normal discs of radius r of the arc $\mathbf{a}_i$ intersect, while if $r > \delta = \frac{1}{2}|\boldsymbol{\alpha}(s) - \boldsymbol{\alpha}(t)|$ with $(s, t) \in dc$ two normal disks from non-adjacent arcs intersect. In either case *exp* is not injective on E_r. ■

The thickness evaluation algorithm uses the characterisation of thickness given in Proposition 7.2. The three basic building blocks of the algorithm explained below are a linear segment approximation, a bisection algorithm and a double critical test.

7.1.1 Linear segment approximation and bisection algorithm

We adopt the description of arcs using Bézier points that was introduced in section 4.3, cf. figure 4.7. If the swept out angle of an arc is small, the arc is close to being straight. Therefore in this case the distance between the two arcs $\mathbf{a}$ and $\mathbf{b}$ given by the Bézier points $\mathbf{a}_0, \mathbf{a}_1, \mathbf{a}_2 \in \mathbb{R}^3$ and $\mathbf{b}_0, \mathbf{b}_1, \mathbf{b}_2 \in \mathbb{R}^3$ is close to the distance between the straight line segments between $\mathbf{a}_0$ and $\mathbf{a}_2$, and $\mathbf{b}_0$ and $\mathbf{b}_2$, which is easy to compute. Lemma 7.3 makes this observation precise.

Lemma 7.3 *For a pair of arcs* $\mathbf{a}$, $\mathbf{b}$ *with* $\angle\mathbf{a} < \pi$ *and* $\angle\mathbf{b} < \pi$, *given by the Bézier points* $\mathbf{a}_0, \mathbf{a}_1, \mathbf{a}_2 \in \mathbb{R}^3$ *and* $\mathbf{b}_0, \mathbf{b}_1, \mathbf{b}_2 \in \mathbb{R}^3$, *denote by* $\mathbf{a}_{02}$ *and* $\mathbf{b}_{02}$ *the closed, straight line segments between* $\mathbf{a}_0$ *and* $\mathbf{a}_2$, *and between* $\mathbf{b}_0$ *and* $\mathbf{b}_2$. *Then,*

$$\left| \min_{(\mathbf{x}_1,\mathbf{x}_2)\in\mathbf{a}_{02}\times\mathbf{b}_{02}} |\mathbf{x}_1 - \mathbf{x}_2| - \min_{(\mathbf{y}_1,\mathbf{y}_2)\in\mathbf{a}\times\mathbf{b}} |\mathbf{y}_1 - \mathbf{y}_2| \right| \leq \epsilon_{\mathbf{a}} + \epsilon_{\mathbf{b}}, \tag{7.1}$$

where

$$\epsilon_{\mathbf{a}} = \omega_{\mathbf{a}} \sqrt{\frac{1-\omega_{\mathbf{a}}}{1+\omega_{\mathbf{a}}}} |\mathbf{a}_0 - \mathbf{a}_1|, \quad \textit{and} \quad \epsilon_{\mathbf{b}} = \omega_{\mathbf{b}} \sqrt{\frac{1-\omega_{\mathbf{b}}}{1+\omega_{\mathbf{b}}}} |\mathbf{b}_0 - \mathbf{b}_1|, \tag{7.2}$$

with $\omega_{\mathbf{a}} = \cos\delta_{\mathbf{a}}$ *and* $\omega_{\mathbf{b}} = \cos\delta_{\mathbf{b}}$*, and* $\delta_{\mathbf{a}}$ *and* $\delta_{\mathbf{b}}$ *are the base angles of the Bézier triangles, cf. figure 4.7.*

Note that the error bound given in (7.1) is optimal, in that it can be achieved.

Proof We define the non-negative numbers $\epsilon_{\mathbf{a}}$, $\epsilon_{\mathbf{b}}$ by

$$\epsilon_{\mathbf{a}} := \left|\mathbf{a}(\tfrac{1}{2}) - \tfrac{1}{2}(\mathbf{a}_0 + \mathbf{a}_2)\right|, \qquad \epsilon_{\mathbf{b}} := \left|\mathbf{b}(\tfrac{1}{2}) - \tfrac{1}{2}(\mathbf{b}_0 + \mathbf{b}_2)\right|. \tag{7.3}$$

Using the Bézier parametrisation (4.8) we find

$$\left|\mathbf{a}(\tfrac{1}{2}) - \tfrac{1}{2}(\mathbf{a}_0 + \mathbf{a}_2)\right| = \left|\frac{\mathbf{a}_0 + 2\omega_{\mathbf{a}}\mathbf{a}_1 + \mathbf{a}_2}{2(1+\omega_{\mathbf{a}})} - \frac{\mathbf{a}_0 + \mathbf{a}_2}{2}\right| = \frac{\omega_{\mathbf{a}}}{2(1+\omega_{\mathbf{a}})}|\mathbf{a}_0 - 2\mathbf{a}_1 + \mathbf{a}_2|, \tag{7.4}$$

where $\omega_{\mathbf{a}} = \cos\delta_{\mathbf{a}}$. Now we use planar vector geometry to obtain

$$|\mathbf{a}_0 - 2\mathbf{a}_1 + \mathbf{a}_2| = |(\mathbf{a}_0 - \mathbf{a}_1) + (\mathbf{a}_2 - \mathbf{a}_1)| = 2\sin\delta_{\mathbf{a}}|\mathbf{a}_0 - \mathbf{a}_1| = 2\sqrt{1-\omega_{\mathbf{a}}^2}|\mathbf{a}_0 - \mathbf{a}_1|.$$

Combining this with equations (7.3) and (7.4) we find

$$\epsilon_{\mathbf{a}} = \frac{\omega_{\mathbf{a}}\sqrt{1-\omega_{\mathbf{a}}^2}}{(1+\omega_{\mathbf{a}})}|\mathbf{a}_0 - \mathbf{a}_1| = \omega_{\mathbf{a}}\sqrt{\frac{1-\omega_{\mathbf{a}}}{1+\omega_{\mathbf{a}}}}|\mathbf{a}_0 - \mathbf{a}_1|.$$

The analogous statement for $\epsilon_{\mathbf{b}}$ is derived in a similar way, to yield (7.2).

For any subset $\mathcal{U} \subset \mathbb{R}^3$, and for any $r > 0$, define the closed r-neighbourhood of $\mathcal{U}$ by

$$\overline{\mathcal{N}}_r(\mathcal{U}) = \bigcup_{\mathbf{x}\in\mathcal{U}} \overline{\mathcal{B}}_r(\mathbf{x}).$$

Simple planar geometry shows $\mathbf{a} \subset \overline{\mathcal{N}}_{\epsilon_{\mathbf{a}}}(\mathbf{a}_{02})$ and $\mathbf{a}_{02} \subset \overline{\mathcal{N}}_{\epsilon_{\mathbf{a}}}(\mathbf{a})$, and similarly $\mathbf{b} \subset \overline{\mathcal{N}}_{\epsilon_{\mathbf{b}}}(\mathbf{b}_{02})$ and $\mathbf{b}_{02} \subset \overline{\mathcal{N}}_{\epsilon_{\mathbf{b}}}(\mathbf{b})$.

Assume that $\min_{(\mathbf{y}_1,\mathbf{y}_2)\in\mathbf{a}\times\mathbf{b}} |\mathbf{y}_1 - \mathbf{y}_2|$ is achieved by $(\mathbf{p}_1, \mathbf{p}_2) \in \mathbf{a} \times \mathbf{b}$. There exist points $\mathbf{z}_1 \in \mathbf{a}_{02}$ and $\mathbf{z}_2 \in \mathbf{b}_{02}$ with $|\mathbf{p}_1 - \mathbf{z}_1| \le \epsilon_{\mathbf{a}}$ and $|\mathbf{p}_2 - \mathbf{z}_2| \le \epsilon_{\mathbf{b}}$. This and the triangle inequality yield

$$\begin{aligned} \min_{(\mathbf{x}_1,\mathbf{x}_2)\in\mathbf{a}_{02}\times\mathbf{b}_{02}} |\mathbf{x}_1 - \mathbf{x}_2| &\le |\mathbf{z}_1 - \mathbf{z}_2| \le \epsilon_{\mathbf{a}} + |\mathbf{p}_1 - \mathbf{p}_2| + \epsilon_{\mathbf{b}} \\ &= \min_{(\mathbf{y}_1,\mathbf{y}_2)\in\mathbf{a}\times\mathbf{b}} |\mathbf{y}_1 - \mathbf{y}_2| + \epsilon_{\mathbf{a}} + \epsilon_{\mathbf{b}}. \end{aligned} \tag{7.5}$$

With the same argument, but starting from the minimum over the straight line segments, we find

$$\min_{(\mathbf{y}_1,\mathbf{y}_2)\in\mathbf{a}\times\mathbf{b}} |\mathbf{y}_1 - \mathbf{y}_2| \le \min_{(\mathbf{x}_1,\mathbf{x}_2)\in\mathbf{a}_{02}\times\mathbf{b}_{02}} |\mathbf{x}_1 - \mathbf{x}_2| + \epsilon_{\mathbf{a}} + \epsilon_{\mathbf{b}}. \tag{7.6}$$

Combining inequalities (7.5) and (7.6) we find the error estimate (7.1). ■

Notation 7.4 *For an arc* $\mathbf{a}$ *and* $m \in \mathbb{N}$ *denote by* $\mathcal{V}_m(\mathbf{a})$ *the set of* 2^m *congruent arcs derived by* m *successive bisections of* $\mathbf{a}$*.*

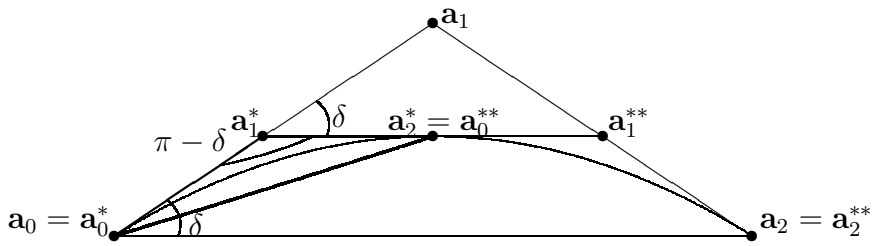

Figure 7.2: Bisecting an arc $\mathbf{a}$ with base angle δ leads to two sub arcs $\mathbf{a}^* \in \mathcal{V}_1(\mathbf{a})$ and $\mathbf{a}^{**} \in \mathcal{V}_1(\mathbf{a})$ with base angles $\frac{1}{2}\delta$.

For an arc $\mathbf{a}$ and for fixed $m \in \mathbb{N}$ all elements $\mathbf{a}^* \in \mathcal{V}_m(\mathbf{a})$ are congruent arcs, and therefore share the same base angle δ^*, base length, and side length. In order to understand how these values for an arc $\mathbf{a}^* \in \mathcal{V}_m(\mathbf{a})$ are related to those for $\mathbf{a}$, we first study the relation between the base angle δ^*, its cosine ω^*, the base length $|\mathbf{a}_2^* - \mathbf{a}_0^*|$, and the side length $|\mathbf{a}_1^* - \mathbf{a}_0^*|$ of an arc $\mathbf{a}^* \in \mathcal{V}_1(\mathbf{a})$, and the base angle δ, its cosine ω, the base length $|\mathbf{a}_2 - \mathbf{a}_0|$, and the side length $|\mathbf{a}_1 - \mathbf{a}_0|$ of the initial arc $\mathbf{a}$.

Lemma 7.5 *Given an arc $\mathbf{a}$ with $\angle\mathbf{a} < \pi$, where δ is the base angle, ω its cosine, and $|\mathbf{a}_2 - \mathbf{a}_0|$ and $|\mathbf{a}_1 - \mathbf{a}_0|$ are the base and side lengths of $\mathbf{a}$, then for an arc $\mathbf{a}^* \in \mathcal{V}_1(\mathbf{a})$ the values of the base angle δ^*, its cosine ω^*, and the base and side length $|\mathbf{a}_2^* - \mathbf{a}_0^*|$ and $|\mathbf{a}_1^* - \mathbf{a}_0^*|$ are*

$$\begin{aligned} \delta^* &= \tfrac{1}{2}\delta, \\ \omega^* &= \sqrt{\tfrac{1}{2}(1+\omega)}, \\ |\mathbf{a}_2^* - \mathbf{a}_0^*| &= \frac{1}{\sqrt{2(1+\omega)}}|\mathbf{a}_2 - \mathbf{a}_0|, \\ |\mathbf{a}_1^* - \mathbf{a}_0^*| &= \frac{\omega}{1+\omega}|\mathbf{a}_1 - \mathbf{a}_0|. \end{aligned}$$

Proof Figure 7.2 illustrates the bisection of $\mathbf{a}$ into the arcs $\mathbf{a}^* \in \mathcal{V}_1(\mathbf{a})$ and $\mathbf{a}^{**} \in \mathcal{V}_1(\mathbf{a})$. Denote the base angle of $\mathbf{a}^*$ by δ^*. The line through $\mathbf{a}_1^*$ and $\mathbf{a}_1^{**}$ is parallel to the line through $\mathbf{a}_0$ and $\mathbf{a}_2$. Therefore the angle $\angle(\mathbf{a}_0, \mathbf{a}_1^*, \mathbf{a}_2^*) = \pi - \delta$. Because interior angles in a triangle sum up to π, $2\delta^* + (\pi - \delta) = \pi$, hence $\delta^* = \frac{1}{2}\delta$.

Define $\omega^* = \cos\delta^*$. Then the fact that $\delta^* = \frac{1}{2}\delta$ and the cosine addition rule give

$$\omega^* = \cos(\tfrac{1}{2}\delta) = \sqrt{\tfrac{1}{2}(\cos(\delta) + 1)} = \sqrt{\tfrac{1}{2}(\omega + 1)}.$$

Using trigonometry with the angle $\angle(\mathbf{a}_2^*, \mathbf{a}_0^*, \mathbf{a}_2) = \frac{1}{2}\delta$ we find

$$|\mathbf{a}_2^* - \mathbf{a}_0^*| = \frac{|\mathbf{a}_2 - \mathbf{a}_0|}{2\omega^*} = \frac{|\mathbf{a}_2 - \mathbf{a}_0|}{\sqrt{2(\omega+1)}}.$$

Using trigonometry with the angles $\angle(\mathbf{a}_1^*, \mathbf{a}_0^*, \mathbf{a}_2^*) = \frac{1}{2}\delta$, $\angle(\mathbf{a}_2^*, \mathbf{a}_0^*, \mathbf{a}_2) = \frac{1}{2}\delta$ and $\angle(\mathbf{a}_1, \mathbf{a}_0, \mathbf{a}_2) = \delta$ we have

$$|\mathbf{a}_1^* - \mathbf{a}_0^*| = \frac{|\mathbf{a}_2^* - \mathbf{a}_0^*|}{2\omega^*} = \frac{|\mathbf{a}_2 - \mathbf{a}_0|}{2\omega^*\ 2\omega^*} = \frac{2\omega|\mathbf{a}_1 - \mathbf{a}_0|}{4{\omega^*}^2},$$

and with $\omega^* = \sqrt{\frac{1}{2}(1+\omega)}$ we find

$$|\mathbf{a}_1^* - \mathbf{a}_0^*| = \frac{2\omega|\mathbf{a}_1 - \mathbf{a}_0|}{4\frac{1}{2}(1+\omega)} = \frac{\omega}{1+\omega}|\mathbf{a}_1 - \mathbf{a}_0|.$$

■

Lemma 7.6 *For an arc* $\mathbf{a}$ *with* $\angle\mathbf{a} < \pi$*, the error term defined in (7.2) of an arc* $\mathbf{a}^* \in \mathcal{V}_1(\mathbf{a})$ *is given by*

$$\epsilon_{\mathbf{a}^*} = \frac{\epsilon_{\mathbf{a}}}{f_{\mathbf{a}}}, \quad \textit{where} \quad f_{\mathbf{a}} = 2 + \sqrt{2(1+\omega)}, \tag{7.7}$$

where ω *is the cosine of the base angle, and* $\epsilon_{\mathbf{a}}$ *is the error term of* $\mathbf{a}$*.*

By the term *error factor* we mean the denominator $f_{\mathbf{a}}$ in the right hand side of equation (7.7).

Proof We have by (7.2)

$$\epsilon_{\mathbf{a}^*} = \omega^*\sqrt{\frac{1-\omega^*}{1+\omega^*}}|\mathbf{a}_0^* - \mathbf{a}_1^*| = \omega^*\frac{\sqrt{1-\omega^{*2}}}{1+\omega^*}|\mathbf{a}_0^* - \mathbf{a}_1^*|.$$

We use Lemma 7.5:

$$\epsilon_{\mathbf{a}^*} = \sqrt{\tfrac{1}{2}(1+\omega)}\frac{\sqrt{1-\frac{1}{2}(1+\omega)}}{1+\sqrt{\frac{1}{2}(1+\omega)}}\frac{\omega}{1+\omega}|\mathbf{a}_1 - \mathbf{a}_0|,$$

and algebra to obtain

$$\begin{aligned}
\epsilon_{\mathbf{a}^*} &= \frac{\sqrt{\frac{1}{2}(1+\omega) - \frac{1}{4}(1+\omega)^2}}{1+\sqrt{\frac{1}{2}(1+\omega)}}\frac{\omega}{1+\omega}|\mathbf{a}_1 - \mathbf{a}_0| \\
&= \frac{\sqrt{\frac{1}{4} - \frac{1}{4}\omega^2}}{1+\sqrt{\frac{1}{2}(1+\omega)}}\frac{\omega}{1+\omega}|\mathbf{a}_1 - \mathbf{a}_0| = \frac{1}{2+\sqrt{2(1+\omega)})}\frac{\sqrt{1-\omega^2}\omega}{1+\omega}|\mathbf{a}_1 - \mathbf{a}_0| \\
&= \frac{1}{2+\sqrt{2(1+\omega)})}\epsilon_{\mathbf{a}},
\end{aligned}$$

as was to be shown. ■

Proposition 7.7 *For a pair of arcs* $\mathbf{a}$*,* $\mathbf{b}$*, and for* $m \to \infty$*, the minima of the minimal euclidean distance between the base segments over all sub-arc pairs* $(\mathbf{a}^*, \mathbf{b}^*) \in \mathcal{V}_m(\mathbf{a}) \times \mathcal{V}_m(\mathbf{b})$ *converges to the minimal euclidean distance between the two arcs:*

$$\min_{(\mathbf{a}^*,\mathbf{b}^*)\in\mathcal{V}_m(\mathbf{a})\times\mathcal{V}_m(\mathbf{b})}\left(\min_{(\mathbf{x}_1,\mathbf{x}_2)\in\mathbf{a}_{02}^*\times\mathbf{b}_{02}^*}|\mathbf{x}_1 - \mathbf{x}_2|\right) \to \min_{(\mathbf{y}_1,\mathbf{y}_2)\in\mathbf{a}\times\mathbf{b}}|\mathbf{y}_1 - \mathbf{y}_2|, \qquad m \to \infty. \tag{7.8}$$

Proof This result is a consequence of Lemmas 7.3 and 7.6. ■

Note that on the left hand side of (7.8) the minimum is taken over 2^{2m} numbers. In practice this would make evaluation of the distance between two arcs to a high tolerance unacceptable slow. Both the double critical test and distance test described below help to avoid this slow down by eliminating unnecessary computations of distance.

7.1.2 Single and double critical test

For two closed, differentiable curves $\mathbf{q} \in C^1(I, \mathbb{R}^3)$ and $\mathbf{r} \in C^1(J, \mathbb{R}^3)$ the euclidean distance is the two-argument function

$$d(s,t) := |\mathbf{q}(s) - \mathbf{r}(t)|, \qquad (s,t) \in I \times J. \tag{7.9}$$

The euclidean distance d is said to have a *single critical point* with respect to s at $(\bar{s}, \bar{t}) \in I \times J$ when

$$\partial_s d(\bar{s}, \bar{t}) = 0, \tag{7.10}$$

and similarly the euclidean distance d has a *single critical point* with respect to t at $(\bar{s}, \bar{t}) \in I \times J$ when

$$\partial_t d(\bar{s}, \bar{t}) = 0. \tag{7.11}$$

We say that the euclidean distance d has a *(double) critical point* at $(\bar{s}, \bar{t}) \in I \times J$ when

$$\partial_s d(\bar{s}, \bar{t}) = 0 \quad \text{and} \quad \partial_t d(\bar{s}, \bar{t}) = 0. \tag{7.12}$$

By extension we will also say that the euclidean distance has a single or double critical point at $(\mathbf{q}(\bar{s}), \mathbf{r}(\bar{t}))$. An equivalent condition for (7.10) to be true is

$$\mathbf{q}'(\bar{s}) \cdot (\mathbf{q}(\bar{s}) - \mathbf{r}(\bar{t})) = 0, \tag{7.13}$$

cf. (2.13), similarly equation (7.11) is true when

$$\mathbf{r}'(\bar{t}) \cdot (\mathbf{q}(\bar{s}) - \mathbf{r}(\bar{t})) = 0, \tag{7.14}$$

hence, the euclidean distance d has a double critical point at $(\bar{s}, \bar{t}) \in I \times J$ only when

$$\mathbf{q}'(\bar{s}) \cdot (\mathbf{q}(\bar{s}) - \mathbf{r}(\bar{t})) = 0 = \mathbf{r}'(\bar{t}) \cdot (\mathbf{q}(\bar{s}) - \mathbf{r}(\bar{t})), \tag{7.15}$$

cf. (2.11). It follows that two non-intersecting differentiable curves $\mathbf{q}$ and $\mathbf{r}$ achieve minimal distance only at points where both tangents are perpendicular to the chord, cf. figure 7.3.

In general the minimum euclidean distance between two circular arcs does not correspond to a critical point of the euclidean distance between the corresponding circles, but can instead be achieved at the end points of the arcs without the tangents being perpendicular to the chord achieving the minimal distance. In order to evaluate the thickness of a closed arc curve $\boldsymbol{\alpha}$, it is important to evaluate the distance only on the set of double critical points. Lemma 7.9 below provides a necessary condition for double critical points on pairs of circular arcs.

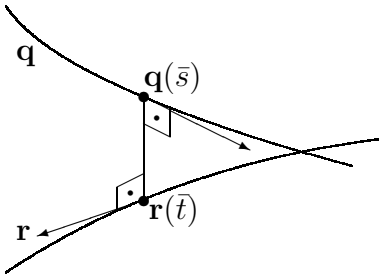

Figure 7.3: Two non-intersecting differentiable curves $\mathbf{q}$ and $\mathbf{r}$ achieve minimal euclidean distance only at points $\mathbf{r}(\bar{t})$ and $\mathbf{q}(\bar{s})$, where both tangents are perpendicular to the chord. In particular the points $(\bar{s}, \bar{t})$ are double critical.

Lemma 7.8 *For a pair of circular arcs* $\mathbf{a}$, $\mathbf{b}$ *with* $\angle\mathbf{a} < \pi$ *and* $\angle\mathbf{b} < \pi$, *given by the Bézier points* $\mathbf{a}_0, \mathbf{a}_1, \mathbf{a}_2 \in \mathbb{R}^3$ *and* $\mathbf{b}_0, \mathbf{b}_1, \mathbf{b}_2 \in \mathbb{R}^3$ *and with the property*

$$|(\mathbf{a}_0 + \mathbf{a}_2) - (\mathbf{b}_0 + \mathbf{b}_2)| > |\mathbf{a}_0 - \mathbf{a}_2| + |\mathbf{b}_0 - \mathbf{b}_2|, \tag{7.16}$$

denote by $\gamma \in (0, \frac{1}{2}\pi)$ *the angle satisfying*

$$\sin\gamma = \frac{|\mathbf{a}_0 - \mathbf{a}_2| + |\mathbf{b}_0 - \mathbf{b}_2|}{|\mathbf{a}_0 + \mathbf{a}_2 - (\mathbf{b}_0 + \mathbf{b}_2)|}, \tag{7.17}$$

and by $\mathbf{w}$ *the unit vector*

$$\mathbf{w} = \frac{\mathbf{a}_0 + \mathbf{a}_2 - (\mathbf{b}_0 + \mathbf{b}_2)}{|\mathbf{a}_0 + \mathbf{a}_2 - (\mathbf{b}_0 + \mathbf{b}_2)|}. \tag{7.18}$$

Denote the unit tangents at the endpoints of the arcs $\mathbf{a}$ *by*

$$\mathbf{t}_0 = \frac{\mathbf{a}_1 - \mathbf{a}_0}{|\mathbf{a}_1 - \mathbf{a}_0|}, \text{ and } \mathbf{t}_1 = \frac{\mathbf{a}_2 - \mathbf{a}_1}{|\mathbf{a}_2 - \mathbf{a}_1|}.$$

If one of the two statements (7.19) and (7.20) is true,

$$\mathbf{w} \cdot \mathbf{t}_0 < -\sin\gamma \quad \text{and} \quad \mathbf{w} \cdot \mathbf{t}_1 < -\sin\gamma, \tag{7.19}$$

$$\mathbf{w} \cdot \mathbf{t}_0 > \sin\gamma \quad \text{and} \quad \mathbf{w} \cdot \mathbf{t}_1 > \sin\gamma, \tag{7.20}$$

then the euclidean distance d *between the two arcs does not have a single critical point with respect to the argument of* $\mathbf{a}$.

Proof We will show that if one of the two statements (7.19) and (7.20) is true, then there is no chord between the two arcs that is perpendicular to any tangent of the arc $\mathbf{a}$, which is an equivalent condition for a single critical point with respect to the argument of $\mathbf{a}$ of the euclidean distance d.

Consider the ball $\mathcal{B}_\mathbf{a}$ centred at $\frac{1}{2}(\mathbf{a}_0 + \mathbf{a}_2)$ with radius $\frac{1}{2}|\mathbf{a}_2 - \mathbf{a}_0|$, and the ball $\mathcal{B}_\mathbf{b}$ centred at $\frac{1}{2}(\mathbf{b}_0 + \mathbf{b}_2)$ with radii $\frac{1}{2}|\mathbf{b}_2 - \mathbf{b}_0|$. Each ball contains an arc, i.e. $\mathbf{a} \subset \mathcal{B}_\mathbf{a}$ and $\mathbf{b} \subset \mathcal{B}_\mathbf{b}$, and by assumption (7.16), they do not intersect. The unit vector $\mathbf{w}$ given by (7.18) is parallel to the line through the two centres of the spheres. Denote by γ the maximum angle between $\mathbf{w}$ and a vector with endpoints in either sphere,

$$\gamma = \max_{\mathbf{z} \in \mathcal{B}_\mathbf{a},\, \widehat{\mathbf{z}} \in \mathcal{B}_\mathbf{b}} \angle(\mathbf{w}, \mathbf{z} - \widehat{\mathbf{z}}).$$

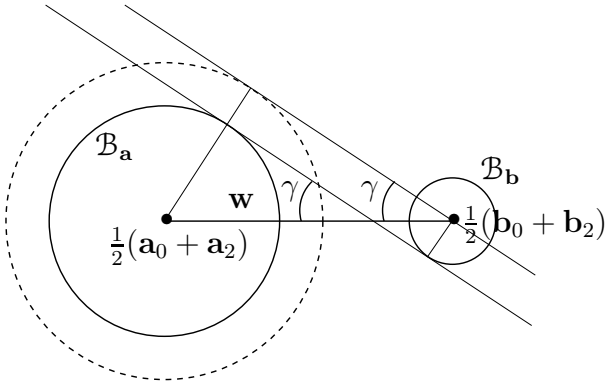

Figure 7.4: The two balls $\mathcal{B}_\mathbf{a}$ and $\mathcal{B}_\mathbf{b}$ contain the two arcs $\mathbf{a}$ and $\mathbf{b}$. The angle γ is the maximum angle between the vector $\mathbf{w}$ and any vector from a point in the ball $\mathcal{B}_\mathbf{b}$ to a point in the ball $\mathcal{B}_\mathbf{a}$.

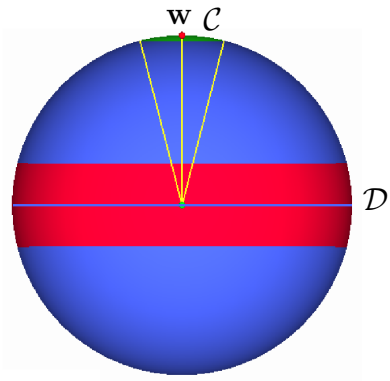

Figure 7.5: The unit sphere S^2 with vector $\mathbf{w}$, the set of chords $\mathcal{C}$ and band $\mathcal{D}$.

Consider Figure 7.4 to find that $\sin\gamma$ can be written as the ratio of the sum of the radii of $\mathcal{B}_\mathbf{a}$ and $\mathcal{B}_\mathbf{b}$ and the distance between the centres of $\mathcal{B}_\mathbf{a}$ and $\mathcal{B}_\mathbf{b}$, that is, (7.17) holds.

Now consider the unit sphere S^2, cf. figure 7.5. Denote by $\mathcal{C}$ the set of normalised vectors from a point in $\mathcal{B}_\mathbf{b}$ to a point in $\mathcal{B}_\mathbf{a}$

$$\mathcal{C} = \{\mathbf{v} \in S^2 : \mathbf{v} \cdot \mathbf{w} \geq \cos\gamma\}, \tag{7.21}$$

and the set of unit vectors that are perpendicular to some $\mathbf{v} \in \mathcal{C}$ by $\mathcal{D}$

$$\mathcal{D} = \{\mathbf{v} \in S^2 : |\mathbf{v} \cdot \mathbf{w}| \leq \sin\gamma\}. \tag{7.22}$$

The tangent indicatrix of a circular arc $\mathbf{a}$ is an arc of a great circle on S^2, and for a circular arc $\mathbf{a}$ with swept out angle $\angle\mathbf{a} < \pi$ it is the smaller arc of the great circle passing through the tangents at the endpoints of the arc. Therefore, it suffices to check the tangents $\mathbf{t}_0$ and $\mathbf{t}_1$ at the end points of the the arc $\mathbf{a}$. If both tangents $\mathbf{t}_0$ and $\mathbf{t}_1$ are in the same component of $S^2\backslash\mathcal{D}$, i.e. if either (7.19) or (7.20) is true, then the tangent indicatrix of $\mathbf{a}$ does not intersect $\mathcal{D}$ and therefore nowhere along the arc $\mathbf{a}$ can the tangent be perpendicular to any vector $\mathbf{v} \in \mathcal{C}$, in particular, no tangent to the arc $\mathbf{a}$ is perpendicular to any vector from a point on $\mathbf{b}$ to a point on $\mathbf{a}$. ■

Corollary 7.9 *For a pair of circular arcs* $\mathbf{a}$, $\mathbf{b}$ *with* $\angle\mathbf{a} < \pi$ *and* $\angle\mathbf{b} < \pi$, *given by the Bézier points* $\mathbf{a}_0, \mathbf{a}_1, \mathbf{a}_2 \in \mathbb{R}^3$ *and* $\mathbf{b}_0, \mathbf{b}_1, \mathbf{b}_2 \in \mathbb{R}^3$ *with the property*

$$|\mathbf{a}_0 + \mathbf{a}_2 - (\mathbf{b}_0 + \mathbf{b}_2)| > |\mathbf{a}_0 - \mathbf{a}_2| + |\mathbf{b}_0 - \mathbf{b}_2|, \tag{7.23}$$

denote by $\gamma \in (0, \frac{1}{2}\pi)$ *the angle satisfying*

$$\sin\gamma = \frac{|\mathbf{a}_0 - \mathbf{a}_2| + |\mathbf{b}_0 - \mathbf{b}_2|}{|\mathbf{a}_0 + \mathbf{a}_2 - (\mathbf{b}_0 + \mathbf{b}_2)|}, \tag{7.24}$$

and by $\mathbf{w}$ *the unit vector*

$$\mathbf{w} = \frac{\mathbf{a}_0 + \mathbf{a}_2 - (\mathbf{b}_0 + \mathbf{b}_2)}{|\mathbf{a}_0 + \mathbf{a}_2 - (\mathbf{b}_0 + \mathbf{b}_2)|}. \tag{7.25}$$

Denote the unit tangents at the endpoints of the arcs $\mathbf{a}$ *and* $\mathbf{b}$ *by*

$$\mathbf{t}_0 = \frac{\mathbf{a}_1 - \mathbf{a}_0}{|\mathbf{a}_1 - \mathbf{a}_0|},\ \mathbf{t}_1 = \frac{\mathbf{a}_2 - \mathbf{a}_1}{|\mathbf{a}_2 - \mathbf{a}_1|},\ \widehat{\mathbf{t}}_0 = \frac{\mathbf{b}_1 - \mathbf{b}_0}{|\mathbf{b}_1 - \mathbf{b}_0|},\ \textit{and}\ \widehat{\mathbf{t}}_1 = \frac{\mathbf{b}_2 - \mathbf{b}_1}{|\mathbf{b}_2 - \mathbf{b}_1|}.$$

If one of the four statements (7.26)-(7.29) is true,

$$\mathbf{w}\cdot\mathbf{t}_0 < -\sin\gamma \quad \textit{and} \quad \mathbf{w}\cdot\mathbf{t}_1 < -\sin\gamma, \tag{7.26}$$

$$\mathbf{w}\cdot\mathbf{t}_0 > \sin\gamma \quad \textit{and} \quad \mathbf{w}\cdot\mathbf{t}_1 > \sin\gamma, \tag{7.27}$$

$$\mathbf{w}\cdot\widehat{\mathbf{t}}_0 < -\sin\gamma \quad \textit{and} \quad \mathbf{w}\cdot\widehat{\mathbf{t}}_1 < -\sin\gamma, \tag{7.28}$$

$$\mathbf{w}\cdot\widehat{\mathbf{t}}_0 > \sin\gamma \quad \textit{and} \quad \mathbf{w}\cdot\widehat{\mathbf{t}}_1 > \sin\gamma, \tag{7.29}$$

then the euclidean distance between the two arcs does not have a double critical point.

Proof If one of the four statements (7.26)-(7.29) is true, then we may apply Lemma 7.8 to find that there is no single critical point of the euclidean distance with respect to either the argument of $\mathbf{a}$ or the argument of $\mathbf{b}$, in particular there can be no double critical point of the euclidean distance.

■

Note that Corollary 7.9 is just a necessary condition for the presence of a double critical point. But the double critical test becomes sharper when we bisect both arcs and apply the test on the four pairs of sub arcs. The next proposition states that when combined with the bisection iteration, the double critical test is sharp in the limit, i.e. in the limit it becomes a sufficient condition. More precisely, given two arcs where the euclidean distance does not have a double critical point, after a finite number of bisection iterations the double critical test on every pair of sub arcs yields that there is no double critical point on the sub arc pair (i.e. for every pair of sub arcs one of the four statements (7.26)-(7.29) is true).

Proposition 7.10 *For any pair of circular arcs* $\mathbf{a}$, $\mathbf{b}$ *where the euclidean distance does not have a double critical point there exists* $m \in \mathbb{N}$ *such that for all* $\mathbf{a}^* \in \mathcal{V}_m(\mathbf{a})$ *and for all* $\mathbf{b}^* \in \mathcal{V}_m(\mathbf{b})$ *one of the four statements (7.26)-(7.29) is true.*

Proof For a pair of circular arcs $\mathbf{a}$, $\mathbf{b}$ where the euclidean distance does not have a critical point we have for some $\epsilon > 0$

$$\left|\mathbf{a}'(s) \cdot \frac{\mathbf{a}(s) - \mathbf{b}(t)}{|\mathbf{a}(s) - \mathbf{b}(t)|}\right| + \left|\mathbf{b}'(t) \cdot \frac{\mathbf{a}(s) - \mathbf{b}(t)}{|\mathbf{a}(s) - \mathbf{b}(t)|}\right| \geq \epsilon > 0. \tag{7.30}$$

For a pair of sub-arcs $(\mathbf{a}^*, \mathbf{b}^*) \in \mathcal{V}_m(\mathbf{a}) \times \mathcal{V}_m(\mathbf{b})$ we denote the unit vector given by (7.25) by $\mathbf{w}_{(\mathbf{a}^*,\mathbf{b}^*)}$, the angle given by (7.24) by $\gamma_{(\mathbf{a}^*,\mathbf{b}^*)}$, and the tangents at the end points by $\mathbf{t}_{0,\mathbf{a}^*}$, $\mathbf{t}_{1,\mathbf{a}^*}$, $\mathbf{t}_{0,\mathbf{b}^*}$, and $\mathbf{t}_{1,\mathbf{b}^*}$.

The triangle inequality yields

$$\begin{aligned}\left|\mathbf{w}_{(\mathbf{a}^*,\mathbf{b}^*)} - \frac{\mathbf{a}^*(s) - \mathbf{b}^*(t)}{|\mathbf{a}^*(s) - \mathbf{b}^*(t)|}\right| &\leq \left|\frac{\mathbf{a}_0^* + \mathbf{a}_2^*}{2} - \mathbf{a}^*(s)\right| + \left|\frac{\mathbf{b}_0^* + \mathbf{b}_2^*}{2} - \mathbf{b}^*(t)\right| \\ &\leq \left|\frac{\mathbf{a}_2^* - \mathbf{a}_0^*}{2}\right| + \left|\frac{\mathbf{b}_2^* - \mathbf{b}_0^*}{2}\right|\end{aligned}$$

for all $s, t \in [0, 1]$. Lemma 7.5 yields the uniform convergence

$$\max_{(\mathbf{a}^*,\mathbf{b}^*)\in\mathcal{V}_m(\mathbf{a})\times\mathcal{V}_m(\mathbf{b})} \left(\max_{s,t\in[0,1]} \left|\mathbf{w}_{(\mathbf{a}^*,\mathbf{b}^*)} - \frac{\mathbf{a}^*(s) - \mathbf{b}^*(t)}{|\mathbf{a}^*(s) - \mathbf{b}^*(t)|}\right|\right) \to 0, \quad \text{as} \quad m \to \infty. \tag{7.31}$$

The convergence (7.31) has two implications. On the one hand, the angles $\gamma_{(\mathbf{a}^*,\mathbf{b}^*)}$ converge uniformly to zero

$$\gamma_{(\mathbf{a}^*,\mathbf{b}^*)} \to 0, \quad \text{as} \quad m \to \infty, \tag{7.32}$$

and by continuity of the sine function we have

$$\max_{(\mathbf{a}^*,\mathbf{b}^*)\in\mathcal{V}_m(\mathbf{a})\times\mathcal{V}_m(\mathbf{b})} \sin\gamma_{(\mathbf{a}^*,\mathbf{b}^*)} \to 0, \quad \text{as} \quad m \to \infty. \tag{7.33}$$

On the other hand,

$$\begin{aligned}\left|\mathbf{w}_{(\mathbf{a}^*,\mathbf{b}^*)} \cdot \mathbf{t}_{0,\mathbf{a}^*} - \frac{\mathbf{a}^*(s) - \mathbf{b}^*(t)}{|\mathbf{a}^*(s) - \mathbf{b}^*(t)|} \cdot \mathbf{t}_{0,\mathbf{a}^*}\right| &= \left|\left(\mathbf{w}_{(\mathbf{a}^*,\mathbf{b}^*)} - \frac{\mathbf{a}^*(s) - \mathbf{b}^*(t)}{|\mathbf{a}^*(s) - \mathbf{b}^*(t)|}\right) \cdot \mathbf{t}_{0,\mathbf{a}^*}\right| \\ &\leq \left|\mathbf{w}_{(\mathbf{a}^*,\mathbf{b}^*)} - \frac{\mathbf{a}^*(s) - \mathbf{b}^*(t)}{|\mathbf{a}^*(s) - \mathbf{b}^*(t)|}\right|,\end{aligned}$$

so that, with (7.31) we find

$$\max_{(\mathbf{a}^*,\mathbf{b}^*)\in\mathcal{V}_m(\mathbf{a})\times\mathcal{V}_m(\mathbf{b})} \left(\max_{s,t\in[0,1]} \left|\mathbf{w}_{(\mathbf{a}^*,\mathbf{b}^*)} \cdot \mathbf{t}_{0,\mathbf{a}^*} - \frac{\mathbf{a}^*(s) - \mathbf{b}^*(t)}{|\mathbf{a}^*(s) - \mathbf{b}^*(t)|} \cdot \mathbf{t}_{0,\mathbf{a}^*}\right|\right) \to 0, \quad \text{as} \quad m \to \infty. \tag{7.34}$$

The analogous statement is true for the tangents $\mathbf{t}_{1,\mathbf{a}^*}$, $\mathbf{t}_{0,\mathbf{b}^*}$, and $\mathbf{t}_{1,\mathbf{b}^*}$. Note that for any pair of sub-arcs $(\mathbf{a}^*, \mathbf{b}^*) \in \mathcal{V}_m(\mathbf{a}) \times \mathcal{V}_m(\mathbf{b})$ the end tangents $\mathbf{t}_{0,\mathbf{a}^*}$, $\mathbf{t}_{1,\mathbf{a}^*}$, $\mathbf{t}_{0,\mathbf{b}^*}$, and $\mathbf{t}_{1,\mathbf{b}^*}$ are the tangent $\mathbf{a}'(s)$, respectively $\mathbf{b}'(t)$, for some $s, t \in [0, 1]$.

Combining the four uniform convergences of the type (7.34), the uniform convergence (7.33), and the property (7.30) yields that there exists $m \in \mathbb{N}$ such that for all $\mathbf{a}^* \in \mathcal{V}_m(\mathbf{a})$ and for all $\mathbf{b}^* \in \mathcal{V}_m(\mathbf{b})$ one of the four statements (7.26)-(7.29) is true. ■

7.1.3 Thickness algorithm

The algorithm built from the linear segment approximation, the bisection algorithm and the double critical test leads to the correct result, but is slow. However, if we apply the additional distance test, explained below, the thickness evaluation becomes much more efficient. The idea of the distance test is simple: In the next iteration ignore the pair of arcs $(\mathbf{a}, \mathbf{b})$, if

$$\min_{(\mathbf{y}_1,\mathbf{y}_2)\in\mathbf{a}_{02}\times\mathbf{b}_{02}} |\mathbf{y}_1 - \mathbf{y}_2| - \epsilon_{\mathbf{a}} - \epsilon_{\mathbf{b}} \geq \min_{\mathbf{a}^*,\mathbf{b}^*\in\mathcal{U}} \left(\min_{(\mathbf{y}_1,\mathbf{y}_2)\in\mathbf{a}^*_{02}\times\mathbf{b}^*_{02}} |\mathbf{y}_1 - \mathbf{y}_2| + \epsilon_{\mathbf{a}^*} + \epsilon_{\mathbf{b}^*} \right), \tag{7.35}$$

where $\mathcal{U}$ is the set of candidates, i.e. pairs of arcs to consider. By *candidate* we refer to a pair of arcs that possibly achieves thickness together with some information about this pair. At the beginning all pairs are candidates. Then, by the double critical test, various candidates are excluded. At every bisection iteration the number of potential candidates is quadrupled, but the distance test and double critical test can be applied to decrease the number of actual candidates. In the code we use as a data format for candidates a vector $\mathbf{c} \in \mathbb{R}^{23}$ where

$$\mathbf{c} = [\mathbf{a}_0^T, \mathbf{a}_1^T, \mathbf{a}_2^T, \mathbf{b}_0^T, \mathbf{b}_1^T, \mathbf{b}_2^T, \epsilon_{\mathbf{a}}, f_{\mathbf{a}}, \epsilon_{\mathbf{b}}, f_{\mathbf{b}}, d_{(\mathbf{a},\mathbf{b})}]^T \in \mathbb{R}^{23}, \tag{7.36}$$

where $\mathbf{a}_0$, $\mathbf{a}_1$, and $\mathbf{a}_2$ are the Bézier points of one arc $\mathbf{a}$, $\mathbf{b}_0$, $\mathbf{b}_1$, and $\mathbf{b}_2$ are the Bézier points of the arc $\mathbf{b}$, $\epsilon_{\mathbf{a}}$ and $\epsilon_{\mathbf{b}}$ are the error terms given by (7.2), $f_{\mathbf{a}}$ and $f_{\mathbf{b}}$ are the error factors defined in (7.7), and $d_{(\mathbf{a},\mathbf{b})}$ is the minimal euclidean distance between the straight line segments $\mathbf{a}_{02}$ and $\mathbf{b}_{02}$.

A flowchart of the algorithm used to compute the thickness of an arc curve $\boldsymbol{\alpha}$ consisting of n arcs is given in figure 7.6. The different steps (boxes) are now explained in more detail.

Input: An arc curve $\boldsymbol{\alpha}$ assembled from n arcs, i.e. a list of triples $(\mathbf{b}_0^i, \mathbf{b}_1^i, \mathbf{b}_2^i)$ of Bezier points associated with the arcs $\mathbf{a}_i$, $1 \leq i \leq n$, and a relative error bound $\bar{\epsilon}_{rel} > 0$.

Local radii and length:

1. Compute radius $r(\mathbf{a}_i)$ and length $\lambda(\mathbf{a}_i)$ of the arc $\mathbf{a}_i$ for all $1 \leq i \leq n$.
2. Compute the length $\lambda(\boldsymbol{\alpha}) = \sum_{i=1}^n \lambda(\mathbf{a}_i)$ of the arc curve $\boldsymbol{\alpha}$ and the smallest radius $r_{\min} = \min_{1\leq i\leq n} r(\mathbf{a}_i)$.

Initial double critical test:

1. Define $C_{crit} := \emptyset$.
2. For $(i,j) \in \{(i,j) \in \mathbb{N}\times\mathbb{N}; 1 \leq i \leq n, 1 \leq j \leq i-2\}\backslash\{(n,1)\}$, that is for pairs that are not on the diagonal and not next neighbours, make the double critical test, cf. Corollary 7.9, on $(\mathbf{a}_i, \mathbf{a}_j)$ and denote the result by $c_{i,j} \in \{0,1\}$, i.e. $c_{i,j} := 1$ if the pair $(\mathbf{a}_i, \mathbf{a}_j)$ passes the test and $c_{i,j} := 0$ if it fails.

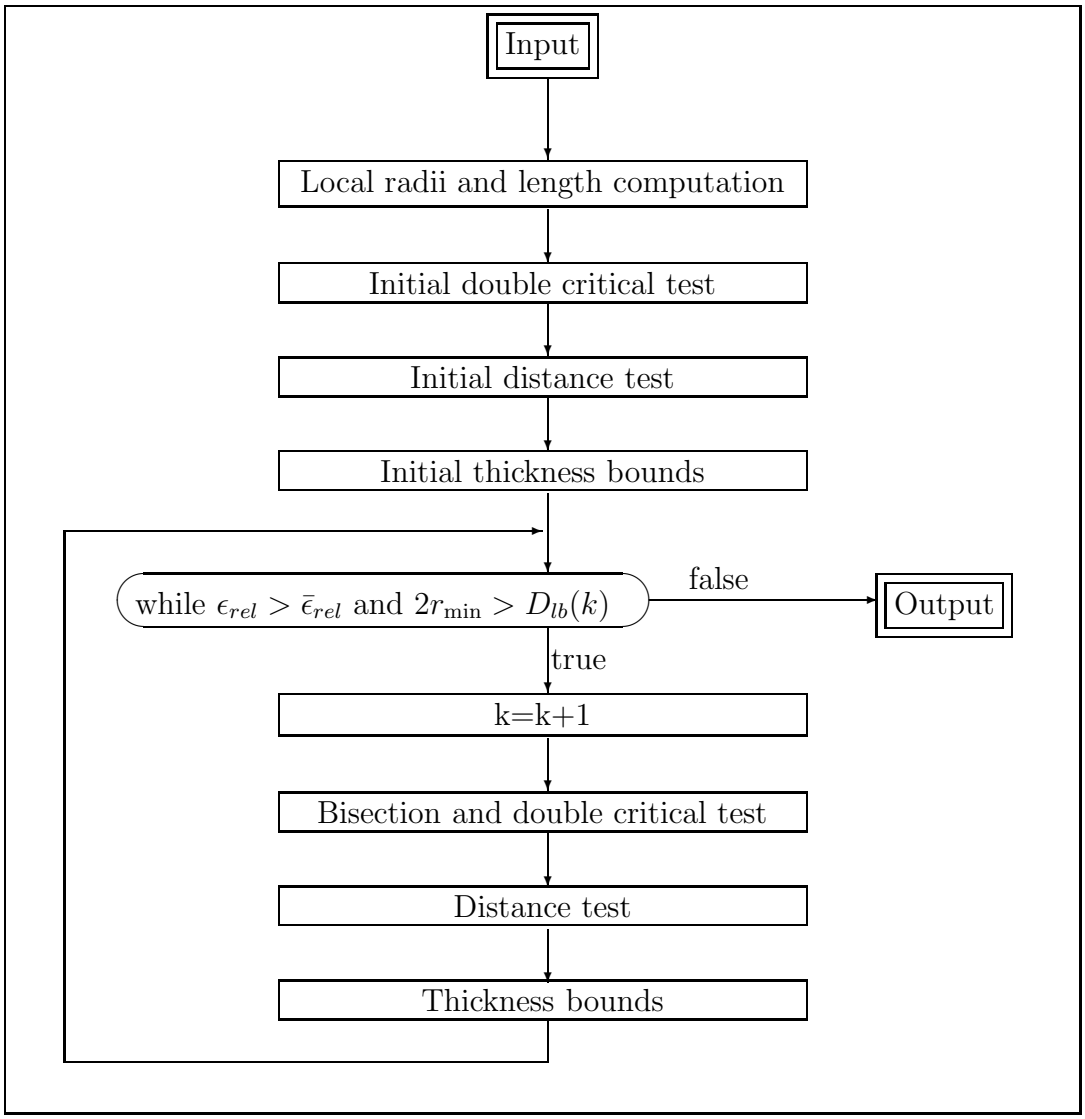

Figure 7.6: Flowchart of the thickness evaluation algorithm for arc curves using as basic building blocks the linear segment approximation cf. Lemma 7.3, the bisection algorithm cf. Proposition 7.7 and the double critical test cf. Corollary 7.9.

3. If $c_{i,j} \neq 0$, compute the initial errors given by (7.2), the error factors given by (7.7), and the minimal euclidean distance between the base segments for the pair $(\mathbf{a}_i, \mathbf{a}_j)$, and append a column in the format (7.36) to the matrix C_{crit}.

Initial distance test:

1. Define $C_{dist} := \emptyset$.

2. Compute $d_b := \min_i\{C_{crit}(19,i) + C_{crit}(21,i) + C_{crit}(23,i)\}$.

3. If $C_{crit}(23,i) - C_{crit}(19,i) - C_{crit}(21,i) \leq d_b$, append a column in the format (7.36) to the matrix C_{dist}.

Initial thickness bounds: Compute initial upper and lower bounds for the minimal distance between double critical points D_{lb} and D_{ub}, the thickness Δ_{lb} and Δ_{ub}, and the rope length $(\lambda/\Delta)_{lb}$ and $(\lambda/\Delta)_{ub}$

$$\begin{aligned} D_{lb} &:= \min_i(C_{dist}(23,i) - C_{dist}(19,i) - C_{dist}(21,i)) \\ D_{ub} &:= \min_i(C_{dist}(23,i) + C_{dist}(19,i) + C_{dist}(21,i)) \\ \Delta_{lb} &:= \min\{r_{\min}, \tfrac{1}{2}D_{lb}\} \\ \Delta_{ub} &:= \min\{r_{\min}, \tfrac{1}{2}D_{ub}\} \\ (\lambda/\Delta)_{ub} &:= \frac{\lambda(\boldsymbol{\alpha})}{\Delta_{lb}} \\ (\lambda/\Delta)_{lb} &:= \frac{\lambda(\boldsymbol{\alpha})}{\Delta_{ub}} \end{aligned}$$

Compute the maximal and relative error, and set the number k of iterations to one.

$$\begin{aligned} \epsilon_{\max} &:= \max_i(C_{dist}(19,i) + C_{dist}(21,i)) \\ \epsilon_{rel} &:= \frac{\epsilon_{\max}}{\Delta_{lb}} \\ k &:= 1 \end{aligned}$$

While iteration: while the relative error is bigger than the relative error bound and the lower bound for the double critical self distance D_{lb} is smaller than the double of the minimal radius, i.e. while

$$\epsilon_{rel} > \bar{\epsilon}_{rel} \text{ and } 2r_{\min} > D_{lb}(k)$$

k=k+1: Add one to the number k of iterations.

Bisection and double critical test:

1. Set $C_{crit} := \emptyset$.

2. For each column of C_{dist}, bisect both arcs and apply the double critical test, cf. Corollary 7.9, to all four pairs, denote the result by $c_1, \ldots, c_4 \in \{0, 1\}$, i.e. $c_i := 1$ for passing the test and $c_i := 0$ for failing.

3. If $c_i \neq 0$, compute the minimal euclidean distance between the base segments for the corresponding sub pair and add a column in the format (7.36) to the matrix C_{crit} according Lemma 7.6 as follows:

$$\mathbf{c} = [\mathbf{a}_0^T, \mathbf{a}_1^T, \mathbf{a}_2^T, \mathbf{b}_0^T, \mathbf{b}_1^T, \mathbf{b}_2^T, \frac{\epsilon_\mathbf{a}}{f_\mathbf{a}}, f_\mathbf{a}, \frac{\epsilon_\mathbf{b}}{f_\mathbf{b}}, f_\mathbf{b}, d_{(\mathbf{a},\mathbf{b})}]^T \in \mathbb{R}^{21}.$$

Distance test:

1. Define $C_{dist} := \emptyset$.

2. Compute $d_b := \min_i\{C_{crit}(19, i) + C_{crit}(21, i) + C_{crit}(23, i)\}$.

3. If $C_{crit}(23, i) - C_{crit}(19, i) - C_{crit}(21, i) \leq d_b$, add a column in the format (7.36) to the matrix C_{dist}.

Thickness bounds: Compute upper and lower bounds for the minimal distance between double critical points D_{lb} and D_{ub}, the thickness Δ_{lb} and Δ_{ub}, and the rope length $(\lambda/\Delta)_{lb}$ and $(\lambda/\Delta)_{ub}$

$$\begin{aligned}
D_{lb} &= [D_{lb}; \min_i(C_{dist}(23, i) - C_{dist}(19, i) - C_{dist}(21, i))] \\
D_{ub} &= [D_{ub}; \min_i(C_{dist}(23, i) + C_{dist}(19, i) + C_{dist}(21, i))] \\
\Delta_{lb} &= [\Delta_{lb}; \min\{2r_{\min},\ \min_i(C_{dist}(23, i) - C_{dist}(19, i) - C_{dist}(21, i))\}] \\
\Delta_{ub} &= [\Delta_{ub}; \min\{2r_{\min},\ \min_i(C_{dist}(23, i) + C_{dist}(19, i) + C_{dist}(21, i))\}] \\
(\lambda/\Delta)_{ub} &= \left[(\lambda/\Delta)_{ub}; \frac{\lambda(\boldsymbol{\alpha})}{\min\{2r_{\min},\ \min_i(C_{dist}(23, i) - C_{dist}(19, i) - C_{dist}(21, i))\}}\right] \\
(\lambda/\Delta)_{lb} &= \left[(\lambda/\Delta)_{lb}; \frac{\lambda(\boldsymbol{\alpha})}{\min\{2r_{\min},\ \min_i(C_{dist}(23, i) + C_{dist}(19, i) + C_{dist}(21, i))\}}\right]
\end{aligned}$$

Compute the maximal and relative error

$$\begin{aligned}
\epsilon_{\max} &= [\epsilon_{\max}; \max_i(C_{dist}(19, i) + C_{dist}(21, i))] \\
\epsilon_{rel} &= \left[\epsilon_{rel}; \frac{\max_i(C_{dist}(19, i) + C_{dist}(21, i))}{\min\{2r_{\min},\ \min_i(C_{dist}(23, i) - C_{dist}(19, i) - C_{dist}(21, i))\}}\right]
\end{aligned}$$

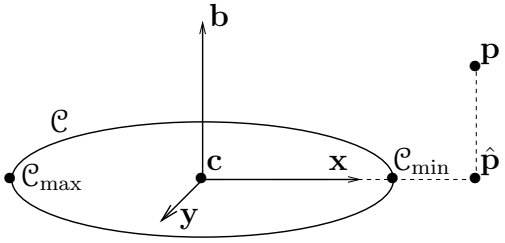

Figure 7.7: Projection of $\mathbf{p}$ onto the plane of the circle $\mathcal{C}$ with centre $\mathbf{c}$ that defines the orthonormal coordinate system $(\mathbf{x}, \mathbf{b}, \mathbf{y})$. The minima and maxima of $\mathsf{pp}(\mathbf{p}, \cdot)$ are achieved at $\mathcal{C}_{\min}$ and $\mathcal{C}_{\max}$.

Output: The algorithm stops after a finite number $\bar{k}$ of iterations with as output: The radii $r(\mathbf{a}_i)$ and lengths $\lambda(\mathbf{a}_i)$, the length $\lambda(\boldsymbol{\alpha})$ of the arc curve $\boldsymbol{\alpha}$, the smallest radius $r_{\min}$, upper and lower bounds for the minimal distance between double critical points $D_{lb} \in \mathbb{R}^{\bar{k}}$ and $D_{ub} \in \mathbb{R}^{\bar{k}}$, the thickness $\Delta_{lb} \in \mathbb{R}^{\bar{k}}$ and $\Delta_{ub} \in \mathbb{R}^{\bar{k}}$, and the rope length $(\lambda/\Delta)_{lb} \in \mathbb{R}^{\bar{k}}$ and $(\lambda/\Delta)_{ub} \in \mathbb{R}^{\bar{k}}$, the maximal and relative error of each iteration $\epsilon_{\max} \in \mathbb{R}^{\bar{k}}$ and $\epsilon_{rel} \in \mathbb{R}^{\bar{k}}$, the set of candidates passing the double critical test of the last iteration C_{crit}, the set of candidates passing the distance test of the last iteration C_{dist}, and the number of candidates in C_{dist} and C_{crit} at each iteration.

For a Matlab code implementing the thickness evaluation algorithm presented in this section see Appendix B.

7.2 Evaluation of ρ_{pt} on arc curves

To evaluate ρ_{pt} on a given arc curve $\boldsymbol{\alpha} \in C^1(I, \mathbb{R}^3)$ we will exploit the necessary conditions given in Lemma 3.6 and the simple geometry of circles. We start with an elementary, classic result.

Lemma 7.11 *For a circle $\mathcal{C}$ parametrised by a parameter $s \in I$, and a point $\mathbf{p}$, consider the euclidean distance function $\mathsf{pp}(\mathbf{p}, \cdot) : s \mapsto \mathsf{pp}(\mathbf{p}, \mathcal{C}(s))$, $s \in I$, where $\mathsf{pp}(\mathbf{p}, \mathcal{C}(s)) = \frac{1}{2}|\mathbf{p} - \mathcal{C}(s)|$. Denote the unit binormal by $\mathbf{b}$, the radius by r, and the centre of the circle $\mathcal{C}$ by $\mathbf{c}$. Then $\mathsf{pp}(\mathbf{p}, \cdot)$ is either constant, whenever $\mathbf{p} \in \mathcal{A}$ (cf. Definition 2.6), or it has exactly one minimum and one maximum, which are achieved at*

$$\mathcal{C}_{\min} = \mathbf{c} + r\frac{\mathbf{p} - \mathbf{c} - \mathbf{b} \cdot (\mathbf{p} - \mathbf{c})\mathbf{b}}{|\mathbf{p} - \mathbf{c} - \mathbf{b} \cdot (\mathbf{p} - \mathbf{c})\mathbf{b}|}, \quad \mathcal{C}_{\max} = \mathbf{c} - r\frac{\mathbf{p} - \mathbf{c} - \mathbf{b} \cdot (\mathbf{p} - \mathbf{c})\mathbf{b}}{|\mathbf{p} - \mathbf{c} - \mathbf{b} \cdot (\mathbf{p} - \mathbf{c})\mathbf{b}|}. \tag{7.37}$$

Proof If the point $\mathbf{p}$ lies on the polar axis $\mathcal{A}$ of the circle $\mathcal{C}$, then the euclidean distance function $\mathsf{pp}(\mathbf{p}, \cdot)$ is constant. Assume now $\mathbf{p} \notin \mathcal{A}$. Project $\mathbf{p}$ onto the plane of $\mathcal{C}$,

$$\hat{\mathbf{p}} = \mathbf{p} - \mathbf{b} \cdot (\mathbf{p} - \mathbf{c})\mathbf{b}.$$

Because $\mathbf{p} \notin \mathcal{A}$, $\hat{\mathbf{p}} - \mathbf{c} \neq 0$. Set $\mathbf{x} := \frac{\hat{\mathbf{p}} - \mathbf{c}}{|\hat{\mathbf{p}} - \mathbf{c}|}$ and $\mathbf{y} := \mathbf{x} \times \mathbf{b}$, then $(\mathbf{x}, \mathbf{b}, \mathbf{y})$ is an

orthonormal coordinate system, cf. Figure 7.7. A parametrisation of the circle $\mathcal{C}$ is given by

$$\mathcal{C}(s) = \mathbf{c} + r\cos(s)\mathbf{x} + r\sin(s)\mathbf{y}, \quad s \in [0, 2\pi].$$

We differentiate the distance function to find

$$\partial_s \left((2\mathsf{pp}(\mathbf{p}, \mathcal{C}(s)))^2 \right) = \partial_s \left(|\mathbf{p} - \mathcal{C}(s)|^2 \right) = 2r\sin(s)(\mathbf{p} - \mathbf{c}) \cdot \mathbf{x}.$$

Because $\mathbf{p} \notin \mathcal{A}$, we have $(\mathbf{p} - \mathbf{c}) \cdot \mathbf{x} \neq 0$. Therefore the only critical points are when $\sin(s) = 0$, i.e. for $s = 0$ and $s = \pi$, which correspond to the two points given in (7.37). ■

The analogous result for the circular distance function pt is less simple.

Lemma 7.12 *For a circle $\mathcal{C}$ parametrised by a parameter $s \in I$, and a point $\mathbf{p} \notin \mathcal{C}$, consider the function $\mathsf{pt}(\mathbf{p}, \cdot) : s \mapsto \mathsf{pt}(\mathbf{p}, \mathcal{C}(s))$, $s \in I$, where $\mathsf{pt}(\mathbf{p}, \mathcal{C}(s))$ is the radius of the circle passing through $\mathbf{p}$ and $\mathcal{C}(s)$ with tangent $\mathcal{C}'(s)$. Denote by $\mathbf{b}$ the binormal to the circle $\mathcal{C}$, and by $\mathbf{c}_\mathcal{S}$ the centre of the sphere $\mathcal{S}$ containing both $\mathcal{C}$ and $\mathbf{p}$. Then either $\mathsf{pt}(\mathbf{p}, \cdot)$ is constant or it assumes either two or four critical points. More precisely, if $\mathbf{p}$ is not contained in the plane of the circle $\mathcal{C}$, then only one of the following three cases occurs:*

1. *When $\mathbf{p} \in \mathcal{A}$, that is when*

$$\left| \frac{\mathbf{p} - \mathbf{c}_\mathcal{S}}{|\mathbf{p} - \mathbf{c}_\mathcal{S}|} \cdot \mathbf{b} \right| = 1,$$

   then $\mathsf{pt}(\mathbf{p}, \cdot)$ is constant,

2. *when*

$$\left| \frac{\mathcal{C}(s) - \mathbf{c}_\mathcal{S}}{|\mathcal{C}(s) - \mathbf{c}_\mathcal{S}|} \cdot \mathbf{b} \right| \leq \left| \frac{\mathbf{p} - \mathbf{c}_\mathcal{S}}{|\mathbf{p} - \mathbf{c}_\mathcal{S}|} \cdot \mathbf{b} \right| < 1, \qquad s \in I, \tag{7.38}$$

   then $\mathsf{pt}(\mathbf{p}, \cdot)$ has two critical points, one minimum and one maximum that are achieved at the minimum and maximum of $\mathsf{pp}(\mathbf{p}, \cdot)$ given in (7.37),

3. *when*

$$0 \leq \left| \frac{\mathbf{p} - \mathbf{c}_\mathcal{S}}{|\mathbf{p} - \mathbf{c}_\mathcal{S}|} \cdot \mathbf{b} \right| < \left| \frac{\mathcal{C}(s) - \mathbf{c}_\mathcal{S}}{|\mathcal{C}(s) - \mathbf{c}_\mathcal{S}|} \cdot \mathbf{b} \right|, \qquad s \in I, \tag{7.39}$$

   then $\mathsf{pt}(\mathbf{p}, \cdot)$ has four critical points, two global maxima equal to the radius of the sphere $\mathcal{S}$ and a global and a local minimum that are respectively the minimum and maximum of $\mathsf{pp}(\mathbf{p}, \cdot)$ given in (7.37).

If $\mathbf{p}$ is contained in the plane of the circle $\mathcal{C}$, cf. Figure 7.8, then only one of the following three cases can occur:

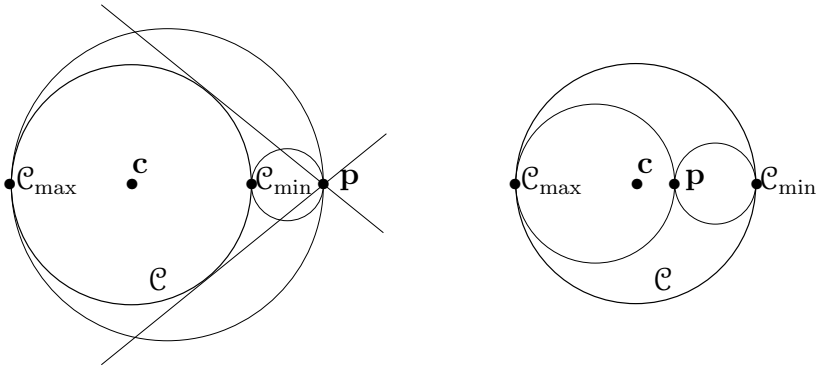

(a) (b)

Figure 7.8: When $\mathbf{p}$ is contained in the plane of the circle $\mathcal{C}$, and (a) $\mathbf{p}$ is outside the circle $\mathcal{C}$, then $\mathsf{pt}(\mathbf{p}, \cdot)$ has two infinities and two (a global and a local) minima that are achieved at the minimum and maximum of the euclidean distance, $\mathcal{C}_{\min}$ and $\mathcal{C}_{\max}$, and (b) when $\mathbf{p}$ is inside the circle $\mathcal{C}$ with $\mathbf{p} \neq \mathbf{c}$, $\mathsf{pt}(\mathbf{p}, \cdot)$ has two critical points, one minimum and one maximum that are achieved at the minimum and maximum of the euclidean distance, $\mathcal{C}_{\min}$ and $\mathcal{C}_{\max}$.

1. *When $\mathbf{p} = \mathbf{c}$, the centre of the circle $\mathcal{C}$, then $\mathsf{pt}(\mathbf{p}, \cdot)$ is constant,*

2. *when $\mathbf{p}$ is inside the circle $\mathcal{C}$ with $\mathbf{p} \neq \mathbf{c}$, then $\mathsf{pt}(\mathbf{p}, \cdot)$ has two critical points, one minimum and one maximum corresponding to the minimum and maximum of $\mathsf{pp}(\mathbf{p}, \cdot)$ achieved at the points given in (7.37),*

3. *when $\mathbf{p}$ is outside the circle $\mathcal{C}$, then $\mathsf{pt}(\mathbf{p}, \cdot)$ has two poles, or infinities, and two critical points, namely one global and one local minimum that are achieved at respectively the minimum and maximum of $\mathsf{pp}(\mathbf{p}, \cdot)$ given in (7.37).*

We remark that the inequalities (7.38) and (7.39) distinguish between the cases in which the projection of the point $\mathbf{p}$ onto the plane of the circle $\mathcal{C}$ lies inside or outside the circle. When $\mathbf{p} \in \mathcal{C}$ then $\mathsf{pt}(\mathbf{p}, \mathcal{C}(s)) = r$ whenever $\mathbf{p} \neq \mathcal{C}(s)$. However as $\mathbf{p}$ approaches $\mathcal{C}$ the function $\mathsf{pt}(\mathbf{p}, \mathcal{C}(s))$ as a function of $\mathbf{p}$ is discontinuous.

Proof If the point $\mathbf{p}$ lies on the polar axis $\mathcal{A}$ of the circle $\mathcal{C}$, then $\mathsf{pt}(\mathbf{p}, \cdot)$ is constant. Assume now $\mathbf{p} \notin \mathcal{A}$. The circle $\mathcal{C}$ and a point $\mathbf{p} \notin \mathcal{C}$ define a unique sphere $\mathcal{S}$ (or plane) containing both $\mathcal{C}$ and $\mathbf{p}$. Every circle $\bar{\mathcal{C}}$ passing through $\mathbf{p}$ and tangent to the circle $\mathcal{C}$ at some point $\mathcal{C}(s)$ lies on the sphere $\mathcal{S}$. By the proof of Lemma 3.6, a critical point of $\mathsf{pt}(\mathbf{p}, \cdot)$ is achieved only at either a point $\mathcal{C}(s)$ that assumes a single critical distance, i.e. $(\mathcal{C}(s) - \mathbf{p}) \cdot \mathcal{C}'(s) = 0$, or when the centre of $\bar{\mathcal{C}}$ lies on the polar axis $\mathcal{A}$ of $\mathcal{C}$. The first case corresponds exactly to the minimum and maximum of the euclidean distance described in (7.37).

We next demonstrate that in the present case of a circle and a point $\mathbf{p} \notin \mathcal{C}$ the centre of $\bar{\mathcal{C}}$ intersects the polar axis of $\mathcal{C}$ if and only if $\bar{\mathcal{C}}$ is a great circle of the sphere $\mathcal{S}$. First note that for a given sphere and a tangent to the sphere at some point, the locus of the centres of all circles lying on the sphere with the prescribed tangent is a circle of half of the radius of the sphere passing through the point and the centre of the sphere

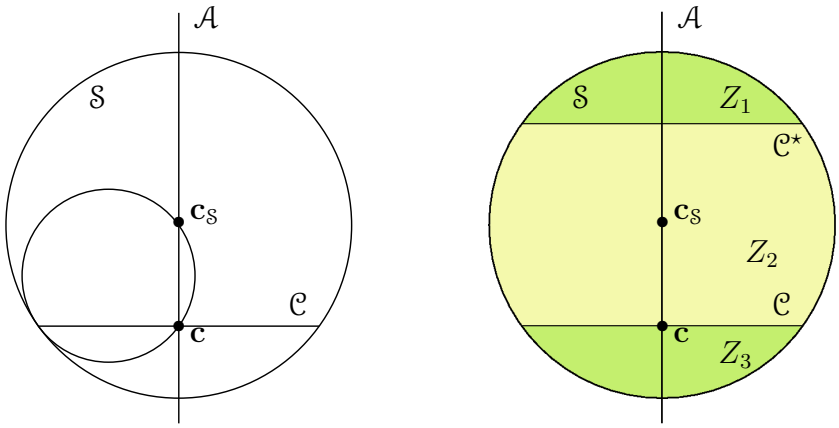

(a) (b)

Figure 7.9: (a) A cut through $\mathbf{c}$ and $\mathbf{c}_{\mathcal{S}}$ perpendicular to a tangent to $\mathcal{C}$, showing the circle that is the locus of the centres of all circles on $\mathcal{S}$ that are tangent to the given tangent of $\mathcal{C}$. (b) Illustration of $\mathcal{S}\backslash(\mathcal{C}\cup\mathcal{C}^\star) = Z_1 \cup Z_2 \cup Z_3$.

and which is contained in the plane perpendicular to the tangent, cf. Figure 7.9(a). In particular this circle intersects the polar axis $\mathcal{A}$ in only two points: the centre $\mathbf{c}$ of $\mathcal{C}$ and the centre $\mathbf{c}_{\mathcal{S}}$ of the sphere $\mathcal{S}$. Therefore the centre of $\bar{\mathcal{C}}$ is either $\mathbf{c}_{\mathcal{S}}$ or $\mathbf{c}$. But the latter can not be true as $\mathbf{p} \notin \mathcal{C}$. Thus, the circle $\bar{\mathcal{C}}$ is a great circle of $\mathcal{S}$.

If $\mathcal{S}$ is a true sphere of finite radius, two cases can happen: (a) $\mathcal{S}$ is the circumsphere of $\mathcal{C}$, or (b) $\mathcal{S}$ is not the circumsphere of $\mathcal{C}$. If $\mathcal{S}$ is the circumsphere of $\mathcal{C}$, then any great circle passing through a point $\mathbf{p} \in \mathcal{S}\backslash\mathcal{C}$ intersects the circle $\mathcal{C}$ with an non-zero angle. Thus, the only critical points of $\mathsf{pt}(\mathbf{p},\cdot)$ are the critical points of $\mathsf{pp}(\mathbf{p},\cdot)$ described in (7.37).

If $\mathcal{S}$ is not the circumsphere of $\mathcal{C}$, we denote by $\mathcal{C}^\star$ the circle on $\mathcal{S}$ in a plane parallel to the plane of $\mathcal{C}$ and with the same radius as $\mathcal{C}$. The two circles $\mathcal{C}$ and $\mathcal{C}^\star$ split the sphere $\mathcal{S}$ into three open components, say $\mathcal{S}\backslash(\mathcal{C}\cup\mathcal{C}^\star) = Z_1 \cup Z_2 \cup Z_3$, with Z_1 and Z_3 bounded by a circle, and Z_2 bounded by both circles, cf. figure 7.9(b). When $\mathbf{p} \in \mathcal{C}^\star$, in which case $\left|\frac{\mathcal{C}(s)-\mathbf{c}_{\mathcal{S}}}{|\mathcal{C}(s)-\mathbf{c}_{\mathcal{S}}|}\cdot\mathbf{b}\right| = \left|\frac{\mathbf{p}-\mathbf{c}_{\mathcal{S}}}{|\mathbf{p}-\mathbf{c}_{\mathcal{S}}|}\cdot\mathbf{b}\right|$, there is only one great circle passing through $\mathbf{p}$ and tangent to $\mathcal{C}$ at some point. This circle is the circle achieving the maximum of $\mathsf{pp}(\mathbf{p},\cdot)$. That is, we have only two critical points of $\mathsf{pt}(\mathbf{p},\cdot)$ and they correspond to the critical points of the euclidean distance $\mathsf{pp}(\mathbf{p},\cdot)$ given in (7.37). When $\mathbf{p} \in (Z_1 \cup Z_3)\backslash\mathcal{A}$, in which case $\left|\frac{\mathcal{C}(s)-\mathbf{c}_{\mathcal{S}}}{|\mathcal{C}(s)-\mathbf{c}_{\mathcal{S}}|}\cdot\mathbf{b}\right| < \left|\frac{\mathbf{p}-\mathbf{c}_{\mathcal{S}}}{|\mathbf{p}-\mathbf{c}_{\mathcal{S}}|}\cdot\mathbf{b}\right| < 1$, then every great circle passing through $\mathbf{p}$ intersects the circle $\mathcal{C}$ with an non-zero angle. Thus, the only critical points of $\mathsf{pt}(\mathbf{p},\cdot)$ are the critical points of $\mathsf{pp}(\mathbf{p},\cdot)$ given in (7.37). But when $\mathbf{p} \in Z_2$, in which case $0 \leq \left|\frac{\mathbf{p}-\mathbf{c}_{\mathcal{S}}}{|\mathbf{p}-\mathbf{c}_{\mathcal{S}}|}\cdot\mathbf{b}\right| < \left|\frac{\mathcal{C}(s)-\mathbf{c}_{\mathcal{S}}}{|\mathcal{C}(s)-\mathbf{c}_{\mathcal{S}}|}\cdot\mathbf{b}\right|$, there are two great circles passing through $\mathbf{p}$ that are tangent to $\mathcal{C}$ at some point. Both circles that correspond to critical points of $\mathsf{pp}(\mathbf{p},\cdot)$ have smaller radii than the great circles, that is they are two local minima of $\mathsf{pt}(\mathbf{p},\cdot)$, and the global maxima of $\mathsf{pp}(\mathbf{p},\cdot)$ is achieved twice by the great circles.

If $\mathcal{S}$ is actually a plane, any circle $\bar{\mathcal{C}}$ passing through $\mathbf{p}$ and tangent to the circle $\mathcal{C}$ at some point lies in this plane. Therefore the centre of $\bar{\mathcal{C}}$ lies also in this plane. The

polar axis $\mathcal{A}$ intersects the plane only in the centre $\mathbf{c}$ of $\mathcal{C}$ (which can not be a centre of a circle $\bar{\mathcal{C}}$ because $\mathbf{p} \notin \mathcal{C}$), and at infinity, in which case $\bar{\mathcal{C}}$ is a straight line. When $\mathbf{p} = \mathbf{c}$, then $\mathsf{pt}(\mathbf{p}, \cdot)$ is constant. When $\mathbf{p}$ is inside the circle $\mathcal{C}$ with $\mathbf{p} \neq \mathbf{c}$, any straight line intersects $\mathcal{C}$, so that the only critical points of $\mathsf{pt}(\mathbf{p}, \cdot)$ correspond to the two critical points of $\mathsf{pp}(\mathbf{p}, \cdot)$ and are achieved at the points given in (7.37). When $\mathbf{p}$ is outside the circle $\mathcal{C}$, then there are exactly two straight line passing through $\mathbf{p}$ and tangent to $\mathcal{C}$ at some point. Therefore the critical points of $\mathsf{pt}(\mathbf{p}, \cdot)$ are two maxima with the value infinity and two minima that correspond to the two critical points of $\mathsf{pp}(\mathbf{p}, \cdot)$. ■

Corollary 7.13 *For a circle $\mathcal{C}$ parametrised by a parameter $s \in I$, and a point $\mathbf{p} \notin \mathcal{C}$, the function $\mathsf{pt}(\mathbf{p}, \cdot)$, $s \in I$, is either constant or has either one or two minima. The global minimum of $\mathsf{pt}(\mathbf{p}, \cdot)$ is the global minimum of $\mathsf{pp}(\mathbf{p}, \cdot)$. If it has two minima, then they are the critical points of $\mathsf{pp}(\mathbf{p}, \cdot)$. That is the maximum of $\mathsf{pp}(\mathbf{p}, \cdot)$ is either a local minimum of $\mathsf{pt}(\mathbf{p}, \cdot)$ or the global maximum of $\mathsf{pt}(\mathbf{p}, \cdot)$.*

It is remarkable that on a circle the minimum of $\mathsf{pt}(\mathbf{p}, \cdot)$ is never achieved by the fifth case of Lemma 3.6, cf. section 7.2.1. Now consider an arc $\mathbf{a}$ instead an entire circle $\mathcal{C}$. To decide if a minimum of $\mathsf{pt}(\mathbf{p}, \cdot)$ is achieved within the arc, we have to consider derivatives at the end points.

Lemma 7.14 *For an arc $\mathbf{a}$ with $\angle\mathbf{a} < \pi$, given by the Bézier points $\mathbf{a}_0, \mathbf{a}_1, \mathbf{a}_2 \in \mathbb{R}^3$, denote by r the radius, and by $\mathbf{c}$ the centre of the arc $\mathbf{a}$. Then for a point $\mathbf{p} \notin \mathbf{a}$,*

1. *When $(\mathbf{a}_1 - \mathbf{a}_0) \cdot (\mathbf{a}_0 - \mathbf{p}) < 0$ and $(\mathbf{a}_2 - \mathbf{a}_1) \cdot (\mathbf{a}_2 - \mathbf{p}) < 0$, then there is no minimum of $\mathsf{pt}(\mathbf{p}, \cdot)$ achieved inside the arc, and the minimum is achieved at an end point,*

2. *When $(\mathbf{a}_1 - \mathbf{a}_0) \cdot (\mathbf{a}_0 - \mathbf{p}) \leq 0$ and $(\mathbf{a}_2 - \mathbf{a}_1) \cdot (\mathbf{a}_2 - \mathbf{p}) \geq 0$, then there is a minimum of $\mathsf{pt}(\mathbf{p}, \cdot)$ achieved inside the arc by the minimum of $\mathsf{pp}(\mathbf{p}, \cdot)$,*

3. *When $(\mathbf{a}_1 - \mathbf{a}_0) \cdot (\mathbf{a}_0 - \mathbf{p}) \geq 0$ and $(\mathbf{a}_2 - \mathbf{a}_1) \cdot (\mathbf{a}_2 - \mathbf{p}) \leq 0$ and if $\mathbf{p}$, $\mathbf{a}_0$, $\mathbf{a}_1$, and $\mathbf{a}_2$ are not coplanar with additionally (7.39) being valid, or if $\mathbf{p}$, $\mathbf{a}_0$, $\mathbf{a}_1$, and $\mathbf{a}_2$ are coplanar with additionally $r < |\mathbf{p} - \mathbf{c}|$, then there is a minimum of $\mathsf{pt}(\mathbf{p}, \cdot)$ achieved inside the arc by the maximum of $\mathsf{pp}(\mathbf{p}, \cdot)$, otherwise there is no minimum of $\mathsf{pt}(\mathbf{p}, \cdot)$ achieved inside the arc,*

4. *When $(\mathbf{a}_1 - \mathbf{a}_0) \cdot (\mathbf{a}_0 - \mathbf{p}) > 0$ and $(\mathbf{a}_2 - \mathbf{a}_1) \cdot (\mathbf{a}_2 - \mathbf{p}) > 0$, then there is no minimum of $\mathsf{pt}(\mathbf{p}, \cdot)$ achieved inside the arc, and the minimum is achieved at an end point.*

Proof Lemma 7.12 implies the results. ■

For a Matlab code implementing the evaluation of ρ_{pt} based on Lemma 7.14 see Appendix B.

7.2.1 Example: Biarc approximation of an Ellipse

In order to verify the proposed algorithms we compare the standard local radius of curvature function ρ, and the global radius of curvature function ρ_{pt} evaluated on an ellipse and on a biarc approximation of the same ellipse. We consider the case of the ellipse with principal axes of length 1.0 and 0.6 discussed in section 3.5.1. We use a biarc curve obtained as an interpolation of 100 point-tangent data pairs non-uniformly distributed in arc length, that were uniformly distributed in the $(\cos(t), 0.6\sin(t))$ parametrisation. The matching rule used here, and in the biarc curves described in chapter 8 is the *midpoint*-matching rule, and we therefore refer to such biarcs as *midpoint-biarcs*.

Notation 7.15 *For a proper point-tangent data pair* $((\mathbf{q}_0, \mathbf{t}_0), (\mathbf{q}_1, \mathbf{t}_1)) \in \mathcal{J} \times \mathcal{J}$ *the* midpoint-biarc *is the biarc that has the mid point of the circular arc of* Σ_{++} *as matching point* $\mathbf{m}$.

By definition 4.12, midpoint-biarcs are proper biarcs. In [54] the midpoint-matching rule is called *Shippey's bisector*, it is a geometrically natural rule with simple associated formulæ. For a short discussion on other possible matching rules see section 9.

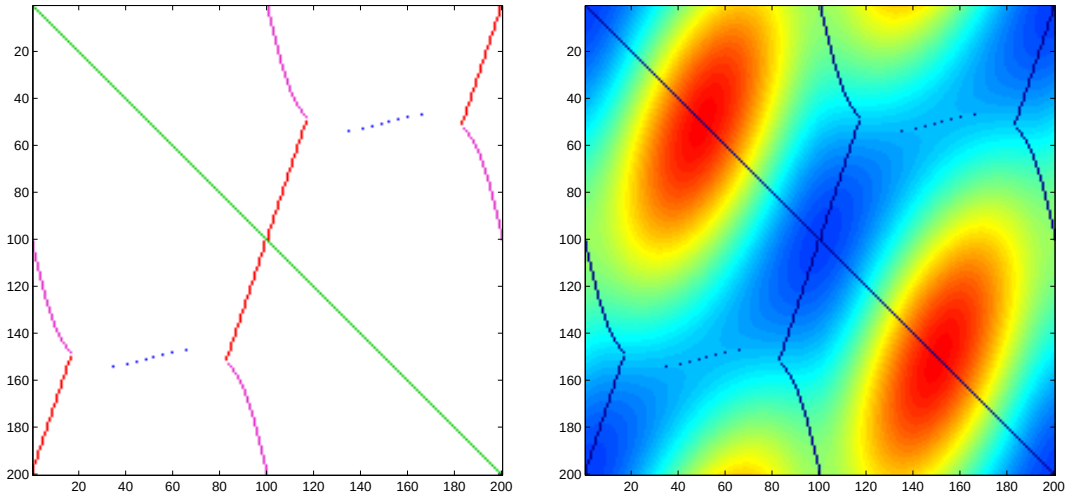

Figure 7.10: (cf. Figure 3.3) The pt function for a 100-midpoint-biarc approximation of an ellipse with principal axes of length 1.0 and 0.6. The vertical index is that of the midpoints $\mathbf{m}_i$ of the arcs $\mathbf{a}_i$, $i = 1, \cdots, 200$, the horizontal index is that of the arcs $\mathbf{a}_j$, $j = 1, \cdots, 200$. (a) The colours indicate how the minimum of $\mathsf{pt}(\mathbf{m}_i, \cdot)$ restricted to the arc $\mathbf{a}_j$ is achieved. Blue: a local minimum of $\mathsf{pt}(\mathbf{m}_i, \cdot)|_{\mathbf{a}_j}$ is achieved at an interior minimum of $\mathsf{pp}(\mathbf{m}_i, \cdot)$, magenta: a local minimum of $\mathsf{pt}(\mathbf{m}_i, \cdot)|_{\mathbf{a}_j}$ is achieved at an interior maximum of $\mathsf{pp}(\mathbf{m}_i, \cdot)$, red: a local minimum of $\mathsf{pt}(\mathbf{m}_i, \cdot)|_{\mathbf{a}_j}$ is achieved at an end point of the arc $\mathbf{a}_j$ which is a (local) minimum of $\mathsf{pt}(\mathbf{m}_i, \cdot)$, and green: the minimum is achieved by the local radius. (b) the minimum of $\mathsf{pt}(\mathbf{m}_i, \cdot)|_{\mathbf{a}_j}$, with a superposed blue dot when the minimum $\mathsf{pt}(\mathbf{m}_i, \cdot)|_{\mathbf{a}_j}$ is a minimum of $\mathsf{pt}(\mathbf{m}_i, \cdot)$.

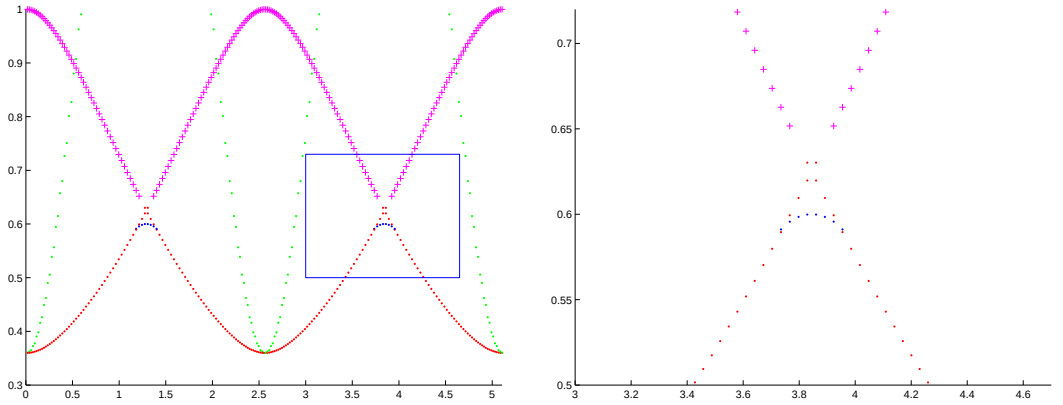

Figure 7.11: (cf. Figure 3.5) (a) Plot of the height of the minimum of $\mathsf{pt}(\mathbf{m}_i, \cdot)|_{\mathbf{a}_j}$ for (i, j) that achieve a minimum of $\mathsf{pt}(\mathbf{m}_i, \cdot)$, the horizontal axis is arc length. Magenta $+$: the minimum of $\mathsf{pt}(\mathbf{m}_i, \cdot)|_{\mathbf{a}_j}$ is achieved at an interior maximum of $\mathsf{pp}(\mathbf{m}_i, \cdot)$, blue dot: the minimum of $\mathsf{pt}(\mathbf{m}_i, \cdot)|_{\mathbf{a}_j}$ is achieved at an interior minimum of $\mathsf{pp}(\mathbf{m}_i, \cdot)$, red dot: the minimum of $\mathsf{pt}(\mathbf{m}_i, \cdot)|_{\mathbf{a}_j}$ is achieved at an end point of the arcs $\mathbf{a}_j$ and it is a (local) minimum of $\mathsf{pt}(\mathbf{m}_i, \cdot)$, green dot: local radius of $\mathbf{a}_i$. For a fixed i, the minimum of the values plotted is $\rho_{\mathsf{tp}}(\mathbf{m}_i)$ shown in figure 7.12, (b) is a zoom of the box in (a).

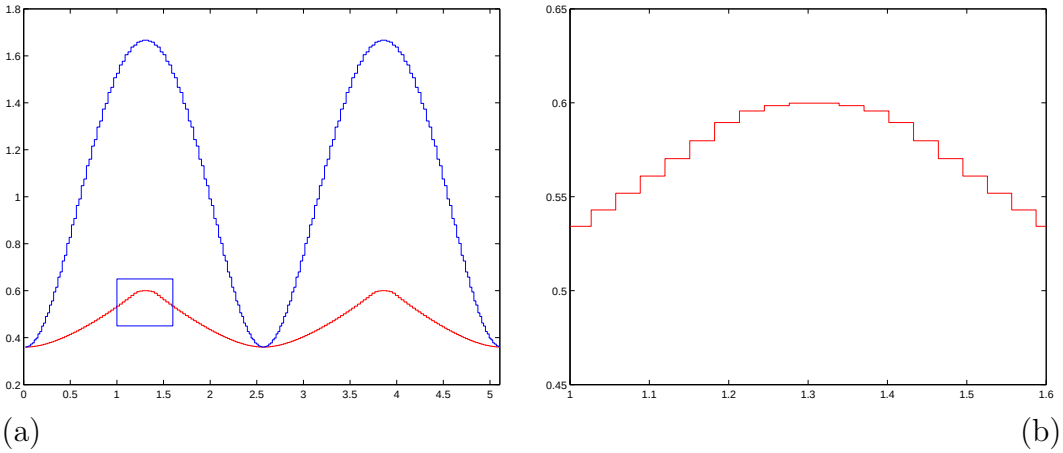

Figure 7.12: (cf. Figure 3.4) (a) Plots of the local and global radius of curvature function ρ and ρ_{pt} for a 100-midpoint-biarc approximation of an ellipse with principal axes of length 1.0 and 0.6, (b) zoom of the box indicated in (a).

We evaluate the global radius of curvature function ρ_{tp} at the mid point $\mathbf{m}_i$ of every one of the 200 arcs $\mathbf{a}_i$. In order to do that we have to study the minima of $\mathsf{pt}(\mathbf{m}_i, \cdot)$ restricted to the arc $\mathbf{a}_j$, i.e. of $\mathsf{pt}(\mathbf{m}_i, \cdot)|_{\mathbf{a}_j}$ for every pair $1 \leq i, j \leq 200$. In particular we seek local minima of $\mathsf{pt}(\mathbf{m}_i, \cdot)|_{\mathbf{a}_j}$ that correspond to local minima of the $\mathsf{pt}(\mathbf{m}_i, \cdot)$. Using Lemma 7.14 we classified all pairs (i, j) as shown in Figure 7.10 (a). Figure 7.10 (b) displays those special pairs of arcs superposed with the height of the minimum value of $\mathsf{pt}(\mathbf{m}_i, \cdot)|_{\mathbf{a}_j}$.

In Figure 7.11 the heights of the minimum of $\mathsf{pt}(\mathbf{m}_i, \cdot)|_{\mathbf{a}_j}$ are plotted against the parameter $t \in [0, 2\pi)$ for pairs appearing in Figure 7.10 (a). Except for two small regions where the minima are given by blue dots, that is by a minimum of $\mathsf{pp}(\mathbf{m}_i, \cdot)$, the minima is given by red dots, that is they are achieved at an end point of the arc. The switch in the way of achieving the minima of $\mathsf{pt}(\mathbf{m}_i, \cdot)|_{\mathbf{a}_j}$ corresponds exactly to the switch observed in Figure 3.5 (d)-(f). Note that the blue line does not stop exactly on the red line, but overlaps it slightly. In particular for a finer mesh one can observe a local minimum of $\mathsf{pt}(\mathbf{m}_i, \cdot)|_{\mathbf{a}_j}$ achieved at an interior minimum of $\mathsf{pp}(\mathbf{m}_i, \cdot)$ that is higher than the value of the local minimum of $\mathsf{pt}(\mathbf{m}_i, \cdot)|_{\mathbf{a}_k}$ achieved at an end point of an arc.

The minimal values (red) of the heights of the minimum of $\mathsf{pt}(\mathbf{m}_i, \cdot)|_{\mathbf{a}_j}$ for pairs appearing in figure 7.10 (a) and the radii $r(\mathbf{a}_i)$ of the arcs $\mathbf{a}_i$ (blue) are plotted against the parameter $t \in [0, 2\pi)$ in Figure 7.12. This is the analogue of the ρ and ρ_{pt} plots in Figure 3.4. The flat region of ρ_{pt} in Figure 7.12 corresponds to the region bounded by the corners of the global radius of curvature function ρ_{pt} visible in figure 3.4.

Chapter 8

Ideal Shapes - Global radius of curvature functions and contact sets

We now consider the specific problem of computation of the ideal shapes that were introduced in section 2.3. We address the two following, related questions: For a given closed, non-intersecting curve, can we quantify how close the given configuration is to being an ideal knot shape? Can we rigorously define a contact set? Both questions require answers in a form that is robust for numerics. We then apply the proposed definitions to shapes obtained by simulated annealing computations using the biarc discretization implemented in a code developed in collaboration with B. Laurie. In particular we test a necessary condition and determine the approximate contact sets of computations of the ideal shapes of the 3.1 (or trefoil) and 4.1 (or figure-eight) knots.

8.1 Ideality test, contact set and μ-contact set

For an ideal shape, as mentioned in section 2.3, the global radius of curvature function ρ_{pt} is constant on curved segments. In general we have the inequality $\rho_{\mathsf{pt}} \leq \rho_{\mathsf{tp}}$ (cf. (3.25)). We next show that on ideal shapes these two global radius of curvature functions agree on curved segments, and therefore the function ρ_{tp} is also constant on curved segments:

Lemma 8.1 *Given a smooth ideal shape* $\mathbf{q}$*, then*

$$\rho_{\mathsf{pt}}(s) = \rho_{\mathsf{tp}}(s) = \Delta[\mathbf{q}] \quad \textit{for } \{s \in I; \kappa(s) \neq 0\}.$$

Proof We know from [18, p. 4771] that $\rho_{\mathsf{pt}}(s) = \Delta[\mathbf{q}]$ when $\kappa(s) \neq 0$. Assume there exists an $s \in I$ with $\rho_{\mathsf{pt}}(s) < \rho_{\mathsf{tp}}(s)$ and $\kappa(s) \neq 0$. Because of the equalities (3.23) and the inequalities (3.25), more precisely because $\rho \geq \rho_{\mathsf{tp}} \geq \rho_{\mathsf{pt}}$, the global radius of curvature function $\rho_{\mathsf{pt}}(s)$ is achieved non-locally, that is, there exists a $t \in I$ with $t \neq s$ and $\rho_{\mathsf{pt}}(s) = \mathsf{pt}(s,t)$. Consider the circumsphere $\mathcal{S}$ of the circle $\mathcal{C}(s,t,t)$. The vector $\mathbf{q}'(s)$ is tangent to the sphere $\mathcal{S}$, because if not, then there exists a circle $\mathcal{C}(s',t,t)$ with $\mathsf{pt}(s',t) < \mathsf{pt}(s,t) = \rho_{\mathsf{pt}}(s) = \Delta[\mathbf{q}]$. Thus, the circle $\mathcal{C}(s,s,t)$ lies on the sphere $\mathcal{S}$, and therefore $\mathsf{tp}(s,t) \leq \mathsf{pt}(s,t) = \rho_{\mathsf{pt}}(s)$ which contradicts $\rho_{\mathsf{pt}}(s) < \rho_{\mathsf{tp}}(s)$. ■

The precise regularity necessary for Lemma 8.1 to remain valid is not clear. The proof of constancy of ρ_{pt} given in [18] uses curve shortening arguments for which C^2 regularity is sufficient, but a gap remains to the known $C^{1,1}$ smoothness of ideal shapes.

Given Lemma 8.1 a comparison of the graphs of both ρ_{pt} and ρ_{tp} with ρ and the thickness gives one indication of how close to ideal a given shape is. By the inequality $\rho_{\mathsf{pt}} \leq \rho_{\mathsf{tp}}$ (cf. (3.25)) the graph of ρ_{tp} will be further from constant than that of ρ_{pt} but because we do not have a rigorous algorithm for the computation of ρ_{tp} in hand, we graph only ρ_{pt}.

Definition 8.2 *For a closed, non-intersecting curve* $\mathbf{q} \in C^1(I, \mathbb{R}^3)$ *we define*

1. *the* contact set $\boldsymbol{\chi}$ *to be the set*

$$\boldsymbol{\chi} := \{(s,\sigma) \in I \times I; \mathsf{pt}(s,\sigma) = \Delta[\mathbf{q}]\},$$

and the set of contact points *in three dimensional space to be the set*

$$\mathcal{C} := \{\mathbf{c} \in \mathbb{R}^3;\ \mathbf{c} \textit{ is the centre of } \mathcal{C}(s,\sigma,\sigma)\ \&\ (s,\sigma) \in \boldsymbol{\chi}\},$$

2. *and for* $\mu > 0$ *the* μ-contact set $\boldsymbol{\chi}_\mu$ *to be the set*

$$\boldsymbol{\chi}_\mu := \{(s,\sigma) \in I \times I; \mathsf{pt}(s,\sigma) \leq \Delta[\mathbf{q}](1+\mu)\ \ \&\ \ \mathsf{pt}(s,\cdot) \textit{ has a local minimum in } \sigma\},$$

and the set of μ-contact points *in three dimensional space to be the set*

$$\mathcal{C}_\mu := \{\mathbf{c} \in \mathbb{R}^3;\ \mathbf{c} \textit{ is the centre of } \mathcal{C}(s,\sigma,\sigma)\ \&\ (s,\sigma) \in \boldsymbol{\chi}_\mu\}.$$

The ideas motivating Definition 8.2 are the following. For a generic curve Γ the contact set $\boldsymbol{\chi}$ will typically be a pair of elements (s,σ) and (σ,s) with $\boldsymbol{\chi}_\mu$, for μ sufficiently small, being a pair of short curve segments containing (s,σ) and (σ,s) respectively. For an exactly ideal shape the constancy of ρ_{pt} implies that the contact set $\boldsymbol{\chi}$ will contain points of the form $(s, I(s))$ for each s, with, presumably, the set being made up of one or more curves in the (s,σ) plane generated by the local minimiser of $\mathsf{pt}(s,\cdot)$ moving with the parameter s. For an approximately ideal shape the contact set $\boldsymbol{\chi}$ should again be one, or a small number of, isolated points, but for μ small $\boldsymbol{\chi}_\mu$ should explode to a much larger set, containing points of the form $(s, I(s))$ for all s. It is also reasonable to anticipate ranges of μ for which $\boldsymbol{\chi}_\mu$ is invariant or changes very little. These expectations are justified by the computations described below.

Trivially we have $\boldsymbol{\chi} \subset \boldsymbol{\chi}_\mu$ for any $\mu > 0$, and $\boldsymbol{\chi} \subset \boldsymbol{\chi}_{\mu_1} \subset \boldsymbol{\chi}_{\mu_2}$ for $\mu_2 > \mu_1 > 0$. Moreover, if $(s,\sigma) \notin \boldsymbol{\chi}$, then there exists a $\mu > 0$ such that $(s,\sigma) \notin \boldsymbol{\chi}_\mu$. Note that both the exact contact set $\boldsymbol{\chi}$ as well as any $\boldsymbol{\chi}_\mu$ can contain contact of the type (s,s). With the definition of μ-contact we have another test in hand: If the shape obtained by simulated annealing computation is close to being converged then we expect that there exists a $\mu > 0$ such that $\boldsymbol{\chi}_{2\mu} \backslash \boldsymbol{\chi}_\mu$ is a small set relative to the number of arcs of the arc curve. The sets of contact points $\mathcal{C}$ and $\mathcal{C}_\mu$ in three dimensional space are useful to give the right spatial picture, but they contain different information than the contact sets

$\boldsymbol{\chi}$ and $\boldsymbol{\chi}_\mu$ in two dimensions. For example the contact set $\mathcal{C}$ of the circle (namely the ideal shape of the trivial knot) contains one single point, but this point is derived from an infinite number of pairs in $\boldsymbol{\chi}$, more precisely one line for local curvature, one line for diametrically opposite points.

An approximate μ-contact set could be defined in other related ways, for example as

$$\boldsymbol{\chi}^*_\mu := \{(s,\sigma) \in I \times I; \mathsf{pt}(s,\sigma) \leq \Delta[\mathbf{q}](1+\mu) \quad \& \quad \partial_\sigma \mathsf{pt}(s,\sigma) = 0\},$$

which is perhaps more useful analytically. Similarly an approximate contact set could instead be based on the function ρ_{tp} and be found via minima of $\mathsf{tp}(s,\cdot)$.

8.2 Computation of an ideal 3.1-knot

We now present the output of simulated annealing computations performed in collaboration with B. Laurie who upgraded an existing code [26] that was based on a piece-wise linear space discretization to the biarc discretization, and implemented the thickness evaluation algorithm described in chapter 7. The basic data format is a list of point-tangent data. The allowed moves are random changes in both points and tangents, but the step sizes have different scales for points and tangents. Throughout we used the midpoint matching rule, cf. Notation 7.15, which is a convenient and simple choice. Nevertheless it is reasonable to believe that it may not be the optimal matching rule to compute ideal shapes. Moreover we do not know the optimal values for parameters such as temperature and cooling rate that need to be set during the simulation. The knot shapes presented here were obtained by low temperature simulated annealing starting from close-to-ideal shapes, in particular we did not attempt to globally search the conformation space of the knot type in order to find all local minima.

The simulated annealing computation of the 3.1 knot was carried out by B. Laurie and J. Smutny. Low temperature simulated annealing was performed starting from a 190-biarc interpolation of a piece-wise linear trefoil configuration obtained from a prior simulated annealing computation of B. Laurie [26]. After some computation a curvature plot seemed to suggest that the shape was close to converged, although three regions corresponding to the inner parts of the knot remained unresolved. The curvature was not very smooth in that region and it was not clear if local curvature was active. In order to address these issues a local (and manual) mesh refinement was performed in these three regions by splitting some biarcs to obtain a 264-biarc shape with a rather nonuniform distribution of biarc lengths. Subsequent low temperature annealing provided the shape $\boldsymbol{\alpha}$ described below which has rope length $\frac{\lambda(\boldsymbol{\alpha})}{\Delta[\boldsymbol{\alpha}]} = 32.74446$. We denote the 528 arcs by $\mathbf{a}_i$, the radii by r_i and the mid point of each arc $\mathbf{a}_i$ by $\mathbf{m}_i$, $1 \leq i \leq 528$. The total time for the simulated annealing computation was several months on a single CPU.

8.2.1 Computing the thickness

Figure 8.1 illustrates the thickness evaluation algorithm presented in section 7.1.3. The horizontal line indicates the number of pairs of arcs of the arc curve, here $(2 \cdot 264)^2 =$

278′784. The number of candidates in achieving thickness after the double critical test (higher curve) and after the distance test (lower curve) of each of the 15 iterations is plotted. With the bisection step the number of pairs of candidates is quadrupled, which is why it is important to combine both tests to reduce computation time. It would probably be worthwhile investigating additional tests to further improve the speed of the thickness evaluation.

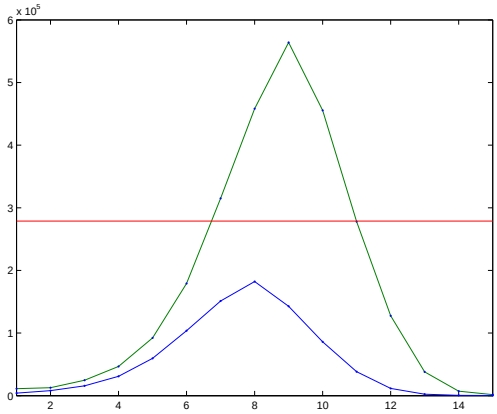

Figure 8.1: The number of candidates in achieving thickness after the double critical test (higher curve) and after the distance test (lower curve), cf. 7.1, for each of the fifteen iteration steps. The horizontal line indicates the original total number $(2 \cdot 264)^2 = 278'784$ of pairs of arcs to be considered.

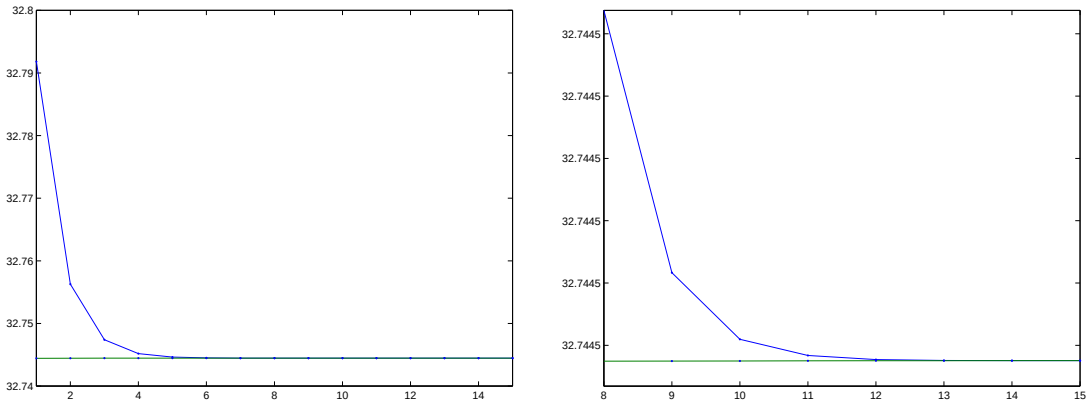

(a) (b)

Figure 8.2: (a) Upper and lower bound of rope length $\frac{\lambda(\boldsymbol{\alpha})}{\Delta[\boldsymbol{\alpha}]}$ of the biarc curve after each of the fifteen iteration steps, (b) is a zoom of Figure (a), the values for the last 8 iteration steps are displayed.

The evolution of upper and lower bounds of rope length $\frac{\lambda(\boldsymbol{\alpha})}{\Delta[\boldsymbol{\alpha}]}$ during the thickness evaluation algorithm is plotted in Figure 8.2. The lower bound of rope length is increasing, but much less rapidly than the upper bound is decreasing. The final bounds of rope length, the length $\lambda(\boldsymbol{\alpha})$ of the arc curve, the minimal radius $\min_i r_i$, and upper

and lower bounds for thickness $\Delta[\boldsymbol{\alpha}]$ are

$$\begin{aligned} \lambda(\boldsymbol{\alpha}) &= 0.99999999997863, \\ \min_i r_i &= 0.03054053096312, \\ 0.03053951779966 \leq \Delta[\boldsymbol{\alpha}] &\leq 0.03053951779968, \\ 32.74445937679887 \leq \tfrac{\lambda(\boldsymbol{\alpha})}{\Delta[\boldsymbol{\alpha}]} &\leq 32.74445937682155. \end{aligned}$$

The thickness was evaluated up to a relative error of 10^{-12}, that is the maximal error divided by the lower bound of thickness is smaller than 10^{-12}. Note that $\min_i r_i$ is slightly higher than the thickness $\Delta[\boldsymbol{\alpha}]$, this observation will be discussed later.

8.2.2 The shape

To display the shape of the knot the centre of mass and principal axes $\mathbf{v}_1$, $\mathbf{v}_2$, and $\mathbf{v}_3$ of inertia (ordered with eigenvalues $\lambda_1 = 3.1161 \cdot 10^{-3} \leq \lambda_2 = 3.1347 \cdot 10^{-3} \leq \lambda_3 = 5.2057 \cdot 10^{-3}$) of the set of end points of all arcs were computed. Figure 8.3 (a) shows the projection of the end points of all arcs onto the $\mathbf{v}_1$-$\mathbf{v}_2$ plane, whereas (b) is the projection of the tangents at the end points of all arcs onto the $\mathbf{v}_1$-$\mathbf{v}_2$ plane. In Figure 8.3 the polar coordinates of (c) the end points and (d) end point tangents along arc length are plotted, with blue the $\mathbf{v}_3$ coordinate, green the radial coordinate $r = \sqrt{v_1^2 + v_2^2}$ and red the angle ϕ in radians scaled by a factor to make variations visible on the same plot. Note that the discontinuities of the scaled angle ϕ (red) in both Figures 8.3 (c) and (d) are not a real feature, but are due to the fact that Matlab displays the angle $\phi \in [-\pi, \pi)$ modulo 2π. Both the curve and the tangent curve appear to be very smooth, but the derivative of the tangent, i.e. the curvature, is large in three small regions, as can be observed in the Figures 8.3 (b) and (d). Figure 8.3 (a)-(d) suggests that the ideal shape of the trefoil is close to having a period three, rotational symmetry about the $\mathbf{v}_3$ axis. Rotational symmetry would imply double eigenvalues of the inertia matrix. Therefore one measure of asymmetry is $\frac{\lambda_2 - \lambda_1}{\lambda_1 + \lambda_2 + \lambda_3} = 1.6233 \cdot 10^{-3}$, thus the presented shape is only close to being, but is not precisely, rotationally symmetric.

The tangent indicatrix of an arc curve is a continuous curve assembled from arcs of great circles, cf. section 4.2. Figures 8.4 (a)-(f) show the tangent indicatrix of the shape from six different directions corresponding to the principal axes $\pm\mathbf{v}_1$, $\pm\mathbf{v}_2$, and $\pm\mathbf{v}_3$. The lengths of the 528 arcs are depicted in Figure 8.5. In the three regions where mesh-refinement was performed the lengths are about three times shorter. Figure 8.6 depicts the radii of the 528 arcs scaled by the thickness Δ. There are three regions with almost constant radii equal 2Δ and three regions with a high variation of the radii, dropping from approximately 2Δ down to Δ then up to 2.8Δ, back down to Δ, and finally back up to end again with 2Δ. In section 8.2.3 we quantify how close the scaled radii are to actually achieving thickness. The regions with constant curvature belong to the large exterior loops visible in Figure 8.3 (a). As will also be seen from torsion plots and in the two dimensional contact map, cf. Figure 8.13, these regions are close to being, but are not precisely, circular arcs.

The angle between the planes of adjacent arcs is plotted in figure 8.7. There are three regions with large angles that correspond to the regions with a high variation of

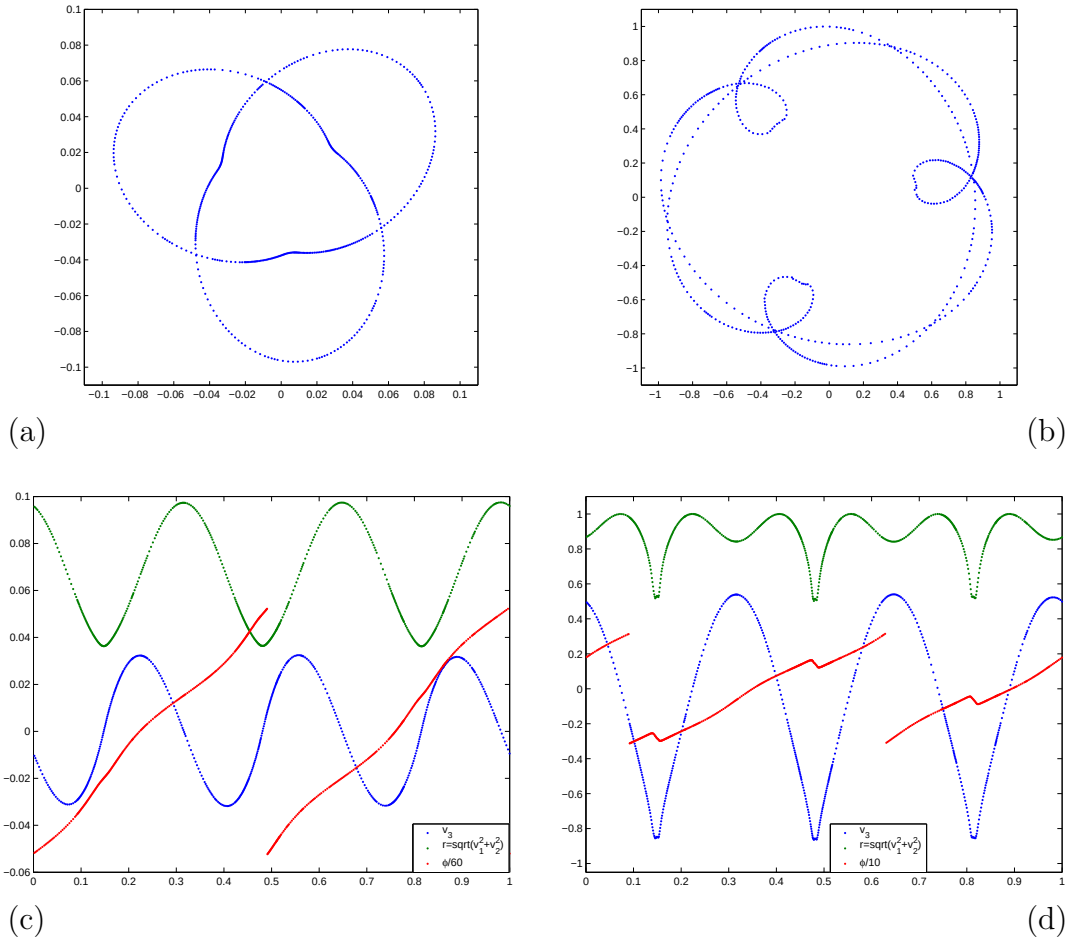

Figure 8.3: Projection onto the plane of the $\mathbf{v}_1$-$\mathbf{v}_2$ inertia axes of (a) the end points of all arcs, and (b) the unit tangents at the end points of all arcs. Plots of the cylindrical polar coordinates v_3, $r = \sqrt{v_1^2 + v_2^2}$ and the (scaled) angle ϕ in radians, of (c) the end points of all arcs w.r.t. the axes of inertia, after translation to the centre of mass, and (d) of the tangents at the end points of all arcs.

the radii, that is to the parts "inside the knot". Note that the angle is given in radians, that is, the maximal value of about 1.2 between adjacent arcs corresponds to an angle of about 70 degrees.

In chapter 5 we derived various approximation results of radius of curvature, its derivative, and torsion for biarcs interpolating an underlying C^3-curve in terms of the circles $\mathcal{C}_0$ and $\mathcal{C}_1$ associated with every point-tangent data pair, cf. Propositions 5.12 and 5.13. Figure 8.8 displays the quantities that approach the values of radius of curvature, its derivative, and torsion for a finite h. But we stress that it is not clear that the ideal shape is a C^3-curve, and, moreover, we have no estimate of the constants involved in the error terms. Both the approximation of the radius of curvature and its derivative suggest that the curvature of the underlying ideal shape is very close to constant on the large loops. The parts of the shape having large oscillations of the derivative of curvature coincide with the parts of large torsion, which takes values up to 700.

The plots of quantities associated with the actual arc curve shape, cf. Figures 8.6

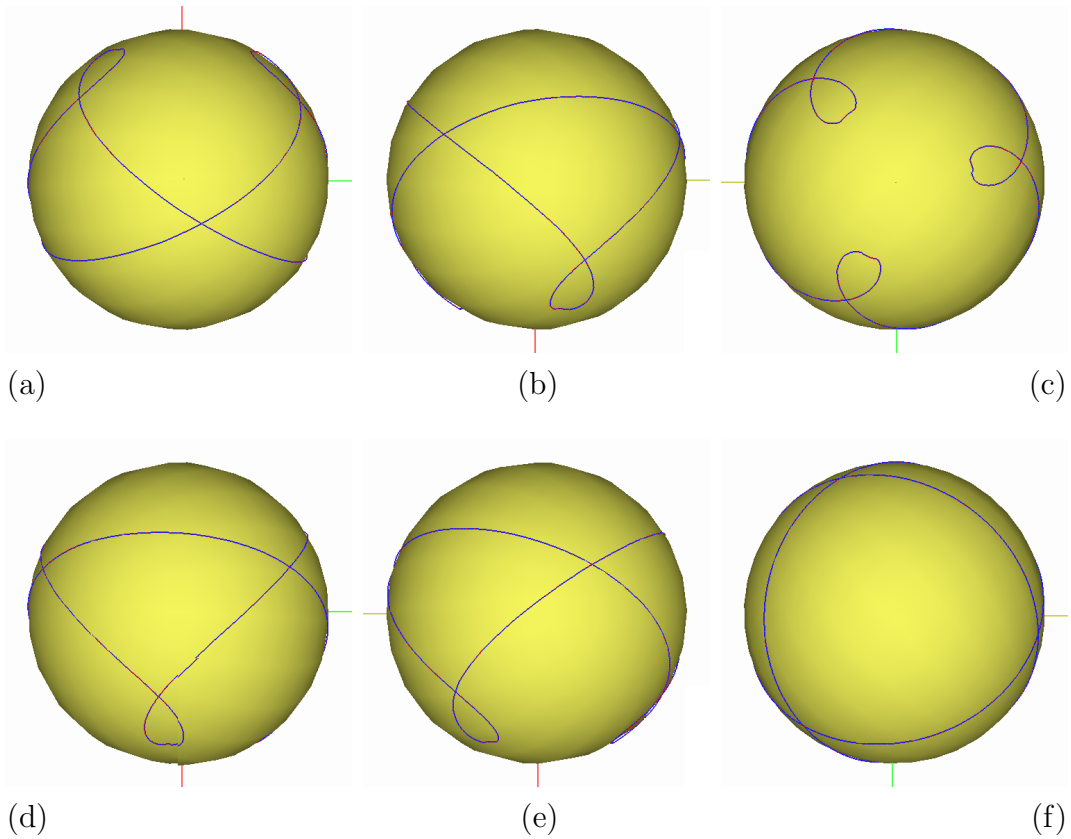

Figure 8.4: Six projections of the tangent indicatrix along principal axes of inertia (a) and (d) $\pm\mathbf{v}_1$, (b) and (e) $\pm\mathbf{v}_2$, and (c) and (f) $\pm\mathbf{v}_3$.

and 8.7, are in agreement with the plots of the approximating finite difference quantities for an assumed underlying curve, cf. Figures 8.8(a)-(b) and 8.8(e)-(f).

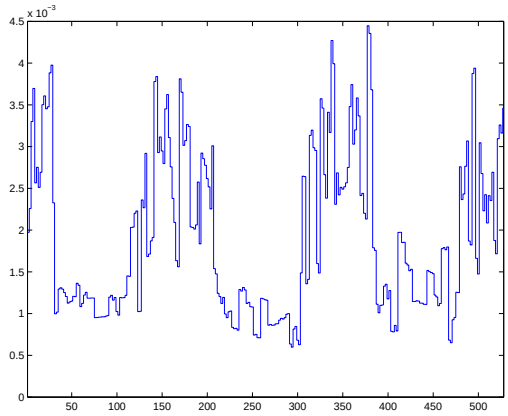

Figure 8.5: The lengths of the 528 arcs in the simulation are non-uniform. A three-periodicity can be observed, where mesh-refinement was performed to resolve the three regions of high local curvature.

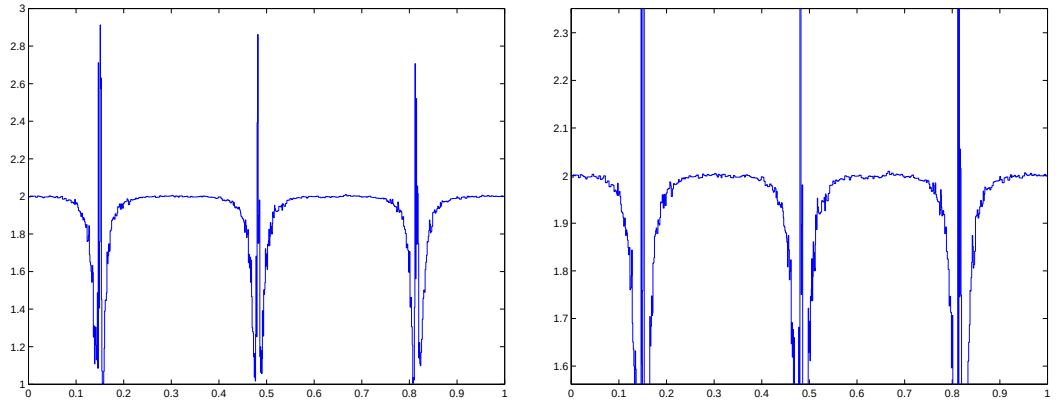

Figure 8.6: (a) Plot of the radii of the arcs scaled by the thickness (non-dimensional), (b) is a zoom of (a).

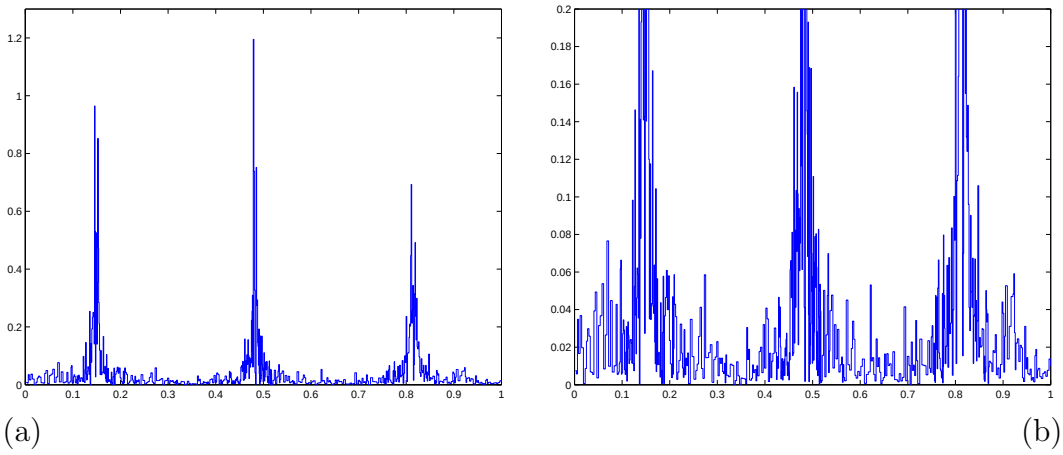

Figure 8.7: Plots of (a) torsion angle, i.e. the angle between the planes of successive arcs in radians and (b) zoom of (a).

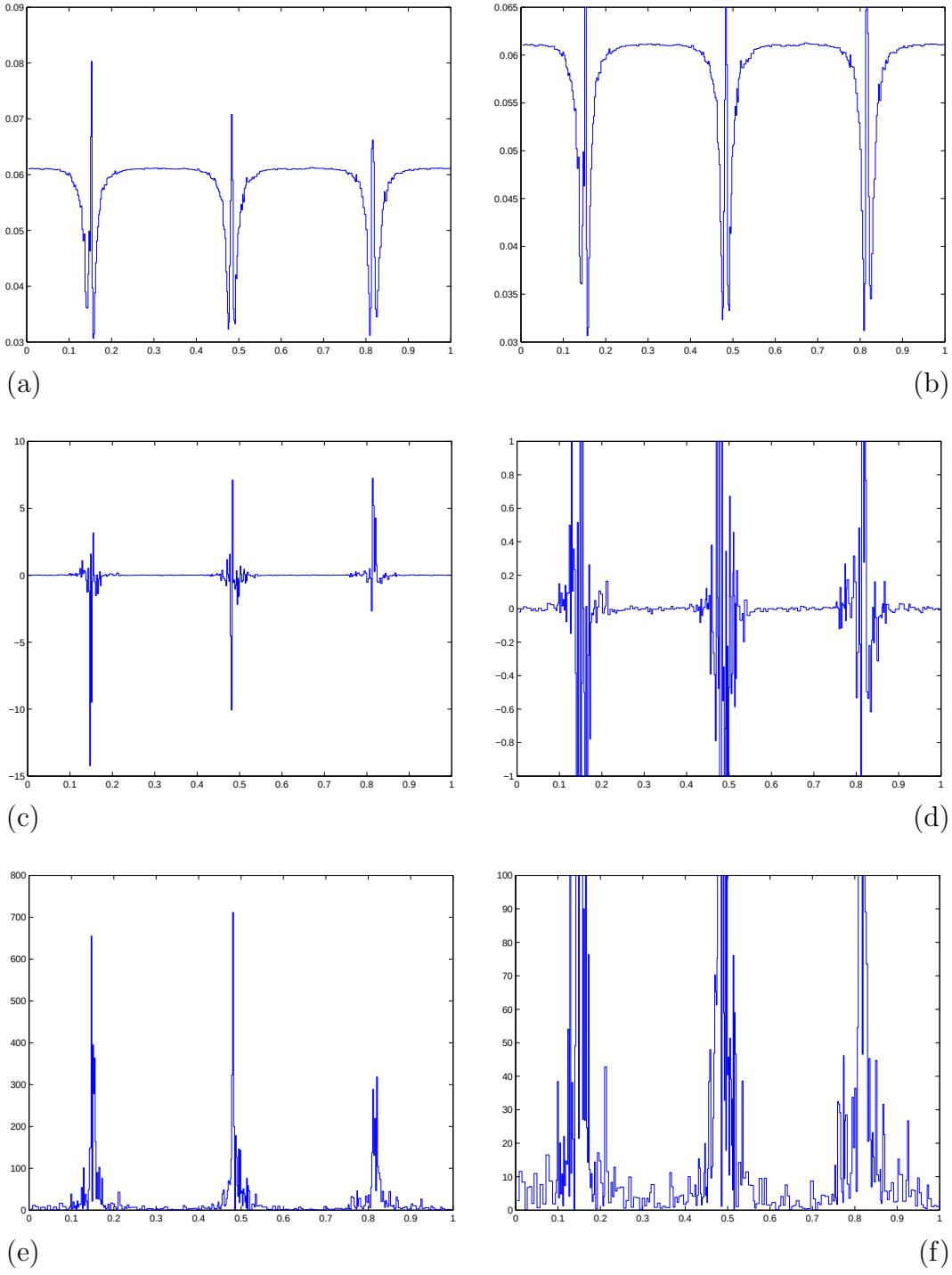

Figure 8.8: Plots of the finite difference approximation of radius of curvature, its derivative, and torsion for an underlying curve. (a) Plot of the approximation of the radius of curvature in terms of the circles $\mathcal{C}_0^h$ and $\mathcal{C}_1^h$, cf. Proposition 5.12, (b) zoom of (a) (units of length). (c) Plot of the approximation of the derivative of the radius of curvature in terms of the circles $\mathcal{C}_0^h$ and $\mathcal{C}_1^h$, cf. Proposition 5.12, (d) zoom of (c) (non-dimensional). (e) Plot of the approximation of the torsion in terms of the circles $\mathcal{C}_0^h$ and $\mathcal{C}_1^h$, cf. Proposition 5.13, (f) zoom of (d) (units reciprocal length).

8.2.3 The contact set and ρ_{pt}

To find an appropriate $\mu > 0$ for a μ-contact set $\boldsymbol{\chi}_\mu$ of Definition 8.2, we use Lemma 7.14 to compute the minimum of $\mathsf{pt}(\mathbf{m}_i, \cdot)$ restricted to the arc $\mathbf{a}_j$ for all pairs $1 \leq i, j \leq 528$. We then classify the minima that correspond to minima of $\mathsf{pt}(\mathbf{m}_i, \cdot)$ along the whole curve as follows, cf. Figure 8.9 and 8.10: The minimum of $\mathsf{pt}(\mathbf{m}_i, \cdot)|_{\mathbf{a}_j}$ is achieved by (a) blue: a minimum of $\mathsf{pp}(\mathbf{m}_i, \cdot)$, (b) magenta: a maximum of $\mathsf{pp}(\mathbf{m}_i, \cdot)$, (c) red: an end point of the arc $\mathbf{a}_j$, and (d) green: a local radius. The only difference between Figures 8.9 and 8.10 is that in the latter the non-uniform lengths of the arcs are taken into account, whereas Figure 8.9 is a plot of index vs. index. Figure 8.10 is smoother and more representative of the overall contact set, while Figure 8.9 provides a magnification of regions where mesh refinement was made. Any pair plotted in figure 8.9 and 8.10 is a priori a candidate to be an element of a μ-contact set $\boldsymbol{\chi}_\mu$. If the value of the minimum of $\mathsf{pt}(\mathbf{m}_i, \cdot)|_{\mathbf{a}_j}$ is smaller than $\Delta(1 + \mu)$, then the arc-length values (s, σ) corresponding to $\mathbf{m}_i$ and the point on the arc $\mathbf{a}_j$ where the minimal value is achieved belong to the μ-contact set $\boldsymbol{\chi}_\mu$.

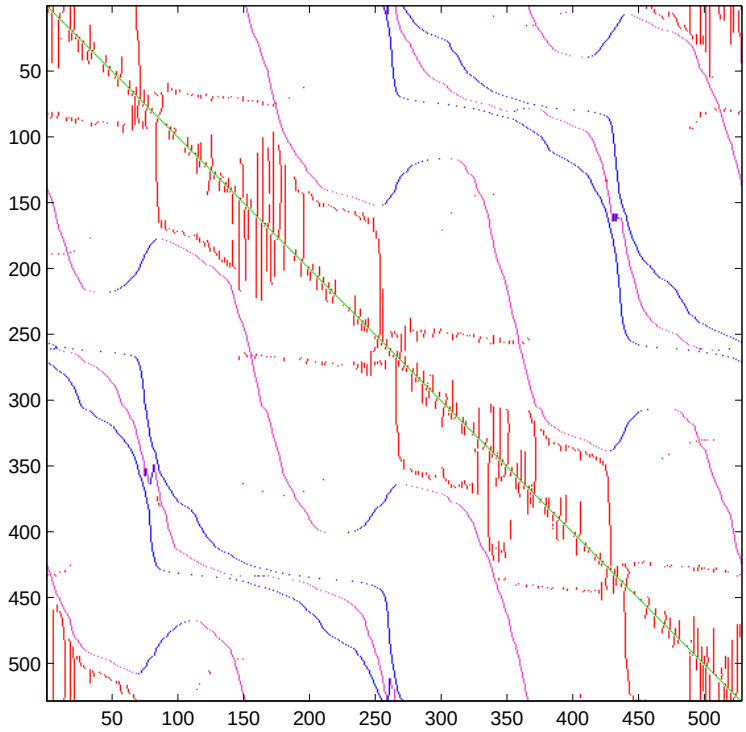

Figure 8.9: The vertical axis stands for the midpoints $\mathbf{m}_i$ of the arcs $\mathbf{a}_i$, $i = 1, \cdots, 528$, the horizontal axis stands for the arcs $\mathbf{a}_j$, $j = 1, \cdots, 528$. The colours indicate how the minimum of $\mathsf{pt}(\mathbf{m}_i, \cdot)$ restricted to the arc $\mathbf{a}_j$ is achieved. Blue: a local minimum of $\mathsf{pt}(\mathbf{m}_i, \cdot)|_{\mathbf{a}_j}$ is achieved at an interior minimum of $\mathsf{pp}(\mathbf{m}_i, \cdot)$, magenta: a local minimum of $\mathsf{pt}(\mathbf{m}_i, \cdot)|_{\mathbf{a}_j}$ is achieved at an interior maximum of $\mathsf{pp}(\mathbf{m}_i, \cdot)$, red: a local minimum of $\mathsf{pt}(\mathbf{m}_i, \cdot)|_{\mathbf{a}_j}$ is achieved at an end point of the arc $\mathbf{a}_j$ which is also a (local) minimum of $\mathsf{pt}(\mathbf{m}_i, \cdot)$, and green: the minimum of $\mathsf{pt}(\mathbf{m}_i, \cdot)|_{\mathbf{a}_j}$is achieved by the local radius. Note that the figure axes represent indices which are a distortion of actual length because of the non uniform mesh.

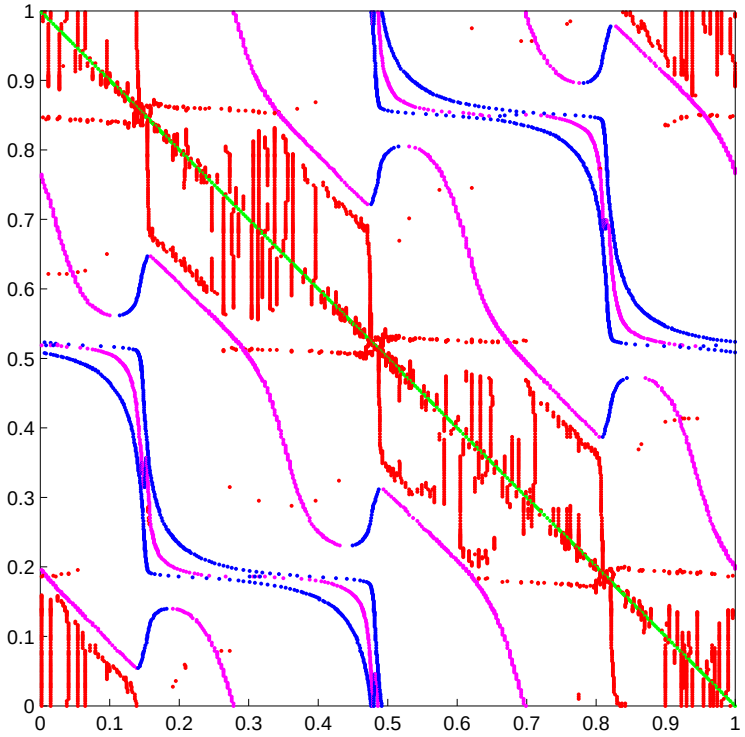

Figure 8.10: As Figure 8.9, but not distorted; the differing lengths of the arcs are taken into account. (Note: the vertical axis label is reversed, $(0,0)$ is at the top left.)

In Figure 8.11 the minimal value of $\mathsf{pt}(\mathbf{m}_i,\cdot)|_{\mathbf{a}_j}$ is plotted using a colour map with blue for low and red for high, except for pairs that appear in figures 8.9 and 8.10. Note that the minima form a very flat valley. Moreover at three places along the diagonal we see double dips approaching very close to the global minimum.

We now have to select an appropriate value of μ. We plot the heights of all minima of $\mathsf{pt}(\mathbf{m}_i,\cdot)|_{\mathbf{a}_j}$ that are candidates for a $\boldsymbol{\chi}_\mu$, i.e. that appear in Figures 8.9 and 8.10, against arc length in various zooms, cf. Figure 8.12 (a)-(d). The heights appearing in Figure 8.12 (b) belong to the lowest line in (a) and correspond to the three "curves" in the blue flat valley in Figure 8.11. The dots in figure 8.12 (c) correspond to the lowest line with the lowest bits of the above structure in (b), and finally, (d) is an ever stronger zoom showing only the lowest line in (b). In figure 8.12 (d) there is a gap above a layer of candidates. We therefore set $\mu := 8.1861 \cdot 10^{-6}$, which is about half of the height of Figure 8.12 (d). Now the μ-contact set $\boldsymbol{\chi}_\mu$ is the set of pairs of arc lengths corresponding to pairs plotted in Figures 8.9 and 8.10 for which the minima of $\mathsf{pt}(\mathbf{m}_i,\cdot)|_{\mathbf{a}_j}$ is smaller or equal to $\Delta(1+\mu)$. And similarly for $\boldsymbol{\chi}_{2\mu}$.

Figure 8.13 displays the μ-contact set $\boldsymbol{\chi}_\mu$ with $\mu = 8.1861 \cdot 10^{-6}$. The contact set appears to be two smooth lines. Indeed, the μ-contact set $\boldsymbol{\chi}_\mu$ has 1058 elements so that the average number of μ-contacts per arc is $\frac{1058}{2\cdot 264} \approx 2.00$. We expect the μ-contact set $\boldsymbol{\chi}_\mu$ to be relatively invariant for small increasing μ, in fact, the number of elements of the 2μ-contact set $\boldsymbol{\chi}_{2\mu}$ is 1062, that is $\boldsymbol{\chi}_{2\mu}\backslash\boldsymbol{\chi}_\mu$ contains only four additional contacts. The change of elements relative to the number or arcs is $\frac{4}{2\cdot 264} = 0.0076$. Figure 8.14 visualises the elements of both contact sets $\boldsymbol{\chi}_\mu$ and $\boldsymbol{\chi}_{2\mu}$: As in Figure 8.12 the height of

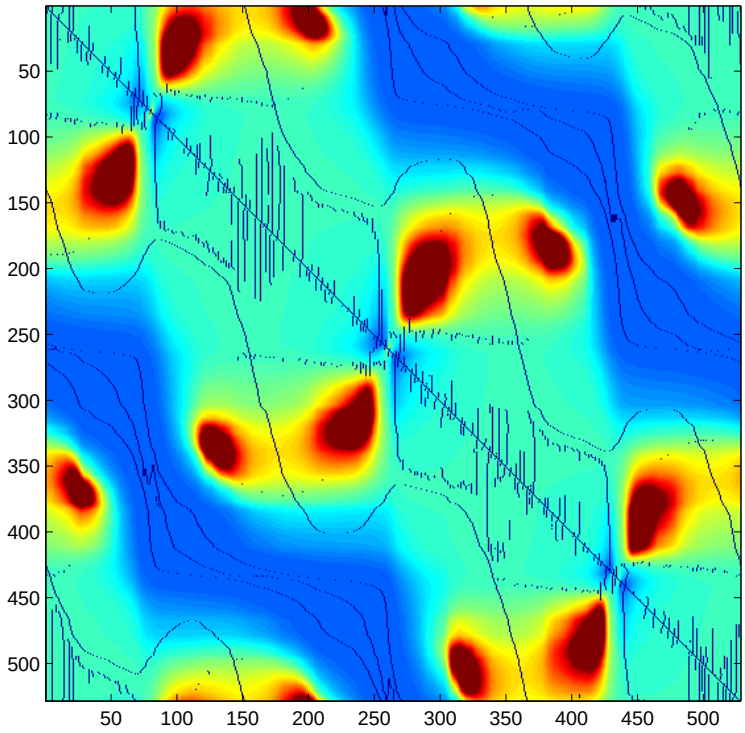

Figure 8.11: The minimum of $\mathsf{pt}(\mathbf{m}_i, \cdot)|_{\mathbf{a}_j}$, a blue dot is drawn when the minimum $\mathsf{pt}(\mathbf{m}_i, \cdot)|_{\mathbf{a}_j}$ is a minimum of $\mathsf{pt}(\mathbf{m}_i, \cdot)$. Note that the figure plots indices along a non uniform mesh. The colour map uses blue for low and red for high values.

the minimum of $\mathsf{pt}(\mathbf{m}_i, \cdot)|_{\mathbf{a}_j}$ is plotted for elements in $\boldsymbol{\chi}_{2\mu}$, but with a different colour coding, namely the lowest value is blue dots, second lowest is red dots, third lowest is green dots, fourth lowest is a blue line. Moreover the vertical axis is now $[\Delta, \Delta(1+2\mu)]$ and the dashed horizontal line indicates the height $\Delta(1+\mu)$. In the upper half plane there are two green dots and two elements belonging to a blue line; these are the four elements of $\boldsymbol{\chi}_{2\mu} \backslash \boldsymbol{\chi}_{\mu}$. As most of the figure 8.14 is only blue or red dots, this confirms that the average number of contacts per arc is two.

The next goal is to understand the three dimensional picture. Figures 8.15 (a)-(c) show three projections of the knot with the set of μ-contact points $\mathcal{C}_\mu$ in three dimensional space together with the associated contact chords. A *contact chord* associated with an element (s, σ) of the contact set $\boldsymbol{\chi}_\mu$ is the straight line segment with end points $\boldsymbol{\alpha}(s)$ and $\boldsymbol{\alpha}(\sigma)$. The mid points of all contact chords are exactly the set of μ-contact points $\mathcal{C}_\mu$ in three dimensional space, cf. Definition 8.2. The green balls in Figures 8.15 (a)-(c) are centred at the mid points $\mathbf{m}_i$ of the arcs $\mathbf{a}_i$, μ-contact points $\mathcal{C}_\mu$ are drawn with red balls, and the contact chords are blue. At this resolution the set of μ-contact points spheres form a tube whose centreline is another trefoil knot. The picture suggests that the contact chords form a surface.

One necessary condition for a configuration to be ideal is constancy of ρ_{pt} on curved segments. The discussed shape is curved everywhere, so for this shape to be ideal the function ρ_{pt} has to be constant everywhere. The value of $\rho_{\mathsf{pt}}(\mathbf{m}_i)$ is the minimum of $\mathsf{pt}(\mathbf{m}_i, \cdot)$ along the curve, that is it is the smallest value $\mathsf{pt}(\mathbf{m}_i, \cdot)|_{\mathbf{a}_j}$ corresponding to

the dots plotted in Figures 8.9 and 8.10. Note that we evaluate ρ_{pt} at a discrete number of points, specifically on the mid points of the arcs, but $\rho_{\mathsf{pt}}(\mathbf{m}_i)$ is exact and not an approximation. Figure 8.16 (a)-(b) is a plot of ρ and ρ_{pt} along arc length. We compute $\max_i \rho_{\mathsf{pt}}(\mathbf{m}_i) - \min_i \rho_{\mathsf{pt}}(\mathbf{m}_i) = 1.6992 \cdot 10^{-8}$ to measure how far from constant the global radius of curvature function ρ_{pt} is.

The μ used for the contact set $\boldsymbol{\chi}_\mu$ provides a useful scale to estimate how close certain local radii are to being active in achieving thickness. Figure 8.16 (c) is a plot of ρ and ρ_{pt} with vertical axis $[\Delta, \Delta(1 + 700\mu)]$, whereas in (d) the vertical axis $[\Delta, \Delta(1 + 5\mu)]$. We can read from figure 8.16 (d) that local radii are not active in achieving thickness for this μ, but are remarkably close.

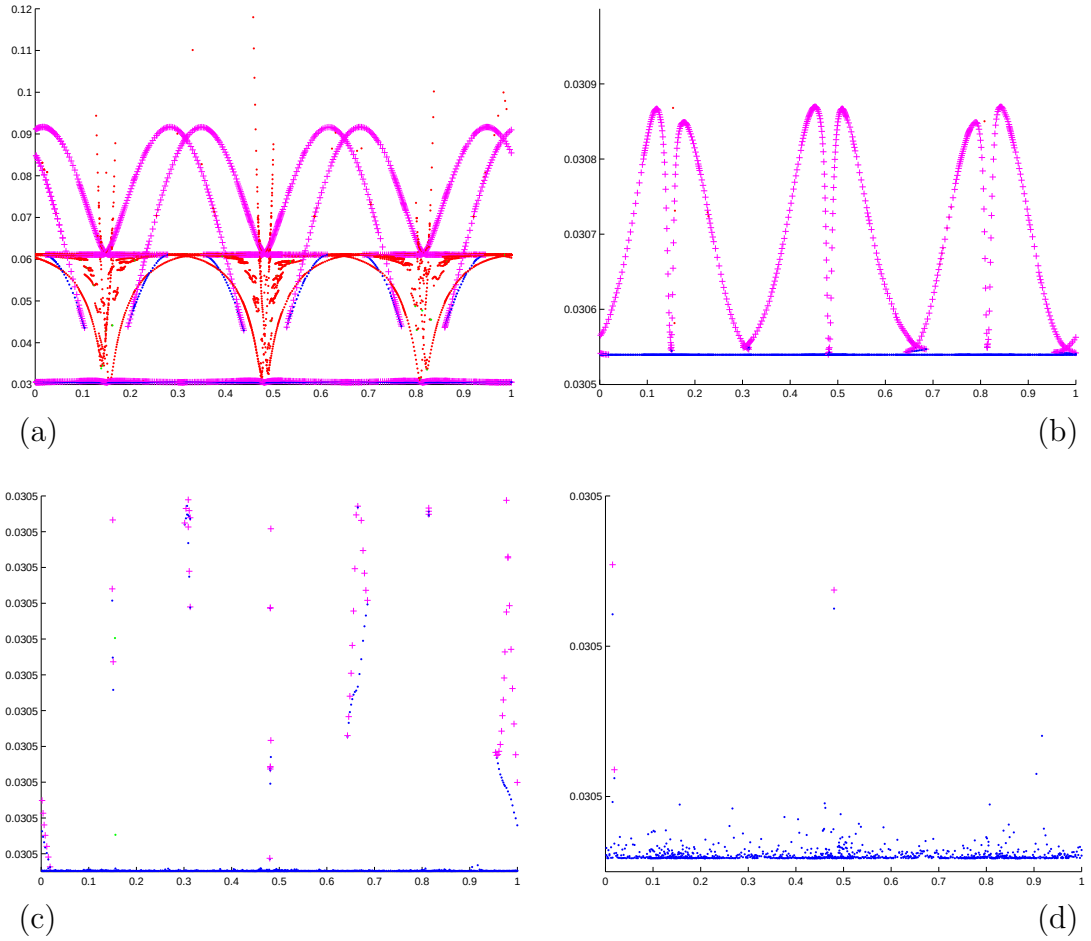

Figure 8.12: (a) Plot of the height of the minimum of $\mathsf{pt}(\mathbf{m}_i, \cdot)|_{\mathbf{a}_j}$ for (i, j) that achieve a minimum of $\mathsf{pt}(\mathbf{m}_i, \cdot)$, the horizontal axis is arc length. Magenta $+$: the minimum of $\mathsf{pt}(\mathbf{m}_i, \cdot)|_{\mathbf{a}_j}$ is achieved at an interior maximum of $\mathsf{pp}(\mathbf{m}_i, \cdot)$, blue dot: the minimum of $\mathsf{pt}(\mathbf{m}_i, \cdot)|_{\mathbf{a}_j}$ is achieved at an interior minimum of $\mathsf{pp}(\mathbf{m}_i, \cdot)$, red dot: the minimum of $\mathsf{pt}(\mathbf{m}_i, \cdot)|_{\mathbf{a}_j}$ is achieved at an end point of the arc $\mathbf{a}_j$ and it is a (local) minimum of $\mathsf{pt}(\mathbf{m}_i, \cdot)$, green dot: local radius is a minimum of $\mathsf{pt}(\mathbf{m}_i, \cdot)$. For a fixed i, the minimum of the values plotted is $\rho_{\mathsf{tp}}(\mathbf{m}_i)$ shown in Figure 8.16, (b) zoom of (a) where the vertical axis is $[0.0305, 0.031]$, (c) zoom of (a) where the vertical axis is $[0.0305395, 0.03055]$, (d) zoom of (a) where the vertical axis is $[0.0305395, 0.03054]$.

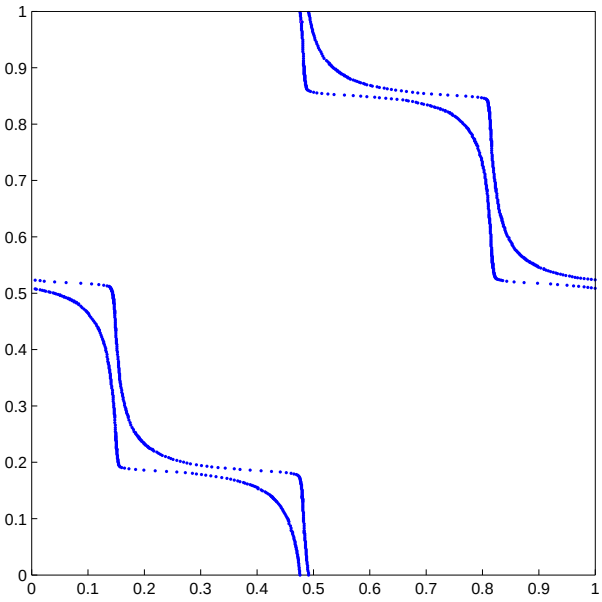

Figure 8.13: The μ-contact set $\boldsymbol{\chi}_\mu$ with $\mu = 8.1861 \cdot 10^{-6}$. (Note: the label of the vertical axis is reversed, $(0, 0)$ is at the top left.)

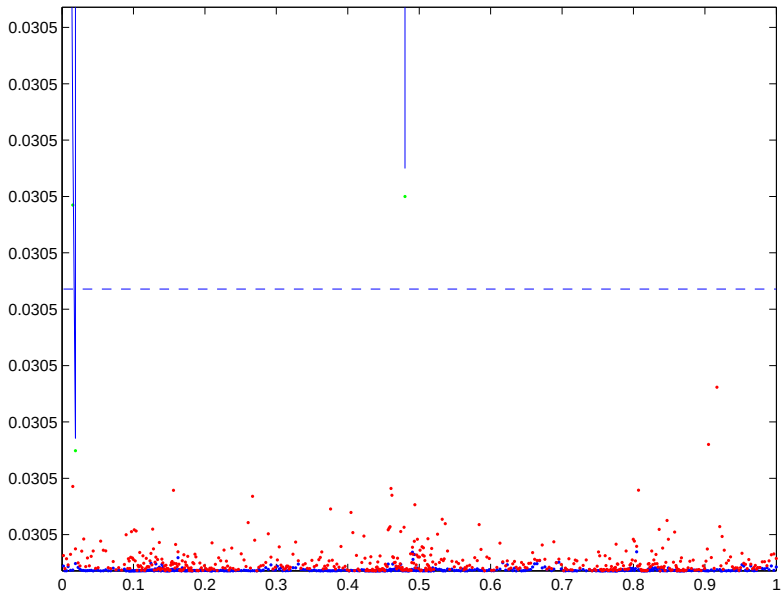

Figure 8.14: The minimum of $\mathsf{pt}(\mathbf{m}_i, \cdot)|_{\mathbf{a}_j}$ of members of the 2μ-contact set $\boldsymbol{\chi}_{2\mu}$ for $\mu = 8.1861 \cdot 10^{-6}$, the vertical axis is $[\Delta, \Delta(1 + 2\mu)]$. The lowest value is blue dots, second lowest is red dots, third lowest is green dots, fourth lowest is blue lines, fifth lowest is red lines and sixth lowest is green lines. The horizontal dashed line is at the height $\Delta(1 + \mu)$.

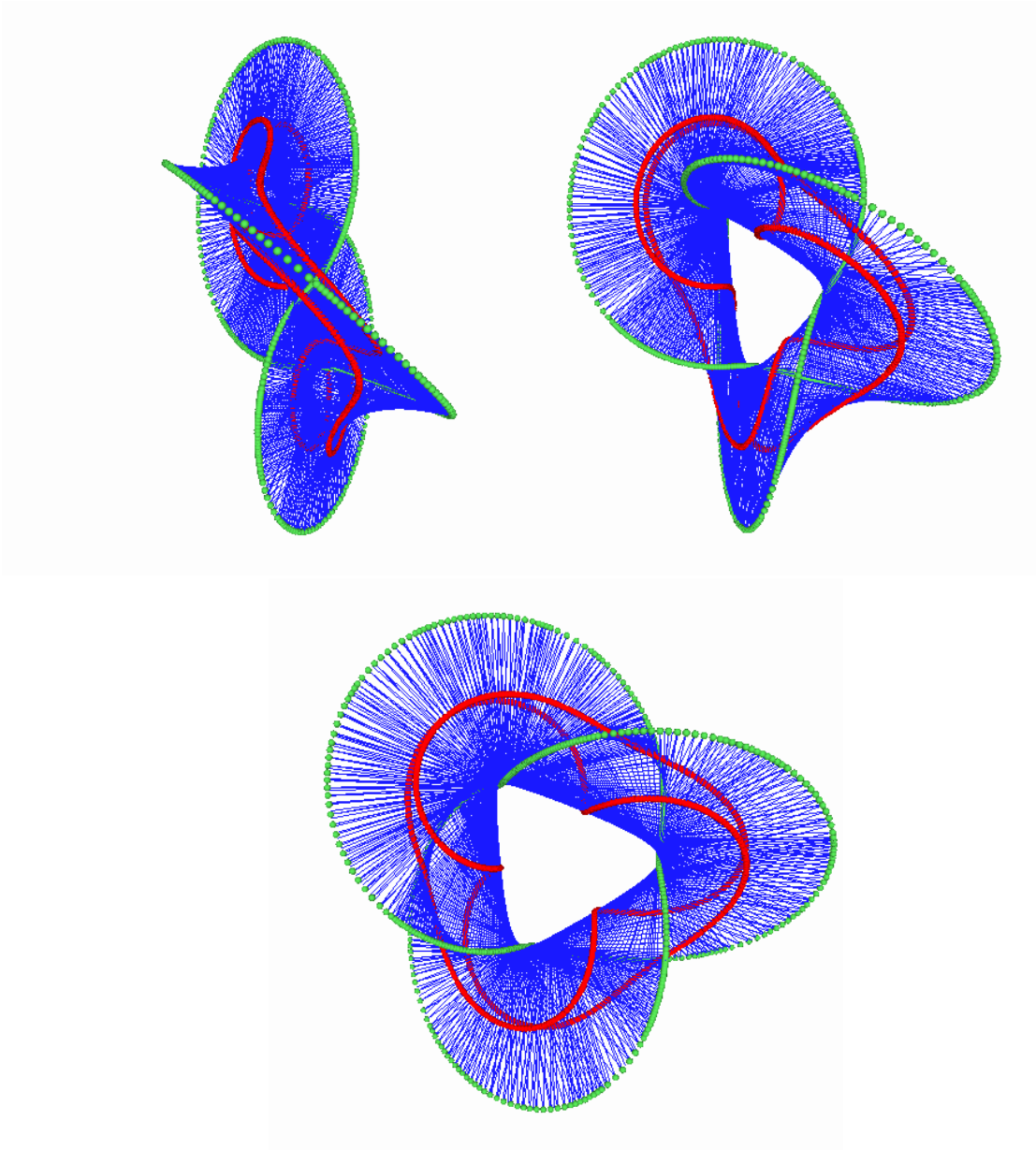

Figure 8.15: Three projections of the approximately ideal trefoil knot (the green balls are centred at the mid points $\mathbf{m}_i$ of the arcs $\mathbf{a}_i$), the set of contact points $\mathcal{C}_\mu$ in three dimensional space (red balls overlapping to form a tube) and associated contact chords (blue line segments) that connect the pairs of points $\boldsymbol{\alpha}(s)$ and $\boldsymbol{\alpha}(\sigma)$ for $(s, \sigma) \in \boldsymbol{\chi}_\mu$ with $\mu = 8.1861 \cdot 10^{-6}$.

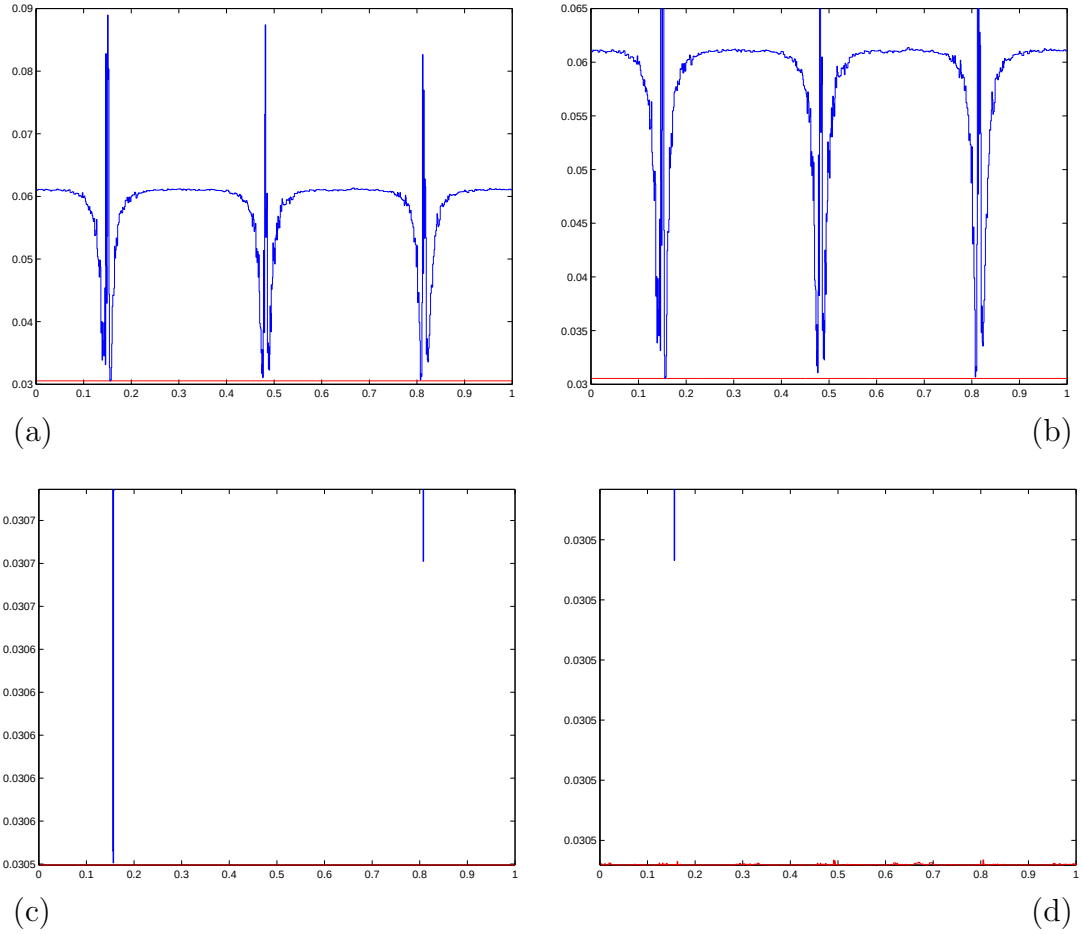

Figure 8.16: (a) Plots of ρ and ρ_{pt}, (b) zoom of (a) with vertical axis $[0.03, 0.065]$, (c) zoom of (a) with vertical axis $[\Delta, \Delta(1 + 700\mu)]$ and (d) zoom of (a) with vertical axis $[\Delta, \Delta(1 + 5\mu)]$, all with $\mu = 8.1861 \cdot 10^{-6}$.

8.3 Computation of an ideal 4.1-knot

The simulated annealing computation of the 4.1 knot was performed by M. Carlen and J. Smutny. Simulated annealing was performed starting from a 208-biarc figure eight knot obtained from biarc interpolation of a piece-wise linear approximately ideal configuration [56, 41][1]. To resolve the dips in radii of curvature that evolved, the number of biarcs was then doubled and by subsequent simulated annealing the present shape $\boldsymbol{\alpha}$ of rope length $\frac{\lambda(\boldsymbol{\alpha})}{\Delta[\boldsymbol{\alpha}]} = 42.11588$ was obtained. We denote the 832 arcs by $\mathbf{a}_i$, the radii by r_i and the mid points of the arcs $\mathbf{a}_i$ by $\mathbf{m}_i$, $1 \leq i \leq 832$. The figures to be presented in sections 8.3.1-8.3.3 are, up to different scales, the precise analogue of the figures shown in sections 8.2.1-8.2.3 for the trefoil knot.

8.3.1 Computing the thickness

Figure 8.17 illustrates the thickness evaluation algorithm presented in section 7.1.3. The horizontal line indicates the number of pairs of arcs of the arc curve, here $(2 \cdot 416)^2 = 692'224$. The number of candidates in achieving thickness after the double critical test (higher curve) and after the distance test (lower curve) at each of the 15 iterations is plotted. In contrast to the thickness evaluation of the 3.1 knot, cf. Figure 8.1, the number of candidates is far below the horizontal line. Therefore the evaluation is faster.

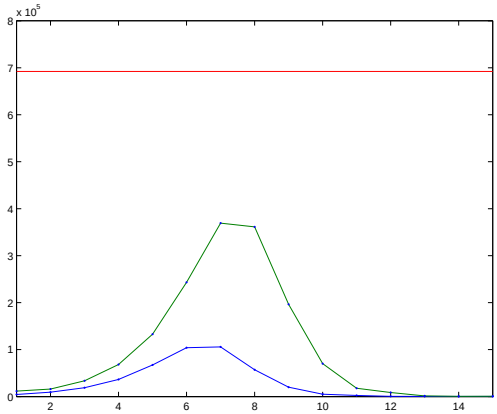

Figure 8.17: The number of candidates after the double critical test (higher curve) and after the distance test (lower curve) cf. section 7.1.3 after each of the fifteen iteration steps. The level of the straight line indicates the number $(2 \cdot 416)^2 = 692'224$ of pairs of arcs to evaluate.

The evolution of upper and lower bounds of rope length $\frac{\lambda(\boldsymbol{\alpha})}{\Delta[\boldsymbol{\alpha}]}$ during the thickness evaluation algorithm is plotted in Figure 8.18. The lower bound of rope length is increasing, but much less rapidly then the upper bound is decreasing. The final bounds of rope length, the length $\lambda(\boldsymbol{\alpha})$ of the arc curve, the minimal radius $\min_i r_i$, and upper

[1] It is a pleasure to thank P. Pieranski for providing this initial data.

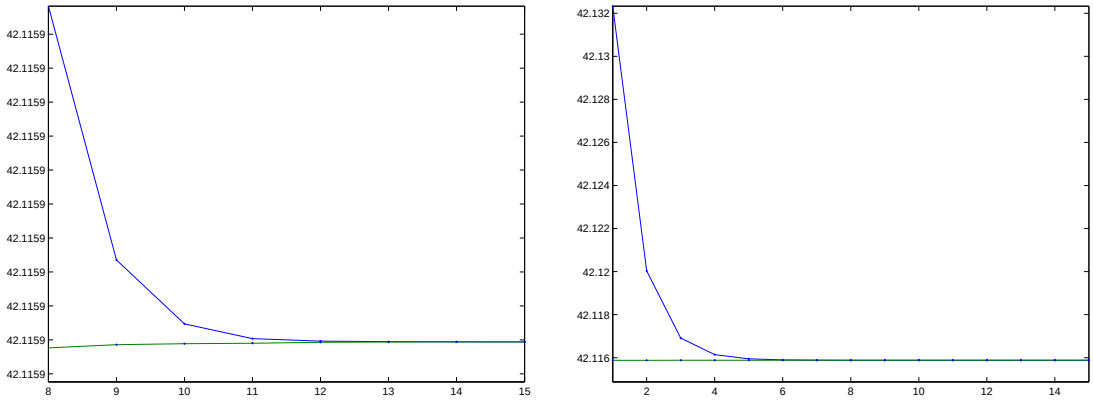

(a) (b)

Figure 8.18: (a) Upper and lower bound of rope length after each of the fifteen iteration steps, (b) is a zoom of Figure (a), the values for the last 8 iteration steps are displayed.

and lower bounds for thickness $\Delta[\boldsymbol{\alpha}]$ are

$$\begin{aligned} & \lambda(\boldsymbol{\alpha}) && = 0.99999999927731 \\ & \min_i r_i && = 0.02374402362244 \\ 0.02374401039630 \leq\ & \Delta[\boldsymbol{\alpha}] && \leq 0.02374401039633 \\ 42.11588449404105 \leq\ & \tfrac{\lambda(\boldsymbol{\alpha})}{\Delta[\boldsymbol{\alpha}]} && \leq 42.11588449409459 \end{aligned}$$

As for the 3.1 knot, thickness was evaluated up to a relative error of 10^{-12}, that is the maximal error divided by the lower bound of thickness is smaller than 10^{-12}. Similarly to the trefoil knot we can observe that $\min_i r_i$ is slightly higher than the thickness $\Delta[\boldsymbol{\alpha}]$; in this case $\min_i r_i$ is much closer to the thickness $\Delta[\boldsymbol{\alpha}]$ than the respective values for the trefoil knot.

8.3.2 The shape

To display the shape of the knot the centre of mass and principal axes $\mathbf{v}_1$, $\mathbf{v}_2$, and $\mathbf{v}_3$ of inertia (ordered with eigenvalues $\lambda_1 = 2.3526 \cdot 10^{-3} \leq \lambda_2 = 2.7632 \cdot 10^{-3} \leq \lambda_3 = 2.8144 \cdot 10^{-3}$) of the set of end points of all arcs were computed. Figure 8.19 (a) shows the projection of the end points of all arcs onto the $\mathbf{v}_2$-$\mathbf{v}_3$ plane, whereas (b) is the projection of the unit tangents at the end points of all arcs onto the $\mathbf{v}_2$-$\mathbf{v}_3$ plane. In figure 8.19 the polar coordinates of (c) the end points, and (d) end point tangents along arc length are plotted, with blue the $\mathbf{v}_1$ coordinate, green the radial coordinate $r = \sqrt{v_2^2 + v_3^2}$ and red the angle ϕ in radians scaled by a factor to make variations visible on the same plot. Note that the discontinuities of the scaled angle ϕ (red) in both Figures 8.19 (c) and (d) are not a real feature, but are due to the fact that Matlab displays the angle $\phi \in [-\pi, \pi)$ modulo 2π. Both the curve and the tangent curve appear to be smooth, but the derivative of the tangent i.e. the curvature is large in four small regions, as can be observed in the Figures 8.19 (b) and (d). The projections of both the curve and the tangent curve onto the $\mathbf{v}_2$-$\mathbf{v}_3$ plane depicted in Figures 8.19 (a) and (b) are close to period four symmetry. One necessary condition for exact symmetry is

equality of eigenvalues λ_2 and λ_3. Here $\frac{\lambda_3-\lambda_2}{\lambda_1+\lambda_2+\lambda_3} = 6.4567 \cdot 10^{-3}$, thus the projections are not precisely rotationally symmetric, and in this measure seem further from rotational symmetric than the trefoil computations described in section 8.2.2. Note that in the 4.1 case the $\mathbf{v}_1$ component of both the curve and the tangent curve in Figures 8.19 (c) and (d) seem close to being period two symmetric.

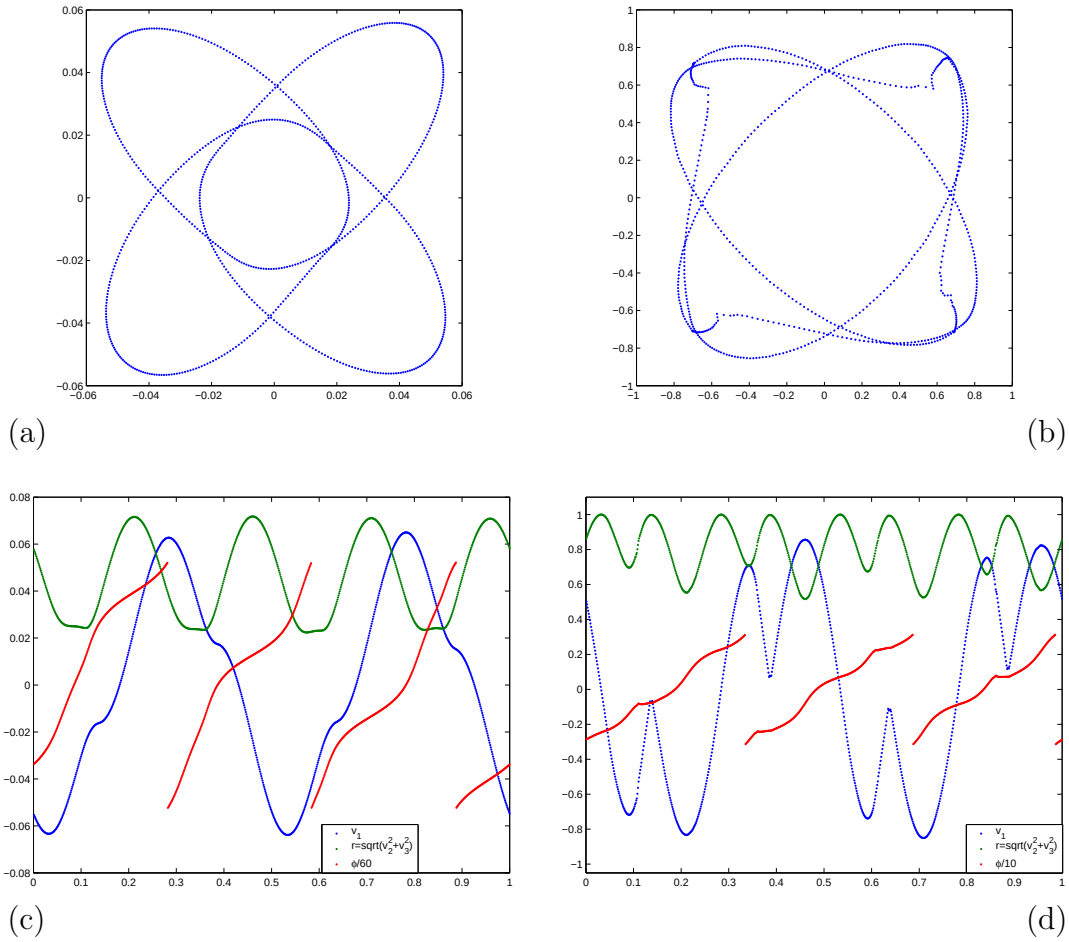

Figure 8.19: Projection onto the plane of the $\mathbf{v}_2$-$\mathbf{v}_3$ inertia axes of (a) the end points of all arcs, and (b) the unit tangents at the end points of all arcs. Plots of the cylindrical polar coordinates v_1, $r = \sqrt{v_2^2 + v_3^2}$ and the (scaled) angle ϕ in radians, of (c) the end points of all arcs w.r.t. the axes of inertia, after translation to the centre of mass, and (d) of the tangents at the end points of all arcs.

The tangent indicatrix of an arc curve is a continuous curve assembled from arcs of great circles, cf. section 4.2. Figures 8.20 (a)-(f) show the tangent indicatrix of the shape from six different directions corresponding to the principal axes $\pm\mathbf{v}_1$, $\pm\mathbf{v}_2$, and $\pm\mathbf{v}_3$.

The lengths of the 832 arcs depicted in Figure 8.21 are rather uniform. Figure 8.22 depicts the radii of the 832 arcs scaled by the thickness Δ. Similarly to the 3.1 knot there are (four) regions with almost constant radii equal 2Δ corresponding to the four loops visible in figure 8.19 (a). But the radii of the 4.1 knot take values from Δ to 55Δ. More precisely, there are four very short regions (approximately two to four arcs) which have

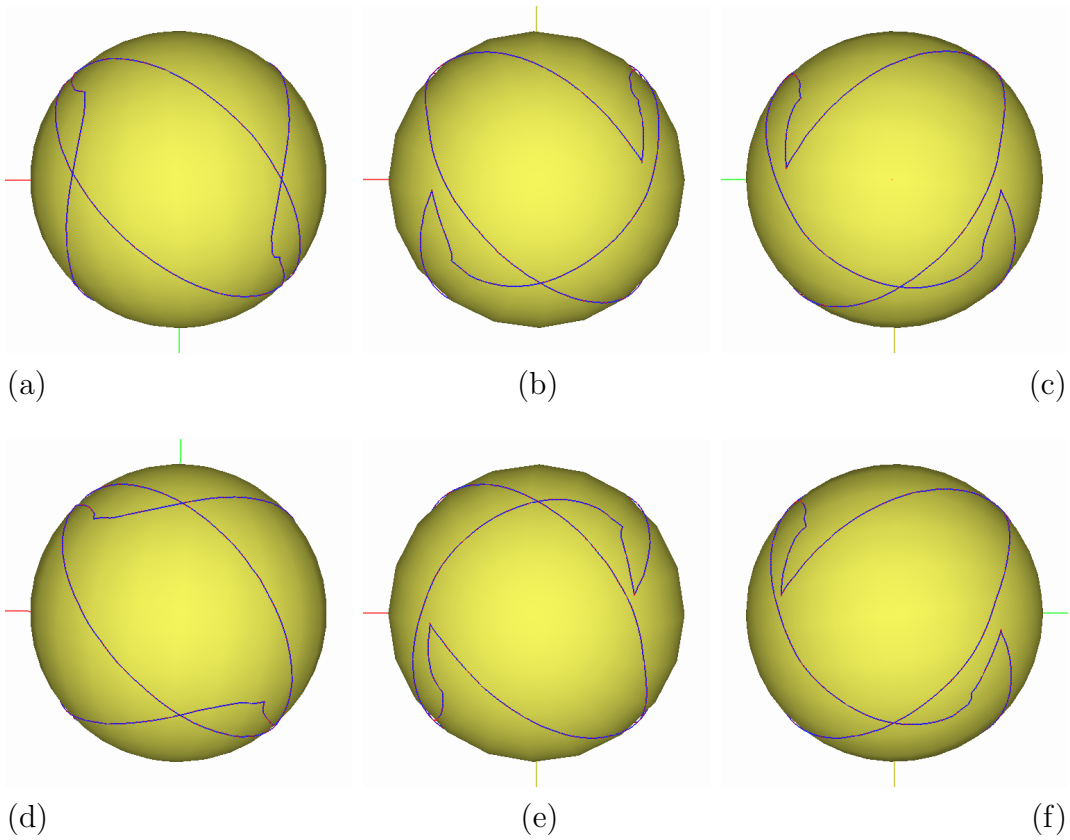

Figure 8.20: Six projections of the tangent indicatrix along principal axes of inertia (a) and (d)$\pm\mathbf{v}_1$, (b) and (e) $\pm\mathbf{v}_2$, and (c) and (f) $\pm\mathbf{v}_3$.

very large radii. On the other hand, there are four even shorter regions (approximately two arcs) situated "inside the knot" where the radii are close to achieving the thickness Δ. As for the trefoil knot we quantify in the next section 8.3.3 how close the radii are to actively achieving thickness.

The angle between the planes of adjacent arcs is plotted in figure 8.23. There are four regions with large angles that correspond to the regions with a high variation of the radii. Figure 8.24 provides a zoom of such a region. In fact in the region where the radii are small, i.e. close to Δ, the torsion angles have a local maximum, and in the region where the radii are very large the torsion angles have another higher maximum. Note that the angle is given in radians, that is, the maximal value of about 3 corresponds to an angle of almost 180 degrees. In other words, at this maximum the arcs are almost straight, but the planes flip by approximately 180 degrees. It seems likely that the underlying ideal shape has a discontinuous Frenet frame at this point.

In chapter 5 we derived various approximation results of radius of curvature, its derivative, and torsion for biarcs interpolating an underlying C^3-curve in terms of the circles $\mathcal{C}_0$ and $\mathcal{C}_1$ associated with every point-tangent data pair, cf. Propositions 5.12 and 5.13. Figure 8.25 displays the quantities that approach the values of radius of curvature, its derivative, and torsion for a finite h. But we stress that it is not clear that the ideal shape is a C^3-curve, and, moreover, we have no estimate of the constants involved in the error terms. Both the approximation of the radius of curvature and its derivative

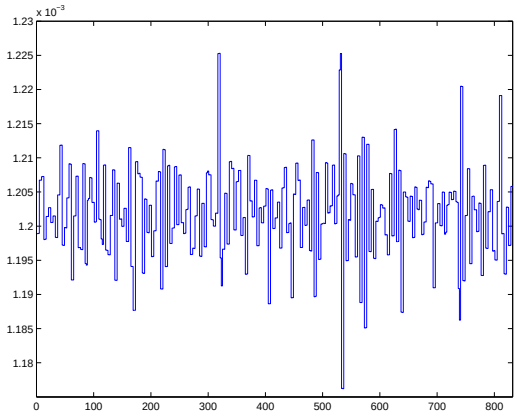

Figure 8.21: The lengths of the 832 arcs are rather uniform.

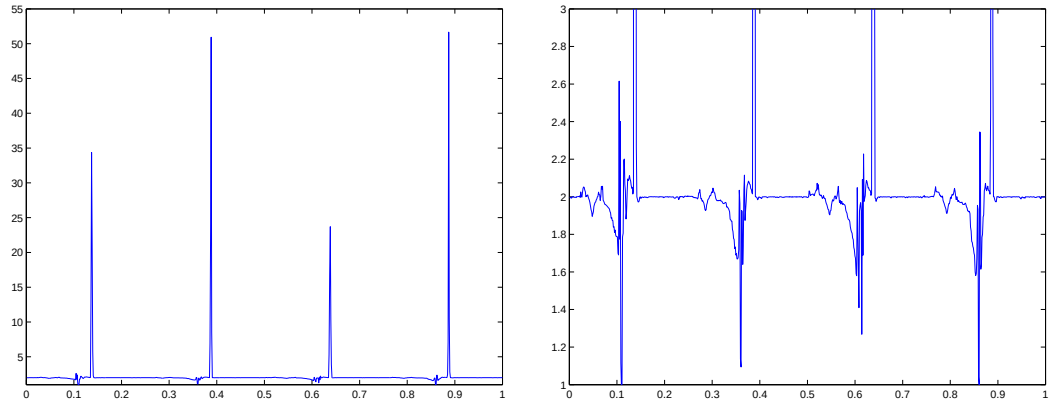

(a) (b)

Figure 8.22: (a) Plot of the radii of the arcs scaled by the thickness (non-dimensional), (b) is a zoom of (a).

suggest that the curvature of the underlying ideal shape is very close to constant on the large four loops. The parts of the shape having large oscillations of the derivative of curvature coincide with the parts of large torsion, which takes values up to 1200.

The plots of quantities associated with the actual arc curve shape, cf. figures 8.22 and 8.23 are in agreement with the plots of approximating finite difference quantities of an assumed underlying curve, cf. Figures 8.25(a)-(b) and 8.25(e)-(f).

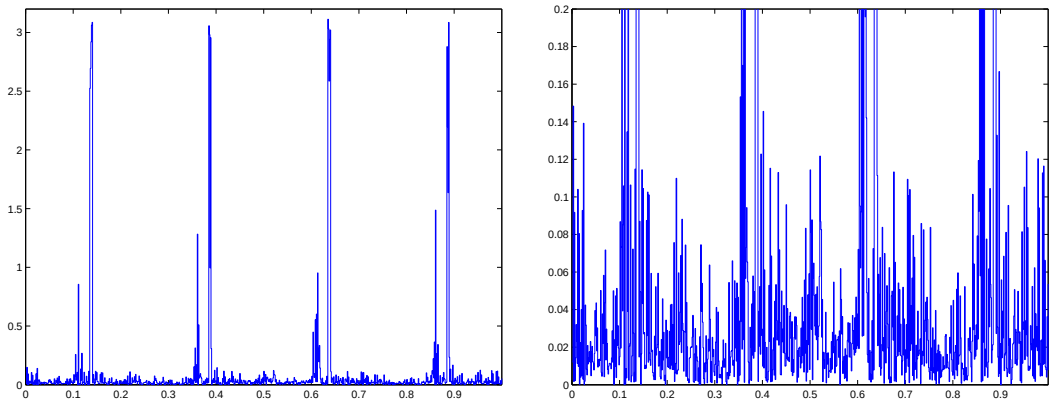

Figure 8.23: Plots of (a) torsion angle, i.e. the angle between the planes of successive arcs in radians, and (b) zoom of (a).

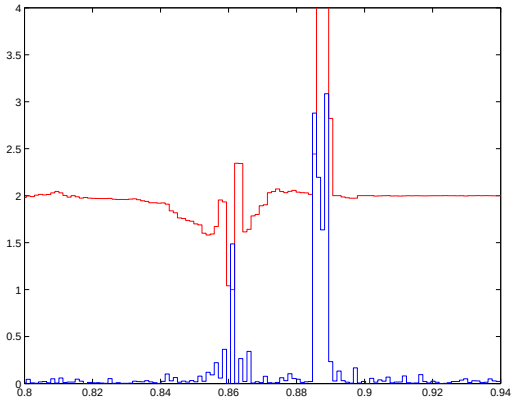

Figure 8.24: Zoom of superposed plots of radii scaled by thickness (red) and torsion angle, i.e. the angle between the planes of successive arcs in radians (blue).

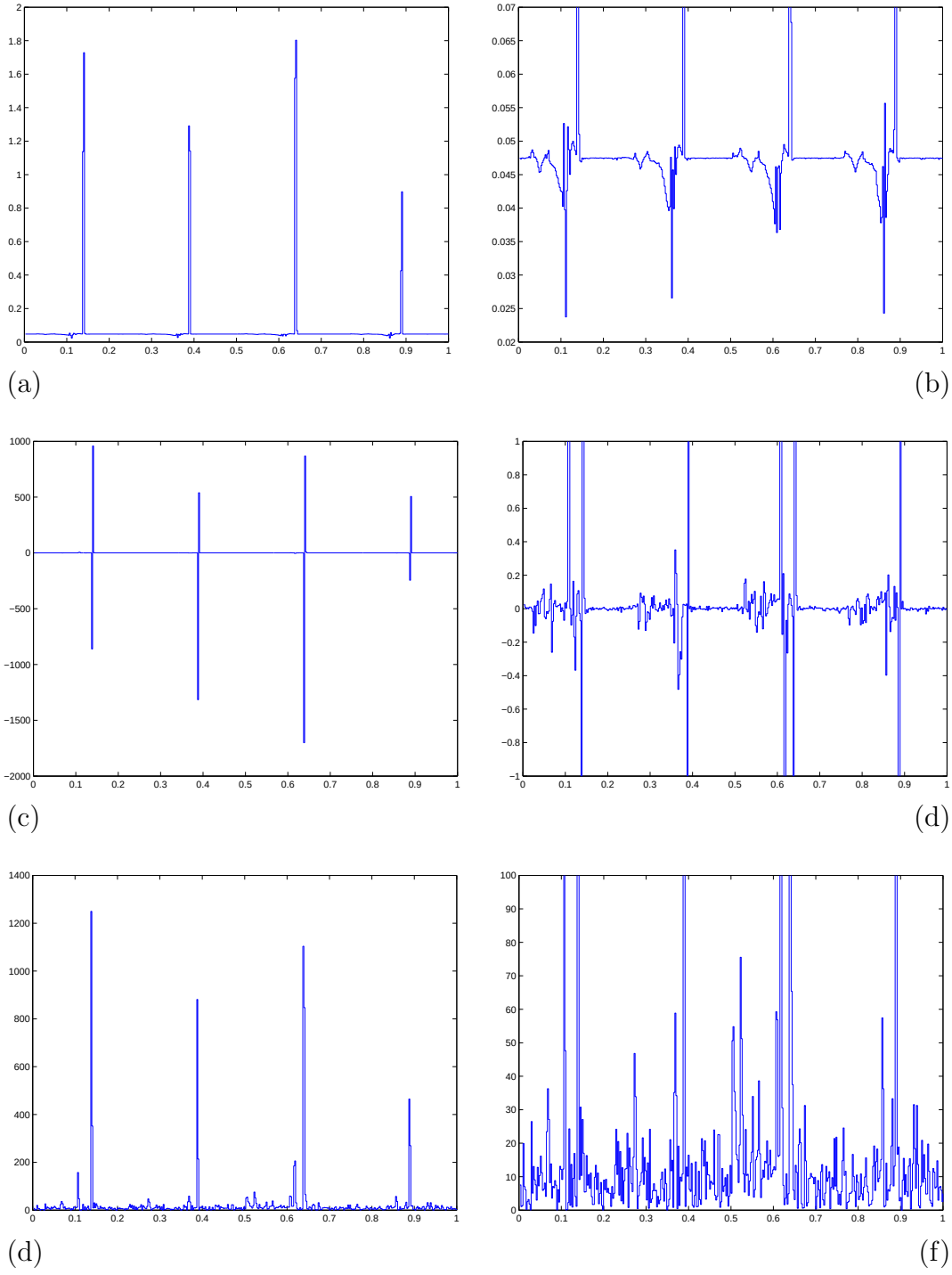

Figure 8.25: Plots of the finite difference approximation of radius of curvature, its derivative, and torsion for an underlying curve. (a) Plot of the approximation of the radius of curvature in terms of the circles $\mathcal{C}_0^h$ and $\mathcal{C}_1^h$, cf. Proposition 5.12, (b) zoom of (a) (units of length). (c) Plot of the approximation of the derivative of the radius of curvature in terms of the circles $\mathcal{C}_0^h$ and $\mathcal{C}_1^h$, cf. Proposition 5.12, (d) zoom of (c) (non-dimensional). (e) Plot of the approximation of the torsion in terms of the circles $\mathcal{C}_0^h$ and $\mathcal{C}_1^h$, cf. Proposition 5.13, (f) zoom of (e) (units reciprocal length).

8.3.3 The contact set and ρ_{pt}

To find an appropriate $\mu > 0$ for a μ-contact set $\boldsymbol{\chi}_\mu$ of Definition 8.2, we use Lemma 7.14 to compute the minimum of $\mathsf{pt}(\mathbf{m}_i, \cdot)$ restricted to the arc $\mathbf{a}_j$ for all pairs $1 \leq i, j \leq 832$. We then classify the minima that correspond to a minima of $\mathsf{pt}(\mathbf{m}_i, \cdot)$ along the whole curve as follows, cf. Figure 8.26: The minimum of $\mathsf{pt}(\mathbf{m}_i, \cdot)|_{\mathbf{a}_j}$ is achieved by (a) blue: a minimum of $\mathsf{pp}(\mathbf{m}_i, \cdot)$, (b) magenta: a maximum of $\mathsf{pp}(\mathbf{m}_i, \cdot)$, (c) red: an end point of the arc $\mathbf{a}_j$, and (d) green: a local radius. Figure 8.26 is a plot of index vs. index. Any pair plotted in Figure 8.26 is a priori a candidate to be an element of a μ-contact set $\boldsymbol{\chi}_\mu$. If the value of the minimum of $\mathsf{pt}(\mathbf{m}_i, \cdot)|_{\mathbf{a}_j}$ is smaller than $\Delta(1+\mu)$ then the arc-length values (s, σ) corresponding to $\mathbf{m}_i$ and the point on the arc $\mathbf{a}_j$ where the minimal value is achieved belong to the μ-contact set $\boldsymbol{\chi}_\mu$.

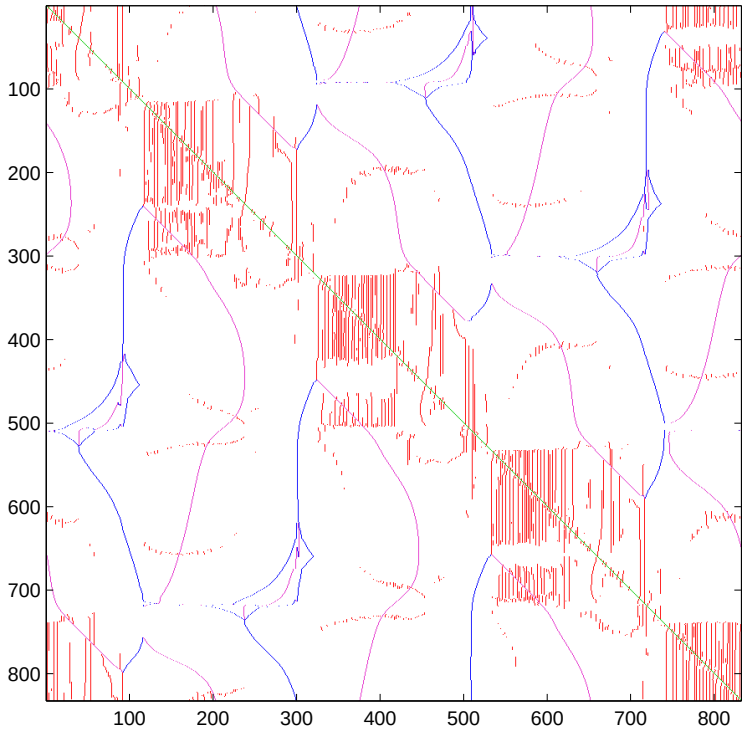

Figure 8.26: The vertical axis stands for the midpoints $\mathbf{m}_i$ of the arcs $\mathbf{a}_i$, $i = 1, \cdots, 832$, the horizontal axis stands for the arcs $\mathbf{a}_j$, $j = 1, \cdots, 832$ (a) the four colours indicate if and how the minimum of $\mathsf{pt}(\mathbf{m}_i, \cdot)$ restricted to the arc $\mathbf{a}_j$ is achieved. Blue: a local minimum of $\mathsf{pt}(\mathbf{m}_i, \cdot)|_{\mathbf{a}_j}$ is achieved at an interior minimum of $\mathsf{pp}(\mathbf{m}_i, \cdot)$, magenta: a local minimum of $\mathsf{pt}(\mathbf{m}_i, \cdot)|_{\mathbf{a}_j}$ is achieved at an iterior maximum of $\mathsf{pp}(\mathbf{m}_i, \cdot)$, red: a local minimum of $\mathsf{pt}(\mathbf{m}_i, \cdot)|_{\mathbf{a}_j}$ is achieved by at an end point of the arc $\mathbf{a}_j$ which is also (local) minimum of $\mathsf{pt}(\mathbf{m}_i, \cdot)$, green: the minimum of $\mathsf{pt}(\mathbf{m}_i, \cdot)|_{\mathbf{a}_j}$ is achieved by the local radius.

In Figure 8.27 the minimal value of $\mathsf{pt}(\mathbf{m}_i, \cdot)|_{\mathbf{a}_j}$ is plotted using a colour map with blue for low and red for high, except for pairs that appear in the figure 8.26. Note that the minima is a very flat valley or hollow. Moreover on the diagonal there is a variation from dark red to blue indicating large differences in radii as we observed in Figure 8.22.

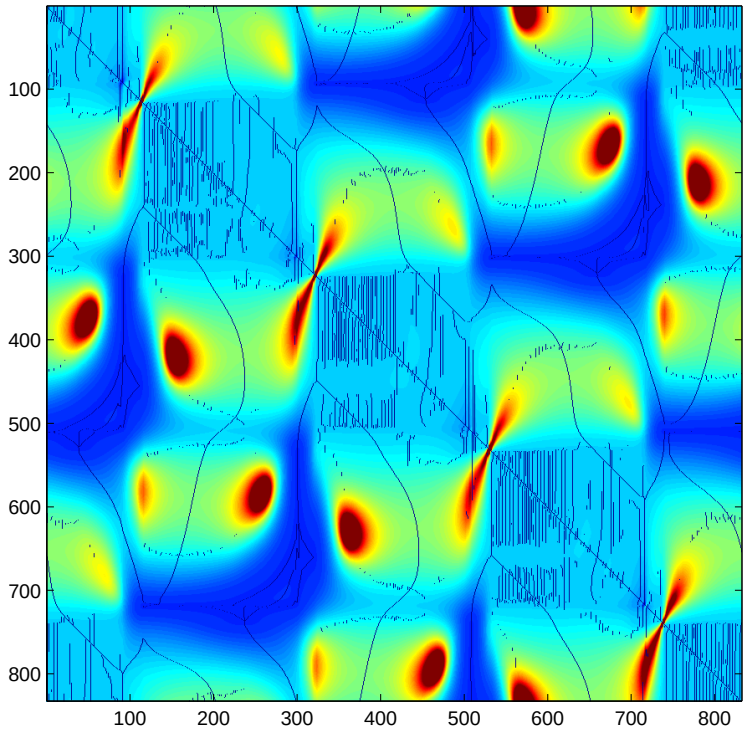

Figure 8.27: The minimum of $\mathsf{pt}(\mathbf{m}_i, \cdot)|_{\mathbf{a}_j}$, a blue dot is drawn when the minimum $\mathsf{pt}(\mathbf{m}_i, \cdot)|_{\mathbf{a}_j}$ is a minimum of $\mathsf{pt}(\mathbf{m}_i, \cdot)$. The colour map uses blue for low and red for high values.

We now have to determine an appropriate value of μ. We plot the heights of all minima of $\mathsf{pt}(\mathbf{m}_i, \cdot)|_{\mathbf{a}_j}$ that are candidates for a $\boldsymbol{\chi}_\mu$, i.e. that appear in figure 8.26 along arc length in various zooms, cf. Figure 8.28 (a)-(c). The heights appearing in Figure 8.28 (b) belong to the lowest line in (a). The dots in the figure 8.28 (c) correspond to the lowest line with the lowest bits of the higher structure in (b). In contrast to the plots for the trefoil, cf. Figure 8.28 (d), the gap above a layer of candidates in Figure 8.28 (c) is less significant. Nevertheless we set $\mu := 4.2115 \cdot 10^{-6}$, which is about half of the height of Figure 8.28 (c). Now the μ-contact set $\boldsymbol{\chi}_\mu$ is the set of pairs of arc lengths corresponding to pairs plotted in Figure 8.26 for which the minima of $\mathsf{pt}(\mathbf{m}_i, \cdot)|_{\mathbf{a}_j}$ is smaller or equal to $\Delta(1 + \mu)$. And similarly for $\boldsymbol{\chi}_{2\mu}$.

Figure 8.29 displays the μ-contact set $\boldsymbol{\chi}_\mu$ with $\mu = 4.2115 \cdot 10^{-6}$. From this plot it is hard to say conclusively if the set $\boldsymbol{\chi}_\mu$ is connected, but certainly is not one or two curves, but at best bits of curves. The μ-contact set $\boldsymbol{\chi}_\mu$ has 1213 elements, so that the average number of μ-contacts per arc is $\frac{1213}{2 \cdot 416} \approx 1.46$, which is much less than for the trefoil knot. We expect the μ-contact set $\boldsymbol{\chi}_\mu$ to be relatively invariant for small increasing μ, in fact, the number of elements of the 2μ-contact set $\boldsymbol{\chi}_{2\mu}$ is 1238, that is $\boldsymbol{\chi}_{2\mu} \backslash \boldsymbol{\chi}_\mu$ contains 25 additional contacts. The change of elements relative to the number or arcs is $\frac{25}{2 \cdot 416} = 0.03$. Figure 8.30 visualises the elements of both contact sets $\boldsymbol{\chi}_\mu$ and $\boldsymbol{\chi}_{2\mu}$: As in Figure 8.28 the height of the minimum of $\mathsf{pt}(\mathbf{m}_i, \cdot)|_{\mathbf{a}_j}$ is plotted for elements in $\boldsymbol{\chi}_{2\mu}$ but with a different colour coding, namely the lowest value is blue dots, second lowest is red dots, third lowest is green dots, fourth lowest is a blue line. Moreover the

vertical axis is now $[\Delta, \Delta(1+2\mu)]$ and the dashed horizontal line indicates the height $\Delta(1+\mu)$. The 25 elements of $\boldsymbol{\chi}_{2\mu} \backslash \boldsymbol{\chi}_{\mu}$ are in the upper half of the figure. We can observe two regimes: there are four parts with almost only blue dots, and four parts with blue and red dots, this confirms that the average number of μ-contact per arc is less than two and, because both regimes are of about the same length, the average number of contacts per arc is about $\frac{1}{2}(1+2) \approx 1.5$.

The next goal is to understand the three dimensional picture. Figures 8.31 (a)-(c) show three projections of the knot with the set of μ-contact points $\mathcal{C}_{\mu}$ in three dimensional space together with the associated contact chords. A *contact chord* associated with an element (s, σ) of the contact set $\boldsymbol{\chi}_{\mu}$ is the straight line segment with end points $\boldsymbol{\alpha}(s)$ and $\boldsymbol{\alpha}(\sigma)$. The mid points of all contact chords are exactly the set of μ-contact points $\mathcal{C}_{\mu}$ in three dimensional space, cf. Definition 8.2. The green balls in Figures 8.31 (a)-(c) are centred at the mid points $\mathbf{m}_i$ of the arcs $\mathbf{a}_i$, μ-contact points $\mathcal{C}_{\mu}$ are drawn with red balls and the contact chords are blue. The behaviour of the set of μ-contact points $\mathcal{C}_{\mu}$ in three dimensional space is radically different from the trefoil, cf. Figures 8.15 (a)-(c). The picture suggests that the set $\mathcal{C}_{\mu}$ is composed of a number of parts of curves. Most of the (mid) points have one or two contact point associated, but there is also small number of points having no contact. The arcs of such points have very large radii.

One necessary condition for a configuration to be ideal is constancy of ρ_{pt} on curved segments. The value of $\rho_{\mathsf{pt}}(\mathbf{m}_i)$ is the minimum of $\mathsf{pt}(\mathbf{m}_i, \cdot)$ along the curve, that is it is the smallest value $\mathsf{pt}(\mathbf{m}_i, \cdot)|_{\mathbf{a}_j}$ corresponding to the dots plotted in Figures 8.26. Note that we evaluate ρ_{pt} at a discrete number of points, specifically on the mid points of the arcs, but $\rho_{\mathsf{pt}}(\mathbf{m}_i)$ is exact and not an approximation. Figure 8.32 (a)-(b) is a plot of ρ and ρ_{pt} along arc length. We compute $\max_i \rho_{\mathsf{pt}}(\mathbf{m}_i) - \min_i \rho_{\mathsf{pt}}(\mathbf{m}_i) = 3.5178 \cdot 10^{-5}$ to measure how far from constant the global radius of curvature function ρ_{pt} is. The variation is three orders of magnitude larger than the corresponding value for the trefoil knot. But, restricting the global radius function ρ_{pt} onto the parts where the radii are not high, the value is of the order $10^{-7} - 10^{-6}$. This can be interpreted in two ways: Either the biarcs approach straight line segments where the global radius of curvature is not expected to be constant, or the shape did not resolve the contact set. Probably both interpretations are correct, the maxima in Figure 8.32 (c) may be real, but not the wiggles in Figure 8.32 (d).

The μ used for the contact set $\boldsymbol{\chi}_{\mu}$ provides a useful scale to estimate how close certain local radii are to being active in achieving thickness. Figure 8.32 (c) is a plot of ρ and ρ_{pt} with vertical axis $[\Delta, \Delta(1+500\mu)]$, whereas in (d) the vertical axis is $[\Delta, \Delta(1+\mu)]$. We can read from figure 8.32 (d) that local radii are active in achieving thickness for this μ in two of the four dips.

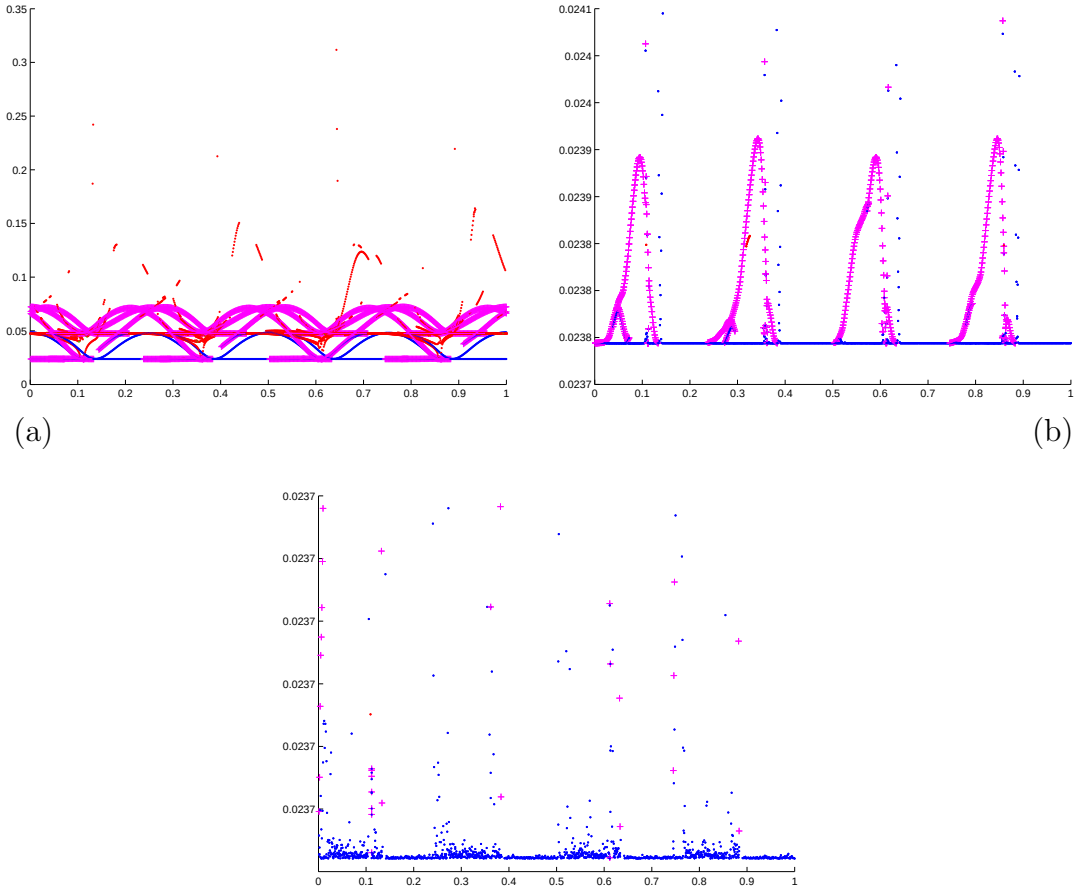

Figure 8.28: (a) Plot of the height of the minimum of $\mathsf{pt}(\mathbf{m}_i, \cdot)|_{\mathbf{a}_j}$ for (i, j) that achieve a minimum of $\mathsf{pt}(\mathbf{m}_i, \cdot)$, the horizontal axis is arc length. Magenta $+$: the minimum of $\mathsf{pt}(\mathbf{m}_i, \cdot)|_{\mathbf{a}_j}$ is achieved at an interior maximum of $\mathsf{pp}(\mathbf{m}_i, \cdot)$, blue dot: the minimum of $\mathsf{pt}(\mathbf{m}_i, \cdot)|_{\mathbf{a}_j}$ is achieved at an interior minimum of $\mathsf{pp}(\mathbf{m}_i, \cdot)$, red dot: the minimum of $\mathsf{pt}(\mathbf{m}_i, \cdot)|_{\mathbf{a}_j}$ is achieved by at an end point of the arcs $\mathbf{a}_j$ and it is a (local) minimum of $\mathsf{pt}(\mathbf{m}_i, \cdot)$, light green dot: local radii is a minimum of $\mathsf{pt}(\mathbf{m}_i, \cdot)$. For a fixed i, the minimum of the values plotted is $\rho_{\mathsf{tp}}(\mathbf{m}_i)$ shown in Figure 8.32, (b) zoom of (a) where the vertical axis is $[0.0237, 0.0241]$, (c) zoom of (a) where the vertical axis is $[0.0237440, 0.0237443]$.

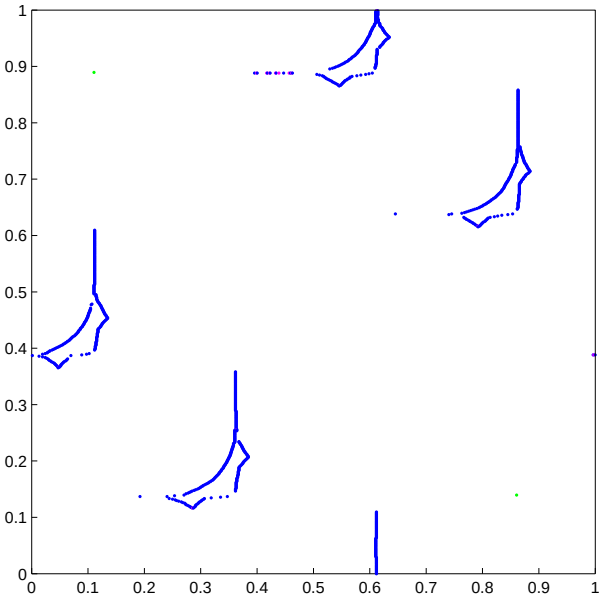

Figure 8.29: The μ-contact set $\boldsymbol{\chi}_\mu$ with $\mu = 4.2115 \cdot 10^{-6}$. The two green dots on the diagonal indicate that two contacts of the type (s, s) are contained in $\boldsymbol{\chi}_\mu$. (Note: the label of the vertical axis is reversed, $(0, 0)$ is at the top left.)

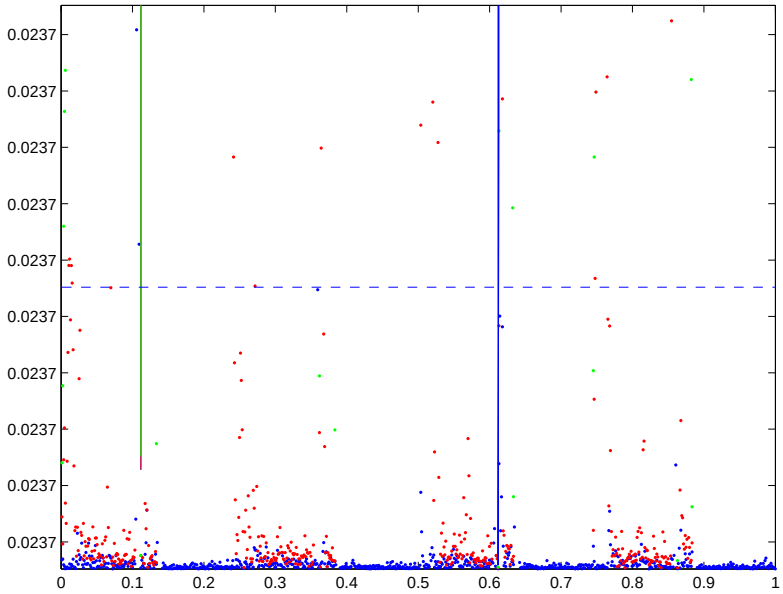

Figure 8.30: The minimum of $\mathsf{pt}(\mathbf{m}_i, \cdot)|_{\mathbf{a}_j}$ of members of the 2μ-contact set $\boldsymbol{\chi}_{2\mu}$ for $\mu = 4.2115 \cdot 10^{-6}$, the vertical axis is $[\Delta, \Delta(1+2\mu)]$ and the height $\Delta(1+\mu)$ is indicated by the dashed line. The lowest value is blue dots, second lowest is red dots, third lowest is green dots, fourth lowest is blue lines, fifth lowest is red lines and sixth lowest is green lines.

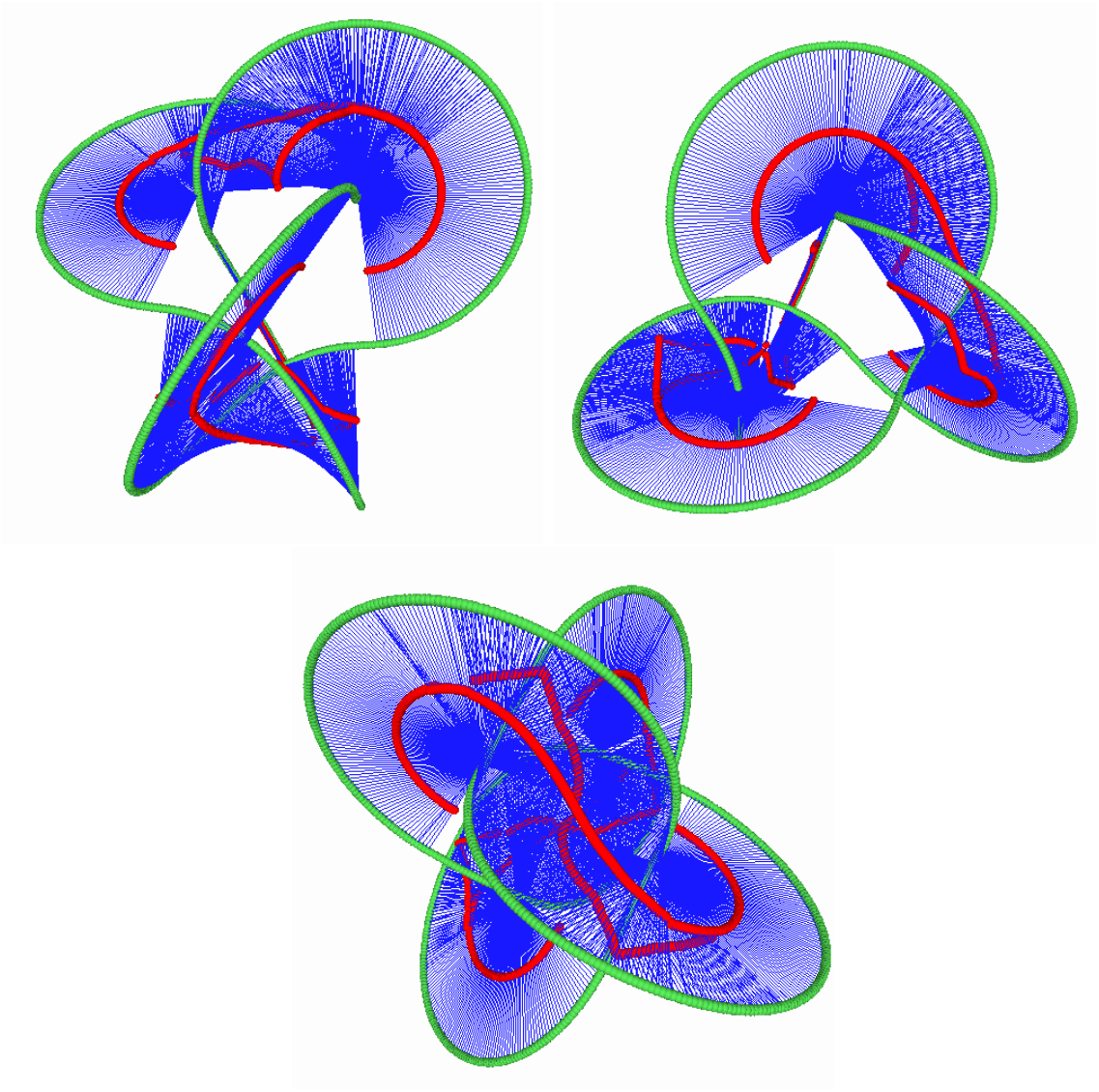

Figure 8.31: Three pictures of the approximately ideal figure eight knot (the green balls are centred at the mid points $\mathbf{m}_i$ of the arcs $\mathbf{a}_i$), the set of contact points $\mathcal{C}_\mu$ in three dimensional space (red balls) and associated contact chords (blue line segments) that connect the pairs of points $\boldsymbol{\alpha}(s)$ and $\boldsymbol{\alpha}(\sigma)$ for a $(s, \sigma) \in \boldsymbol{\chi}_\mu$ with $\mu = 4.2115 \cdot 10^{-6}$.

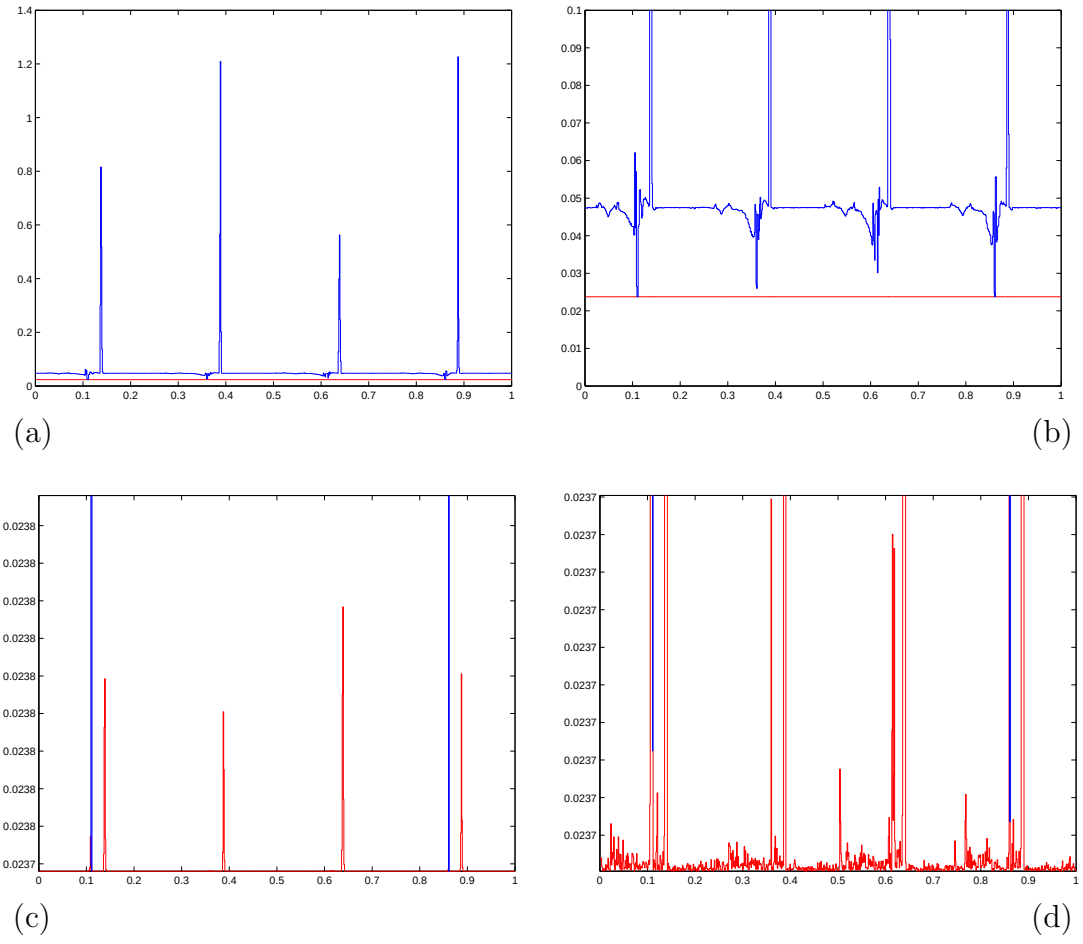

Figure 8.32: (a) Plots of ρ and ρ_{pt}, (b) zoom of (a) with vertical axis $[0, 1]$, (c) zoom of (a) with vertical axis $[\Delta, \Delta(1+500\mu)]$ and (d) zoom of (a) with vertical axis $[\Delta, \Delta(1+\mu)]$, all with $\mu = 4.2115 \cdot 10^{-6}$.

8.4 Critique of the Computations

We believe that the shapes of the 3.1 and 4.1 knots described in section 8.2 and 8.3 are the closest known shapes to the ideal knot configurations. Nevertheless the computations perhaps raise as many questions as they answer. The stochastic approach of simulated annealing, which requires no derivative information, is largely dictated by the fact that little is currently known analytically to be able to formulate and justify a constrained gradient flow that would be guaranteed to converge, essentially because it is far from simple to be able to write down the appropriate constrained derivatives. On the other hand, the evaluation of thickness and the ρ_{pt} function on a given biarc curve, whatever its source, is rigorous and accurate to a prescribed tolerance. In this way we achieved the upper bounds on rope length for the trefoil (with 528 arcs) of 32.74446, and for the figure eight (with 832 arcs) of 42.11588. The only bounds close to these, known to us were achieved by Rawdon [47], using the method of inscribing arcs of circles onto a piecewise linear shape, of 32.90 and 32.77 for the trefoil with respectively 160 and 1332 linear segments, and 42.38 for the figure eight knot with 208 linear segments.

In point of fact we believe that it is perhaps of more interest to understand the properties of the curve realising the optimal rope thickness rather than the value of thickness itself, and it seems that rather significant changes in, for example, local curvature of the configuration can be necessary to obtain extremely small improvements in rope length. A striking and previously unobserved feature in our simulations of both the 3.1 and 4.1 knots is the rapid and large scale variations in local curvature in, respectively, three and four narrow regions corresponding to the curve passing through the "centre" of the knot. This was first observed in a 192-biarc, 3.1 computation, whereupon the number of biarcs was doubled in the three regions of interest to obtain the 264-biarc shapes described here. Upon continued simulated annealing the features persisted, and indeed sharpened. For this reason, and the fact that the features have the appropriate period three, respectively four, behaviour we believe them to be real, and not numerical artifacts.

In both the 3.1 and 4.1 knots the same features are associated with both a) extremely large torsion angles, suggesting a singularity in the second derivative, and b) small radii of curvature that approach the lower bound provided by the thickness. It has been generally assumed that for simple knots like the trefoil, local radius of curvature was never close to achieving thickness. We now suspect that this belief has been based upon limitations of previously adopted numerical schemes, either due to the general exclusion of nearest neighbour effects as done by many authors using point or piecewise linear discretizations, or due to the curve shortening algorithm that was used [18]. On the other hand, while our biarc computations seem decisive in suggesting that local curvature is extremely close to being active in achieving thickness in both the 3.1 and 4.1 ideal shapes, they are not quite conclusive in whether or not thickness is truly achieved locally. This question is of some consequence for the analysis of ideal shapes, because exclusion of the possibility of local curvature being active simplifies various arguments. It therefore seems worthwhile to pursue this issue further, either analytically or through further computation.

One additional piece of evidence concerning the achievement of thickness locally is provided by a third simulation involving a 568-biarc discretization of the composite +3.1#−3.1-knot. This simulation, currently with rope length 58.27448, is much less converged than either the 3.1 or 4.1 computations described above, as can be seen both from the large variations in the local curvature plot shown in figure 8.33, and the fact that the variation $\max \rho_{\mathsf{pt}} - \min \rho_{\mathsf{pt}} \approx 2 \cdot 10^{-4}$ in the global radius of curvature function on curved segments is respectively one and four orders of magnitude higher than the respective values for the 4.1 and 3.1 simulations. Although the local radius of curvature function ρ is not at all smooth, the global radius of curvature function ρ_{pt} shown in 8.33 (a) is by comparison quite close to constant on curved segments. We include the preliminary results from this simulation because of two features. First there are upward spikes in ρ_{pt} on segments of the curve that are close to straight, which confirms for our biarc simulations a phenomenon first observed in the point discretization simulations of [18]. Second, as shown in 8.33 (b), in this simulation there are multiple arcs on which ρ_{pt} is achieved by local curvature, and which achieve thickness to within a relative error of 10^{-7}. This strongly suggests that local curvature is active in realising thickness for the ideal shape of the +3.1#−3.1-knot.

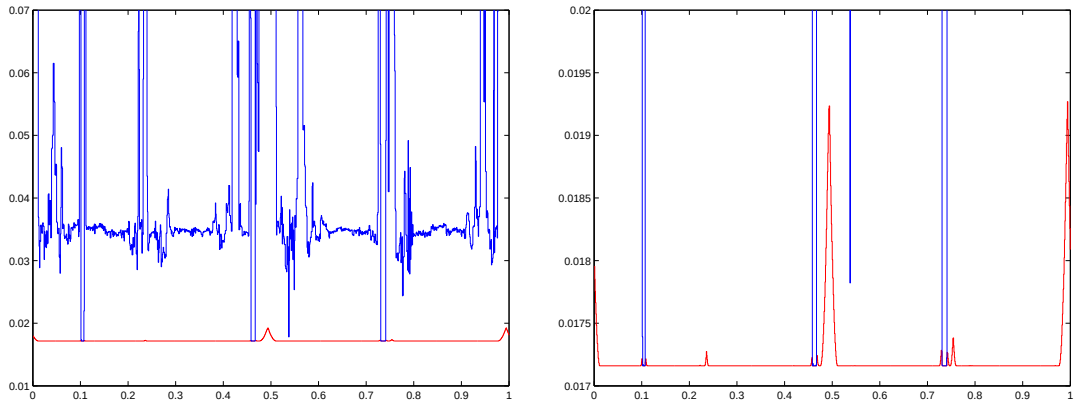

(a) (b)

Figure 8.33: Plots of radius of curvature ρ and global radius of curvature ρ_{pt} on a 568-biarc composite +3.1#−3.1-knot, (b) is a zoom of (a).

The resolution of our biarc simulation seems sufficient to conclude that, as shown in Figure 8.15 the contact chords of the 3.1 knot span a surface and the contact points themselves form a trefoil knot. In contrast, as shown in figure 8.31 the contact chords associated with $\boldsymbol{\chi}_\mu$ of the figure eight knot are split into two disjoint components, with the contact points in each component forming a loop with two tails.

Two further lines of investigation present themselves. First the tolerance to which the necessary condition of [52], which requires that the principal normals to the curve should lie in the convex hull of the contact chords, could be checked on our computed shapes. Second, simulated annealing could be carried out for both 3.1 and 4.1 knots but with period three, respectively two, rotational symmetry forced a priori. The results of such computations should clarify whether or not the current simulations, which predict shapes that are close to, but not exactly symmetric, are picking up real, but small

deviations from symmetry, or whether the simulations are merely reflecting a very slow elimination of asymmetry, perhaps due to the entirely local nature of the moves used in the simulated annealing.

Chapter 9

Conclusions and discussion

The main goal of this thesis is to present an analysis that justifies a new way to compute with self-avoiding curves. We approached the problem from two sides: On the one hand we explored functions related to thickness that are candidates for an analytically attractive characterisation of thickness, on the other hand we introduced a higher-order space curve discretization, namely biarcs, to be able to compute in the regularity class where self-avoiding curves are known to lie. We then demonstrated that distance from self-avoidance can be efficiently evaluated on this discretization. Finally we illustrated all of the theory with computations of ideal knot shapes.

In chapter 3, following the idea of *global radius of curvature* [18] we introduced all twelve possible non-trivial global radius of curvature functions to discover that for either closed or infinite, smooth curves, the functions are nested, and many are in fact identical, cf. inequalities (3.20)-(3.21), Proposition 3.3 and Lemma 3.4:

$$\rho_{\mathsf{os}} \geq \left\{ \begin{array}{c} \rho = \rho^{\star}_{\mathsf{cp}} \geq \rho_{\mathsf{tp}} = \rho_{\mathsf{tt}} = \rho_{\mathsf{tpp}} \\ \rho_{\mathsf{pc}} \end{array} \right\} \geq \rho_{\mathsf{pt}} = \rho_{\mathsf{ppp}} = \rho_{\mathsf{ptp}} = \rho_{\mathsf{ppt}} = \rho_{\mathsf{pppp}} \geq 0.$$

The above inequalities are sharp in the sense that there exist curves for which each inequality is strict at some points. On the other hand there is always a common minimal value of

$$\rho_{\mathsf{tp}} = \rho_{\mathsf{tt}} = \rho_{\mathsf{tpp}} \quad \text{and} \quad \rho_{\mathsf{pt}} = \rho_{\mathsf{ppp}} = \rho_{\mathsf{ptp}} = \rho_{\mathsf{ppt}} = \rho_{\mathsf{pppp}}, \tag{9.1}$$

and this common minimum equals the curve thickness $\Delta[\mathbf{q}]$, cf. Lemma 3.8.

Most of the explicit formulæ for circle and sphere radii given in chapter 3 are restricted to generic sets of distinct points, but we are inevitably drawn to the consideration of coalescent and nongeneric limits. Most of these limits offer no difficulty. This fact is fortunate because we note that a priori exceptional cases, such as cocircular points and tangents, appear to be more typical than might be thought in the realization of global radius of curvature functions, at least on approximately ideal shapes. In most circumstances it is convenient to define a spherical radius on cocircular data to be the radius of the smallest compatible sphere. Consideration of smooth curves lying on a single sphere then reveals that the choice of smallest possible radius makes it inevitable that spherical radii can be discontinuous, even on a smooth curve, but this presents no

real difficulty. The one limiting case which does remain problematic is that in which the derivative of curvature κ' and the torsion τ vanish at a common point. The interpretation of the classic local osculating sphere is ambiguous at such points, and it is therefore only natural that the global spherical functions can suffer the same ambiguity. In fact our biarc prescription for a space discretization involves arcs of circles where κ' and the torsion τ vanish a.e. and in particular wherever they are defined. But then the fact that the curve is known to be assembled from exact arcs of circles allows a special treatment.

Each of the two sets of equivalent global radius of curvature functions (9.1) involve at least one derived from a circular distance function, and others derived from spherical distance functions. For computations it is more convenient to work with a circular global radius of curvature function from each class because of the possibility that a spherical global radius of curvature function could be realised as the minimum of a discontinuous spherical radius function. Accordingly, we focussed our attention on the two distinct circular global radius of curvature functions ρ_{tp} and ρ_{pt}. Section 3.3 characterises the ways that ρ_{tp} and ρ_{pt} can be achieved on smooth functions. It remains to investigate the minimal regularity hypotheses on the curve $\mathbf{q}$ necessary for the results of chapter 3 to remain valid. Except for section 3.3 the results of chapter 3 have been published in [19].

In chapter 4, we developed, in a wide generality, the geometry of biarcs that interpolate a given point-tangent data pair. We assembled results appearing in the Computer Aided Design (or CAD) literature in a consistent notation and with rigorous mathematical proofs. We also described new results, in particular the tangent indicatrix properties of biarcs presented in Proposition 4.9. We note that these tangent indicatrix properties offer a route to an efficient and accurate numerical evaluation on biarc curves of the Writhe [16] and Average Crossing Number, which are quantities of considerable interest in the study of ideal shapes [5, 57]. We further remark that results in the flavour of Lemma 4.13 can be obtained for non-proper biarcs cf. Definition 4.12, but we did not stress this line of development because those cases have little interest for approximation purposes.

In chapter 5 we assembled the local convergence results of biarcs needed later in the derivation of the global convergence results that are presented in chapter 6. When the point-tangent data to be interpolated is drawn from a nested family of meshes on an underlying base curve $\mathbf{q}$, and the number of interpolation points is sent to infinity, various convergence properties follow. If $\mathbf{q}$ is a $C^{1,1}$ arc length parametrised curve, then the arc length of the biarc approximation $\boldsymbol{\beta}_{h_j}$ approaches that of $\mathbf{q}$ quadratically, cf. Corollary 6.9. Given convergence of arc lengths, various convergences of the curves themselves can be obtained, as detailed in Table 9.1. We remark that in the case that $\mathbf{q}$ is C^2, Proposition 6.15 shows that each arc of the biarc curve approaches the osculating circle of the base curve at the appropriate mesh point, and it follows that there is convergence of the curvature a.e.

We conjecture that the convergence results summarised in Table 9.1 are close to being sharp, but have proven no result in that direction. It would be of interest to consider analogous *approximation* results along the lines of determining a maximal distance of

	$\|\mathbf{q}-\mathbf{B}_{h_j}\|_C$	$\|(\mathbf{q}-\mathbf{B}_{h_j})'\|_C$	$K_{(\mathbf{q}-\mathbf{B}_{h_j})'}$
$\mathbf{q}\in C^{1,1}$	$O(h_j^2)$	$O(h_j)$	-
$\mathbf{q}\in C^{2}$	$o(h_j^2)$	$o(h_j)$	$o(1)$
$\mathbf{q}\in C^{2,1}$	$O(h_j^3)$	$O(h_j^2)$	$O(h_j)$

Table 9.1: Summary of rates of convergence of interpolating biarc curves $\mathbf{B}_{h_j}$ as established in Theorems 6.13, 6.17, and 6.20 for various norms, and differing assumed regularities of the base curve $\mathbf{q}$.

any curve $\mathbf{q}$ of prescribed regularity and arc length from a given set of biarcs with a fixed number of sub-arcs, but again we have not pursued such an investigation.

The convergence theorems of chapter 6 can all be appropriately extended to curves parametrised on the half- or whole real line. The case for $\mathbf{q}\in C^{1,1}$ is described in section 6.7. For an infinite domain and results with the assumption $\mathbf{q}\in C^2$, the second derivative $\mathbf{q}''$ must additionally be assumed to be uniformly continuous on I.

Throughout the presentation we have focused on the case of curves embedded in $\mathbb{R}^3$, but all results carry over straightforwardly to curves in $\mathbb{R}^n$. As previously remarked in section 4.1 (cf. p. 42) any generic, proper, point-tangent data pair is contained in a unique three-dimensional affine subspace $\mathcal{V}\in\mathbb{R}^n$, and a biarc interpolation of the data lies on the unique, double tangent two-sphere $\mathcal{S}$ contained in $\mathcal{V}$. Moreover the Bézier parametrisation (4.8) of circular arcs is unaltered, except that now the control points are themselves points in $\mathbb{R}^n$. Accordingly, it is simple to see that the biarc parameters Λ and $\bar{\Lambda}$ can be defined just as in the $\mathbb{R}^3$ case. Then all our convergence proofs carry over because they rely only upon the biarc parameters and Taylor expansions, which are both independent of dimension.

Because each biarc curve in $\mathbb{R}^n$ is locally low-dimensional, in the sense that each component biarc lies in the appropriate three dimensional affine subspace $\mathcal{V}$, it can be argued that biarc curves are a rather natural, geometrically simple, way to generalise the $C^{0,1}$ Lagrange interpolation of points by piecewise linear functions, to the $C^{1,1}$ Hermite interpolation of point-tangent data. The more standard approach of cubic splines does not have this property of local low-dimensionality. As is the case with cubic splines, biarc curves could also be used for the $C^{1,1}$ Lagrange interpolation of only point data, with the freedom of the tangents at the node points being set by an additional criterion, such as minimal arc length, minimal total square curvature, etc. Precisely because the geometry of biarcs is so simple, the discrete approximation and subsequent minimisation of such functionals seems to be straightforward, although we have again not, as yet, pursued this avenue of investigation.

Ultimately a biarc curve is nothing other than an ordered sequence of circular arcs. However in order to have locality it is important to focus on a biarc curve as being an ordered sequence of *pairs* of circular arcs related through a matching condition. In this interpretation when the point-tangent data at one mesh point is varied, the changes in

the overall biarc curve propagate only to one upstream and one downstream biarc, i.e. only four arcs change. In contrast, it is easy to see, using the n-dimensional generalisation of the rotation matrix $\mathbf{R}(\mathbf{e})$ defined in (4.2), that a sequence of single circular arcs can be used to interpolate an ordered list of points, with the only freedom being the tangent direction at a single point. In contrast to the biarc case, this interpolation is entirely rigid; a change at any node point propagates globally.

We mention that the osculating arc splines of Leopoldseder [27], comprise another spline made up of an ordered sequence of circular arcs. In an osculating arc spline every other circular arc is by construction a sub-arc of an osculating circle to the curve, with the intervening arcs yielding an overall C^1 assembly. As explained in [28] this construction can only be achieved by adjusting the choice of mesh along the base curve. While there is no guarantee that any arc of a biarc curve is part of an osculating circle for the base curve, we do know, from Proposition 6.15, that when the base curve is C^2 all arcs of the biarc approach osculating arcs in the limit of mesh refinement.

While we believe that it is important to regard a biarc curve as a sequence of pairs of arcs related by a matching rule, it is also important to observe that both our local and global convergence results are largely independent of the specific choice of matching rule. The matching condition for proper biarc curves is that the matching point $\mathbf{m}$ must lie on the arc Σ_{++} defined in Definition 4.8, which is open in the sense that the end points are not allowed. If an end point is taken as matching point, then the subsequent biarc curve would not in general even be C^1. For our convergence results we merely require that the matching points are bounded away from the end points of Σ_{++} in the non-dimensional way expressed in the bounds (5.42) or (6.2) on the biarc parameters Λ and $\bar{\Lambda}$.

The Taylor expansions derived in chapter 5 immediately yield various finite difference formulæ via suppression of the error term, some of which are exploited in the examination of approximately ideal shapes that was presented in chapter 8. It is apparent that the finite difference formulæ that are derived are not exhaustive. In particular if a higher order regularity of the underlying curve were assumed, consideration of appropriate linear combinations of the higher order versions of the expansions described here would provide higher order discrete approximations to quantities such as curvature and torsion in terms of the radii and angles between various circles.

While our primary interest is in the approximation properties of biarcs, we do note that expansions, such as in Lemma 5.8, remain valid in the formal limit $\Lambda \to 1$, in which case they yield finite difference formulæ just in terms of the given point-tangent data $(\mathbf{q}_i, \mathbf{t}_i)$, independent of the chosen interpolant. Indeed while biarcs have good approximation properties for curvature and the osculating circle, the only convergent finite difference approximations of torsion that we describe are in terms of only the data. While convergence of curvature of biarcs is certainly desirable, the situation is not so clear for torsion, because we apply the biarc discretization to problems where the solutions are only known to be $C^{1,1}$, i.e. curvature exists a.e., but it is plausible that the solution is no better than that.

Various authors have discussed which matching rules are best according to various criteria, both in the planar [60], [32], [50] and 3D cases [54], [35]. For us there is no overall

best choice yet apparent. It is, for example, plausible that faster convergences than those proven here could perhaps be obtained for specific matching rules. It is perhaps also the case that to obtain convergence of torsion for biarcs it would be necessary to specify a particular matching rule. Alternatively, in the spirit of Lagrange interpolation using higher order splines, the free matching parameters might be set via minimisation of an auxiliary side function, subject to the bounds (6.2). In our computations of ideal knot shapes we adopted the simplest, or mid-point, matching rule.

The fact that biarc curves have explicit, simple geometry and closed form expressions for arc length and curvature make them attractive in a number of contexts, for example as a replacement for the piecewise linear space discretization used in numerical simulations of optimal packing problems involving curves with a prescribed minimal thickness [31, 30]. The missing element before biarcs can be adopted in such computations is the construction of an algorithm, as provided in chapter 7, that allows thickness to be efficiently evaluated on an arc curve up to a prescribed accuracy. With the improved understanding of how ρ_{pt} is achieved provided by Lemma 3.6, we further showed that ρ_{pt} can be evaluated precisely on arc curves, cf. Lemma 7.14. Specifically all the possibilities described in Lemma 3.6, can be simply classified on arc curves because for a given point $\mathbf{p}$ and arc $\mathbf{a}$, all circles that pass through $\mathbf{p}$ and that are somewhere tangent to $\mathbf{a}$ lie on the sphere defined by $\mathbf{a}$ and $\mathbf{p}$, and a simple geometric picture arises. It would be of interest to find an analogous simple and precise way to evaluate ρ_{tp} on arc curves to have another test for closeness to ideality of computed knot shapes.

The convergence results of Theorems 6.13, 6.17, and 6.20 and the algorithm for efficient thickness evaluation described in section 7.1 lay a foundation for rigorous computations involving self-avoiding curves. The example we adopted to illustrate the use of biarcs as a computational tool are the special self-avoiding curves that arise in the optimal packing problem of finding *ideal knot shapes* [57, 5].

The computed approximations of ideal 3.1 and 4.1 knots described in sections 8.2-8.3 were obtained with a simulated annealing code developed in collaboration with B. Laurie. The detailed evaluations of thickness, ρ_{pt} and various finite difference approximations, presented in chapter 8 were obtained from an independent post-processing on the computed biarc curves using the Matlab scripts detailed in Appendix B. In particular the all important length and thickness of the computed biarc approximation of ideal configurations were each evaluated twice, using two independently written codes, with complete agreement to the specified tolerance.

We do not believe the current version of the simulated annealing code to be particularly efficient. Specifically, and in the first instance, only the simplest possible moves were used, namely random, small, independent, changes to an individual node or tangent. It seems likely that significant gains in efficiency could be obtained by the introduction of a set of more sophisticated moves. For example, because we now know how to compute the contact set accurately, one could bias the moves of non-active points to be arc length shortening. It also seems likely that the addition of some nonlocal, cooperative moves could speed convergence. One potentially interesting choice for global moves seems to be inversion in a sphere, which maps a biarc curve to another biarc curve. Moreover arbitrary pairs of inversions leave the knot type unaltered, and

pairs can be constructed either to give very large deformations, or to be close to the identity. In addition to a more suitable choice of moves, a more suitable choice for the matching rule, or indeed using the matching parameters as additional free variables in the simulated annealing, could improve efficiency of computation. Similarly, while the algorithm for computing thickness is robust and accurate to an arbitrary precision, it is likely that still more efficient, and faster algorithms could be constructed. For example one might compute thickness by deriving estimates of the error between the minimum of $\rho_{\mathsf{pt}}(s_i)$ at a discrete set of points s_i and the continuous minimum over arc length, combined with a bisection iteration.

As is typically the case for any stochastic algorithm, we have no rigorous stopping or convergence criterion for the computation. Such stopping criteria would presumably have to be based upon an analytical set of sufficient conditions for at least local ideality of a knot shape. Such a set of sufficient conditions are not currently known. Of course relative changes in the rope length could be taken as the stopping criterion, but this appears to be a rather bad choice. Our computations indicate that the actual configuration of a knot can change quite significantly, particularly its features involving higher order quantities such as curvature, with extremely small associated changes in rope length. Fortunately, the fact that the theory of chapter 7 allows the thickness and ρ_{pt} functions of a biarc curve to be computed to an arbitrary accuracy means that we can efficiently examine the degree to which the necessary condition of constancy of ρ_{pt} on curved segments is satisfied. In particular $\max \rho_{\mathsf{pt}} - \min \rho_{\mathsf{pt}}$, where the max and min are taken independently over curved segments, is one indication of how close to ideal the shape is.

The definition 8.2 of the μ-contact set $\boldsymbol{\chi}_\mu$ provides a second approach to quantify closeness to ideality via a construction of the set of pairs of points that are close to contact, and the dependence of the set on the tolerance parameter μ, for example the difference between the sets $\boldsymbol{\chi}_\mu$ and $\boldsymbol{\chi}_{2\mu}$. During the computations the form of the contact set has proven to be very sensitive, so that an accurate evaluation of thickness during the simulated annealing process seems to be necessary. We chose to compute with a relative error bound of 10^{-12} on thickness. The sensitivity of the contact set means that it provides a more rigorous test of closeness to ideality than a study of only the function ρ_{pt} itself.

In summary we claim that biarc curves are an efficient choice of space discretization for self avoiding curves, particularly so for optimal packing problems. For the specific optimal packing problem of ideal knots, the biarc discretization kills two birds with one stone: on the one hand, because of their simple geometry, biarcs allow evaluation of thickness and the global radius of curvature function ρ_{pt} efficiently and to a prescribed tolerance, while on the other hand they lie in the right regularity class, so that all biarc shapes that are obtained, by whatever means, provide rigorous lower bounds on thickness, independent of any discretization error. As a consequence we have obtained the best known upper bounds for rope length of the ideal 3.1 and 4.1 knots. Perhaps more importantly, the biarc discretization allows a close and detailed inspection of the approximately ideal shapes, and the contact and approximate contact sets can be resolved. Computation with biarcs has yielded an improved understanding of the rather

complicated contact sets which give a measure of closeness to ideality. Accurate computations permit the verification of known necessary conditions for optimality, such as constancy of ρ_{pt}, and offer insights which may lead to the discovery of further necessary, and perhaps sufficient, analytic conditions for optimality.

Appendix A

Construction of a sequence of reparametrisation functions

In this appendix we prove that the conditions (C1)-(C7) of section 6.3 can be satisfied by giving an explicit construction of a sequence of reparametrisation functions $\{\varphi_j\}$. Basically, we take straight lines with gradient $\frac{\lambda(\boldsymbol{\beta}_{h_j})}{\lambda(\mathbf{q})}$, and add correction terms using weighted cosine functions in order to satisfy condition (C3).

Let hypotheses (H0)-(H2) hold. Define ψ and $\psi_h \in C^\infty(\mathbb{R},\mathbb{R})$ by

$$\psi(\tau) = \tfrac{1}{2} + \tfrac{1}{2}\cos(2\pi\tau + \pi) = \tfrac{1}{2} - \tfrac{1}{2}\cos(2\pi\tau), \quad \psi_h(\tau) = h\psi\left(\tfrac{\tau}{h}\right), \tag{A.1}$$

for $\tau \in \mathbb{R}$ and for $0 < h < 1$. Then

$$\begin{aligned}
\int_0^1 \psi(\tau)d\tau &= \left(\frac{t}{2} - \frac{1}{4\pi}\sin(2\pi t)\right)\Big|_0^1 = \tfrac{1}{2}, \\
\int_0^h \psi_h(\tau)d\tau &= h\int_0^h \psi(\frac{\tau}{h})d\tau = h\int_0^1 \psi(\tau)hd\tau = \frac{h^2}{2}.
\end{aligned}$$

Now define the reparametrisation function φ_j by

$$\begin{aligned}
\varphi_j(s) &= \frac{\lambda(\boldsymbol{\beta}_{h_j})}{\lambda(\mathbf{q})}s + \sum_{i=1}^{m(s)-1}\left(a_{j,i}\int_0^{h_{j,i}}\psi_{h_{j,i}}(\tau)d\tau\right) \\
&+ a_{j,m(s)}\int_0^{s-s_{j,m(s)-1}}\psi_{h_{j,m(s)}}(\tau)d\tau, \qquad (A.2)\\
&= \frac{\lambda(\boldsymbol{\beta}_{h_j})}{\lambda(\mathbf{q})}s + \tfrac{1}{2}\textstyle\sum_{i=1}^{m(s)-1} a_{j,i}h_{j,i}^2 \\
&+ a_{j,m(s)}h_{j,m(s)}^2\left(\frac{s-s_{j,m(s)-1}}{2h_{j,m(s)}} - \frac{1}{4\pi}\sin\left(\frac{2\pi(s-s_{j,m(s)-1})}{h_{j,m(s)}}\right)\right),
\end{aligned}$$

where $m(s) \in \mathcal{N}(j)$ is such that $s \in (s_{j,m(s)-1}, s_{j,m(s)}]$ and where $a_{j,i}$ is such that

$$\lambda((\mathbf{a},\bar{\mathbf{a}})_{j,i}) = \frac{\lambda(\boldsymbol{\beta}_{h_j})}{\lambda(\mathbf{q})}h_{j,i} + a_{j,i}\int_0^{h_{j,i}}\psi_{h_{j,i}}(\tau)d\tau = \frac{\lambda(\boldsymbol{\beta}_{h_j})}{\lambda(\mathbf{q})}h_{j,i} + a_{j,i}\frac{h_{j,i}^2}{2}.$$

In other words, the factor $a_{j,i}$ is given by

$$a_{j,i} = \frac{2}{h_{j,i}^2}\left[\lambda((\mathbf{a},\bar{\mathbf{a}})_{j,i}) - \frac{\lambda(\boldsymbol{\beta}_{h_j})}{\lambda(\mathbf{q})}h_{j,i}\right] \in \mathbb{R}, \tag{A.3}$$

which can be estimated as

$$\frac{|a_{j,i}|}{h_{j,i}} \leq 2\left(\frac{|\lambda((\mathbf{a},\bar{\mathbf{a}})_{j,i}) - h_{j,i}|}{h_{j,i}^3} + \frac{|h_{j,i} - \frac{\lambda(\boldsymbol{\beta}_{h_j})}{\lambda(\mathbf{q})}h_{j,i}|}{h_{j,i}^3}\right).$$

Both terms on the right hand side are uniformly bounded in $i \in \mathcal{N}(j)$ by Lemma 6.8 and Corollary 6.9, hence

$$a_{j,i} = O(h_{j,i}) \tag{A.4}$$

with the constant being uniform.

The sequence of reparametrisation functions $\{\varphi_j\}$ given by (A.1), (A.2) and (A.3) can now be shown to satisfy each condition (C1)-(C7):

Condition (C1): By the definition we have immediately $\varphi_j \in C^\infty((s_{j,i-1}, s_{j,i}), \mathbb{R})$ for all $i \in \mathcal{N}(j),\ j \in \mathbb{N}$. More precisely, for $s \in (s_{j,i-1}, s_{j,i})$ we have

$$\varphi_j'(s) = \frac{\lambda(\boldsymbol{\beta}_{h_j})}{\lambda(\mathbf{q})} + a_{j,i}\frac{h_{j,i}}{2}\left[1 - \cos\left(\frac{2\pi(s - s_{j,i-1})}{h_{j,i}}\right)\right], \tag{A.5}$$

$$\varphi_j''(s) = a_{j,i}\pi \sin\left(\frac{2\pi(s - s_{j,i-1})}{h_{j,i}}\right), \tag{A.6}$$

$$\varphi_j'''(s) = a_{j,i}\frac{2\pi^2}{h_{j,i}}\cos\left(\frac{2\pi(s - s_{j,i-1})}{h_{j,i}}\right). \tag{A.7}$$

At the points $s_{j,i}$ one computes the left and right limits.

$$\begin{aligned}\varphi_j'(s_{j,i}) &= \frac{\lambda(\boldsymbol{\beta}_{h_j})}{\lambda(\mathbf{q})},\\ \varphi_j''(s_{j,i}) &= 0,\end{aligned}$$

and

$$\varphi_{h_j-}'''(s_{j,i}) = a_{j,i}\pi\frac{2\pi}{h_{j,i}}, \quad \varphi_{h_j+}'''(s_{j,i}) = a_{j,i+1}\pi\frac{2\pi}{h_{j,i+1}}.$$

Thus, the functions $\varphi_j, \varphi_j', \varphi_j''$ are continuous and $\varphi_j \in C^2(I, I_j)$. But φ_j'' is in general only piecewise differentiable, so that $\varphi_j \in C^{2,1}\backslash C^3$.

Condition (C2): This follows from (C6), i.e. from the fact that φ_{h_j}' converges uniformly to one as $j \to \infty$.

Conditions (C3)-(C5): By construction, i.e. by (A.3), we have $\mathbf{q}(s_{j,i}) = \boldsymbol{\beta}_{h_j}(\varphi_j(s_{j,i}))$ for $i \in \mathcal{N}(j),\ j \in \mathbb{N}$. In the proof of (C1) we find (C4)-(C5).

Condition (C6): Convergence in C^1: We use equation (A.5), Corollary 6.9 and equation (A.4) to obtain

$$\begin{aligned} |\varphi_j'(s) - 1| &\leq \left| \frac{\lambda(\boldsymbol{\beta}_{h_j})}{\lambda(\mathbf{q})} - 1 \right| + |a_{j,i}| \frac{h_{j,i}}{2} \left| 1 - \cos\left(\frac{2\pi(s - s_{j,i-1})}{h_{j,i}} \right) \right| \\ &\leq \left| \frac{\lambda(\boldsymbol{\beta}_{h_j})}{\lambda(\mathbf{q})} - 1 \right| + |a_{j,i}| h_{j,i} = O(h_j^2), \end{aligned}$$

uniformly in s.

Convergence in C^2: With equations (A.6) and (A.4) we conclude the uniform convergence

$$|\varphi_j''(s)| \leq |a_{j,i}| \pi \left| \sin\left(\frac{2\pi(s - s_{j,i-1})}{h_{j,i}} \right) \right| \leq |a_{j,i}| \pi = O(h_j).$$

Condition (C7): Equations (A.7) and (A.4) imply

$$\|\varphi_j'''\|_{L^\infty} \leq \sup_{i \in \mathcal{N}(j)} a_{j,i} \frac{2\pi^2}{h_{j,i}} \cos\left(\frac{2\pi(s - s_{j,i-1})}{h_{j,i}} \right) \leq \mathsf{c},$$

for all $j \in \mathbb{N}$.

Appendix B

Listing of MATLAB codes

We list five Matlab scripts. The three scripts `crit_test.m`, `min_dist_segment.m`, and `ropelength.m` are used for the thickness evaluation algorithm as described in section 7.1.3, the script `frho_pt.m` computes ρ_{pt} and candidates for a μ-contact set $\boldsymbol{\chi}_\mu$ following Lemma 7.14, and finally, for a given μ the $\boldsymbol{\chi}_\mu$ and $\boldsymbol{\chi}_{2\mu}$ are computed in the script `fcontact.m`.

```
function [c]=crit_test(a0,a1,a2,b0,b1,b2);
% if c=2, then nothing can be said, balls intersect,
% if c=1, then nothing can be said,
% if c=0, then no critical point (of euclidean distance) inside arcs.
%---------------------------------------
% the tangents at the ends of the arcs
ta1=(a1-a0)/norm(a1-a0);
ta2=(a2-a1)/norm(a2-a1);
tb1=(b1-b0)/norm(b1-b0);
tb2=(b2-b1)/norm(b2-b1);
% check if the balls intersect, if c=2 balls intersect
if norm(a0+a2-b0-b2)<=norm(a0-a2)+norm(b0-b2)
c=2;
else
sin_alpha=(norm(a0-a2)+norm(b0-b2))/norm(a0+a2-b0-b2);
w=(a0+a2-b0-b2)/norm(a0+a2-b0-b2);
%---------------------------------------
if w'*ta1<-sin_alpha & w'*ta2<-sin_alpha
c=0;
elseif w'*ta1>sin_alpha & w'*ta2>sin_alpha
c=0;
elseif w'*tb1<-sin_alpha & w'*tb2<-sin_alpha
c=0;
elseif w'*tb1>sin_alpha & w'*tb2>sin_alpha
c=0;
else
```

```
c=1;
end
%---------------------------------------
end
%---------------------------------------



function [minima]=min_dist_segment(b0,b1,d0,d1);
%---------------------------------------
% Given twice 2 points in 3d space (colums),
% Computes min distance minima between segments.
% The set candidates is:
% - min_corners=minimal distance between end of the segments.
% - inner_dist=minimal distance between the lines,
%   set to inf if not attained inside the segment.
% - d0_dist=minimal distance of projection of end do onto the segment of b,
%   set to inf if not attained inside the segment.
%   Analogously for: d1_dist, b0_dist, b1_dist.
%---------------------------------------
min_corners=min([norm(b0-d0) norm(b0-d1)  norm(b1-d0) norm(b1-d1)]);
%---------------------------------------
% distance between lines
lambda=1/(norm(b1-b0)^2*norm(d1-d0)^2-((b1-b0)'*(d1-d0))^2)*
[-(b1-b0)'*(b0-d0)*norm(d1-d0)^2+(b1-b0)'*(d1-d0)*(d1-d0)'*(b0-d0);
norm(b1-b0)^2*(d1-d0)'*(b0-d0)-(b1-b0)'*(b0-d0)*(b1-b0)'*(d1-d0)];

% check if minimal distance achieved inside segements
if lambda(1)<1 & lambda(2)<1 & lambda(1)>0 & lambda(2)>0
inner_dist=norm(b0+lambda(1).*(b1-b0)-d0-lambda(2).*(d1-d0));
else
inner_dist=inf;
end
%---------------------------------------
% project d0 onto b-segment:
p_d0=(d0-b0)'*(b1-b0)/norm(b1-b0)^2*(b1-b0)+b0;
% check if inside segment
if norm(p_d0-b0)+norm(p_d0-b1)-norm(b1-b0)<=0.00000001
d0_dist=norm(p_d0-d0);
else
d0_dist=inf;
end
%---------------------------------------
% project d1 onto b-segment:
```

```
p_d1=(d1-b0)'*(b1-b0)/norm(b1-b0)^2*(b1-b0)+b0;
% check if inside segment
if norm(p_d1-b0)+norm(p_d1-b1)-norm(b1-b0)<=0.00000001
d1_dist=norm(p_d1-d1);
else
d1_dist=inf;
end
%----------------------------------------
% project b0 onto d-segment:
p_b0=(b0-d0)'*(d1-d0)/norm(d1-d0)^2*(d1-d0)+d0;
% check if inside segment
if norm(p_b0-d0)+norm(p_b0-d1)-norm(d1-d0)<=0.00000001
b0_dist=norm(p_b0-b0);
else
b0_dist=inf;
end
%----------------------------------------
% project b1 onto d-segment:
p_b1=(b1-d0)'*(d1-d0)/norm(d1-d0)^2*(d1-d0)+d0;
% check if inside segment
if norm(p_b1-d0)+norm(p_b1-d1)-norm(d1-d0)<=0.00000001
b1_dist=norm(p_b1-b1);
else
b1_dist=inf;
end
%----------------------------------------
minima=min([min_corners inner_dist d0_dist d1_dist b0_dist b1_dist]);
%----------------------------------------




function [length,total_length,length_added,min_r,r,sizecritC,sizedist
C,critC,distC,lb_dcsd,ub_dcsd,lb_thickness,ub_thickness,ub_ropelength,
lb_ropelength,max_error,rel_error]=ropelength(B0,B1,B2,rel_error_b
ound);
%----------------------------------------
% given a list of arcs by Bezier points (=n colums with 3 rows),
% computes the length and thickness of the arccurve
% with double critical test, with distance test
%----------------------------------------
[three,n]=size(B1);

% local: radii of arcs and lengths
for i=1:n
```

```
T(:,i)=(B1(:,i)-B0(:,i))/norm(B1(:,i)-B0(:,i));   % normed tangent
E(:,i)=(B2(:,i)-B0(:,i))/norm(B2(:,i)-B0(:,i));   % normed chord
eta(i)=acos(E(:,i)'*T(:,i));
r(i)=norm(B2(:,i)-B0(:,i))/2/sqrt(1-(E(:,i)'*T(:,i))^2);
length(i)=2*r(i)*eta(i);
end
[min_r min_r_arc]=min(r);

total_length=0;
for i=1:n
total_length=total_length+length(i);
length_added(i)=total_length;
end
%---------------------------------------
% initial criticality test
critC=[];
for i=1:n
for j=1:i-2             %we do not evaluate next neighbours
if ~ (i==n & j==1)      %(*) neighbours

[c_v4]=crit_test_v4(B0(:,i),B1(:,i),B2(:,i),B0(:,j),B1(:,j),B2(:,j));
if c_v4~=0

% compute initial error and factor
w_a=(B1(:,i)-B0(:,i))'*(B2(:,i)-B0(:,i))/(norm(B1(:,i)-B0(:,i))
*norm(B2(:,i)-B0(:,i)));
error_a=w_a*sqrt((1-w_a)/(1+w_a))*norm(B1(:,i)-B0(:,i));
w_b=(B1(:,j)-B0(:,j))'*(B2(:,j)-B0(:,j))/(norm(B1(:,j)-B0(:,j))
*norm(B2(:,j)-B0(:,j)));
error_b=w_b*sqrt((1-w_b)/(1+w_b))*norm(B1(:,j)-B0(:,j));
factor_a=2*(1+sqrt((1+w_a)/2));
factor_b=2*(1+sqrt((1+w_b)/2));

[min_dist_seg]=min_dist_segment(B0(:,i),B2(:,i),B0(:,j),B2(:,j));
critC=[critC [B0(:,i);B1(:,i);B2(:,i);B0(:,j);B1(:,j);B2(:,j);error_a;
factor_a;error_b;factor_b;min_dist_seg]];

end %from if
end %from if (*)
end %from for
end %from for

sizecritC=size(critC); % distC = initial intermediate set of candidates
%---------------------------------------
```

```
% initial distance test:
distC=[];
dist_bound=min(critC(19,:)+critC(21,:)+critC(23,:));
[twentythree colncritC]=size(critC);
for i=1:colncritC
if critC(23,i)-critC(19,i)-critC(21,i)<=dist_bound
distC=[distC critC(:,i)];
end %from if
end %from for
sizedistC=size(distC);  % distC = initial set of candidates
%---------------------------------------
% initial values:

lb_dcsd=min(distC(23,:)-distC(19,:)-distC(21,:));
ub_dcsd=min(distC(23,:)+distC(19,:)+distC(21,:));

lb_thickness=min([2*min_r lb_dcsd]);
ub_thickness=min([2*min_r ub_dcsd]);

ub_ropelength=total_length/lb_thickness;
lb_ropelength=total_length/ub_thickness;

max_error=max(distC(19,:)+distC(21,:));
rel_error=max_error/lb_thickness;
iteration=1;
%---------------------------------------
% Iteration:
%---------------------------------------
while rel_error(iteration)>rel_error_bound & 2*min_r>lb_dcsd(iteration)
iteration=iteration+1;
C=distC;
critC=[];
[twentythree colnC]=size(C);

for k=1:colnC
%---------------------------------------
% bisect the arcs

w1_a=(C(7:9,k)-C(1:3,k))'/norm(C(7:9,k)-C(1:3,k))*(C(4:6,k)-C(1:3,k))
/norm(C(4:6,k)-C(1:3,k));
midpt_a=((1/2)*(C(1:3,k)+C(7:9,k))+w1_a*C(4:6,k))/(1+w1_a);

w1_b=(C(16:18,k)-C(10:12,k))'/norm(C(16:18,k)-C(10:12,k))*(C(13:15,k)
-C(10:12,k))/norm(C(13:15,k)-C(10:12,k));
```

```
midpt_b=((1/2)*(C(10:12,k)+C(16:18,k))+w1_b*C(13:15,k))/(1+w1_b);

A0=C(1:3,k);
A1=C(1:3,k)+((midpt_a-C(1:3,k))'*(midpt_a-C(1:3,k)))/2/((midpt_a-C(1:
3,k))'*(C(4:6,k)-C(1:3,k)))*(C(4:6,k)-C(1:3,k));
A2=midpt_a;

B0=midpt_a;
B1=C(7:9,k)+((midpt_a-C(1:3,k))'*(midpt_a-C(1:3,k)))/2/((midpt_a-C(1:
3,k))'*(C(4:6,k)-C(1:3,k)))*(C(4:6,k)-C(7:9,k));
B2=C(7:9,k);

C0=C(10:12,k);
C1=C(10:12,k)+((midpt_b-C(10:12,k))'*(midpt_b-C(10:12,k)))/2/((midpt_
b-C(10:12,k))'*(C(13:15,k)-C(10:12,k)))*(C(13:15,k)-C(10:12,k));
C2=midpt_b;

D0=midpt_b;
D1=C(16:18,k)+((midpt_b-C(10:12,k))'*(midpt_b-C(10:12,k)))/2/((midpt_
b-C(10:12,k))'*(C(13:15,k)-C(10:12,k)))*(C(13:15,k)-C(16:18,k));
D2=C(16:18,k);
%----------------------------------------
% criticality test

[c_v4_AC]=crit_test_v4(A0,A1,A2,C0,C1,C2);
[c_v4_AD]=crit_test_v4(A0,A1,A2,D0,D1,D2);
[c_v4_BC]=crit_test_v4(B0,B1,B2,C0,C1,C2);
[c_v4_BD]=crit_test_v4(B0,B1,B2,D0,D1,D2);

if c_v4_AC~=0
[min_dist_segAC]=min_dist_segment(A0,A2,C0,C2);
critC=[critC [A0;A1;A2;C0;C1;C2;C(19,k)/C(20,k);C(20,k);C(21,k)/C(22,
k);C(22,k);min_dist_segAC]];
end %from if

if c_v4_AD~=0
[min_dist_segAD]=min_dist_segment(A0,A2,D0,D2);
critC=[critC [A0;A1;A2;D0;D1;D2;C(19,k)/C(20,k);C(20,k);C(21,k)/C(22,
k);C(22,k);min_dist_segAD]];
end %from if

if c_v4_BC~=0
[min_dist_segBC]=min_dist_segment(B0,B2,C0,C2);
critC=[critC [B0;B1;B2;C0;C1;C2;C(19,k)/C(20,k);C(20,k);C(21,k)/C(22,
```

```
k);C(22,k);min_dist_segBC]];
end %from if

if c_v4_BD~=0
[min_dist_segBD]=min_dist_segment(B0,B2,D0,D2);
critC=[critC [B0;B1;B2;D0;D1;D2;C(19,k)/C(20,k);C(20,k);C(21,k)/C(22,
k);C(22,k);min_dist_segBD]];
end %from if
%----------------------------------------
end %from for k=1:colnC
sizecritC=[sizecritC; size(critC)]; % critC=intermediate set of candidates

%----------------------------------------
% distance test:
distC=[];
dist_bound=min(critC(19,:)+critC(21,:)+critC(23,:));
[twentythree colncritC]=size(critC);
for i=1:colncritC
if critC(23,i)-critC(19,i)-critC(21,i)<=dist_bound
distC=[distC critC(:,i)];
end %from if
end %from for
sizedistC=[sizedistC; size(distC)];  % distC = set of candidates
%----------------------------------------

lb_dcsd=[lb_dcsd;min(distC(23,:)-distC(19,:)-distC(21,:))];
ub_dcsd=[ub_dcsd;min(distC(23,:)+distC(19,:)+distC(21,:))];

lb_thickness=[lb_thickness;min([2*min_r min(distC(23,:)-distC(19,:)-d
istC(21,:))])];
ub_thickness=[ub_thickness;min([2*min_r min(distC(23,:)+distC(19,:)+d
istC(21,:))])];

ub_ropelength=[ub_ropelength;total_length/(min([2*min_r min(distC(23,
:)-distC(19,:)-distC(21,:))]))];
lb_ropelength=[lb_ropelength;total_length/(min([2*min_r min(distC(23,
:)+distC(19,:)+distC(21,:))]))];

max_error=[max_error;max(distC(19,:)+distC(21,:))];
rel_error=[rel_error;max(distC(19,:)+distC(21,:))/(min([2*min_r min(d
istC(23,:)-distC(19,:)-distC(21,:))]))];
%----------------------------------------
end %from while
%----------------------------------------
```

```
function [rho_pt,pt_A,pt_V,pt_CV,pt_C]=frho_pt(small,M,B0,B1,B2,r,len
gth_added);
%---------------------------------------
% Check if rho_pt is achieved inside arc or not.
% If not achieved inside arc pt_V=minima of pt on end point.
% If achieved inside arc, single critical test and pt_V=pp.
%---------------------------------------
% pt_A(i,j)=0 if local i.e. i==j
% pt_A(i,j)=1 if minimum achieved inside and by pp-min
%             (or at endpoints with the necessary cond satisfied).
% pt_A(i,j)=2 if minimum achieved inside and by pp-max
%             (or at endpoints with the necessary cond satisfied).
% pt_A(i,j)=4 if minimum achieved at endpoints.
%
% pt_C(i,j)=0 if pt_A(i,j)=0 and if local radius is minimum
% pt_C(i,j)=4 if pt_A(i,j)=0 and if local radius is not minimum
% pt_C(i,j)=pt_A(i,j) if pt_A(i,j)=1,2
% pt_C(i,j)=3 if the endpoint is minima
% pt_C(i,j)=4 if the endpoint is not minima
%
% pt_CV(i,j)=0 if pt_C(i,j)=0,1,2,3  and
% pt_CV(i,j)=pt_V(i,j) if pt_C(i,j)=4.
%
% pt_V(i,j)=minimal value of pt(midpoint,arc) on that pair
%---------------------------------------
[three n]=size(B0);

for i=1:n
for j=1:n
%------------------%------------------
if i==j
pt_A(i,j)=0;
pt_V(i,j)=r(j);

elseif i~=j
f0=(B0(:,j)-M(:,i))'*(B1(:,j)-B0(:,j));
f2=(B2(:,j)-M(:,i))'*(B2(:,j)-B1(:,j));
%------------------%------------------%------------------
if f0<0 & f2<0
pt_A(i,j)=4;

T=(B1(:,j)-B0(:,j))/norm(B1(:,j)-B0(:,j));
cos_phi=(1/norm(M(:,i)-B0(:,j)))*(M(:,i)-B0(:,j))'*T;
r_quad=norm(M(:,i)-B0(:,j))^2/(4*(1-cos_phi^2));
```

```
pt0=sqrt(r_quad);
T=(B1(:,j)-B2(:,j))/norm(B1(:,j)-B2(:,j));
cos_phi=(1/norm(M(:,i)-B2(:,j)))*(M(:,i)-B2(:,j))'*T;
r_quad=norm(M(:,i)-B2(:,j))^2/(4*(1-cos_phi^2));
pt2=sqrt(r_quad);

pt_Vij=min([pt0 pt2]);
pt_V(i,j)=pt_Vij;
%------------------%------------------%------------------
elseif f0>0 & f2>0
pt_A(i,j)=4;

T=(B1(:,j)-B0(:,j))/norm(B1(:,j)-B0(:,j));
cos_phi=(1/norm(M(:,i)-B0(:,j)))*(M(:,i)-B0(:,j))'*T;
r_quad=norm(M(:,i)-B0(:,j))^2/(4*(1-cos_phi^2));
pt0=sqrt(r_quad);
T=(B1(:,j)-B2(:,j))/norm(B1(:,j)-B2(:,j));
cos_phi=(1/norm(M(:,i)-B2(:,j)))*(M(:,i)-B2(:,j))'*T;
r_quad=norm(M(:,i)-B2(:,j))^2/(4*(1-cos_phi^2));
pt2=sqrt(r_quad);

pt_Vij=min([pt0 pt2]);
pt_V(i,j)=pt_Vij;
%------------------%------------------%------------------
elseif f0<=0 & f2>=0
pt_A(i,j)=1;
%---------%---------
Bino=cross((B0(:,j)-B1(:,j)),(B2(:,j)-B1(:,j)))/norm(cross((B0(:,j)-B
1(:,j)),(B2(:,j)-B1(:,j))));
%---------
T0=(B1(:,j)-B0(:,j))/norm((B1(:,j)-B0(:,j)));
Chord=(B2(:,j)-B0(:,j))/norm((B2(:,j)-B0(:,j)));
cos_phi=Chord'*T0;
center=B0(:,j)+(r(j)/sqrt(1-cos_phi^2))*Chord-(r(j)*cos_phi/sqrt(1-co
s_phi^2))*T0;
%---------
% point on whole circle, where pp-min is achieved:
ppmin=center+r(j)*(M(:,i)-center-Bino'*(M(:,i)-center)*Bino)/norm(M(:
,i)-center-Bino'*(M(:,i)-center)*Bino);
pt_V(i,j)=.5*norm(ppmin-M(:,i));

%------------------%------------------%------------------
elseif f0>=0 & f2<=0
```

```
%---------%---------%---------
% check if coplanar
if det([(B0(:,j)-B1(:,j)) (B2(:,j)-B1(:,j)) (M(:,i)-B1(:,j))])==0

% compute center of arc:
T2=(B1(:,j)-B0(:,j))/norm(B1(:,j)-B0(:,j));
Chord=(B2(:,j)-B0(:,j))/norm(B2(:,j)-B0(:,j));
cos_phi=Chord'*T2;
center=B0(:,j)+(r(j)/sqrt(1-cos_phi^2))*Chord-(r(j)*cos_phi/sqrt(1-co
s_phi^2))*T2;
%---------%---------
if r(j)<norm(M(:,i)-center)
pt_A(i,j)=2;

Bino=cross((B0(:,j)-B1(:,j)),(B2(:,j)-B1(:,j)))/norm(cross((B0(:,j)-B
1(:,j)),(B2(:,j)-B1(:,j))));
%---------
T0=(B1(:,j)-B0(:,j))/norm((B1(:,j)-B0(:,j)));
Chord=(B2(:,j)-B0(:,j))/norm((B2(:,j)-B0(:,j)));
cos_phi=Chord'*T0;
center=B0(:,j)+(r(j)/sqrt(1-cos_phi^2))*Chord-(r(j)*cos_phi/sqrt(1-co
s_phi^2))*T0;
%---------
% point on whole circle, where pp-max is achieved:
ppmax=center-r(j)*(M(:,i)-center-Bino'*(M(:,i)-center)*Bino)/norm(M(:
,i)-center-Bino'*(M(:,i)-center)*Bino);
pt_V(i,j)=.5*norm(ppmax-M(:,i));

%---------%---------
else
pt_A(i,j)=4;

T=(B1(:,j)-B0(:,j))/norm(B1(:,j)-B0(:,j));
cos_phi=(1/norm(M(:,i)-B0(:,j)))*(M(:,i)-B0(:,j))'*T;
r_quad=norm(M(:,i)-B0(:,j))^2/(4*(1-cos_phi^2));
pt0=sqrt(r_quad);
T=(B1(:,j)-B2(:,j))/norm(B1(:,j)-B2(:,j));
cos_phi=(1/norm(M(:,i)-B2(:,j)))*(M(:,i)-B2(:,j))'*T;
r_quad=norm(M(:,i)-B2(:,j))^2/(4*(1-cos_phi^2));
pt2=sqrt(r_quad);

pt_Vij=min([pt0 pt2]);
pt_V(i,j)=pt_Vij;
```

```
end %from if r(j)<norm etc.
%---------%---------

%---------%---------%---------
else %from if det==0

% compute center of arc:
T2=(B1(:,j)-B0(:,j))/norm(B1(:,j)-B0(:,j));
Chord=(B2(:,j)-B0(:,j))/norm(B2(:,j)-B0(:,j));
cos_phi=Chord'*T2;
center=B0(:,j)+(r(j)/sqrt(1-cos_phi^2))*Chord-(r(j)*cos_phi/sqrt(1-co
s_phi^2))*T2;
% compute binormal of arc:
Bino=cross((B0(:,j)-B1(:,j)),(B2(:,j)-B1(:,j)))/norm(cross((B0(:,j)-B
1(:,j)),(B2(:,j)-B1(:,j))));
% compute center of arc-point-sphere
centersph=center+(Bino'*(M(:,i)-center))*Bino;

circ_cos=norm((B0(:,j)-centersph)'*Bino)/norm(B0(:,j)-centersph);
point_cos=norm((M(:,i)-centersph)'*Bino)/norm(M(:,i)-centersph);
%---------%---------
if point_cos<circ_cos   %condition (7.43)

pt_A(i,j)=2;

Bino=cross((B0(:,j)-B1(:,j)),(B2(:,j)-B1(:,j)))/norm(cross((B0(:,j)-B
1(:,j)),(B2(:,j)-B1(:,j))));
%---------
T0=(B1(:,j)-B0(:,j))/norm((B1(:,j)-B0(:,j)));
Chord=(B2(:,j)-B0(:,j))/norm((B2(:,j)-B0(:,j)));
cos_phi=Chord'*T0;
center=B0(:,j)+(r(j)/sqrt(1-cos_phi^2))*Chord-(r(j)*cos_phi/sqrt(1-co
s_phi^2))*T0;
%---------
% point on whole circle, where pp-max is achieved:
ppmax=center-r(j)*(M(:,i)-center-Bino'*(M(:,i)-center)*Bino)/norm(M(:
,i)-center-Bino'*(M(:,i)-center)*Bino);
pt_V(i,j)=.5*norm(ppmax-M(:,i));

%---------%---------
else
pt_A(i,j)=4;

T=(B1(:,j)-B0(:,j))/norm(B1(:,j)-B0(:,j));
```

```
cos_phi=(1/norm(M(:,i)-B0(:,j)))*(M(:,i)-B0(:,j))'*T;
r_quad=norm(M(:,i)-B0(:,j))^2/(4*(1-cos_phi^2));
pt0=sqrt(r_quad);
T=(B1(:,j)-B2(:,j))/norm(B1(:,j)-B2(:,j));
cos_phi=(1/norm(M(:,i)-B2(:,j)))*(M(:,i)-B2(:,j))'*T;
r_quad=norm(M(:,i)-B2(:,j))^2/(4*(1-cos_phi^2));
pt2=sqrt(r_quad);

pt_Vij=min([pt0 pt2]);
pt_V(i,j)=pt_Vij;
end
%---------%---------
end %from if det==0
%---------%---------%---------

%---------%---------
end %if f0<0 & f2<0 etc.
end %from if i~=j
%------------------%------------------
end %from for
end %from for
%----------------------------------------

%----------------------------------------
% compute rho_pt:
for k=1:n
rho_pt(k)=min(pt_V(k,:));
end
%----------------------------------------
% compute pt_C:
% find corner-min where pt_A(i,j)=4:
for i=1:n
for j=2:n-1
%----%----%----%----
if pt_A(i,j)~=4
% local
if i==j
pt_C(i,j)=0;
pt_CV(i,j)=0;
elseif i~=j
pt_C(i,j)=pt_A(i,j);
pt_CV(i,j)=0;
end
%-------------
```

```
else
if norm(pt_V(i,j)-pt_V(i,j+1))<small & pt_A(i,j+1)==4
pt_C(i,j)=3;
pt_CV(i,j)=0;
else
pt_C(i,j)=4;
pt_CV(i,j)=pt_V(i,j);
end %from if
%----
end %from if
%----%----
end %from for j=2:n-1
%----%----%----%----

%----%----%----%----
% for j=1
if pt_A(i,1)~=4
% local
if i==1
pt_C(i,1)=0;
pt_CV(i,1)=0;
elseif i~=1
pt_C(i,1)=pt_A(i,1);
pt_CV(i,1)=0;
end
%-------------
else
if norm(pt_V(i,1)-pt_V(i,2))<small & pt_A(i,2)==4
pt_C(i,1)=3;
pt_CV(i,1)=0;
else
pt_C(i,1)=4;
pt_CV(i,1)=pt_V(i,1);
end %from if
%----
end %from if
%----%----%----%----

%----%----%----%----
% for j=n
if pt_A(i,n)~=4
% local
if i==n
pt_C(i,n)=0;
```

```
pt_CV(i,n)=0;
elseif i~=n
pt_C(i,n)=pt_A(i,n);
pt_CV(i,n)=0;
end
%-------------
else
if norm(pt_V(i,n)-pt_V(i,1))<small & pt_A(i,1)==4
pt_C(i,n)=3;
pt_CV(i,n)=0;
else
pt_C(i,n)=4;
pt_CV(i,n)=pt_V(i,n);
end %from if
%----
end %from if
%----%----
%----%----%----%----
end %from for i=1:n

% Plots:
figure(1)
stairs(length_added,rho_pt,'r')
hold on
stairs(length_added,r,'b')
hold off
figure(2)
image(pt_CV*34),axis('square'),
figure(3)
imagesc(pt_C),axis('square')
colormap([0 .8 0;0 0 1;0.9 0.2 0.8; 1 0 0; 1 1 1])
%---------------------------------------




function [IC,IC2,ICcount,IC2count,Cr_index,Cr]=fcontact(thickness,muc
,M,B0,B1,B2,length_added,rho_pt,pt_V,pt_CV,pt_C);
%---------------------------------------
% note: do not use mu as a variable in matlab, it is taken!
%---------------------------------------
% IC(i,j)=0, when there is a muc-contact
% IC(i,j)=1, when there is no muc-contact
%---------------------------------------
[three n]=size(length_added);
```

```
%---------------------------------------
ICcount=0;
IC2count=0;

for i=1:n
for j=1:n
if pt_C(i,j)~=4 & pt_V(i,j)<=thickness*(1+muc)
IC(i,j)=0;
ICcount=ICcount+1;
IC2(i,j)=0;
IC2count=IC2count+1;
elseif pt_C(i,j)~=4 & pt_V(i,j)<=thickness*(1+2*muc)
IC(i,j)=1;
IC2(i,j)=0;
IC2count=IC2count+1;
else
IC(i,j)=1;
IC2(i,j)=1;
end
end
end

% Plots:
figure(4)
imagesc(IC),,axis('square'),colormap([0 0 0; 1 1 1])
figure(5)
imagesc(IC2),,axis('square'),colormap([0 0 0; 1 1 1])
%---------------------------------------


%---------------------------------------
Cr=[];
Cr_index=[];
for i=1:n
vec=[];
i_index=[];
%-------%-------%
for j=1:n
if pt_C(i,j)~=4
vec=[vec pt_V(i,j)];
i_index=[i_index j];
end
end
```

```
%-------%-------
[vec index]=sort(vec);
vec=vec(1:6);
index=index(1:6);
Cr=[Cr;vec];
Index=i_index(index);
Cr_index=[Cr_index; Index];
end

% for each i, (i.e. each Midpoint of an arc, usually)
% puts six lowest values of pt_V(i,:) where pt_C~=4,
% into a vector vec. Vectors are rows of matrix Cr.

% Plots:
figure(6)
plot(length_added,Cr(:,1),'.b',length_added,Cr(:,2),'.r',length_added
,Cr(:,3),'.g',length_added,Cr(:,4),'b',length_added,Cr(:,5),'r',lengt
h_added,Cr(:,6),'g'),axis([0 1 thickness thickness*(1+muc)])
figure(7)
plot(length_added,Cr(:,1),'b.',length_added,Cr(:,2),'r.',length_added
,Cr(:,3),'g.',length_added,Cr(:,4),'b',length_added,Cr(:,5),'r',lengt
h_added,Cr(:,6),'g',[length_added(1) length_added(n)],[thickness*(1+m
uc) thickness*(1+muc)],'b--'),axis([0 1 thickness thickness*(1+2*muc)])
%---------------------------------------
```

Bibliography

[1] M. Berger, *Geometry I*, Springer, Berlin Heidelberg (1987).

[2] K. M. Bolton, Biarc curves, *Computer-Aided Design* **7** (1975), 89–92.

[3] G. Buck and J. Simon, *Energy and length of knots*, in Lectures at Knots96, ed. Suzuki, S., World Scientific Publishing, Singapore (1997), 219–234.

[4] G. Burde, H. Zieschang, *Knots*, Second Edition, Walter de Gruyter, Berlin (2003).

[5] J. A. Calvo, K. C. Millett and E. J. Rawdon (Eds), *Physical Knots: Knotting, Linking, and Folding. Geometric Objects in* $\mathbb{R}^3$, Contemporary Mathematics **304**, (2002).

[6] J. Cantarella, R. B. Kusner and J. M. Sullivan, On the minimum ropelength of knots and links, *Inventiones mathematicae* **150**(2) (2002), 257–286.

[7] H. S. M. Coxeter, *Introduction to Geometry*, Second Edition, Wiley, New York (1969).

[8] G. Dietler, P. Pieranski, S. Kasas and A. Stasiak, The rupture of knotted strings under tension, *Contemporary Mathematics* **304** (2002), 217–222.

[9] M. P. Do Carmo, *Differential Geometry of Curves and Surfaces*, Prentice-Hall, New Jersey (1976).

[10] M. P. Do Carmo, *Riemannian Geometry*, Birkäuser, Boston, Basel, Berlin (1992).

[11] O. C. Durumeric, Thickness Formula and C^1-Compactness for $C^{1,1}$ Riemannian Submanifolds, arXiv:math.DG/0204050, (2002).

[12] O. C. Durumeric, Local structure of ideal shapes of knots, arXiv:math.GT/0204063 (2002).

[13] D. H. Eberly, *3D game engine design a practical approach to real-time computer graphics*, Morgan Kaufmann Publishers, San Francisco, (2001).

[14] L. C. Evans and R. F. Gariepy, *Measure Theory and Fine Properties of Functions*, CRC Press, Boca Raton, Florida, 1992.

[15] G. Farin, *Curves and Surfaces for Computer-Aided Geometric Design*, Academic Press, Boston, 1990.

[16] F. B. Fuller, Decomposition of the Linking Number of a Closed Ribbon: A Problem from Molecular Biology, *Proc. Natl. Acad. Sci. USA* **75**(8) (1978), 3557–3561.

[17] O. Gonzalez and R. de la Llave, Existence of ideal knots, *J. of Knot Theory and its Ramifications* **12**(1) (2003), 123–133.

[18] O. Gonzalez and J. H. Maddocks, Global curvature, thickness, and the ideal shapes of knots, *Proc. Natl. Acad. Sci. USA* **96**(9) (1999), 4769–4773.

[19] O. Gonzalez, J. H. Maddocks, and J. Smutny, Curves, circles, and spheres, *Contemporary Mathematics* **304** (2002), 195–215.

[20] O. Gonzalez, J. H. Maddocks, F. Schuricht and H. von der Mosel, Global curvature and self-contact of nonlinearly elastic curves and rods, *Calc. Var. Partial Differential Equations* **14**(1) (2002), 29–68.

[21] W. C. Graustein, *Differential Geometry*, Dover Publications, New York (1966).

[22] H. W. Guggenheimer, *Differential Geometry*, Dover, New York (1977).

[23] J. Hoschek, Circular Splines, *Computer-Aided Design* **24**(11) (1992), 611–618.

[24] R. Kusner and J. M. Sullivan, *Möbius-Invariant Knot Energies.* Chpt. 17 of [57].

[25] V. Katritch, J. Bednar, D. Michoud, R. G. Scharein, J. Dubochet, and A. Stasiak, *Geometry and physics of knots*, Nature **384** (1996), 142–145.

[26] B. Laurie, *Annealing Ideal Knots and Links: Methods and Pitfalls*, Chpt. 3 of [57].

[27] S. Leopoldseder, *Cone spline surfaces and spatial arc splines*, PhD Thesis, Technische Universität Wien, 1998.

[28] S. Leopoldseder, Algorithms on cone spline surfaces and spatial osculating arc splines, *Computer Aided Geometric Design* **18**(6) (2001), 503–608.

[29] R. A. Litherland, J. Simon, O. Durumeric, and E. Rawdon, *Thickness of knots*, Topology and its Applications **91** (1999), 233–244.

[30] D. Marenduzzo and C. Micheletti, Thermodynamics of DNA packaging inside a viral capsid: the role of DNA intrinsic thickness, *J. of Molecular Biology* **330** (2003), 485–492.

[31] A. Maritan, C. Micheletti, A. Trovato, and J. R. Banavar, Optimal shapes of compact strings, *Nature* **406** (2000), 287–290.

[32] D. S. Meek and D. J. Walton, Approximation of discrete data by G^1 arc splines, *Computer-Aided Design* **24** (1992), 301–306.

[33] Z. A. Melzak, *Invitation to Geometry*, Wiley, New York (1983).

[34] C. A. Neff, Finding the distance between two circles in three-dimensional space, *IBM J. Res. Develop.*, **34**(5) (1990), 770–775.

[35] A. W. Nutbourne and R. R. Martin, *Differential geometry applied to curve and surface design*, Vol. 1: Foundations, Ellis Horwood, Chichester (1988).

[36] J. O'Hara, *Energy of Knots*, Chpt. 16 of [57].

[37] C. J. Ong, Y. S. Wong, H. T. Loh, and X. G. Hong, An optimization approach for biarc curve-fitting of B-spline curves, *Computer-Aided Design* **28**(12) (1996), 951–959.

[38] D. B Parkinson and D. N. Moreton, Optimal biarc-curve fitting, *Computer-Aided Design* **23** (1991), 411–419.

[39] D. B. Parkinson, Optimised biarc curves with tension, *Computer-Aided Geometric Design* **9**(3) (1992), 207–218.

[40] L. A. Piegl and W. Tiller, Biarc approximation of NURBS curves, *Computer-Aided Design* **34**(11) (2002), 807–814.

[41] P. Pieranski, *In Search of Ideal Knots*, Chpt. 2 of [57].

[42] P. Pieranski and S. Przybyl, Ideal trefoil knot, *Physical Review E*, **64**, 031801 (2001).

[43] P. Pieranski, S. Przybyl, and A. Stasiak, Tight open knots, *European Physical Journal E*, **6**(2) (2001), 123–128.

[44] P. Pieranski and S. Przybyl, In Search of the Ideal Trefoil Knot, *Contemporary Mathematics* **304** (2002), 153–162.

[45] E. J. Rawdon, *Approximating the Thickness of a Knot*, Chpt. 9 of [57].

[46] E. J. Rawdon, Approximating smooth thickness, *J. of Knot Theory and its Ramifications* **9** (1) (2000), 113–145.

[47] E. J. Rawdon, Can computers discover ideal knots?, *Experimental Mathematics*, to appear.

[48] E. J. Rawdon, Program TOROS (Thickness Or Ropelength Optimizing System), http://www.mathcs.duq.edu/ rawdon/manual.html.

[49] D. Rolfsen, *Knots and Links*, Publish or Perish, Berkeley (1976).

[50] J. Schonherr, Smooth biarc curves, *Computer-Aided Design* **25** (1993), 365–370.

[51] F. Schuricht, H. von der Mosel, *Global curvature for rectifiable loops*, Mathematische Zeitschrift, **243** (2003), 37–77.

[52] F. Schuricht and H. von der Mosel, Characterization of ideal knots, *Calc. Var.*, **19** (2004), 281–305.

[53] T. J. Sharrock, *Surface Design with Cyclide Patches*, PhD Thesis, University of Cambridge, Engineering Department, 1985.

[54] T. J. Sharrock, Biarcs in three dimensions, in *The Mathematics of Surfaces II*, Ed. R. R. Martin, Oxford Univ. Press, New York, (1987), 395–411.

[55] A. Stasiak, V. Katritch, J. Bednar, D. Michoud, and J. Dubochet, Electrophoretic Mobility of DNA Knots, *Nature*, **384**, (1996), 122.

[56] A. Stasiak, J. Dubochet, V. Katritch, and P. Pieranski, *Ideal Knots and Their Relation to the Physics of Real Knots*, Chpt. 1 of [57].

[57] A. Stasiak, V. Katritch and L. H. Kauffman (Eds), *Ideal knots*, Ser. Knots Everything **19**, World Sci. Publishing, River Edge, NJ (1998).

[58] A. Stasiak and J. H. Maddocks, *Best packing in proteins and DNA*, Nature **406** (2000) 251–253.

[59] D. J. Struik, *Lectures on Classical Differential Geometry*, Second Edition, Dover, New York (1988).

[60] B. Su and C. Liu, Computational Geometry, Curve and Surface Modeling, Academic Press, San Diego, (1989).

[61] P. G. Tait, *Scientific papers*, Vol. II, Cambridge University Press, (1900), 403.

[62] A. V. Vologodskii, N. J. Crisona, B. Laurie, P. Pieranski, V.Katritch, J. Dubochet, and A. Stasiak, Sedimentation and Electrophoretic Migration of DNA Knots and Catenanes, *J. Mol. Biol.*, **278**, (1998), 1–3.

[63] David Vranek, Fast and accurate circle-circle and circle-line 3d distance computation, *Journal of graphics tools*, **7** (1) (2002), 23–32.

[64] W. Wang and B. Joe, Classification and properties of space biarcs, in *SPIE: Curves and surfaces in computer vision and graphics III*, Boston, **1830** (1992), 184–195.

Curriculum Vitæ

I was born on February 26th 1973 in Brugg, Switzerland, as the second child of Olga and Josef Smutny. Together with my two and a half year older sister I spent a happy childhood growing up in Windisch. I went to primary (1980-1985) and secondary school (1985-1989) in Windisch, then continued my education at the Cantonal school of Baden (1989-1993), graduating in January 1993 with the Maturity C (natural sciences). I studied Mathematics at the University of Zürich (1993-1999) with Mineralogy and Petrography, and Computer Science as subsidiary subjects and obtained my diploma with Prof. H. Amann in November 1999. From January to August 2000 I worked in Stansstad for a company called Artificial Life as a Knowledge Base Engineer before I decided to pursue the challenge of a doctorate.